Herpes viruses and neuroinflammation

Doorduin, Janine

Herpes viruses and neuroinflammation: PET imaging and implication in schizophrenia

ISBN: 978-90-367-4128-6

The research in this thesis was funded by the Stanley Medical Research Institute, Grant-ID 05-NV-001.

The printing of this thesis was financially supported by:
Rijksuniversiteit Groningen, School of Behavioral and Cognitive Neuroscience (BCN) and Veenstra Instruments.

Printed by Ipskamp Drukkers, Enschede, the Netherlands

RIJKSUNIVERSITEIT GRONINGEN

Herpes viruses and neuroinflammation: PET imaging and implication in schizophrenia

Proefschrift

ter verkrijging van het doctoraat in de
Medische Wetenschappen
aan de Rijksuniversiteit Groningen
op gezag van de
Rector Magnificus, dr. F. Zwarts,
in het openbaar te verdedigen op
woensdag 6 januari 2010
om 14:45 uur

door

Janine Doorduin

geboren op 26 december 1980
te Maassluis

Promotor:	Prof. dr. R.A. Dierckx
Copromotores:	Dr. H.C. Klein
	Dr. E.F.J. de Vries
Beoordelingscommissie:	Prof. dr. K. Audenaert
	Prof. dr. H.W.G.M. Boddeke
	Prof. dr. P.P. van Rijk

Paranimfen: Jonne Doorduin

Mirella Struijck

Contents

Chapter 1

General introduction

Schizophrenia

Schizophrenia is a chronic, severe and disabling brain disease that is characterized by abnormal mental function and disturbed behavior. At the beginning of the 20th century, the first comprehensive description of schizophrenia was provided by Emil Kraeplin when he called it dementia praecox [1]. He believed that schizophrenia was a degenerative disease that started out in the early childhood and would eventually lead to deterioration of personality and mind. Dementia praecox was renamed into schizophrenia by Eugen Bleuler [2] when he realized that the disorder did not necessarily lead to mental decline and did not always occur in young people. Schizophrenia literally means 'split mind', referring to the loss of capacity to guide thought processes by concepts that were correctly linked together. The term schizophrenia is, however, still controversial since it often leads to misinterpretation of the disease as being a multiple personality disorder.

Approximately 1% of the human population world-wide is affected by schizophrenia [3] and besides the disorder being devastating for most patients, it is very costly for families and society. The age of onset of schizophrenia is often between 16 and 25 years of age, and rarely before puberty or after 40 years of age. Diagnosis is made according to the appearance of positive and negative symptoms [4]. Symptoms are referred to as positive when they represent abnormal behavior, such as hallucinations, delusions and unorganized thinking. The positive symptoms of schizophrenia are characteristic of psychosis and appear in episodes of time. The negative symptoms refer to the absence of normal behavior, resulting in, amongst others, social withdrawal, flattened emotion and the lack of spontaneous thinking. In addition to the positive and negative symptoms, schizophrenic patients show cognitive symptoms, with impairments of attention, memory and executive functions, as well as mood symptoms, such as suicidality and hopelessness.

In general, schizophrenic patients are treated with antipsychotic drugs to control the symptoms. The first generation of antipsychotics, the so-called typical antipsychotics, were only effective in controlling the positive symptoms of schizophrenia. However, the second generation of atypical antipsychotics were also found to control the negative and cognitive symptoms. Although in many of the schizophrenic patients the symptoms are successfully treated, the cure for schizophrenia has not yet been found. Perhaps one of the most important reasons for the lack of a cure for schizophrenia is that the etiology of the disease is still unknown.

Although the etiology of schizophrenia is not known, many structural and functional brain abnormalities have been found. The main structural abnormalities include a reduction in grey matter volume, mainly in the prefrontal and temporal brain regions, and/or an increase in ventricular volume [5]. In addition, the connections between neurons are thought to be altered in schizophrenia, which was measured post-mortem [6], but also with diffusion tensor imaging [7]. Altered neuronal connections, may consequently lead to changes in neurotransmission. The neurotransmitter that was originally thought to underlie the etiology of schizophrenia was dopamine. This was mainly based on the finding that drugs that increase dopamine in the brain, such as amphetamines and cocaine, cause psychotic symptoms. In addition, it was accidently discovered that drugs that antagonized the binding of dopamine caused a decrease in psychotic symptoms. It was later shown that the neurotransmitter glutamate is also involved in schizophrenia. Glutamatergic dysfunction is thought to be related to a hypofunction of the glutamate NMDA-receptor, since the NMDA-antagonists ketamine, phencyclidine (PCP) and dizocilpine (MK-801) were found to induce a condition that resembles schizophrenia. Since both dopamine and glutamate play a role in schizophrenia it is most likely that they interact in inducing schizophrenia, involving also GABAergic and cholinergic systems [8].

Although the findings mentioned before indicate abnormalities in the schizophrenic brain, they do not explain the etiology per se. Both gene mutations and various environmental factors have been suggested to play a role in the etiology of schizophrenia, but neither of these single factors can explain the entire disease process. It is therefore generally agreed that environmental factors underlie the development of schizophrenia only in genetically predisposed individuals. When focusing on environmental factors, one could think of factors such as substance abuse and stressful life events, but also infectious agents are thought to play an important role in the etiology of schizophrenia.

Kraeplin and Bleuler [1,2] were one of the first to propose that infectious agents might play a role in schizophrenia and its development. After half a century of silence, the interest in the infectious hypothesis of schizophrenia revived [9]. Early studies showed a winter and spring seasonality of birth of individuals who developed schizophrenia later in life, which was, amongst others, suggested to be caused by infectious agents [10,11]. Indeed, a significant correlation was found between schizophrenic births and the occurrence of measles, Varicella-Zoster virus and polio [12], as well as influenza [13], suggesting the role of infectious agents in the

development of schizophrenia. In addition, it has also been shown that serious viral infections of the brain during childhood were associated with later development of schizophrenia [14]. These studies indirectly provided evidence for the involvement of infectious agents in schizophrenia and are just a small selection of all the work done.

The infectious agents that are most likely to be involved in schizophrenia are viruses, which show preference for infecting the central nervous system and have the ability to establish latency in the human body. If viruses (or other infectious agents) are proven to play a role in schizophrenia, this can lead to improved treatment and thus better treatment outcome. It is therefore of great value to provide more evidence for the involvement of viruses in schizophrenia, which can, amongst others, be obtained by determining antibodies in serum and cerebrospinal fluid, as well as antigens in the central nervous system. Since most of these studies focused on herpes viruses, only these viruses and their role in schizophrenia will be discussed in more detail.

Herpes viruses in schizophrenia

Herpes viruses are a family of DNA viruses, of which 8 types are known to infect humans. These include the herpes simplex virus type-1 (HSV-1), herpes simplex virus type-2 (HSV-2), Varicella-Zoster virus (VZV), Epstein Barr virus (EBV), cytomegalovirus (CMV) and the human herpes viruses 6, 7 and 8 (HHV 6-8). Herpes viruses are large, enveloped viruses that contain double-stranded DNA, surrounded by an icosadeltahedral capsid [15] (figure 1). The viral envelope contains many glycoproteins that are used for viral attachment, fusion and for escaping immune control. The replication of herpes viruses is initiated when viral glycoproteins interact with cell surface receptors. Following interaction, the capsid is released into the cell and delivers the DNA into the nucleus, where it is transcribed and replicated. Transcription of herpes viruses is regulated by both viral and cellular nuclear factors, which determine whether the infection is lytic, persistent or latent. The ability of herpes viruses to establish latency in the human body makes them attractive candidates for a role in schizophrenia. Primary infection with the majority of the herpes viruses mainly occurs during childhood, without the appearance of clinical symptoms. Periodical reactivation of the viruses later in life could explain the episodes of positive symptoms (psychosis) that schizophrenic patients experience.

Evidence for the role of viruses in schizophrenia can be obtained by measuring viral antibodies in serum and cerebrospinal fluid in schizophrenic patients. Over twenty

studies investigated antibodies against several herpes viruses, but were inconclusive, since both negative and positive associations between schizophrenia and herpes viruses were found (reviewed in [9]). A more direct approach is to study the viral presence in the schizophrenic brain. However, studies on the herpes virus genome in the post-mortem schizophrenic patient predominately showed negative results [9,16]. In one study it has clearly been shown that HSV-1 is present in the schizophrenic brain, but this was not found to be different in comparison with healthy controls. The problem, however, with post-mortem brain research is that the virus could have been present in brain areas that were not tested, that the viral genome cannot be detected by the techniques used or that the virus is latently present at the time of death.

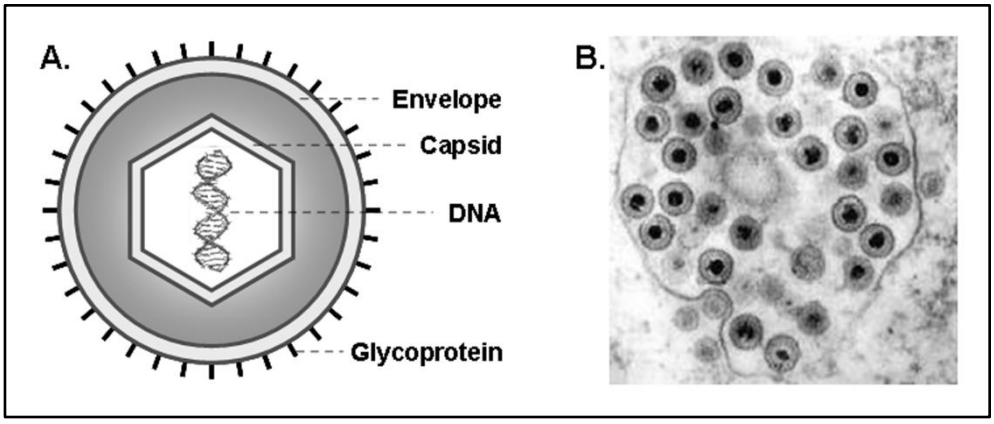

Figure 1 Herpes viruses. **A.** Structure of the herpes virion. **B.** Thin section of virions as they leave the nucleus of an infected cell (magnification of approximately 40.000x); micrograph from F. A. Murphy, School of Veterinary Medicine, University of California, Davis, USA.

More convincing evidence for the role of herpes viruses is provided by studies which showed associations between serum antibodies against herpes viruses and brain abnormalities or disturbances. In MRI studies, it was found that schizophrenic patients that were seropositive for HSV-1 had increased cortical atrophy when compared to seronegative patients [17], and that HSV-1 seropositive first-episode schizophrenic patients had a significant reduction in prefrontal grey matter volume, when compared to seropositive healthy controls and seronegative first-episode schizophrenic patients [18]. In addition, it has been shown that HSV-1 seropositive schizophrenic patients had a lower cognitive functioning than seronegative patients, as

measured by the neuropsychological status of the patients [19]. Seropositivity for other herpes virus, including HSV-2, CMV, EBV and VZV, was not associated with cognitive functioning. In contrast, it was shown by Shirts *et al.* [20] that not only schizophrenic patients that were seropositive for HSV-1, but also CMV seropositive patients showed impaired cognitive function, when compared to seronegative patients, as measured by visual conceptual and visuo-motor tracking. When it was investigated if the anti-herpes virus drug valacyclovir could reduce symptoms in schizophrenic patients, a significant improvement in the total score on the PANNS was found, in CMV seropositive patients [21]. Improvement was not found in patients that were seropositive for other herpes viruses. Taken together, these studies suggest that herpes viruses in schizophrenic patients could, in part, be responsible for the found brain abnormalities, deficits in cognitive functioning and symptoms.

There is thus evidence suggesting that herpes viruses are involved in schizophrenia, however, additional research is necessary to further unravel the role of herpes virus in (the etiology of) schizophrenia. Although herpes viruses may be involved in schizophrenia, a possible involvement of immune mechanisms in schizophrenia has, in addition, been proposed.

Immune mechanisms and neuroinflammation in schizophrenia

The immune system functions as a defense of the body against infectious agents, to prevent disease development. There are two components of the immune system, being the innate and adaptive immune systems. The innate immune system provides an immediate but non-specific response, involving macrophages, granulocytes and natural killer cells. A stronger immune response is provided by the adaptive immune system, characterized by B- and T-lymphocytes, and has an immunological memory. Important signaling molecules for both the innate and adaptive immune systems are cytokines, which can have anti-inflammatory or pro-inflammatory properties. Mainly based on the cytokines expressed, the T-helper lymphocytes are classified into type-1 and type-2, which work together in the immune response. Schizophrenia has been associated with an increase of cytokines in serum and cerebrospinal fluid [22], suggesting the presence of an inflammatory process. In addition, it has been proposed that an imbalance between the type-1 and type-2 immune response is involved in schizophrenia [23]. This imbalance is suggested to indirectly affect dopaminergic and glutamatergic neurotransmission.

In the brain, the innate immune system is represented by microglia cells, which provide the first line of defense against infectious agents or injury, resulting in neuroinflammation. Microglia cells are thought to be derived from monocytes in bone marrow [24]. In the healthy adult brain, microglia cells have a ramified morphology, characterized by a small body with long processes that are continuously used to survey the microenvironment. The morphology of the microglia cells changes into a reactive and amoeboid form when the brain is infected or injured, in response to signals from damaged neurons. Transformation of resting into activated microglia cells is a rapid process and can be divided into two stages. The first stage is characterized by non-phagocytic activated microglia cells, while in the second stage the microglia cells become phagocytic brain macrophages [25]. Activated microglia can express a variety of neurotrophic, anti-inflammatory molecules as well as neurotoxic, pro-inflammatory molecules, such as cytokines, depending on the stage of activation. It remains to be elucidated which factors determine if microglia cells express neurotrophic or neurotoxic molecules, but it has been proposed that in response to acute injury, the microglia cells express neurotrophic molecules, whereas neurotoxic molecules are expressed in chronic disease [26]. Although microglia cells play an important role in neuroinflammation, they do not act alone. Astrocytes are also activated in response to brain injury. The molecules expressed by the activated microglia cells and astrocytes recruit T-lymphocytes and macrophages from the periphery, which are also important for the neuroinflammatory process.

Neuroinflammation was found to be a feature of many neurological disorders, such as Parkinson's disease, Alzheimer's disease, multiple sclerosis and viral encephalitis, as measured in the post-mortem brain and by non-invasive imaging techniques. In addition, neuroinflammation was also implicated in schizophrenia. Studies that were performed to determine if neuroinflammation was present in the schizophrenic brain have mainly been focused on the detection of microglia cells in the postmortem brain. These studies gave conflicting results, since some studies report an increase in the presence of activated microglia cells in the schizophrenic brain [27,28], when compared to the healthy brain, while others could not find such an increase [29,30]. The discrepancy could be due to a variety of factors, like the methods used, the selection of brain areas and the type of schizophrenic patients that were studied. Related to the type of studied schizophrenic patients, it has been shown that activated microglia cells were only found to be present in the brain of schizophrenic patients that committed suicide during acute psychosis [31].

In addition to the postmortem studies, an increased activation of microglia cells in recent-onset schizophrenic patients has been shown by positron emission tomography (PET) imaging [32] with [^{11}C]-PK11195. Logically, the main advantage of PET is that the presence of activated microglia cells can be studied in living schizophrenic patients, at all stages of disease.

Positron emission tomography

Positron emission tomography (PET) is a non-invasive imaging technique used to study functional processes in the body. The principle of PET is based on the coincidence detection of two gamma rays emitted by radioactive isotopes, which are attached to a particular biologically active molecule (figure 2).

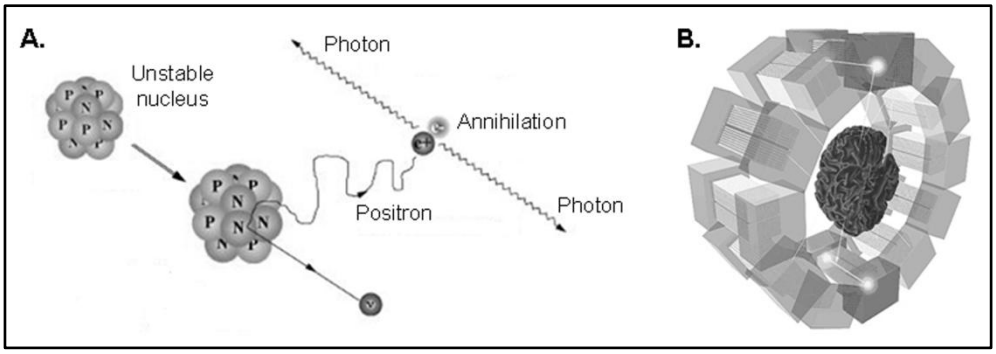

Figure 2 The principle of positron emission tomography. **A.** Positron emission by an unstable nucleus, followed by annihilation with an electron. Annihilation results in two photons that travel in opposite direction. Adapted from: http://depts.washington.edu/nucmed/IRL/pet_intro/intro_src/section2.html. **B.** Coincidence detection of photons by the detectors in the PET camera. From: http://neurocenter.unige.ch/groups/zaidi.php.

The radioactive isotopes used for PET are positron emitters. Positron emitters are isotopes that have an unstable nucleus, which decays by the conversion of a proton into a neutron, during which a positron is emitted. A positron has the same mass as an electron, but has a positive charge instead of the negative charge of electrons and is thus the antiparticle of an electron. Because of the abundance of electrons, the emitted positron will soon meet with an electron. When a positron has lost most of its kinetic energy and meets an electron, they annihilate and the total mass of both particles is

converted into energy according to Einstein's formula $E=mc^2$. The energy is emitted as a pair of photons of 511 keV each, that travel in opposite direction from the site of annihilation.

Most radioactive isotopes that are used in PET are produced by a cyclotron. In the cyclotron, a proton or deuteron beam is accelerated within a magnetic field to gain enough energy before it is ejected to target molecules. When the proton hits the nucleus of the target atom, radioactive isotopes are formed. Depending on which target atom used, different isotopes can be produced. Historically, the most commonly used isotopes for PET are ^{15}O, ^{13}N, ^{11}C and ^{18}F. The half-life of these isotopes, i.e. the time in which half of the radioactivity decays, are 2 min, 10 min, 20 min and 110 min, respectively. Nowadays, other isotopes are applied as well, such as ^{68}Ga, ^{82}Rb, ^{89}Zr, ^{124}I and ^{64}Cu. The radioactive isotope is used for chemical synthesis of the radiotracer. The radiotracer is then the biologically active molecule of interest, for studying a particular process in the body, labeled with a radioactive isotope.

After the radiotracer is injected, it will take part in the biological process of interest and the decay of the radioactivity can be imaged by a PET camera. The PET camera consists of a ring of detectors that can detect the two photons by coincidence detection. Only when two photons are detected within a short time-window by detectors that are approximately at opposite positions, they are considered to be coincident. All coincidence detections are assigned to a line of response, enabling calculation of the position of annihilations. All the annihilations together are used to create a 3D image in which the functional process is visualized. The images can be used for visual examination of, for example, abnormalities or for quantification of the functional process by use of pharmacokinetic models. Because PET is an attractive technique for studying functional processes within the body, it is widely used for both clinical and research purposes, of which the latter also involves animal studies using dedicated small animal PET cameras.

Aim and outline of the thesis

Driven by the viral hypothesis of schizophrenia, the aim was to further study the role of herpes viruses in schizophrenia. Therefore, three different goals were postulated:

1. To study the behavioral and functional consequences of herpes virus infections in rats;
2. To determine if neuroinflammation is present in the brain of schizophrenic patients;
3. To determine if active herpes viruses could be detected in the schizophrenic brain.

The major tool that was used to achieve these goals was PET, since this technique can be used to non-invasively study functional processes in the brain.

Chapter 2 to chapter 5 describe the validation of PET as a tool for imaging of neuroinflammation and active herpes viruses in the brain. *Chapter 2* reviews the use of PET for imaging of neuroinflammation, with a particular focus on the peripheral benzodiazepine receptors as the target for disease and therapy monitoring. In *chapter 3* it was evaluated if PET could be used to study neuroinflammation and active herpes viruses in the rat brain, with [^{11}C]-PK11195 and [^{18}F]-FHBG, respectively. *Chapter 4* and *chapter 5* describe the evaluation of three potential new PET tracers for imaging of neuroinflammation in rats, since the only PET tracer validated for clinical studies, [^{11}C]-PK11195, may not be sensitive enough to visualize mild neuroinflammation.

In chapter 6 to chapter 8, the behavioral and functional consequences of herpes virus infection of the rat brain were described. *Chapter 6* describes the possible link between herpes virus infection, neuroinflammation and neurotransmitters. Antipsychotic treatment in herpes virus infected rats was evaluated in *chapter 7*. In *chapter 8* the possible link between herpes virus induced neuroinflammation and treatment resistance in schizophrenia was studied.

The human PET studies are described in chapter 9 to chapter 11. In *chapter 9* it was studied if neuroinflammation was present in schizophrenic patients and in *chapter 10* it was determined if active herpes viruses could be detected in the schizophrenic brain. In *chapter 11* the role of PET in unraveling the role of herpes viruses in schizophrenia was discussed.

In the final chapters the thesis is summarized in *chapter 12* and *chapter* 13 describes the future perspectives, with concluding remarks. A Dutch version of the summary is provided in *chapter 14*.

References

1 Kraeplin, E. and Barclay, R. M. Dementia praecox and paraphrenia. Edinburgh: E and S Livingstone, 1919

2 Bleuler, E. Dementia praecox or the group of schizophrenias. New York: International Universities Press, 1911

3 World Health Organization. Neurological disorders; public health challenges.: WHO, 2006

4 Lewis DA, Lieberman JA. Catching up on schizophrenia: natural history and neurobiology. Neuron 2000; 28:325-334

5 Davatzikos C, Shen D, Gur RC, et al. Whole-brain morphometric study of schizophrenia revealing a spatially complex set of focal abnormalities. Arch.Gen.Psychiatry 2005; 62:1218-1227

6 Benes FM. Emerging principles of altered neural circuitry in schizophrenia. Brain Res.Brain Res.Rev. 2000; 31:251-269

7 Kyriakopoulos M, Bargiotas T, Barker GJ, Frangou S. Diffusion tensor imaging in schizophrenia. Eur.Psychiatry 2008; 23:255-273

8 Lisman JE, Coyle JT, Green RW, et al. Circuit-based framework for understanding neurotransmitter and risk gene interactions in schizophrenia. Trends Neurosci. 2008; 31:234-242

9 Yolken RH, Torrey EF. Viruses, schizophrenia, and bipolar disorder. Clin.Microbiol.Rev. 1995; 8:131-145

10 Torrey EF, Torrey BB, Peterson MR. Seasonality of schizophrenic births in the United States. Arch.Gen.Psychiatry 1977; 34:1065-1070

11 Torrey EF, Bowler AE, Rawlings R, Terrazas A. Seasonality of schizophrenia and stillbirths. Schizophr.Bull. 1993; 19:557-562

12 Torrey EF, Rawlings R, Waldman IN. Schizophrenic births and viral diseases in two states. Schizophr.Res. 1988; 1:73-77

13 Mednick SA, Machon RA, Huttunen MO, Bonett D. Adult schizophrenia following prenatal exposure to an influenza epidemic. Arch.Gen.Psychiatry 1988; 45:189-192

14 Dalman C, Allebeck P, Gunnell D, et al. Infections in the CNS during childhood and the risk of subsequent psychotic illness: a cohort study of more than one million Swedish subjects. Am.J.Psychiatry 2008; 165:59-65

15 Murray, P. K., Rosenthal, K. S., Kobayasi, G. S., and Pfaller, M. A. Medical Microbiology. St. Louis: C.V. Mosby, 2002

16 Stevens JR, Langloss JM, Albrecht P, Yolken R, Wang YN. A search for cytomegalovirus and herpes viral antigen in brains of schizophrenic patients. Arch.Gen.Psychiatry 1984; 41:795-801

17 Pandurangi AK, Pelonero AL, Nadel L, Calabrese VP. Brain structure changes in schizophrenics with high serum titers of antibodies to herpes virus. Schizophr.Res. 1994; 11:245-250

18 Prasad KM, Shirts BH, Yolken RH, Keshavan MS, Nimgaonkar VL. Brain morphological changes associated with exposure to HSV1 in first-episode schizophrenia. Mol.Psychiatry 2007; 12:105-113

19 Dickerson FB, Boronow JJ, Stallings C, Origoni AE, Ruslanova I, Yolken RH. Association of serum antibodies to herpes simplex virus 1 with cognitive deficits in individuals with schizophrenia. Arch.Gen.Psychiatry 2003; 60:466-472

20 Shirts BH, Prasad KM, Pogue-Geile MF, Dickerson F, Yolken R, Nimgaonkar VL. Antibodies to cytomegalovirus and Herpes Simplex Virus 1 associated with cognitive function in schizophrenia. Schizophr.Res. 2008; 106:268-274

21 Dickerson FB, Boronow JJ, Stallings CR, Origoni AE, Yolken RH. Reduction of symptoms by valacyclovir in cytomegalovirus-seropositive individuals with schizophrenia. Am.J.Psychiatry 2003; 160:2234-2236

22 Potvin S, Stip E, Sepehry AA, Gendron A, Bah R, Kouassi E. Inflammatory cytokine alterations in schizophrenia: a systematic quantitative review. Biol.Psychiatry 2008; 63:801-808

23 Muller N, Schwarz MJ. A psychoneuroimmunological perspective to Emil Kraepelins dichotomy: schizophrenia and major depression as inflammatory CNS disorders. Eur.Arch.Psychiatry Clin.Neurosci. 2008; 258:97-106

24 Ferrer I, Bernet E, Soriano E, del RT, Fonseca M. Naturally occurring cell death in the cerebral cortex of the rat and removal of dead cells by transitory phagocytes. Neuroscience 1990; 39:451-458

25 Kreutzberg GW. Microglia: a sensor for pathological events in the CNS. Trends Neurosci. 1996; 19:312-318

26 Nakajima K, Kohsaka S. Microglia: neuroprotective and neurotrophic cells in the central nervous system. Curr.Drug Targets Cardiovasc.Haematol.Disord. 2004; 4:65-84

27 Bayer TA, Buslei R, Havas L, Falkai P. Evidence for activation of microglia in patients with psychiatric illnesses. Neurosci.Lett. 1999; 271:126-128

28 Radewicz K, Garey LJ, Gentleman SM, Reynolds R. Increase in HLA-DR immunoreactive microglia in frontal and temporal cortex of chronic schizophrenics. J.Neuropathol.Exp.Neurol. 2000; 59:137-150

29 Steiner J, Mawrin C, Ziegeler A, et al. Distribution of HLA-DR-positive microglia in schizophrenia reflects impaired cerebral lateralization. Acta Neuropathol. 2006; 112:305-316

30 Wierzba-Bobrowicz T, Lewandowska E, Lechowicz W, Stepien T, Pasennik E. Quantitative analysis of activated microglia, ramified and damage of processes in the frontal and temporal lobes of chronic schizophrenics. Folia Neuropathol. 2005; 43:81-89

31 Steiner J, Bielau H, Brisch R, et al. Immunological aspects in the neurobiology of suicide: elevated microglial density in schizophrenia and depression is associated with suicide. J.Psychiatr.Res. 2008; 42:151-157

32 van Berckel BN, Bossong MG, Boellaard R, et al. Microglia Activation in Recent-Onset Schizophrenia: A Quantitative (R)-[(11)C]PK11195 Positron Emission Tomography Study. Biol.Psychiatry 2008; 64:820-822

Chapter 2

PET imaging of the peripheral benzodiazepine receptor: monitoring disease progress and therapy response in neurodegenerative disorders

Janine Doorduin, Erik F.J. de Vries, Rudi A. Dierckx and Hans C. Klein

Curr Pharm Design 2008; 14: 3297-3315

Abstract

It is important to gain more insight into neurodegenerative diseases, because these debilitating diseases cannot be cured. A common characteristic of many neurological diseases is neuroinflammation, which is accompanied by the presence of activated microglia cells. In activated microglia cells, an increase in the expression of peripheral benzodiazepine receptors (PBR) can be found. The PBR was suggested as a target for monitoring disease progression and therapy efficacy with positron emission tomography (PET). The PET tracer [^{11}C]-PK11195 has been widely used for PBR imaging, but the tracer has a high lipophilicity and high non-specific binding which makes it difficult to quantify uptake. Therefore, efforts are being made to develop more sensitive radioligands for the PBR. Animal studies have yielded several promising new tracers for PBR imaging, such as [^{11}C]DAA1106, [^{18}F]FEDAA1106, [^{11}C]PBR28, [^{11}C]DPA713 and [^{11}C]CLINME. However, the potential of these new PBR ligands is still under investigation and as a consequence [^{11}C]PK11195 is used so far to image activated microglia cells in neurological disorders. With [^{11}C]PK11195, distinct neuroinflammation was detected in multiple sclerosis, Parkinson's disease, encephalitis and other neurological diseases. Because neuroinflammation plays a central role in the progression of neurodegenerative diseases, anti-inflammatory drugs have been investigated for therapeutic intervention. Especially minocycline and cyclooxygenase inhibitors have shown in vivo anti-inflammatory, hence neuroprotective properties, that could be detected by PET imaging of the PBR with [^{11}C]PK11195. The imaging studies published so far showed that the PBR can be an important target for monitoring disease progression, therapy response and determining the optimal drug dose.

Introduction

Neurological disorders are often debilitating diseases, in which the symptoms can be treated, but the disease cannot be cured. It is therefore of importance to gain more insight in the aetiology of the disease in order to develop better - or perhaps even curative - treatment. The hallmarks and symptoms of various neurological disorders generally differ distinctly, but there may also be some overlap. Alzheimer's disease, for example, is a progressive neurological disease that is characterised by amyloid plaques and neurofibrillary tangles that are formed after misfolding and aggregation of proteins, respectively. Clinical signs are behavioural and psychological symptoms of dementia (BPSD). On the other hand, Parkinson's disease is also a progressive neurodegenerative disease, which is, associated by the loss of dopamine-producing cells in the central nervous system and characterised by tremor, rigidity and bradykinesia. In contrast, encephalitis is an acute infection of the brain caused by, for example, viruses or bacteria that is characterised by fever, psychiatric symptoms like hallucinations and personality changes, and coma. Despite the large differences between the aforementioned neurological diseases, but also other neurological diseases, all share an important characteristic: neuroinflammation. Neuroinflammation was found to play a role in many neurological disorders. In Alzheimer's disease, the presence of the amyloid β (Aβ) fibrils, which form the amyloid plaques, can induce a local inflammatory response [1]. In Parkinson's disease, the degeneration of dopaminergic neurons by, for example, environmental factors or genetic mutations can induce neuroinflammation that might be responsible for further degeneration of the neurons [2]. Moreover, it has been shown that patients with Alzheimer's and Parkinson's disease may benefit from treatment with non-steroidal anti-inflammatory drugs (NSAIDs) [3,4].

Although it has been shown that neuroinflammation has a role in neurological diseases, the question remains whether neuroinflammation precedes the pathology or that it is a secondary response. Moreover, it is not yet known whether the neuroinflammation is beneficial, detrimental or incidental in the progression of neurological disorders. This review focuses on an important characteristic of neuroinflammation: the PBR. During neuroinflammation, the activation of microglia cells and the accompanied increased expression of the peripheral benzodiazepine receptor (PBR) play a central role. The PBR is widely used as target for nuclear imaging of neuroinflammation and is therefore an ideal target for monitoring the course of the disease and the effect of treatment.

Neuroinflammation

It has long been thought that the brain was an 'immune privileged organ' since it was shown that allografts fare better in the brain [5]. This 'immune privilege' was attributed to the presence of the blood-brain barrier and the lack of classic lymph vessels in the brain. However, during the last 10-15 years data has been accumulated that showed that acute and innate responses do exist in the brain, although they are different from the responses in the periphery, and the term neuroinflammation was introduced.

Neuroinflammation refers to the idea that responses and actions of microglia cells and astrocytes in the brain have an inflammation-like character which plays a role in many neurodegenerative diseases and involves many complex cellular responses. To discuss these complex responses is beyond the scope of this review, but the next paragraph provides a brief overview of the cells involved in neuroinflammation.

In response to injury to the brain, both the cells that are present in the brain and cells that are recruited from the periphery participate in the immune response [6]. In the brain, the first line of defence comprises the activation of microglia cells and astrocytes. Activated microglia cells and astrocytes produce a variety of cytokines and chemokines that are, amongst others, important in the recruitment of T-lymphocytes from the periphery. Perivascular macrophages also play an important role in neuroinflammation, since they continuously enter the brain and may return to the lymphoid organs [7]. They are able to activate microglia cell and function as antigen presenting cell for T-lymphocytes. Next to the peripheral macrophages, activated microglia cells and astrocytes can also function as antigen presenting cells, since they were found to express the major histocompatibility complex (MHC) class II [8]. Neurons in the brain are less important in the immune response, but they were found to express cytokines and also MHC class I so they function as antigen presenting cells[9].

The recruitment of T-lymphocytes from the periphery involves the presence of the appropriate cytokines, chemokines and cell adhesion molecules (CAM) [10]. Different expression of the aforementioned proteins allows recruitment of different T-lymphocytes and therefore eliciting the recruitment of specific T-lymphocytes. CAMs are important for the entry of T-lymphocytes into the brain and, as for cytokines and chemokines, different sets of CAM mediate the entry of different types of T-lymphocytes. When T-lymphocytes entered the brain, they can recognize the antigens

that are presented by the antigen presenting cells and in response to recognition, they can secrete cytokines that make the inflammatory process persist. These cytokines can damage the blood-brain barrier and thereby allow the entry of others cells like B-lymphocytes, natural killer cells and mast cells. Microglia play a central role in orchestrating the activity of other immune cells in the brain and the activated state of microglia is associated with expression of a receptor that is the subject of tracer binding studies with PET monitoring. Thus, although many cells play an important role in neuroinflammation, the activation of microglia cells provide an ideal target for monitoring the course of diseases involving neuroinflammation and the effect of treatment.

Microglia cells

Microglia cells are the largest population of macrophages in the brain and are responsible for the first response to injury or infection in brain tissue. The leading hypothesis is that microglia cells are derived from monocytes in bone marrow, and migrate to the brain in early development to phagocytose cellular debris from naturally occurring cell death during embryonic and postnatal stages of development [11] and to eliminate specific axonal projections [12]. In the adult brain, microglia cells have a ramified morphology, which is characterized by a small body with long processes that are used to survey the microenvironment of the microglia. Although the ramified morphology is often referred to as the 'resting state' of microglia cells, it was recently shown that the ramified processes are highly motile and are continuously extracted and retracted [13,14]. In response to brain injury or infection, the microglia cells change from the ramified morphology in a reactive or amoeboid form. In this form, the microglia cells function as macrophages. An inflammatory response is induced and the number of activated microglia cells strongly increase at the affected site. Once activated, the microglia cells can produce neurotoxic molecules, like reactive oxygen species and cytokines such as TNFα and IL-1β, and thereby increasing the incidence of neuronal cell death [15]. On the other hand, activated microglia cells can also release neurotrophic molecules, like brain derived neurotropic factor (BDNF), nerve growth factor (NGF) and cytokines of the IL-6 family, which have a protective effect on brain cells [16]. It still remains to be elucidated which factors determine if microglia cells exert neurotoxic and/or neurotropic effects and which mechanisms are involved in this process. Nevertheless, various studies have shown that activation of microglia cells is not an all-or-none phenomenon and that several states of activation exist.

These activation states depend on the activation environment, the cell type that causes the activation and the activating molecule [16]. The dual character of microglia cells was clearly demonstrated *in vitro* by treatment of NSC-34 neurons with lipopolysaccharide (LPS) stimulated BV-2 microglial conditioned medium [17]. When the neurons were treated with low concentrations of the medium, the viability of the neurons increased, whereas treatment with high concentrations of the medium resulted in a reduction of the viability and apoptosis. This may (in part) be explained by the differential upregulation of the expression of the cytokines IL-6, TNFα or IL-1β by the microglia after LPS stimulation. Another recent study demonstrated that microglia cells also behave differently when cortical neuronal cultures were exposed to mild, moderate or severe hypoxia [18]. Neurotrophic factors (BDNF and GDNF) were found to be equally upregulated by microglia cells in response to media from neurons, irrespective of the severity of the hypoxia, while neurotoxic factors (TNFα , IL-1β and NO) were only upregulated by medium from moderately injured neurons. This difference in the states of microglia activation may be an important feature in neurological disorders associated with microglia cell activation. It has been proposed by Nakajima and Kohsaka [16] that acute injuries such as trauma and axotomy go through a transient process characterized by release of neurotrophic factors from activated microglia cells resulting in repair en regeneration of neurons. On the other hand, chronic diseases such as Alzheimer's disease and multiple sclerosis display a more complex response that leads to neuronal cell death as a result of microglia cells that release neurotoxic molecules.

The peripheral benzodiazepine receptor

Besides the release of neurotoxic and neuroprotective molecules, activation of microglia cells is also accompanied by an increase in the number of mitochondria per cell and by an increase in the density of the PBR in the mitochondrial membrane. The PBR was first discovered by researchers, who were searching for binding sites of the benzodiazepine diazepam in peripheral tissue [19,20]. Because these diazepam binding sites were found outside the brain, they were named 'peripheral' benzodiazepine receptors, in order to distinguish them from the central benzodiazepine receptor, which is a part of the $GABA_A$ receptor complex. In peripheral tissue, the highest level of PBR is found in the adrenals, kidney, lung, heart and hormone secreting tissue [21,22]. Although the PBR was first discovered in peripheral tissue, it was later found that the PBR is also expressed in glia cells in the brain.

The PBR, also often named the peripheral benzodiazepine binding site (PBBS), is a heteromeric complex found in the outer mitochondrial membrane that consists of at least three different subunits, including the isoquinolone binding protein of 18 kDa, a voltage-dependent anion channel of 32 kDa and an adenine nucleotide carrier of 30 kDa. The minimal functional unit (the binding site) of the heteromeric complex is the 18 kDa protein and it was recently suggested to rename the 18 kDa protein part of the PBR into translocator protein (TSPO), because it is predominately localized in mitochondria, its importance does not depend only on ligand binding but also to the subsequent effects of binding and because transport is the main function [23].

It is not exactly known what the endogenous ligands of the PBR are, however a few candidates have been proposed, such as the diazepam-binding inhibitor (DBI) and porphyrins [21]. The PBR is thought to be involved in numerous functions, of which its role in steroidogenesis [24] and mitochondrial functioning [25] are probably the best characterized. The role of the PBR in mitochondrial functioning consists of the PBR being a sensor for cellular oxygen, mediating protective effects for neurons against damage caused by reactive oxygen species (ROS) and regulating the function of the mitochondrial permeability transition pore in response to apoptose triggering signals [25]. These functions of the PBR may be important in controling neuronal damage and they can therefore be the reason for upregulation of the PBR in activated microglia cells.

The PBR may also play an important role in nerve regeneration via steroidogenesis. The steroidogenesis in begins with the conversion of cholesterol to pregnenolone, which is catalyzed by the enzyme P-450_{scc} that is located on the matrix side of the inner mitochondrial membrane. Pregnenolone is then metabolized into neurosteroids, such as androgens, estrogens, glucocorticoids and mineralocorticoids. To form pregnenolone, cholesterol has to be transported from its cellular stores across the mitochondrial membrane and the PBR was suggested to play a major role in this transport process [21]. It was shown that both freeze injury of a peripheral sensory nerve (reversible damage) and nerve transection (permanent damage) increased the density of PBR and the levels of its endogenous ligand octadecaneuropeptide (ODN; a cleavage product of DBI) [26]. After regeneration of the freeze lesioned nerve the PBR density and the ODN levels decreased, whereas it remained elevated in nerve transaction. In addition, it was shown that the PBR agonist Ro5-4864 increased the local levels of pregnenolone in the nerve. The increased level of pregnenolone may be important for nerve regeneration, since it has been shown that steroids possess

neurotrophic activity [27]. Furthermore, the increased number of PBR enabling increased transport of cholesterol may be needed for biogenesis of the inner mitochondrial membrane, which may be required for mitochondrial biogenesis to support the accelerated microglia cell proliferation [24,28].

PET imaging of neuroinflammation

Because of the inaccessability of the brain, early diagnosis and early therapy reponse monitoring of neurological diseases is difficult and often rely on non-invasive imaging techniques. Nuclear imaging techniques like positron emission tomography (PET) and single photon emission computed tomography (SPECT) offer the unique opportunity to provide biochemical and physiological information on processes that occur in the brain. For both these nuclear imaging techniques, a radioactively labeled tracer molecule that participates in the process of interest is injected in the patient. The distribution of the tracer is recorded with a dedicated scanner and converted in 3-dimensional tomographic images. For imaging of the inflammatory response in the brain, PET seems to be the more attractive tool, as it combines a higher resolution and sensitivity with the ability to quantify the biochemical or physiological parameter of interest using pharmacokinetics models. Therefore, this review will focus on PET imaging only. For PET imaging of neuroinflammation in neurological diseases, the increase in expression of the PBR in activated microglia cells is an attractive target. Several tracers have now been developed that specifically bind with high affinity to the PBR. An important aspect of PBR-based PET imaging of neuroinflammation is the fact that in the brain not only activated microglia cells showed increased expression of PBR Activated astroglia cells and infiltrating macrophages also express PBR. What the relative contributions of activated microglia, activated astroglia cells and infiltrating macrophages to the overall PBR expression level in neuroinflammation, and thus to the imaging signal, is not known. However, Banati *et al.* [29] showed that activated microglia cells are the main source of lesion-induced increase in PBR expression when the blood-brain barrier is intact. More importantly, the PBR is also present in the muscle cells of small- and medium-sized intraparenchymal arteries, in leptomeningeal arteries, in perivascular macrophages, in lymphocytes and neutrophils, in the choroids plexus and in the ependyma [30]. Specific binding of the PET tracers to the PBR in these regions is likely to cause a low background binding of the PET tracers and should be taken into account.

PET tracers for PBR imaging

[^{11}C]PK11195

[^{11}C]PK11195 is not only one of the first used PET tracer for PBR imaging, but until a few years ago also the only PET tracer that has been applied to image microglia activation in humans. Many studies demonstrate that [^{11}C]PK11195 PET can detect inflammation-induced microglia activation in various neurological and psychiatric diseases. The results of these studies will be discussed in the next sections of this article. Despite the large number of successful [^{11}C]PK11195 PET studies in human disease, [^{11}C]PK11195 exhibits also several distinct limitations, especially for brain imaging. [^{11}C]PK11195 shows high plasma protein binding and relatively poor penetration of the blood-brain barrier, which results in low levels of tracer accumulation in the brain. In addition, the high lipophilicity of [^{11}C]PK11195 causes relatively high levels of non-specific binding and thus poor signal-to-noise ratios. Consequently, mild neuroinflammation is difficult to detect with [^{11}C]PK11195 PET, if at all. Often, visual or semi-quantitative analysis of [^{11}C]PK11195 PET images is insufficient and quantitative analysis by pharmacokinetic modeling is required. This was clearly demonstrated by the first publications on [^{11}C]PK11195 PET imaging in patients with Alzheimer's disease. The first publication reported no increase in brain region-to-cerebellum ratios of tracer accumulation in patients, as compared to healthy volunteers [31]. A few years later, a [^{11}C]PK11195 PET study on Alzheimer patients, in which pharmacokinetic modeling was applied to convert tracer uptake to binding potentials, was published, in which a significant increase in [^{11}C]PK11195 binding potentials in temporal, parietal and posterior cingulate brain regions of Alzheimer patients was demonstrated [32]. Although quantitative analysis of the PET images gives more detailed and sensitive information, it is also more laborious and causes more discomfort to the patient, as generally arterial blood sampling is required due to the absence of a suitable reference brain region that lacks PBR expression. For the aforementioned reasons, the search for novel PET tracers for the PBR with better imaging properties than [^{11}C]PK11195 has been increased enormously in the past decade. Figure 1 shows a compilation of tracers that have been proposed as alternatives for [^{11}C]PK11195. The current status of these alternative PET tracers for the PBR will be briefly discussed below.

[^{11}C]Ro5-4864

[^{11}C]Ro5-4864 (4'-chlorodiazepam) was also among the first PBR ligands to be radiolabeled for PET imaging [33]. Unfortunately, no increased uptake of this tracer could be detected in human gliomas, with a high density of the PBR, when compared to normal brain tissue [34]. In addition, [^{11}C]Ro5-4864 showed much lower in vitro binding to glioma sections than [^{11}C]PK11195. Thus, it can be concluded that [^{11}C]Ro5-4864 is not a good tracer for PET imaging.

[^{18}F]PK14105

[^{18}F]PK14105 is a structural analogue of PK11195 with comparable lipophilicity, selectivity and affinity for the PBR. PK14105 was labeled with fluorine-18 (half-life 110 min) to provide a longer-lived tracer PET that allows distribution of the compound to satellite centers without a cyclotron [35]. In unilateral lesioned rats, [^{18}F]PK14105 displayed specific uptake in the lesioned striatum, but the specific binding decrease more rapidly over time than that of [^{3}H]PK11195 [36], which makes the tracer less attractive for PET imaging.

[^{11}C]VC193M, [^{11}C]VC195, [^{11}C]VC198M and [^{11}C]VC701

[^{11}C]VC193M, [^{11}C]VC195, [^{11}C]VC198M and [^{11}C]VC701 are quinoline-2-carboxamide derivatives with a high affinity for the PBR that have been labeled with carbon-11 [37]. For all these tracers, ex vivo biodistribution studies in healthy rats demonstrated specific binding in several peripheral organs with high PBR expression [37,38]. Only [^{11}C]VC193M, [^{11}C]VC195 and [^{11}C]VC198M were also evaluated in a preclinical disease model and compared with [^{11}C]PK11195. In unilateral lesioned rats, induced by striatal injection of quinolinic acid, the novel tracers did not outperform [^{11}C]PK11195. Lesioned-to-unlesioned striatum uptake ratios were highest for [^{11}C]PK11195, slightly inferior for [^{11}C]VC195 and substantially lower for [^{11}C]VC193M and [^{11}C]VC198M [39]. The absolute uptake of [^{11}C]VC195 in the lesioned striatum was approximately 70% higher than that of [^{11}C]PK11195, but its clearance from plasma and normal brain was much slower. Thus, [^{11}C]VC195 could be a potential candidate for PBR imaging, but the high background levels of the tracer in the brain, may reduce its sensitivity. [^{11}C]VC701 needs to be further evaluated in disease models and compared with an established tracer, before any conclusion can be drawn.

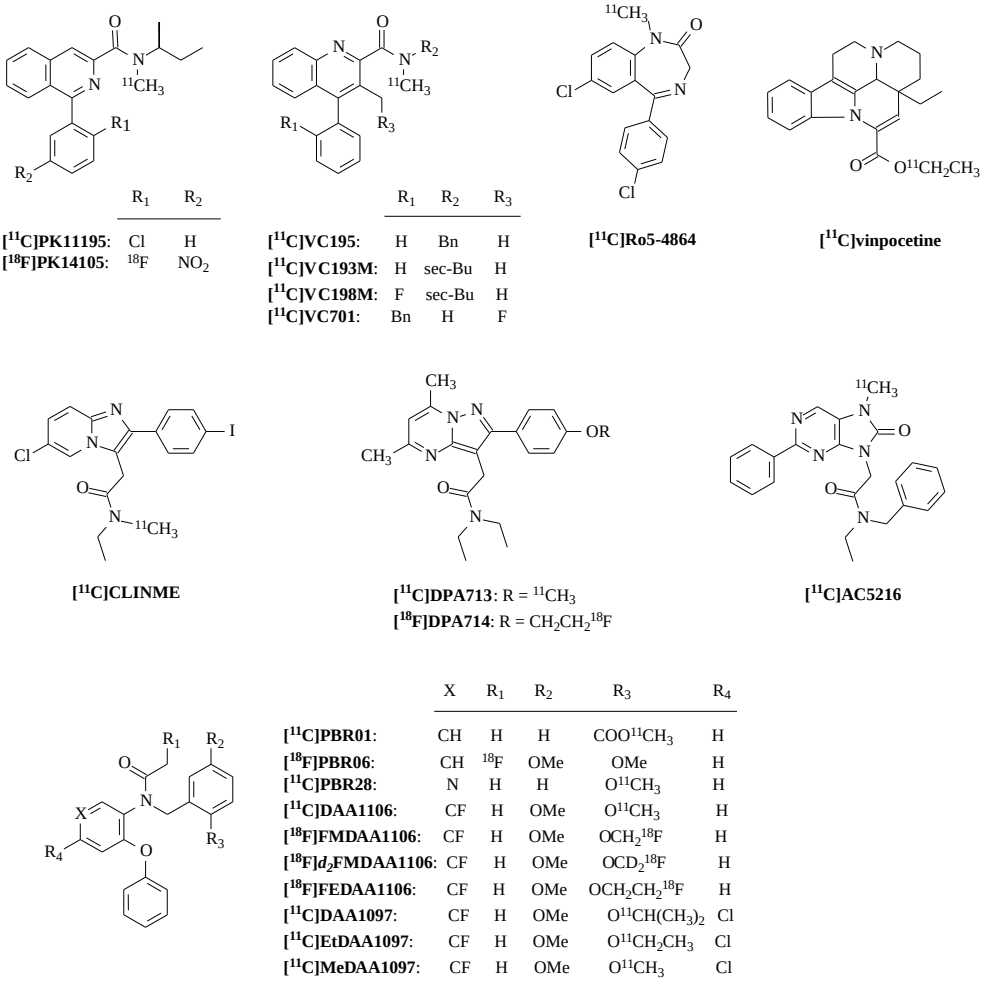

	X	R_1	R_2	R_3	R_4
[^{11}C]PBR01:	CH	H	H	$COO^{11}CH_3$	H
[^{18}F]PBR06:	CH	^{18}F	OMe	OMe	H
[^{11}C]PBR28:	N	H	H	$O^{11}CH_3$	H
[^{11}C]DAA1106:	CF	H	OMe	$O^{11}CH_3$	H
[^{18}F]FMDAA1106:	CF	H	OMe	$OCH_2{}^{18}F$	H
[^{18}F]*d*$_2$FMDAA1106:	CF	H	OMe	$OCD_2{}^{18}F$	H
[^{18}F]FEDAA1106:	CF	H	OMe	$OCH_2CH_2{}^{18}F$	H
[^{11}C]DAA1097:	CF	H	OMe	$O^{11}CH(CH_3)_2$	Cl
[^{11}C]EtDAA1097:	CF	H	OMe	$O^{11}CH_2CH_3$	Cl
[^{11}C]MeDAA1097:	CF	H	OMe	$O^{11}CH_3$	Cl

Figure 1 Chemical structures of various PET tracers for imaging of the peripheral benzodiazepine receptor.

[^{11}C]Vinpocetine

[^{11}C]Vinpocetine is a Vinca minor alkaloid that has been used as a neuroprotective drug in the treatment and prevention of cerebrovascular diseases, such as ischemic stroke. Vinpocetine was found to bind specifically to the PBR and was subsequently investigated as a PET tracer. In cynomolgous monkeys, [^{11}C]vinpocetine showed a

heterogeneous distribution in the brain. Cerebral uptake of [^{11}C]vinpocetine was found to be 5-fold higher than that of [^{11}C]PK11195 [40]. Pretreatment with 3 mg/kg of unlabeled vinpocetine resulted in a 22% reduction of [^{11}C]PK11195 brain uptake. Remarkably, pretreatment with 1 mg/kg of unlabeled PK11195 caused a 36% increase in [^{11}C]vinpocetine brain uptake. The increased brain uptake is caused by displacement of [^{11}C]vinpocetine from the PBR in peripheral tissue like the lung by unlabeled PK11195, leading to an increased delivery of tracer to the brain. Quantitative analysis, however, revealed that the global binding potential of [^{11}C]vinpocetine in the brain was 40% reduced after pretreatment with unlabeled PK11195. Also in human brain, rapid uptake, up to 3.7 % of the injected dose, was observed [41]. In the brain of normal subjects, highest uptake was found in thalamus, as is the case for [^{11}C]PK11195. [^{11}C]vinpocetine is rapidly metabolized in vivo. In human plasma, 25-30% of the radioactivity consists of unchanged tracer at 50 minutes after tracer injection [41]. The main radioactive metabolite of [^{11}C]vinpocetine is [^{11}C]ethanol. Studies in monkeys showed that this metabolite behaves as a flow tracer and most likely does not significantly contribute to the brain radioactivity pattern of [^{11}C]vinpocetine [42]. To evaluate the value of [^{11}C]vinpocetine in human disease, a small pilot study was performed, in which the tracer was compared to [^{11}C]PK11195 in four patients with multiple sclerosis who had their last active period 3 – 17 months before the investigation [43]. In these patients, global and maximum brain uptake of [^{11}C]vinpocetine was approximately 40% higher than that of [^{11}C]PK11195. The apparent [^{11}C]PK11195 binding potential (reference tissue Logan analysis) in and around the lesions was increased in only one patient, whereas the apparent binding potentials of [^{11}C]vinpocetine were increased in all patients. Remarkably, coregistered [^{11}C]vinpocetine and [^{11}C]PK11195 images showed only minimal overlap in peak uptake. These results raise the question whether [^{11}C]vinpocetine and [^{11}C]PK11195 bind to same binding sites after all.

[^{11}C]CLINME

[^{11}C]CLINME (2-[6-chloro-2-(4-iodophenyl)-imidazo[1,2-α]pyridine-3-yl]-N-ethyl-N-methyl-acetamide) is a new PBR ligand that was recently labeled with carbon-11 for PET imaging [44]. The imaging properties of [^{11}C]CLINME were compared to those of [^{11}C]PK11195 in a rat model of local acute neuroinflammation, induced by striatal injection of α-amino-3-hydroxy-5-methylisoxazole-4-propionic acid (AMPA) [45]. Both tracers displayed similar pharmacokinetics in the lesioned striatum, but

[^{11}C]CLINME was significantly faster cleared from the contralateral side, resulting in higher lesioned-to-unlesioned ratios for this new tracer. Pharmacokinetic modeling, using a reference tissue model, revealed that the tracer delivery to the brain was similar for [^{11}C]CLINME and [^{11}C]PK11195, but the apparent binding potential of [^{11}C]CLINME (1.07 ± 0.30) in the lesioned brain was approximately 60% higher than that of [^{11}C]PK11195 (0.66 ± 0.15). However, one should keep in mind that these apparent binding potentials do not purely represent binding in the lesioned striatum, but are also affected by binding in the reference tissue, the contralateral striatum, which contains PBR as well [46]. Metabolite analysis revealed that the in vivo stability of [^{11}C]CLINME is fairly high, with 72% of the tracer in plasma still intact 30 minutes after injection and no metabolites in the brain. Taken together, these data indicate that [^{11}C]CLINME could be a good alternative for [^{11}C]PK11195 as PET tracer for PBR imaging, especially because of its faster clearance for normal brain tissue.

[^{11}C]DPA-713

[^{11}C]DPA-713 (N,N-diethyl-2-(2-(4-[^{11}C]methoxyphenyl)-5,7-dimethylpyrazolo(1,5-a)pyrimidin-3-yl)acetamide) is a pyrazolopyrimidine derivative that was recently labeled with carbon-11 [47,48]. This compound was proposed as a PET tracer for the PBR, because DPA713 has a lower lipophilicity, higher selectivity and approximately 2-fold higher affinity for the PBR than PK11195 [47]. [^{11}C]DPA713 showed specific binding in the brain of healthy baboon with slow brain uptake kinetics, which could be favorable for quantitative analysis of PBR binding [47]. [^{11}C]DPA713 was compared to [^{11}C]PK11195 in rats with a unilateral AMPA-induced striatal lesion [49]. Despite slower pharmacokinetics, [^{11}C]DPA713 uptake in the lesioned striatum was comparable to that of [^{11}C]PK11195. However, tracer accumulation in the control striatum was significantly lower for [^{11}C]DPA713 than for [^{11}C]PK11195. The apparent binding potential, determined with a simplified reference tissue model, was 2.4-fold higher for [^{11}C]DPA713 then for [^{11}C]PK11195 (1.57 ± 0.36 vs. 0.66 ± 0.15). Again, the difference in binding potential is partly due to differences in binding in the reference tissue. We have also compared [^{11}C]DPA713 and [^{11}C]PK11195, but in a HSV encephalitis rat model [50]. Although this model is more variable in the intensity of neuroinflammation, results obtained in this model were comparable to those described above. Metabolism of [^{11}C]DPA713 in plasma was acceptable (about 60% intact tracer after 30 min) and no radioactive brain metabolites were found [49]. These results suggest that [^{11}C]DPA713 is a good candidate PET tracer for PBR imaging.

[^{18}F]DPA714

[^{18}F]DPA714 (N,N-diethyl-2-(2-(4-[2-fluoro-1-ethoxy]phenyl)-5,7-dimethylpyrazolo(1,5-a)pyrimidin-3-yl)acetamide), a full agonist of the PBR, was evaluated in unilateral quinolinic acid lesioned rats. Ex vivo biodistribution demonstrated an 8-fold higher uptake of [^{18}F]DPA714 in the lesioned striatum than in control striatum [51]. The uptake in the lesion was reduced to the level of the contralateral striatum by pretreatment with unlabeled PK11195, DPA713 or DPA714. PET studies in baboon showed rapid uptake and retention of the tracer in the brain, which could be blocked by unlabeled PK11195 and displaced by DPA714. We investigated [^{18}F]DPA714 in rats with viral encephalitis that was induced by intranasal inoculation with HSV type 1 (manuscript submitted). In control animals, brain uptake of [^{18}F]DPA714 is much lower than that of [^{11}C]PK11195 and [^{11}C]DPA713, which may be beneficial for detecting mild infection. In the HSV encephalitis model, however, the specific uptake of [^{18}F]DPA714 in inflamed brain regions was substantially lower than that of [^{11}C]PK11195 and [^{11}C]DPA713, which makes [^{18}F]DPA714 less attractive for PBR imaging than the other tracers.

[^{11}C]AC5216

[^{11}C]AC5216 (N-benzyl-N-ethyl-2-(7-methyl-8-oxo-2-phenyl-7,8-dihydro-9H-purin-9-yl)acetamide) is a high affinity, selective PBR ligand (2-fold higher affinity than PK11195) with anti-anxiety and anti-depressant properties [52]. [^{11}C]AC5216 showed specific binding in brain regions with highest PBR density in normal mouse, rat and monkey, as was demonstrated in receptor blocking studies with unlabeled AC-5216 or PK11195 [53,54]. Maximum radioactivity levels of [^{11}C]AC5216 in the monkey brain were 4-6 times higher than those of [^{11}C]PK11195. In vitro en ex-vivo autoradiography studies in rats with unilateral striatal lesions induced by kainic acid infusion demonstrated approximately 3 times higher tracer uptake in the ipsilateral striatum, cerebral cortex and hippocampus, as compared to the contralateral brain regions [53]. In the plasma of monkey and rat, formation of high amounts of a more polar metabolite of [^{11}C]AC5216 was detected. However, this metabolite does hardly penetrate the blood-brain barrier, as no metabolites were found in the brains of mice and rats [53,54]. In vitro and ex vivo autoradiography studies in mice with PBR expressing tumors indicated that the tracer distribution of [^{11}C]AC5216 in the tumor was flow dependent [55]. The flow dependency of [^{11}C]AC5216 accumulation in the brain has not been investigated yet, but if [^{11}C]AC5216 brain uptake would prove to

be flow dependent, quantification of PBR expression will not be possible with this tracer.

[^{11}C]PBR01

[^{11}C]PBR01 (N-acetyl-N-(2-methoxycarbonylbenzyl)-2-phenoxyaniline) and [^{18}F]PBR06 N-fluoroacetyl-N-(2,5dimethoxybenzyl)-2-phenoxyaniline) belong to a class phenoxyanilide derivatives that have been evaluated as PET tracers in healthy rhesus monkeys [56,57]. Both compounds show a high degree of displaceable specific binding in the brain, but also rapid metabolism in plasma. Among these tracers, [^{11}C]PBR01 appears least suitable for PBR imaging. Uptake of [^{11}C]PBR01 in rhesus monkey brain was lower than that of [^{18}F]PBR06 [57] and [^{11}C]PBR28 [56]. In addition, compartment modeling yielded inaccurate estimates of the distribution volumes of [^{11}C]PBR01, probably due to its slow kinetics relative to its short half-life. In contrast, [^{18}F]PBR06 has adequate kinetics for quantitative analysis, which in combination with relatively low non-specific uptake would make this a promising tracer. However, further evaluation of this tracer in disease models has not been published yet.

[^{11}C]PBR28

[^{11}C]PBR28 (N-(2-methoxybenzyl)-N-(4-phenoxypyridin-3-yl)acetamide) is a PBR ligand with a lower lipophilicity than for example PK11195, PBR01 and DAA1106 [56]. [^{11}C]PBR28 showed high brain uptake in monkey brain, which peaked at 40 minutes after tracer injection [58]. Highest uptake was found in the choroid plexus of the 4th ventricle, consistent with known PBR distribution in monkey. [^{11}C]PBR28 brain uptake could be blocked with 3 mg/kg of DAA1106 with >95% of the brain uptake being displaceable binding. In contrast to [^{11}C]PBR01, compartmental modeling could be applied to quantify brain uptake of [^{11}C]PBR28 within 100-110 minutes of data acquisition. This could be could be due to the lower affinity and lipophilicity of [^{11}C]PBR28 as compared to [^{11}C]PBR01 [58]. [^{11}C]PBR28 was rapidly metabolized by N-debenzylation in monkey, with only 4% intact tracer after 30 min. However, in the brain >97% of the radioactivity consisted of the intact tracer [56]. [^{11}C]PBR28 was further evaluated in the permanent middle cerebral artery occlusion model, a rat model for stroke [59]. [^{11}C]PBR28 PET images showed higher tracer uptake in the peri-ischemic core than in either the ischemic core or the contralateral hemisphere. The distribution of [^{11}C]PBR28 uptake correlated well with PBR

expression as demonstrated by in-vitro [^{3}H]PK11195 autoradiography on brain sections of the same animal (r^2 = 0.80). Radiation dosimetry studies indicate that [^{11}C]PBR28 causes an acceptable radiation burden to the patient (6.6 μSv/MBq) [60]. Organs with high PBR density, like lung, spleen and kidney, receive the highest radiation dose. The distribution volume of [^{11}C]PBR28 was approximately 20 times lower in the brain of healthy volunteers than in monkey brain [61]. A substantial fraction of the human volunteers (14%) did not show any PBR binding in the brain or in peripheral organs. Apparently, in these subjects no binding sites for the tracer are available, which might be due to genetic polymorphism of the receptor. It is still unclear whether this lack of specific binding in a small portion of the subjects is specific for [^{11}C]PBR28 or also occurs with other tracers.

[^{11}C]DAA1097

[^{11}C]DAA1097 (N-(4-chloro-2-phenoxyphenyl)-N-(2-isopropoxybenzyl)acetamide) and its ethyl and methyl homologues were labeled with carbon-11 and evaluated with ex vivo autoradiography in rat brain [62]. For all these homologues, highest uptake was observed in the olfactory bulbs and cerebellum, the regions with highest PBR expression. For all tracers, uptake in the olfactory bulbs and cerebellum could be blocked by co-administration with unlabeled DAA1106. In monkey brain, [^{11}C]DAA1097 uptake in the PBR-rich occipital cortex was slightly lower than that of its ethyl and methyl homologues, which is in agreement with the relative binding affinity of the tracers in vitro [62]. However, the level of specific binding of the [^{11}C]DAA1097 homologues in the occipital cortex of the monkey was lower than those of [^{11}C]DAA1106 and [^{18}F]FEDAA1106.

[^{11}C]DAA1106

[^{11}C]DAA1106 (N-(2,5-dimethoxybenzyl)-N-(5-fluoro-2-phenoxyphenyl)acetamide) is a 2-phenoxy-5-fluoroanilide derivative with high affinity and selectivity for the PBR that was radiolabeled with carbon-11 for PET imaging [63,64]. In mice, [^{11}C]DAA1106 rapidly penetrated the blood-brain barrier. Maximum brain uptake was achieved after 30 minutes, with highest uptake in the olfactory bulbs and cerebellum [64]. [^{11}C]DAA1106 was rapidly metabolized by debenzylation (6% of unchanged [^{11}C]DAA1106 in plasma after 60 minutes), but no metabolites were found in the brain. Co-injection of the non-radioactive PBR ligands PK11195 or DAA1106, but not the CBR ligand Ro15-1788, resulted in a strong reduction of tracer uptake in these

brain regions. Similar results were obtain in rat and monkey. Although the areas with highest uptake were different, the results were in accordance to the species differences in the PBR distribution in the brain [65]. Global [^{11}C]DAA1106 brain uptake was 4 times higher than that of [^{11}C]PK11195, which probably reflects the better brain penetration of the former tracer due to its higher lipophilicity. [^{11}C]DAA1106 was also able to detect activation of microglia in several rat models of inflammation. Unilateral injection of kainic acid in the dorsal rat striatum caused a 2-fold increase in [^{11}C]DAA1106 binding in the lesioned hippocampus compared to the contralateral region, as was determined by ex vivo autoradiography [65]. Similar results were found in the controlled cortical impact model of traumatic brain injury [66], unilateral lipopolysaccaride lesioned rats [67] and unilateral 6-hydroxydopamine lesioned rats [67]. Uptake of [^{11}C]DAA1106 was enhanced in areas of brain damage in all these models. In addition, all these studies showed that [^{11}C]DAA1106 uptake in the damaged brain region was higher than that of [^{11}C]PK11195. In rats with neuronal insults that were induced by intrastriatal micro-infusion of ethanol, increased retention of [^{11}C]DAA1106 in the lesion was also observed. The enhanced tracer uptake lasted from day 3 until at least day 90 after injury and coincided with the increase in activated microglia and astrocytes in the affected striatum [68]. Interesting, multi-linear regression indicated that the enhanced [^{11}C]DAA1106 retention predominantly depended on the number of activated microglia, not on the level of activated astrocytes. In humans, the metabolism of [^{11}C]DAA1106 is acceptable, but binding kinetics (especially receptor dissociation) are slow [69]. Highest binding potential (5.54) was found in the thalamus, which is consistent with [^{11}C]PK11195 data. For quantification of [^{11}C]DAA1106 binding, the non-linear least-square method with the two-compartment model was the most reliable method. However, the binding potentials and the distribution volumes estimated by this method did not correlate. So far, no [^{11}C]DAA1106 PET studies in human disease were published.

[^{18}F]FMDAA1106

[^{18}F]FMDAA1106 (N-(5-fluoro-2-phenoxyphenyl)-N-(2-fluoromethyl-5-methoxybenzyl)-acetamide), a fluoro analogue of [^{11}C]DAA1106, was developed as a PET tracer with a longer half-life [70]. However, [^{18}F]FMDAA1106 showed extensive defluorination in vivo and therefore is not useful for PET imaging. To reduce the metabolic rate of the tracer, the deuterium-substituted analogue [^{18}F]d_2FMDAA1106 was developed [71]. The isotope effect should reduce the rate of carbene formation

and thus increase the stability of the compound. In mice, defluorination was indeed reduced, as was evident from the decreased accumulation of radioactivity in bone. In monkey, however, still avid defluorination occurred [71]. Thus, the deuterated analogue of [^{18}F]FMDAA1106 is also not suited as a PET tracer.

[^{18}F]FEDAA1106

[^{18}F]FEDAA1106 (N-(5-fluoro-2-phenoxyphenyl)-N-(2-fluoroethyl-5-methoxybenzyl)-acetamide) is the fluoroethyl homologue of [^{11}C]DAA1106. The distribution of [^{18}F]FEDAA1106 in mouse and monkey brain was consistent with the known distribution of PBR [70]. The uptake of [^{18}F]FEDAA1106 in the occipital cortex of monkeys was 1.5 and 6 times higher than [^{11}C]DAA1106 and [^{11}C]PK11195, respectively. As for most other DAA1106 derivatives, [^{18}F]FEDAA1106 was metabolized by N-debenzylation into a radioactive metabolite that does not cross the blood-brain barrier. No defluorination was observed. [^{18}F]FEDAA1106 was able to detect activated microglia in an ethanol-induced neuronal insult rat model of neuroinflammation. One month after ethanol injection, small animal PET imaging showed increased [^{18}F]FEDAA1106 uptake in the damaged brain region [68]. [^{18}F]FEDAA1106 was also successfully applied to monitor the neuroinflammatory response to treatment in an animal model of Alzheimer's disease [72]. [^{18}F]FEDAA1106 PET could detect substantial neuroinflammation in the hippocampus of amyloid precursor protein transgenic mice after local immunization with an antibody against amyloid β peptide. In contrast, no increased levels of [^{18}F]FEDAA1106 could be seen in the brain upon immunization of wild-type animals that lack amyloid plaques. In healthy human volunteers, [^{18}F]FEDAA1106 rapidly accumulated into the brain, followed by a very slow wash-out [73]. Differences in tracer uptake between different brain regions were small. Brain uptake of [^{18}F]FEDAA1106 was approximately 6 times higher than that of [^{11}C]PK11195. Because of the slow tracer kinetics, quantification by the Logan plot or multi-linear analysis methods resulted in 10-20% underestimation of [^{18}F]FEDAA1106 binding. Non-linear least-square proved the most reliable method for quantification [73].

As follows from the above, several promising PET tracers for the PBR have been developed. A number of these tracers were shown to have more favorable characteristics for PET imaging than [^{11}C]PK11195. Based on animal data, [^{11}C]DAA1106, [^{18}F]FEDAA1106, [^{11}C]PBR28, [^{11}C]DPA713 and [^{11}C]CLINME are among the most promising new tracers for PBR imaging. However, it is impossible to

select the tracer that shows best imaging properties, because the tracers have been evaluated in different manners in various animal models. The use of different animal models to select the best PET tracer is also complicated by the different affinities of the PBR ligands depending on PBR function. The PBR can be involved in apoptosis or steroidogenesis which can be different in the used animal models. The apoptotic sites were found to have a lower affinity for [^{11}C]PK11195 than the steroidogenic sites [74], which makes interpretation of the data complicated. Furthermore, a comparison of the new tracers with the golden standard, [^{11}C]PK11195, is not available for all compounds. Besides [^{11}C]PK11195, only [^{11}C]vinpocetine, [^{11}C]PBR28, [^{11}C]DAA1106 and [^{18}F]FEDAA1106 were used in healthy volunteers, whereas only [^{11}C]vinpocetine was used in patients. The first results in humans indicate that also the new PET tracers are not ideal yet. [^{11}C]vinpocetine distribution in the brain of multiple sclerosis patients did not correlate with that of [^{11}C]PK11195. [^{11}C]PBR28 did not bind to the PBR in a substantial fraction of the volunteers. [^{11}C]DAA1106 and [^{18}F]FEDAA1106 display very slow pharmacokinetics, which hampers quantification. Thus, it can be concluded that more research is required to find and validate a better alternative for [^{11}C]PK11195 as tracer for the PBR imaging.

PET imaging of neuroinflammation in human disease

As follows from the above, many tracers for imaging of PBR expression have been developed and some of them appear to be promising. With one exception, to date all PET imaging studies on neuroinflammation in human disease have been performed with [^{11}C]PK11195 as the tracer (table 1). The following paragraphs will give an overview of the results of human [^{11}C]PK11195 PET imaging studies in various neurological diseases.

Dementia

Alzheimer's disease

The role of neuroinflammation in dementia was first studied in Alzheimer patients with mild to moderate dementia, but no regions with increased [^{11}C]PK11195 were found when compared to healthy volunteers [31]. In contrast to the aforementioned finding, another study on patients with mild to moderate dementia in Alzheimer's disease showed increased regional binding of [^{11}C]PK11195 that correlated with

decreased glucose metabolism in the same regions [32]. MRI scans that were made as follow-up after 12 to 24 months showed the highest rate of atrophy in the regions where high [^{11}C]PK11195 uptake was found. The conflicting results of these studies can be explained by methodological differences between these studies. The first study used racemic [^{11}C]PK11195, while the second study used the (R)-enantiomer of [^{11}C]PK11195 which has a higher affinity for the PBR. In addition, the second study used a 3D-scanning mode and used tracer kinetic modeling with cluster analysis to determine a reliable input function which allows to determine the binding potential of [^{11}C]PK11195. In Alzheimer's disease, the increased binding of [^{11}C]PK11195 can be due to neuroinflammation, resulting either from the presence of amyloid plaques or from the process of neurodegeneration.

Frontotemporal lobar degeneration

Cagnin *et al.* [75] studied patients with frontotemporal lobar degeneration (FTLD). They reported increased binding of [^{11}C]PK11195 in frontotemporal regions, which is different from the increased [^{11}C]PK11195 uptake found in Alzheimer's disease. The [^{11}C]PK11195 uptake in dementia precedes atrophy that can be visualized by MRI, which makes [^{11}C]PK11195 PET an important tool for disease monitoring and follow-up of therapeutic intervention. As already mentioned by Cagnin e*t al.* [76], the presence of activated microglia cells in brain tissue is an indirect measure of the activity of the disease. [^{11}C]PK11195 PET may be useful in determining if the activation of microglia cells as a result of the disease and/or may contribute to monitoring the progress of the disease.

HIV-associated dementia

Dementia is also a common neurological condition associated with HIV (human immunodeficiency virus) infection. HIV infects glial cells in the brain, resulting in the release of cytokines and chemokines that, together with viral neurotoxins, contribute to neuronal damage. In patients with HIV-associated dementia, a significant higher binding of [^{11}C]PK11195 was found in 5 of the 8 studied brain regions as compared to healthy controls, whereas HIV patients without dementia did not show significantly higher [^{11}C]PK11195 binding [77]. While the activation of microglia cells is associated with dementia in HIV patients [^{11}C]PK11195 PET was not able to detect differences between HIV patients with minor neurocognitive impairment and controls [78]. This may be due to insufficient sensitivity of [^{11}C]PK11195 PET to detect mild activation of microglia in minor neurocognitive impairment.

Table 1 Overview of the PET imaging studies on neuroinflammation in human disease performed with [^{11}C]PK11195.

Neurological disease	Areas with increased [^{11}C]PK11195 uptake	Correlation with	Lack of correlation with
Alzheimer's disease	Inferior and middle temporal gyri, fusiform gyri, left parahippocampal gyrus, left mygdala, left posterior cingulate, inferior parietal lobules, putamen, right pallidum [32]	Rate of atrophy and regional glucose hypometabolism [32]	
Frontotemporal lobar degeneration	Left dorsolateral prefrontal cortex, right hippocampus, parahippocampus, putamen [75,76]		
Corticobasal degeneration	Caudate nucleus, frontal lobe, putamen, thalamus, pallidum, substantia nigra, pons in affected hemisphere [79,80]	Decreased glucose metabolism in affected hemisphere [79]	
Huntington's disease	Striatum, caudate, putamen, pallidum, frontal lobe, parietal lobe, occipital lobe, temporal lobe [81,82]	Pre-symptomatic patients: loss of dopamine binding and the 5-year probability of developing Huntington's disease [82] Symptomatic patients: loss of dopamine binding, higher CAG indexes and clinical severity (Unified Huntington's Disease Rating Scale) [81]	
Parkinson's disease	Midbrain, striatum, pallidum, thalamus, precental gyrus, frontal lobe, anterior cingulate gyrus, posterior cingulate gyrus, pons [83,84]	Midbrain: motor deficit severity (Unified Parkinson's Disease Rating Scale) and loss of presynaptic dopamine transporters [83] Anterior and posterior cingulate and thalamus: clinical duration of symptoms [84]	
Multiple system atrophy	Dorsolateral prefrontal cortex, caudate, putamen, pallidum, thalamus, substantia nigra, pons [85]		
Progressive supranuclear palsy	Caudate nucleus, putamen, pallidum, thalamus, midbrain, substantia nigra, pons, cerebellum, frontal lobe [84]		
Amyotropic lateral sclerosis	Motor cortex, pons, frontal lobe region, thalamus [86]	Increased clinical Upper Motor Neuron scores, both for motor cortex and thalamus [86]	ALS Functional Rating Scale Score and disease duration [86]
Multiple sclerosis	Acute white matter lesions, thalamus, brainstem and normal appearing white matter [87-90]	MRI findings of acute white matter lesions [87,88], the Expanded Disability Status Scale [88], the degree of disease progression [90] and decrease in brain parenchymal volume [90]	

Ischemic stroke	Stroke-defined lesions, thalamus and pons ipsilateral to affected hemisphere, along subcortical white matter tracts [91-93]	MRI-defined lesions (but not within one week after stroke) [92,93]	Contrast-enhanced CT lesions [91]
Encephalitis	Affected temporoparietal lobe [95], limbic system [96], thalamus [96]		
Hepatic encephalopathy	Pallidum, right putamen, right dorsolateral prefrontal region [97-99]	Cognitive impairment [97]	Duration of liver disease, severity of liver disease and blood ammonia levels [97]
Peripheral nerve injury	Thalamus contralateral to the side of injury [100]		

Corticobasal degeneration

Corticobasal degeneration is a progressive neurological disorder characterised by a loss of nerve cells and atrophy in multiple brain areas, including the cerebral cortex and basal ganglia. The symptoms of the disease are similar to those found in Parkinson's disease. In a patient with clinical diagnosis of corticobasal degeneration and left-sided symptoms, higher binding potentials of [^{11}C]PK11195 were found in the right basal ganglia and in the right pons [79]. The increased binding of [^{11}C]PK11195 was accompanied by a decrease in glucose metabolism as measured by [^{18}F]FDG PET, while the MRI scan did not reveal structural changes in any of the areas of high [^{11}C]PK11195 and low [^{18}F]FDG uptake. In another study, significant increased [^{11}C]PK11195 binding was found in the striatum, substantia nigra, pons and in corresponding cortical areas, when compared to healthy controls [80]. These two small studies showed the involvement of microglial cell activation in corticobasal degeneration, however, the exact role of microglia cells needs to be addressed in a larger longitudinal study.

Huntington's disease

Huntington's disease (HD) is a genetic disease caused by a CAG repeat expansion in the HD gene on chromosome 4, resulting in a mutant form of the Huntington protein, which causes degeneration of neurons, especially in the frontal lobe and striatum. In the process of neurodegeneration, microglia cells are thought to play an important role in disease progression. In the first study involving [^{11}C]PK11195 PET in Huntington's disease, increased binding potentials of [^{11}C]PK11195 were found in the whole striatum, in the frontal lobe and in the parietal lobe of symptomatic patients, when compared to age-matched healthy controls [81]. The higher binding

potential in the striatum correlated with a lower striatal [^{11}C]raclopride binding potential (loss of dopamine D_2-receptor binding) and also with a higher CAG repeat length. Subsequently, presymptomatic gene carriers (PGC) were studied and also a higher [^{11}C]PK11195 binding potential was found in the striatum and in cortical areas [82]. The striatal [^{11}C]PK11195 binding potential in PGC was lower than that of symptomatic Huntington's disease patients, but this was not statistically significant. Microglia cell activation thus appears to be an early event in Huntington's disease. Although it is unlikely that microglia cell activation is the cause of the disease it may play an important role in disease progression. Inhibition of microglia cell activation in PGC may cause a delay in the onset of clinical symptoms and [^{11}C]PK11195 PET can be an important tool to monitor this process and may provide prognostic information.

Parkinson syndromes

Parkinson's disease

Parkinson's disease is characterized by progressive degeneration of dopamine neurons in the substantia nigra and the related loss of dopamine nerve terminals in the striatum. Ouchi *et al.* [83] studied the relation between loss of density of the pre-synaptic dopamine transporter and the presence of activated microglia cells. In drug-naïve patients, a higher uptake of [^{11}C]PK11195 was found in the midbrain as compared to age-matched healthy controls. The higher uptake of [^{11}C]PK11195 in the midbrain correlated positively with motor impairment severity of the patients and with loss of pre-synaptic density of the dopamine transporter as determined with [^{11}C]CFT PET. The increased binding of [^{11}C]PK11195 in the striatum was found to be negatively correlated to the [^{11}C]CFT binding in the dorsal putamen. This suggests that microglia cell activation plays an important role in initiating and maintaining Parkinson's disease. Gerhard *et al.* [84] studied longitudinal aspects of microglia cell activation in patients with Parkinson's disease and correlated this with the severity and the duration of the disease. In addition, the levels of microglia cell activation were studied over time, in a follow-up study 18 to 28 months after the first [^{11}C]PK11195 PET scan. Increased [^{11}C]PK11195 binding was found in brain areas in the basal ganglia, cortex and in the brainstem, when patients were compared to age-matched healthy volunteers. An increased binding was also found in the substantia nigra, but this did not reach statistical significance. The contradictory result between both studies can be attributed to methodological differences and to differences in patient population, that contained more early stage patients in the study of Ouchi *et al.* [83].

However, Gerhard *et al.* [84] found no correlation between [^{11}C]PK11195 uptake and disease severity. In patients that were studied 18 to 28 months after the baseline PET scan, the disease process progressed, as determined by increased UPDRS (Unified Parkinson's Disease Rating Scale) and reductions in dopamine storage capacity, determined by [^{18}F]DOPA PET. However, in these patients no differences in [^{11}C]PK11195 uptake were found when compared to baseline uptake. It was suggested that the stable levels of microglia cell activation in Parkinson's disease represent a marker of ongoing disease activity, in which activated microglia cells promote disease progression. This would have interesting implications for the use of microglia cell activation, i.e. PBR expression, as a target for monitoring disease progression and for therapeutic intervention. When activated microglia cells are a key factor in progression of Parkinson's disease, therapeutic treatment directed at reduction of microglia cell activation, may slow down the progression of the disease.

Multiple system atrophy

Multiple system atrophy is a progressive brain disorder that is characterised by damage to the autonomic nervous sytem, muscle rigidity and cerebral dysfyunction. As compared to healthy controls, patients with multiple system atropy showed increased binding potenials of [^{11}C]PK11195 in the dorsolateral prefrontal cortex, striatum, pallidum, thalamus, substantia nigra and the pons [85]. The distribution of increased [^{11}C]PK11195 uptake corresponded well with the known neuropathological distrbution of microglia cells. The data did not indicate a simple correlation between the symptoms of the disease and the degree of microglia cell activation, although the power to make a correlation between microglia activation and clinical features was not high enough because of a small number of patients. A larger longitudinal study is therefore in progress.

Progressive supranuclear palsy

The symptoms of progressive supranuclear palsy, that are caused by gradual deterioriation and death of nerve cells, involve loss of balance and falling, slowing of movement, changes in personality and dementia. In four patients, an increased binding of [^{11}C]PK11195 was found in the striatum, pallidum, thalamus, midbrain, substantia nigra, pons, cerebellum and frontal lobe, when compared to healthy contols [84]. This increased binding is consistent with the known neuropathological distribution of microglia cell activation. Because of the low number of patient in this study, [^{11}C]PK11195 uptake was not intended to be correlated to clinical features and

a larger longitudinal study is necessary to determine the exact role of microglia cells in progressive supranuclear palsy.

Amyotrophic lateral sclerosis

Amyotropic lateral sclerosis is caused by the degeneration of motor neurons. A significantly higher uptake of [^{11}C]PK11195 was found in the region of the motor cortex, pons, frontal lobe region and thalamus, when compared to healthy controls [86]. In addition, a correlation was found between the individual [^{11}C]PK11195 binding potentials and the number of pathological upper motor neuron signs. Although only a small number of patients were included, this study showed that microglia cells are an important feature of amyotropic lateral sclerosis and that disease progression does not only involve the motor areas, but also extends to extra-motor areas.

Multiple sclerosis

Multiple sclerosis (MS) is a chronic disease that is characterized by degeneration of myelin in the white matter of the brain. Active myelin degeneration is accompanied by an inflammatory response, involving not only activated microglia cells and astrocytes, but also lymphocytes and macrophages from the periphery. The first study on imaging of the inflammatory response to myelin degeneration with [^{11}C]PK11195 showed that there was increased uptake in acute white matter lesions, but not in chronic lesions [87]. In a subsequent study, Banati *et al.* [88] used kinetic modeling to quantify the uptake of [^{11}C]PK11195. They found increased focal binding of [^{11}C]PK11195 in MS patients, when compared to healthy controls. In areas where the blood-brain barrier was disrupted, as visualized by contrast-enhancing lesions in T1-weighted MRI, the highest overlap with increased [^{11}C]PK11195 uptake was found. In contrast, old lesions (black holes in T1-weighted MRI) showed little uptake of [^{11}C]PK11195, although during relapse of the disease the binding in the old lesions doubled. The binding of [^{11}C]PK11195 in hypointensive areas in the T1-weighted MRI, showed a positive correlation with the increasing disability of the patients, as measured by the Expanded Disability Status Scale (EDSS). More interesting, [^{11}C]PK11195 binding was found in brain areas beyond the focal lesions and it was therefore discussed that [^{11}C]PK11195 binding would be a better parameter of clinical change than the measurements of disease activity by the EDSS. Consistent with the results of Banati *et al.*, Debruyne *et al.* [89] found an increased [^{11}C]PK11195 uptake in active focal lesions

that were defined by contrast-enhanced T1-weighted MRI images. In addition, they found a trend towards a higher [^{11}C]PK11195 uptake in white matter that on the MRI appears as normal (normal appearing white matter (NAWM)). In a second study by the same group, the higher uptake of [^{11}C]PK11195 in NAWM was confirmed and it was found to correlate positively with the degree of disease progression and the decrease in brain parenchymal volume [90].

The increased [^{11}C]PK11195 binding in the focal lesions that is found in these studies is may theoretically be due to binding to the PBR in infiltrating macrophages from the periphery because of disruption of the blood-brain barrier. In contrast, the increased binding in lesions beyond the focal lesion and in the NAWM, without disruption of the blood-brain barrier, is most likely predominantly due to binding of [^{11}C]PK11195 to the PBR expressed by activated microglia cells. The focal lesions can be visualized by both MRI and PET, however, more interesting for monitoring of the disease progression and probably also for therapeutic intervention is [^{11}C]PK11195 PET. The activation of microglia cells precedes the development of focal lesions that can be visualized by MRI and therefore [^{11}C]PK11195 PET may be a better predictor of disease progression.

Ischemic Stroke

Ischemic stroke is characterized by loss of brain function and necrosis due to decreased blood supply to a certain brain area. [^{11}C]PK11195 PET imaging of stroke has been performed to study the early and late effects of focal ischemia, as well as to study disease progression. In one single patient, [^{11}C]PK11195 PET was performed on day 6, 13 and 20 following a stroke in the left hemisphere [91]. On day 6, increased uptake could just be discerned around the borders of the lesion, while on day 13 after stroke larger well-defined areas of increased [^{11}C]PK11195 uptake were found in the left hemisphere. Tracer uptake was even higher at day 20 after stroke. When contrast enhanced CT images were compared with [^{11}C]PK11195 PET images, it was found that the general distributions of abnormalities in the left hemisphere were similar, but that there was no close resemblance of the detailed distribution abnormalities within brain regions. Another study on imaging of stroke with [^{11}C]PK11195 PET, in two patients, showed that from 5 to 53 days after stroke, the areas with increased uptake corresponded well with lesions shown by MRI [92]. Although the area of [^{11}C]PK11195 binding appeared to be larger than the lesion area shown by MRI, this difference was not statistically significant. One patient was scanned on both day 5 and

day 13 after stroke and it was shown that [^{11}C]PK11195 binding in the lesion areas was more pronounced on day 13. Pappata *et al.* studied patients with chronic middle cerebral artery infarcts and found an increased uptake of [^{11}C]PK11195 in the thalamus ipsilateral to the affected hemisphere 2 to 24 months after stroke, but not in the contralateral thalamus [93]. Increased [^{11}C]PK11195 binding was also found around lesion areas and in degenerating neuronal tracts through the internal capsule. The studies that are mentioned above mainly focused on the activation of microglia cells at a certain time point after stroke. Gerhard *et al.* [94] studied the time course of microglia cell activation from day 3 to day 150 after stroke. Before day 6 after stroke, the area of increased [^{11}C]PK11195 uptake was found to be smaller than the size of the lesion as defined by MRI, while between 9 and 28 days after stroke the area of increased [^{11}C]PK11195 uptake was increased in size relative to the MRI-defined lesion. In two patients that were scanned on two time points after stroke, the second scan not only showed increased [^{11}C]PK11195 uptake in the primary lesion, but also in areas beyond the primary lesion.

The activated microglia cells that are present in the lesion area after stroke may produce neuroprotective molecules to repair the neurons that were only a little damaged, or may serve as macrophages in order to remove the neurons from the brain tissue that are too damaged to recover. The presence of activated microglia cells beyond the lesion area is probably due to damage of neuronal projections, resulting in antero- or retrograde activation of microglia cells. Activated microglia may be beneficial or detrimental, [^{11}C]PK11195 PET may be a useful tool to discriminate between possible beneficial (around the lesion area) and detrimental (distant from the lesion area) activation of microglia cells and could be used to monitor the effect of pharmacological treatment of stroke.

Encephalitis

Rasmussen's encephalitis, also chronic focal encephalitis, is a progressive disease that is characterized by frequent and severe seizures and by neuroinflammation in a single cerebral hemisphere. In two patients with Rasmussen's encephalitis, it was shown that the binding potential of [^{11}C]PK11195 was approximately 10-fold higher in the affected hemisphere, as compared to the unaffected hemisphere [95]. [^{11}C]PK11195 uptake in the unaffected hemisphere was comparable to the uptake in the brain of healthy volunteers, while the binding potential in the affected hemisphere was significantly higher than in the control group. MRI scans revealed regions of atrophy

in the affected hemisphere, however, increased focal and diffuse [^{11}C]PK11195 uptake was also found in brain regions that appeared normal on MRI. This may suggest that [^{11}C]PK11195 can diagnose Rasmussen's encephalitis in a more subtle stage than MRI and thus can be useful in understanding the disease progress, especially because it is not known whether the microglia cell activation has a causal role in the disease, or is a response to the neurological damage caused by the seizures.

In addition to Rasmussen's encephalitis, [^{11}C]PK11195 PET has also been used to image activated microglia cells in herpes encephalitis [96]. Herpes encephalitis is mostly caused by the herpes simplex virus type-1 and is characterised by severe brain damage, that occurs also distant from the primary lesion site. [^{11}C]PK11195 PET in two patients, 5 and 8 months after onset of the disease, revealed high specific binding in limbic regions and in anatomically connected regions (i.e. areas that where beyond the areas that showed atrophy on the MRI scan) [96]. In a follow-up study after antiviral treatment, respectively 12 and 6 months later, the MRI scan showed marked atrophy in the brain areas where increased [^{11}C]PK11195 uptake was found on the first [^{11}C]PK11195 PET scan. In addition, [^{11}C]PK11195 PET revealed a largely maintained, but wider distribution of [^{11}C]PK11195 uptake. These data showed that microglia cell activation in response to brain damage can be found not only at the primary lesion, but also in brain areas that are connected to the primary lesion. Activated microglia cells beyond the primary lesions are predictive for future neurodegeneration. The activated microglia cells, that were found in the follow-up study is unlikely to be due to the presence of virus in the brain and can be a result of a self-induced immune activation involving microglia cells. The microglia cells, and thus the PBR, may therefore be a useful target for predicting the progression of the inflammatory response into neurodegeneration.

Hepatic encephalopathy

Hepatic encephalopathy is a reversible neuropsychiatric disorder, which is accompanied by impaired function of brain cells, which is caused by the presence of toxic substances in the blood, as a result of liver failure. Increased binding of [^{11}C]PK11195 was found in the pallidum, right putamen and the right dorsolateral prefrontal region in patients as compared to healthy controls [97]. The increased uptake in the pallidum is consistent with the well known involvement of the pallidum in liver disease and with T1-weighted MRI signal hyperintensities in this brain region. No correlation between the severity of liver disease and [^{11}C]PK11195 binding was

found, but the patients with the highest [^{11}C]PK11195 binding were cognitively most impaired. This study supports the hypothesis of a role of activated PBR in the pathophysiology of hepatic encephalopathy. Ammonia may be one of the toxic substances that is causing the brain damage in hepatic encephalopathy. It has been shown that hyperammonaemia resembles the symptoms of hepatic encephalopathy and results in increased PK11195 binding and brain pregnenolone synthesis [98]. This suggests a neurotrophic role of the PBR in this disease. In contrast to the aforementioned study, no difference in the volume of distribution of [^{11}C]PK11195 was observed between patients with alcohol liver cirrhosis with acute hepatic encephalopathy and healthy controls [99]. The difference between the two studies can be explained by differences between patient groups, because the arterial level of ammonia was higher in the study were a significant higher [^{11}C]PK11195 uptake was found. Another explanation could be methodological differences. In one study [97], The uptake of [^{11}C]PK11195 is expressed as the binding potential using a reference tissue model (with the reference tissue being determind by cluster analysis), while in the other study [99] it is expressed as volume of distribution using a plasma input curve. The binding potential may be a more accurate measurement of [^{11}C]PK11195 uptake. To determine the role of the PBR in hepatic encephalopathy more studies with larger number of patients are necessary.

Peripheral nerve injury

[^{11}C]PK11195 PET was used to study microglia cell activation in patients with injuries at different levels of the sensory pathway, like rupture of the brachial plexus or avulsion of the spinal cord sensory root [100]. Significantly higher binding of [^{11}C]PK11195 was found in the thalamus contralateral to the side of injury, when compared to the uptake in healthy controls. This higher uptake was found even two decades after the event and was not accompanied by atrophy in the thalamus and did not correlate with the size of the thalamus.

Therapy monitoring

PET is not only an attractive technique for detection of neuroinflammation and studying disease progression, but it could also be a valuable tool for monitoring of therapy response. In oncology therapy monitoring with [^{18}F]FDG PET is routine clinical practice. For more than a decade the decision to continue or to stop cytostatic

therapy in lung cancer, Hodgkin and non-Hodgkin lymphoma, liver metastases and others is based on FDG PET [101,102].

There are several reasons for therapy monitoring based on PBR expression in inflammatory brain diseases. As follows from the above, microglia cell activation is associated with many neurological diseases and there is evidence that microglia cell activation precedes neurodegeneration [103,104]. So, this provides an interesting opportunity to select patients with ongoing neuroinflammation for anti-inflammatory therapy to prevent neurodegeneration. For example, PET imaging with the PBR ligand [^{11}C]PK11195 can localize ongoing inflammation after traumatic nerve lesions, after herpes simplex encephalitis, in Alzheimer's disease or in Parkinson's disease. Patients with neuroinflammatory foci can be specifically subjected to anti-inflammatory therapy, whereas patients that show no inflammation can be safeguarded against ineffective treatment with anti-inflammatory drugs. In this way, PET imaging with PBR ligands can help to select patients that will benefit from the therapy. In these selected patients the effectiveness of therapy can then be evaluated on hard measures of inflammation reduction in the lesions previously found. Dose finding can be performed, preventing under-treatment and also preventing potential toxic effects of anti-inflammatory drugs. Like in cancer therapy, dose change, therapy continuation or therapy discontinuation are then decided in a rational way.

In addition, the hypothesis is that low grade expression of the PBR may be neuroprotective and high level expression neurodestructive. It seems therefore very important to be able to evaluate the actual expression of inflammatory mediating molecules *in vivo* in patients for evalutation of therapy effectiveness and understanding of variable effects of anti-inflammatory drugs. Ideally, the anti-inflammatory drugs shift the inflammatory status from neurodestructive to neuroprotective levels. It is very probable that effective lowering of upregulated PBR signal in PET images is associated with patient cases that show improvement of their clinical profile. Although there are other imaging techniques like CT and MRI that can detect abnormalities in the brain, in monitoring treatment effects on neuroinflammation PET is superior. In both HIV dementia and herpes simplex encephalitis early measurements of brain inflammation with MRI showed insufficient sensitivity. In addition, PET imaging is superior in detection sensitivity in lesions distant from acute infection [96].

In most neurological diseases, anti-inflammatory treatment may prevent severe neuronal damage and neurodegeneration, and the effect of this treatment can be monitored by PET imaging of the PBR. There are a few anti-inflammatory drugs with

potentially neuroprotective properties that have already been evaluated in both animal studies and clinical trials. Among these drugs, minocycline and COX inhibitors have received most attention.

Minocycline

Minocycline is a member of the broad spectrum tetracycline antibiotics and is mostly used to treat acne and other skin infections. In animal models, minocycline decreases microglia cell activation and protects against, amongst others, multiple sclerosis like lesions [105] and virus induced glutamate and IL-1 toxicity [106,107]. In an animal model of schizophrenia, minocycline was also found to protect against the toxic effects of the NMDA-receptor antagonist MK801 [108]. In addition, minocycline is neuroprotective in various animal models of viral brain infection [106,107,109].

One of the mechanism by which minocycline might exert its neuroprotective role is the prevention of microglia cell activation by preventing destructive pressure of cytokines such as TNF-alpha [110]. Paradoxically minocycline can induce elevation of TNF-alpha in stimulated peripheral monocytes [107]. Other mechanism of the effect of minocycline are suggested to be attenuation of apoptosis or suppression of free-radical production [111]. However, the effect of minocycline on the brain is highly disease specific and probably dependent on the precise dosage regimen. For example, in stress (glucocorticoid) related [112] and glutamate related [113] models of neurotoxicity minocycline attenuates damage. In contrast, minocycline exacerbated MPTP-induced damage to dopaminergic neurons in mice and increased symptoms of parkinsonism in MPTP-treated monkeys [114,115]. Minocycline has different immune modulatory effects in demyelination models. This pharmaceutical aggravates inflammatory damage in a non-immune demyelination model [116], but not in an ischemic demylination model [117]. Straightforward paradoxical are the effects of minocycline on infectious diseases in the brain. In the simian model of HIV dementia [109,118], minocycline reduces viral load but also attenuates the inflammatory responses in the brain. Anti inflammatory effect of minocycline may actually improve viral resistance in the brain, which is a paradox that is not yet solved. Probably minocycline has a complex immune modulatory effect (as opposed to a general anti-inflammatory effect) that favours viral clearance.

Although there are contradicting results, most animal studies showed the neuroprotective effect of minocycline and it has already been used and shown to be

effective in clinical studies. In 10 patients with relapsing remitting multiple sclerosis it was found that after two months of treatment with minocycline no contrast-enhanced MRI lesions were found, whereas they were found in the period before and during the first two months of treatment [119]. Follow-up of these patients after 12 and 24 months of treatment showed no relapse and no active lesions on contrast-enhanced MRI [120]. An effect of minocycline treatment was also found in patients when treated for 5 consecutive days at the acute stage of stroke [121]. The reductions in the score on the NIH stroke scale were significantly larger for the minocycline treated patients, as compared non-treated patients. In Huntington's disease, a stabilization of neurological and neuropsychological function was found, as well as an improvement in global psychiatric scoring [122]. Neuroinflammation may also play an important role in schizophrenia and post-mortem studies showed increased activated microglia in schizophrenic brains as compared to healthy brains [123,124]. Treatment with minocycline has been shown be effective in the treatment of acute schizophrenia with predominately catatonic symptoms[125]. Larger studies on the effect of minocycline on cognitive functioning in schizophrenia are in progress.

As mentioned above, there are a few clinical studies that investigate the role of minocycline on various neurological diseases. However, the MRI measurement that are used determine the effect of treatment may not be sensitive enough and only detect large treatment effects. PET imaging of the PBR is likely to be more sensitive, especially with the new PET tracers that are under development, because it directly measures microglia cell activity. It has already been shown that treatment with minocycline causes a reduction in PBR expression. In gerbils with global cerebral ischemia an increase was found in [^{3}H]PK11195 binding in the hippocampus, while treatment with minocycline significantly reduced the increase in [^{3}H]PK11195 binding by 36% [126]. In addition, nodose ganglionectomy in rats resulted in an increase in [^{3}H]PK11195 binding in multiple brainstem nuclei which was significantly decreased by minocycline treatment [127]. Imaging of the PBR may therefore be an important tool in monitoring minocycline treatment in neurodegenerative diseases.

COX inhibitors

Cyclooxygenase (COX) is an enzyme that is responsible for the formation of prostanoids, like prostaglandins and thromboxane and inhibitors of COX have analgesic, antipyretic and anti-inflammatory properties. There are two COX isoforms:

COX-1, which is expressed in most tissues, and COX-2, which is related to inflammation, mainly in the brain. COX-2 inhibitors, like celecoxib and rofecoxib, have found application in the quest for therapy of possibly immune mediated neurodegenerative diseases.

In experimental autoimmune encephalomyelitis (EAE), an animal model for multiple sclerosis, it was found that celecoxib [128] and rofecoxib [129] strongly inhibited the development of EAE. Celecoxib was also found to reduce the inflammatory response to the injection of lipopolysaccharide in the striatum, which results in the activation of microglia cells [130]. In contrast, rofecoxib was not neuroprotective in an experimental mouse model of Parkinson's disease, in which dopaminergic neurons in the striatum were destroyed by MPTP [131]. In this model an increase was found in COX-2 expression, but the damage to the dopaminergic neurons by MPTP in this model might have been too severe for rofecoxib to have a neuroprotective effect. In a mouse model of amyotrophic lateral sclerosis, activated microglia cells were found in the lumbar enlargement of the spinal cord and treatment with rofecoxib resulted in a delay in the onset of motor deficit, although it did not affect survival of the mice [132]. Although there are numerous studies that show the neuroprotective properties of COX-2 inhibitor, there is only one study up till now that used [^{11}C]PK11195 PET to monitor the effect of treatment with a COX-2 inhibitor. Injection of 6-OHDA in the striatum of rats, which is a rat model of Parkinson's disease, resulted in an increased uptake of [^{11}C]PK11195 while after treatment with celecoxib no uptake was present [133].

As mentioned before, the presence of PBR expression as measured with [^{11}C]PK11195 is demonstrated in Alzheimers disease, amyotrophic lateral sclerosis, herpes encephalitis and in Parkinson disease [103]. The evidence of elevated COX-2 expression in these diseases is less robust [134]. Most clinical trials on the effect of treatment with COX inhibitors were conducted in Alzheimer's disease patients. In the first studies performed it was found that indomethacin, a COX-1/COX-2 inhibitor, protected against the decline in cognitive impairment in patients with mild to moderate Alzheimer's disease [135] and that diclofenac treatment, also a COX-1/COX-2 inhibitor, in a small number of patients showed a trend towards less deterioration of the disease [136]. In contrast to these results it was found that 1 year of treatment with rofecoxib did not slow the cognitive decline in Alzheimer's disease patients [137,138] and that 4 years of treatment did not delay the onset of Alzheimer's disease in patients with mild cognitive impairment [139]. Treatment with COX

inhibitor have shown to be effective in psychiatric disorders as it is efficacious e.g. as adjunctive therapy in schizophrenia [140] and may have value in the treatment of major depressive disorders [141].

Although in-vitro and in-vivo data suggested that COX inhibitors are neuroprotective, data in Alzheimer's disease showed no improvement in patients after treatment. Although this is often contributed to the timing of treatment and the choice and dosage of drugs, this can also be attributed to the lack of appropriate selection of patients and due to lack of a sensitive tool for therapy monitoring. Although cognitive functioning is an important feature because it directly reflects the well-being of patients, it might not be the best way for selecting patients for anti-inflammatory therapy. If subtle changes in neuroinflammation can be seen early during treatment by [^{11}C]PK11195 PET, that may predict therapy efficacy and rescue of cognition that occurs after continued treatment. Therefore, it can provide a tool for determining the timing of treatment and the choice and dosage of drugs. It may possibly be demonstrated in the future that the variation in clinical effect of potential anti-inflammatory drugs can be explained by co-variation of the central anti-inflammatory effect with [^{11}C]PK11195 PET.

Conclusion

Because of the degenerative outcome of neurological diseases, it is of great importance to gain more insight in the etiology and progression of the disease and consequently to find adequate therapy and tools to monitor therapy response. As a non-invasive tool, PET could be of help to this respect. Since activated microglia cells play a central role in neurodegeneration, they are an interesting target for imaging. Because the PBR is highly upregulated in activated microglia cells, PET tracers that bind to this receptor have been used for this purpose and new PET tracers for the PBR are under development. Thus far, only the PET tracer [^{11}C]PK11195 has been used in numerous human studies to investigate the role of microglia cell activation in neurological diseases. Although there are not many studies that focus on imaging of the PBR as a tool to monitor therapy yet, this application can be of great importance. Studies with anti-inflammatory drugs, like minocycline and COX inhibitors, have shown that these drugs have neuroprotective potential, and that this effect is disease specific and probably dosage dependent. This neuroprotective effect is likely to be due to inhibition of activated microglia cells and a reduction in PK11195 binding to the

PBR has been shown in response to therapy. The PBR is therefore an important target that can play a decisive role in monitoring the disease progression and the effect of therapy.

Acknowledgements

This study was funded by the Stanley Medical Research Institute, Grant-ID 05-NV-001, and in part by the EC - FP6-project DiMI, LSHB-CT-2005-512146.

References

1 Eikelenboom P, Veerhuis R, Scheper W, Rozemuller AJ, van Gool WA, Hoozemans JJ. The significance of neuroinflammation in understanding Alzheimer's disease. J.Neural Transm. 2006; 113:1685-1695

2 Bartels AL, Leenders KL. Neuroinflammation in the pathophysiology of Parkinson's disease: evidence from animal models to human in vivo studies with [11C]-PK11195 PET. Mov Disord. 2007; 22:1852-1856

3 Esposito E, Di M, V, Benigno A, Pierucci M, Crescimanno G, Di GG. Non-steroidal anti-inflammatory drugs in Parkinson's disease. Exp.Neurol. 2007; 205:295-312

4 Weggen S, Rogers M, Eriksen J. NSAIDs: small molecules for prevention of Alzheimer's disease or precursors for future drug development? Trends Pharmacol.Sci. 2007; 28:536-543

5 Medawar PB. Immunity to homologous grafted skin. III. The fate of skin homografts transplanted to the brain, to subcutaneous tissue, and to the anteriour chamber of the eye. Br J Exp Path 1948; 29:58-74

6 Chavarria A, Alcocer-Varela J. Is damage in central nervous system due to inflammation? Autoimmun.Rev. 2004; 3:251-260

7 Polfliet MM, van d, V, Dopp EA, et al. The role of perivascular and meningeal macrophages in experimental allergic encephalomyelitis. J.Neuroimmunol. 2002; 122:1-8

8 Piehl F, Lidman O. Neuroinflammation in the rat--CNS cells and their role in the regulation of immune reactions. Immunol.Rev. 2001; 184:212-225

9 Olsson T, Kelic S, Edlund C, et al. Neuronal interferon-gamma immunoreactive molecule: bioactivities and purification. Eur.J Immunol. 1994; 24:308-314

10 Matyszak MK. Inflammation in the CNS: balance between immunological privilege and immune responses. Prog.Neurobiol. 1998; 56:19-35

11 Ferrer I, Bernet E, Soriano E, del RT, Fonseca M. Naturally occurring cell death in the cerebral cortex of the rat and removal of dead cells by transitory phagocytes. Neuroscience 1990; 39:451-458

12 Killackey HP. Glia and the Elimination of Transient Cortical Projections. Trends in Neurosciences 1984; 7:225-226

13 Davalos D, Grutzendler J, Yang G, et al. ATP mediates rapid microglial response to local brain injury in vivo. Nat.Neurosci. 2005; 8:752-758

14 Nimmerjahn A, Kirchhoff F, Helmchen F. Resting microglial cells are highly dynamic surveillants of brain parenchyma in vivo. Science 2005; 308:1314-1318

15 Chao CC, Hu SX, Molitor TW, Shaskan EG, Peterson PK. Activated Microglia Mediate Neuronal Cell Injury Via A Nitric-Oxide Mechanism. Journal of Immunology 1992; 149:2736-2741

16 Nakajima K, Kohsaka S. Microglia: neuroprotective and neurotrophic cells in the central nervous system. Curr.Drug Targets Cardiovasc.Haematol.Disord. 2004; 4:65-84
17 Li L, Lu J, Tay SS, Moochhala SM, He BP. The function of microglia, either neuroprotection or neurotoxicity, is determined by the equilibrium among factors released from activated microglia in vitro. Brain Res. 2007; 1159:8-17
18 Lai AY, Todd KG. Differential regulation of trophic and proinflammatory microglial effectors is dependent on severity of neuronal injury. Glia 2008; 56:259-270
19 Braestrup C, Squires RF. Specific benzodiazepine receptors in rat brain characterized by high-affinity (3H)diazepam binding. Proc.Natl.Acad.Sci.U.S.A 1977; 74:3805-3809
20 Braestrup C, Albrechtsen R, Squires RF. High densities of benzodiazepine receptors in human cortical areas. Nature 1977; 269:702-704
21 Gavish M, Bachman I, Shoukrun R, et al. Enigma of the peripheral benzodiazepine receptor. Pharmacol.Rev. 1999; 51:629-650
22 Marangos PJ, Patel J, Boulenger JP, Clark-Rosenberg R. Characterization of peripheral-type benzodiazepine binding sites in brain using [3H]Ro 5-4864. Mol.Pharmacol. 1982; 22:26-32
23 Papadopoulos V, Baraldi M, Guilarte TR, et al. Translocator protein (18kDa): new nomenclature for the peripheral-type benzodiazepine receptor based on its structure and molecular function. Trends Pharmacol.Sci. 2006; 27:402-409
24 Papadopoulos V, Lecanu L, Brown RC, Han Z, Yao ZX. Peripheral-type benzodiazepine receptor in neurosteroid biosynthesis, neuropathology and neurological disorders. Neuroscience 2006; 138:749-756
25 Casellas P, Galiegue S, Basile AS. Peripheral benzodiazepine receptors and mitochondrial function. Neurochem.Int. 2002; 40:475-486
26 Lacor P, Gandolfo P, Tonon MC, et al. Regulation of the expression of peripheral benzodiazepine receptors and their endogenous ligands during rat sciatic nerve degeneration and regeneration: a role for PBR in neurosteroidogenesis. Brain Res. 1999; 815:70-80
27 Schumacher M, Akwa Y, Guennoun R, et al. Steroid synthesis and metabolism in the nervous system: trophic and protective effects. J.Neurocytol. 2000; 29:307-326
28 Lacapere JJ, Papadopoulos V. Peripheral-type benzodiazepine receptor: structure and function of a cholesterol-binding protein in steroid and bile acid biosynthesis. Steroids 2003; 68:569-585
29 Banati RB, Myers R, Kreutzberg GW. PK ('peripheral benzodiazepine')--binding sites in the CNS indicate early and discrete brain lesions: microautoradiographic detection of [3H]PK11195 binding to activated microglia. J.Neurocytol. 1997; 26:77-82
30 Turkheimer FE, Edison P, Pavese N, et al. Reference and target region modeling of [11C]-(R)-PK11195 brain studies. J.Nucl.Med. 2007; 48:158-167

31 Groom GN, Junck L, Foster NL, Frey KA, Kuhl DE. PET of peripheral benzodiazepine binding sites in the microgliosis of Alzheimer's disease. J.Nucl.Med. 1995; 36:2207-2210
32 Cagnin A, Brooks DJ, Kennedy AM, et al. In-vivo measurement of activated microglia in dementia. Lancet 2001; 358:461-467
33 Watkins GL, Jewett DM, Mulholland GK, Kilbourn MR, Toorongian SA. A captive solvent method for rapid N-[11C]methylation of secondary amides: application to the benzodiazepine, 4'-chlorodiazepam (RO5-4864). Int.J.Rad.Appl.Instrum.[A] 1988; 39:441-444
34 Junck L, Olson JM, Ciliax BJ, et al. PET imaging of human gliomas with ligands for the peripheral benzodiazepine binding site. Ann.Neurol. 1989; 26:752-758
35 Pascali C, Luthra SK, Pike VW, et al. The radiosynthesis of [18F]PK 14105 as an alternative radioligand for peripheral type benzodiazepine binding sites. Int.J.Rad.Appl.Instrum.[A] 1990; 41:477-482
36 Price GW, Ahier RG, Hume SP, et al. In vivo binding to peripheral benzodiazepine binding sites in lesioned rat brain: comparison between [3H]PK11195 and [18F]PK14105 as markers for neuronal damage. J.Neurochem. 1990; 55:175-185
37 Matarrese M, Moresco RM, Cappelli A, et al. Labeling and evaluation of N-[11C]methylated quinoline-2-carboxamides as potential radioligands for visualization of peripheral benzodiazepine receptors. J.Med.Chem. 2001; 44:579-585
38 Cappelli A, Matarrese M, Moresco RM, et al. Synthesis, labeling, and biological evaluation of halogenated 2-quinolinecarboxamides as potential radioligands for the visualization of peripheral benzodiazepine receptors. Bioorg.Med.Chem. 2006; 14:4055-4066
39 Belloli S, Moresco RM, Matarrese M, et al. Evaluation of three quinoline-carboxamide derivatives as potential radioligands for the in vivo pet imaging of neurodegeneration. Neurochem.Int. 2004; 44:433-440
40 Gulyas B, Halldin C, Vas A, et al. [11C]vinpocetine: a prospective peripheral benzodiazepine receptor ligand for primate PET studies. J.Neurol.Sci. 2005; 229-230:219-223
41 Gulyas B, Halldin C, Sandell J, et al. PET studies on the brain uptake and regional distribution of [11C]vinpocetine in human subjects. Acta Neurol.Scand. 2002; 106:325-332
42 Gulyas B, Vas A, Halldin C, et al. Cerebral uptake of [ethyl-11C]vinpocetine and 1-[11C]ethanol in cynomolgous monkeys: a comparative preclinical PET study. Nucl.Med.Biol. 2002; 29:753-759
43 Vas A, Shchukin Y, Karrenbauer VD, et al. Functional neuroimaging in multiple sclerosis with radiolabelled glia markers: Preliminary comparative PET studies with [(11)C]vinpocetine and [(11)C]PK11195 in patients. J.Neurol.Sci. 2008; 264:9-17

44 Thominiaux C, Mattner F, Greguric I, et al. Radiosynthesis of 2-[6-chloro-2-(4-iodophenyl)imidazo [1,2-a]pyridin-3-yl]-N-ethyl-N-[C-11]methyl-acetamide, [C-11]CLINME, a novel radioligand for imaging the peripheral benzodiazepine receptors with PET. J.Label.Compd.Radiopharm. 2007; 50:229-236

45 Boutin H, Chauveau F, Thominiaux C, et al. In vivo imaging of brain lesions with [(11)C]CLINME, a new PET radioligand of peripheral benzodiazepine receptors. Glia 2007; 55:1459-1468

46 Kropholler MA, Boellaard R, Schuitemaker A, Folkersma H, van Berckel BN, Lammertsma AA. Evaluation of reference tissue models for the analysis of [11C](R)-PK11195 studies. J.Cereb.Blood Flow Metab 2006; 26:1431-1441

47 James ML, Fulton RR, Henderson DJ, et al. Synthesis and in vivo evaluation of a novel peripheral benzodiazepine receptor PET radioligand. Bioorg.Med.Chem. 2005; 13:6188-6194

48 Thominiaux C, Dolle F, James ML, et al. Improved synthesis of the peripheral benzodiazepine receptor ligand [11C]DPA-713 using [11C]methyl triflate. Appl.Radiat.Isot. 2006; 64:570-573

49 Boutin H, Chauveau F, Thominiaux C, et al. 11C-DPA-713: a novel peripheral benzodiazepine receptor PET ligand for in vivo imaging of neuroinflammation. J.Nucl.Med. 2007; 48:573-581

50 Doorduin J, Klein HC, Dierckx RA, James M, Kassiou M, de Vries EFJ. [(11)C]-DPA-713 and [(18)F]-DPA-714 as New PET Tracers for TSPO: A Comparison with [(11)C]-(R)-PK11195 in a Rat Model of Herpes Encephalitis. Mol.Imaging Biol. 2009; DOI: 10.1007/s11307-009-0211-6-

51 James ML, Fulton RR, Vercoullie J, et al. DPA-714, a new translocator protein (18kDa) (TSPO) ligand: synthesis, radio-fluorination and pharmacological characterisation. Journal of Nuclear Medicine 2008; In press

52 Kita A, Kohayakawa H, Kinoshita T, et al. Antianxiety and antidepressant-like effects of AC-5216, a novel mitochondrial benzodiazepine receptor ligand. Br.J.Pharmacol. 2004; 142:1059-1072

53 Yanamoto K, Zhang MR, Kumata K, Hatori A, Okada M, Suzuki K. In vitro and ex vivo autoradiography studies on peripheral-type benzodiazepine receptor binding using [11C]AC-5216 in normal and kainic acid-lesioned rats. Neurosci.Lett. 2007; 428:59-63

54 Zhang MR, Kumata K, Maeda J, et al. 11C-AC-5216: a novel PET ligand for peripheral benzodiazepine receptors in the primate brain. J.Nucl.Med. 2007; 48:1853-1861

55 Amitani M, Zhang MR, Noguchi J, et al. Blood flow dependence of the intratumoral distribution of peripheral benzodiazepine receptor binding in intact mouse fibrosarcoma. Nucl.Med.Biol. 2006; 33:971-975

56 Briard E, Zoghbi SS, Imaizumi M, et al. Synthesis and evaluation in monkey of two sensitive 11C-labeled aryloxyanilide ligands for imaging brain peripheral benzodiazepine receptors in vivo. J.Med.Chem. 2008; 51:17-30

57 Imaizumi M, Briard E, Zoghbi SS, et al. Kinetic evaluation in nonhuman primates of two new PET ligands for peripheral benzodiazepine receptors in brain. Synapse 2007; 61:595-605
58 Imaizumi M, Briard E, Zoghbi SS, et al. Brain and whole-body imaging in nonhuman primates of [(11)C]PBR28, a promising PET radioligand for peripheral benzodiazepine receptors. Neuroimage. 2008; 39:1289-1298
59 Imaizumi M, Kim HJ, Zoghbi SS, et al. PET imaging with [11C]PBR28 can localize and quantify upregulated peripheral benzodiazepine receptors associated with cerebral ischemia in rat. Neurosci.Lett. 2007; 411:200-205
60 Brown AK, Fujita M, Fujimura Y, et al. Radiation Dosimetry and Biodistribution in Monkey and Man of 11C-PBR28: A PET Radioligand to Image Inflammation. J.Nucl.Med. 2007; 48:2072-2079
61 Fujita M, Imaizumi M, Zoghbi SS, et al. Kinetic analysis in healthy humans of a novel positron emission tomography radioligand to image the peripheral benzodiazepine receptor, a potential biomarker for inflammation. Neuroimage. 2008; 40:43-52
62 Zhang MR, Ogawa M, Maeda J, et al. [2-11C]isopropyl-, [1-11C]ethyl-, and [11C]methyl-labeled phenoxyphenyl acetamide derivatives as positron emission tomography ligands for the peripheral benzodiazepine receptor: radiosynthesis, uptake, and in vivo binding in brain. J.Med.Chem. 2006; 49:2735-2742
63 Probst KC, Izquierdo D, Bird JL, et al. Strategy for improved [(11)C]DAA1106 radiosynthesis and in vivo peripheral benzodiazepine receptor imaging using microPET, evaluation of [(11)C]DAA1106. Nucl.Med.Biol. 2007; 34:439-446
64 Zhang MR, Kida T, Noguchi J, et al. [(11)C]DAA1106: radiosynthesis and in vivo binding to peripheral benzodiazepine receptors in mouse brain. Nucl.Med.Biol. 2003; 30:513-519
65 Maeda J, Suhara T, Zhang MR, et al. Novel peripheral benzodiazepine receptor ligand [11C]DAA1106 for PET: an imaging tool for glial cells in the brain. Synapse 2004; 52:283-291
66 Venneti S, Wagner AK, Wang G, et al. The high affinity peripheral benzodiazepine receptor ligand DAA1106 binds specifically to microglia in a rat model of traumatic brain injury: implications for PET imaging. Exp.Neurol. 2007; 207:118-127
67 Venneti S, Lopresti BJ, Wang G, et al. A comparison of the high-affinity peripheral benzodiazepine receptor ligands DAA1106 and (R)-PK11195 in rat models of neuroinflammation: implications for PET imaging of microglial activation. J.Neurochem. 2007; 102:2118-2131
68 Maeda J, Higuchi M, Inaji M, et al. Phase-dependent roles of reactive microglia and astrocytes in nervous system injury as delineated by imaging of peripheral benzodiazepine receptor. Brain Res. 2007; 1157:100-111

69 Ikoma Y, Yasuno F, Ito H, et al. Quantitative analysis for estimating binding potential of the peripheral benzodiazepine receptor with [(11)C]DAA1106. J.Cereb.Blood Flow Metab 2007; 27:173-184

70 Zhang MR, Maeda J, Ogawa M, et al. Development of a new radioligand, N-(5-fluoro-2-phenoxyphenyl)-N-(2-[18F]fluoroethyl-5-methoxybenzyl)acetami de, for pet imaging of peripheral benzodiazepine receptor in primate brain. J.Med.Chem. 2004; 47:2228-2235

71 Zhang MR, Maeda J, Ito T, et al. Synthesis and evaluation of N-(5-fluoro-2-phenoxyphenyl)-N-(2-[(18)F]fluoromethoxy-d(2)-5-methoxybenzy l)acetamide: a deuterium-substituted radioligand for peripheral benzodiazepine receptor. Bioorg.Med.Chem. 2005; 13:1811-1818

72 Maeda J, Ji B, Irie T, et al. Longitudinal, quantitative assessment of amyloid, neuroinflammation, and anti-amyloid treatment in a living mouse model of Alzheimer's disease enabled by positron emission tomography. J.Neurosci. 2007; 27:10957-10968

73 Fujimura Y, Ikoma Y, Yasuno F, et al. Quantitative analyses of 18F-FEDAA1106 binding to peripheral benzodiazepine receptors in living human brain. J.Nucl.Med. 2006; 47:43-50

74 Veenman L, Papadopoulos V, Gavish M. Channel-like functions of the 18-kDa translocator protein (TSPO): regulation of apoptosis and steroidogenesis as part of the host-defense response. Curr.Pharm.Des 2007; 13:2385-2405

75 Cagnin A, Rossor M, Sampson EL, Mackinnon T, Banati RB. In vivo detection of microglial activation in frontotemporal dementia. Ann.Neurol. 2004; 56:894-897

76 Cagnin A, Kassiou M, Meikle SR, Banati RB. In vivo evidence for microglial activation in neurodegenerative dementia. Acta Neurol.Scand.Suppl 2006; 185:107-114

77 Hammoud DA, Endres CJ, Chander AR, et al. Imaging glial cell activation with [11C]-R-PK11195 in patients with AIDS. J.Neurovirol. 2005; 11:346-355

78 Wiley CA, Lopresti BJ, Becker JT, et al. Positron emission tomography imaging of peripheral benzodiazepine receptor binding in human immunodeficiency virus-infected subjects with and without cognitive impairment. J.Neurovirol. 2006; 12:262-271

79 Henkel K, Karitzky J, Schmid M, et al. Imaging of activated microglia with PET and [11C]PK 11195 in corticobasal degeneration. Mov Disord. 2004; 19:817-821

80 Gerhard A, Watts J, Trender-Gerhard I, et al. In vivo imaging of microglial activation with [11C](R)-PK11195 PET in corticobasal degeneration. Mov Disord. 2004; 19:1221-1226

81 Pavese N, Gerhard A, Tai YF, et al. Microglial activation correlates with severity in Huntington disease: a clinical and PET study. Neurology 2006; 66:1638-1643

82 Tai YF, Pavese N, Gerhard A, et al. Microglial activation in presymptomatic Huntington's disease gene carriers. Brain 2007; 130:1759-1766

83 Ouchi Y, Yoshikawa E, Sekine Y, et al. Microglial activation and dopamine terminal loss in early Parkinson's disease. Ann.Neurol. 2005; 57:168-175

84 Gerhard A, Pavese N, Hotton G, et al. In vivo imaging of microglial activation with [11C](R)-PK11195 PET in idiopathic Parkinson's disease. Neurobiol.Dis. 2006; 21:404-412

85 Gerhard A, Banati RB, Goerres GB, et al. [11C](R)-PK11195 PET imaging of microglial activation in multiple system atrophy. Neurology 2003; 61:686-689

86 Turner MR, Cagnin A, Turkheimer FE, et al. Evidence of widespread cerebral microglial activation in amyotrophic lateral sclerosis: an [11C](R)-PK11195 positron emission tomography study. Neurobiol.Dis. 2004; 15:601-609

87 Vowinckel E, Reutens D, Becher B, et al. PK11195 binding to the peripheral benzodiazepine receptor as a marker of microglia activation in multiple sclerosis and experimental autoimmune encephalomyelitis. J.Neurosci.Res. 1997; 50:345-353

88 Banati RB, Newcombe J, Gunn RN, et al. The peripheral benzodiazepine binding site in the brain in multiple sclerosis: quantitative in vivo imaging of microglia as a measure of disease activity. Brain 2000; 123 (Pt 11):2321-2337

89 Debruyne JC, Versijpt J, Van Laere KJ, et al. PET visualization of microglia in multiple sclerosis patients using [11C]PK11195. Eur.J.Neurol. 2003; 10:257-264

90 Versijpt J, Debruyne JC, Van Laere KJ, et al. Microglial imaging with positron emission tomography and atrophy measurements with magnetic resonance imaging in multiple sclerosis: a correlative study. Mult.Scler. 2005; 11:127-134

91 Ramsay SC, Weiller C, Myers R, et al. Monitoring by PET of macrophage accumulation in brain after ischaemic stroke. Lancet 1992; 339:1054-1055

92 Gerhard A, Neumaier B, Elitok E, et al. In vivo imaging of activated microglia using [11C]PK11195 and positron emission tomography in patients after ischemic stroke. Neuroreport 2000; 11:2957-2960

93 Pappata S, Levasseur M, Gunn RN, et al. Thalamic microglial activation in ischemic stroke detected in vivo by PET and [11C]PK1195. Neurology 2000; 55:1052-1054

94 Gerhard A, Schwarz J, Myers R, Wise R, Banati RB. Evolution of microglial activation in patients after ischemic stroke: a [11C](R)-PK11195 PET study. Neuroimage. 2005; 24:591-595

95 Banati RB, Goerres GW, Myers R, et al. [11C](R)-PK11195 positron emission tomography imaging of activated microglia in vivo in Rasmussen's encephalitis. Neurology 1999; 53:2199-2203

96 Cagnin A, Myers R, Gunn RN, et al. In vivo visualization of activated glia by [11C] (R)-PK11195-PET following herpes encephalitis reveals projected neuronal damage beyond the primary focal lesion. Brain 2001; 124:2014-2027

97 Cagnin A, Taylor-Robinson SD, Forton DM, Banati RB. In vivo imaging of cerebral "peripheral benzodiazepine binding sites" in patients with hepatic encephalopathy. Gut 2006; 55:547-553

98 Itzhak Y, Roig-Cantisano A, Dombro RS, Norenberg MD. Acute liver failure and hyperammonemia increase peripheral-type benzodiazepine receptor binding and pregnenolone synthesis in mouse brain. Brain Res. 1995; 705:345-348

99 Iversen P, Hansen DA, Bender D, et al. Peripheral benzodiazepine receptors in the brain of cirrhosis patients with manifest hepatic encephalopathy. Eur.J.Nucl.Med.Mol.Imaging 2006; 33:810-816

100 Banati RB, Cagnin A, Brooks DJ, et al. Long-term trans-synaptic glial responses in the human thalamus after peripheral nerve injury. Neuroreport 2001; 12:3439-3442

101 Avril NE, Weber WA. Monitoring response to treatment in patients utilizing PET. Radiol.Clin.North Am. 2005; 43:189-204

102 Strauss LG. Positron Emission Tomography: Current Role for Diagnosis and Therapy Monitoring in Oncology. Oncologist. 1997; 2:381-388

103 Cagnin A, Kassiou M, Meikle SR, Banati RB. Positron emission tomography imaging of neuroinflammation. Neurotherapeutics. 2007; 4:443-452

104 De Vries EFJ, Dierckx RA, Klein HC. Nuclear imaging of inflammation in neurologic and psychiatric disorders. Current Clinical Pharmacology 2006; 1:229-242

105 Maier K, Merkler D, Gerber J, et al. Multiple neuroprotective mechanisms of minocycline in autoimmune CNS inflammation. Neurobiol.Dis. 2007; 25:514-525

106 Darman J, Backovic S, Dike S, et al. Viral-induced spinal motor neuron death is non-cell-autonomous and involves glutamate excitotoxicity. J.Neurosci. 2004; 24:7566-7575

107 Irani DN, Prow NA. Neuroprotective interventions targeting detrimental host immune responses protect mice from fatal alphavirus encephalitis. J.Neuropathol.Exp.Neurol. 2007; 66:533-544

108 Levkovitz Y, Levi U, Braw Y, Cohen H. Minocycline, a second-generation tetracycline, as a neuroprotective agent in an animal model of schizophrenia. Brain Res. 2007; 1154:154-162

109 Si Q, Cosenza M, Kim MO, et al. A novel action of minocycline: inhibition of human immunodeficiency virus type 1 infection in microglia. J.Neurovirol. 2004; 10:284-292

110 Giuliani F, Hader W, Yong VW. Minocycline attenuates T cell and microglia activity to impair cytokine production in T cell-microglia interaction. J.Leukoc.Biol. 2005; 78:135-143

111 Yong VW, Wells J, Giuliani F, Casha S, Power C, Metz LM. The promise of minocycline in neurology. Lancet Neurol. 2004; 3:744-751

112 Nair A, Bonneau RH. Stress-induced elevation of glucocorticoids increases microglia proliferation through NMDA receptor activation. J.Neuroimmunol. 2006; 171:72-85

113 Tikka TM, Koistinaho JE. Minocycline provides neuroprotection against N-methyl-D-aspartate neurotoxicity by inhibiting microglia. J.Immunol. 2001; 166:7527-7533

114 Diguet E, Fernagut PO, Wei X, et al. Deleterious effects of minocycline in animal models of Parkinson's disease and Huntington's disease. Eur.J.Neurosci. 2004; 19:3266-3276

115 Yang L, Sugama S, Chirichigno JW, et al. Minocycline enhances MPTP toxicity to dopaminergic neurons. J.Neurosci.Res. 2003; 74:278-285
116 Li WW, Setzu A, Zhao C, Franklin RJ. Minocycline-mediated inhibition of microglia activation impairs oligodendrocyte progenitor cell responses and remyelination in a non-immune model of demyelination. J.Neuroimmunol. 2005; 158:58-66
117 Cho KO, La HO, Cho YJ, Sung KW, Kim SY. Minocycline attenuates white matter damage in a rat model of chronic cerebral hypoperfusion. J.Neurosci.Res. 2006; 83:285-291
118 Zink MC, Uhrlaub J, DeWitt J, et al. Neuroprotective and anti-human immunodeficiency virus activity of minocycline. JAMA 2005; 293:2003-2011
119 Metz LM, Zhang Y, Yeung M, et al. Minocycline reduces gadolinium-enhancing magnetic resonance imaging lesions in multiple sclerosis. Ann.Neurol. 2004; 55:756-
120 Zabad RK, Metz LM, Todoruk TR, et al. The clinical response to minocycline in multiple sclerosis is accompanied by beneficial immune changes: a pilot study. Mult.Scler. 2007; 13:517-526
121 Lampl Y, Boaz M, Gilad R, et al. Minocycline treatment in acute stroke: an open-label, evaluator-blinded study. Neurology 2007; 69:1404-1410
122 Bonelli RM, Hodl AK, Hofmann P, Kapfhammer HP. Neuroprotection in Huntingtons disease: a 2-year study on minocycline. International Clinical Psychopharmacology 2004; 19:337-342
123 Radewicz K, Garey LJ, Gentleman SM, Reynolds R. Increase in HLA-DR immunoreactive microglia in frontal and temporal cortex of chronic schizophrenics. J.Neuropathol.Exp.Neurol. 2000; 59:137-150
124 Wierzba-Bobrowicz T, Lewandowska E, Lechowicz W, Stepien T, Pasennik E. Quantitative analysis of activated microglia, ramified and damage of processes in the frontal and temporal lobes of chronic schizophrenics. Folia Neuropathol. 2005; 43:81-89
125 Miyaoka T, Yasukawa R, Yasuda H, Hayashida M, Inagaki T, Horiguchi J. Possible antipsychotic effects of minocycline in patients with schizophrenia. Prog.Neuropsychopharmacol.Biol.Psychiatry 2007; 31:304-307
126 Cornet S, Spinnewyn B, Delaflotte S, et al. Lack of evidence of direct mitochondrial involvement in the neuroprotective effect of minocycline. Eur.J.Pharmacol. 2004; 505:111-119
127 Roulston CL, Lawrence AJ, Widdop RE, Jarrott B. Minocycline treatment attenuates microglia activation and non-angiotensin II [125I] CGP42112 binding in brainstem following nodose ganglionectomy. Neuroscience 2005; 135:1241-1253
128 Miyamoto K, Miyake S, Mizuno M, Oka N, Kusunoki S, Yamamura T. Selective COX-2 inhibitor celecoxib prevents experimental autoimmune encephalomyelitis through COX-2-independent pathway. Brain 2006; 129:1984-1992

129 Ni J, Shu YY, Zhu YN, et al. COX-2 inhibitors ameliorate experimental autoimmune encephalomyelitis through modulating IFN-gamma and IL-10 production by inhibiting T-bet expression. J.Neuroimmunol. 2007; 186:94-103

130 Hunter RL, Dragicevic N, Seifert K, et al. Inflammation induces mitochondrial dysfunction and dopaminergic neurodegeneration in the nigrostriatal system. J.Neurochem. 2007; 100:1375-1386

131 Przybylkowski A, Kurkowska-Jastrzebska I, Joniec I, Ciesielska A, Czlonkowska A, Czlonkowski A. Cyclooxygenases mRNA and protein expression in striata in the experimental mouse model of Parkinson's disease induced by 1-methyl-4-phenyl-1,2,3,6-tetrahydropyridine administration to mouse. Brain Res. 2004; 1019:144-151

132 Azari MF, Profyris C, Le Grande MR, et al. Effects of intraperitoneal injection of Rofecoxib in a mouse model of ALS. Eur.J.Neurol. 2005; 12:357-364

133 Sanchez-Pernaute R, Ferree A, Cooper O, Yu M, Brownell AL, Isacson O. Selective COX-2 inhibition prevents progressive dopamine neuron degeneration in a rat model of Parkinson's disease. J.Neuroinflammation. 2004; 1:6-

134 Minghetti L. Cyclooxygenase-2 (COX-2) in inflammatory and degenerative brain diseases. J.Neuropathol.Exp.Neurol. 2004; 63:901-910

135 Rogers J, Kirby LC, Hempelman SR, et al. Clinical trial of indomethacin in Alzheimer's disease. Neurology 1993; 43:1609-1611

136 Scharf S, Mander A, Ugoni A, Vajda F, Christophidis N. A double-blind, placebo-controlled trial of diclofenac/misoprostol in Alzheimer's disease. Neurology 1999; 53:197-201

137 Aisen PS, Schafer KA, Grundman M, et al. Effects of rofecoxib or naproxen vs placebo on Alzheimer disease progression: a randomized controlled trial. JAMA 2003; 289:2819-2826

138 Reines SA, Block GA, Morris JC, et al. Rofecoxib: no effect on Alzheimer's disease in a 1-year, randomized, blinded, controlled study. Neurology 2004; 62:66-71

139 Thal LJ, Ferris SH, Kirby L, et al. A randomized, double-blind, study of rofecoxib in patients with mild cognitive impairment. Neuropsychopharmacology 2005; 30:1204-1215

140 Akhondzadeh S, Tabatabaee M, Amini H, Ahmadi Abhari SA, Abbasi SH, Behnam B. Celecoxib as adjunctive therapy in schizophrenia: A double-blind, randomized and placebo-controlled trial. Schizophr.Res. 2007; 90:179-185

141 Muller N, Riedel M, Schwarz MJ. Psychotropic effects of COX-2 inhibitors--a possible new approach for the treatment of psychiatric disorders. Pharmacopsychiatry 2004; 37:266-269

Chapter 3

Positron emission tomography as an imaging tool to study herpes simplex virus type-1 infection of the brain and the accompanied microglia cell activation

Janine Doorduin, Hans C. Klein, Rudi A. Dierckx and Erik F.J. de Vries

Submitted for publication

Abstract

The herpes simplex virus type-1 (HSV-1) is implicated in the etiology of neurological disorders, like schizophrenia and Alzheimer's disease. Studying the behavior of HSV-1 infection of the brain and the accompanied microglia cells activation in animal models can be of great interest. It was therefore investigated if PET could be used to longitudinally study HSV-1 infection of the brain with [^{18}F]-FHBG and the accompanied microglia cell activation with [^{11}C]-(R)-PK11195, in a rat model of HSV-1 encephalitis (HSE).

Rats were intranasally inoculated with 1x10^{7} PFU of HSV-1. At day 7 after inoculation a PET scan was made with [^{18}F]-FHBG or [^{11}C]-(R)-PK11195, followed by ex vivo biodistribution. To longitudinally study microglia cell activation, rats were intranasally inoculated with 1x10^{3}, 1x10^{4} or 1x10^{5} PFU of HSV-1. PET imaging with [^{11}C]-(R)-PK11195 was performed at day 7 and 14 after inoculation.

Increased ex vivo uptake of [^{18}F]-FHBG (53-84%) and [^{11}C]-(R)-PK11195 (25-62%) was found in the bulbus olfactorius, cerebral cortex, brainstem and cerebellum of HSE rats, when compared to control rats. PET imaging showed similar results for [^{11}C]-(R)-PK11195, but not for [^{18}F]-FHBG. Inoculation with 1x10^{3} PFU resulted in microglia cell activation that was significantly lower (18-55%) when compared to inoculation with 1x10^{7} PFU. Inoculation with 1x10^{4} and 1x10^{5} PFU resulted in microglia cell activation similar to inoculation with 1x10^{7} PFU. Not all rats inoculated with lower dosages survived until day 14, but for those who did survive no differences in brain uptake of [^{11}C]-(R)-PK11195 were found between day 7 and 14 after inoculation.

PET has proven to be a specific and sensitive tool for monitoring HSV-1 and the related microglia cell activation in rats with herpes simplex encephalitis. Especially longitudinal follow-up of the activation of microglia cells in response to HSV-1 infection of the brain is possible using [^{11}C]-(R)-PK11195 PET. Due to spill-over effects [^{18}F]-FHBG is not suitable for PET imaging of HSE in rats.

Introduction

The herpes simplex virus type-1 (HSV-1) is a neurotropic DNA virus that is present in a large percentage of the human population and is the most common cause of viral encephalitis in the Western world [1,2]. Herpes simplex encephalitis (HSE) is an acute infection of the brain, predominately caused by HSV-1, leading to mortality in 70% of the patients if not treated with anti-viral drugs [2]. The incidence of HSE is estimated at two to four cases per million per year [3].

After primary infection, which is in general without clinical symptoms, HSV-1 establishes latency in the trigeminal ganglion. Reactivation of HSV-1 from the trigeminal ganglion can occur spontaneously or can be caused by a variety of factors, including stress, UV-light, and immunosuppression. HSV-1 reactivation usually results in herpes labialis (cold sore) by anterograde transport [1,3,4], but reactivation of HSV-1 can also result in retrograde transport of the virus to the brain causing HSE. This infection of the brain mainly involves the temporal cortex and limbic system structures. The clinical signs of HSE include headache, fever, changes in consciousness, confusion and sometimes psychosis [5-7].

The psychosis that occurs in HSE resembles the psychosis related to psychiatric diseases like schizophrenia. HSV-1 and other herpes viruses, like the cytomegalovirus (CMV), have been associated with schizophrenia, its cognitive deficits and changes in brain morphology [8-11]. In addition to schizophrenia, HSV-1 is also implicated in Alzheimer's disease. HSV-1 was found to affect the same brain areas which are affected in Alzheimer's disease and the long-term effects of HSE include memory loss and cognitive decline, which are also characteristic of Alzheimer's disease [12]. It has been shown that HSV-1 is present in the brains of healthy subjects [13] and it has been proposed that reactivation of HSV-1 that is present in the brain plays a role in Alzheimer's disease and causes the psychotic episodes of schizophrenic patients. Because environmental or genetic factors influence the HSV-1 infection of the brain, different diseases can emerge from reactivation of the virus.

One common finding in HSE, schizophrenia and Alzheimer's disease is the presence of neuroinflammation [14-18]. Neuroinflammation is characterized by the presence of activated microglia cells, which are the resident macrophages of the brain. In the healthy, brain microglia cells are resting, but in response to brain injury by for example HSV-1 infection the microglia cells become activated. Activated microglia cells can help damaged neurons to recover and remove irreversibly damaged neurons by

phagocytosis. It is not known when the activation of microglia cells in brain injury is beneficial or detrimental, but it has been proposed that it is beneficial in acute injury and will lead to neuronal cell death in chronic disease [19]. It has been shown with immunohistochemistry and brain cell isolation that HSV-1 infection of the rodent brain resulted in microglia cell activation [20-22]. In addition, microglia cell activation was found in HSE patients, even beyond the primary focal lesion, which persisted many months after anti-viral treatment [14].

With respect to the implications of HSV-1 infection of the brain, including its potential role in neuroinflammation in schizophrenia and Alzheimer's disease, it can be of great interest to further study the physiology of HSV-1 infection in animal models of these diseases. Positron emission tomography (PET), a non-invasive imaging technique, provides an unique tool for studying HSV-1 infection of the brain and the accompanied neuroinflammation in living subjects. The advantage of using PET over techniques such as immunohistochemistry, for which animals have to be sacrificed, is that the relation between HSV-1 and neuroinflammation can in principle be studied longitudinally in the same animal, reducing variability between individual animals and the total number of animals needed.

HSV-1 infection of the brain can be imaged using the PET tracer 9-(4-[^{18}F]-fluoro-3-hydroxymethylbutyl)guanine ([^{18}F]-FHBG). [^{18}F]-FHBG is the radiolabelled form of the antiviral drug penciclovir, which is a prodrug that is activated by phosphorylation by HSV thymidine kinase (HSVtk). HSVtk is only expressed by active, replicating viruses. In cells where active HSV-1 is present, [^{18}F]-FHBG will be phosphorylated by HSVtk, resulting in trapping of phosphorylated [^{18}F]-FHBG inside the cell [23]. [^{18}F]-FHBG is not phosphorylated by innate human or rodent thymidine kinase, thus increased uptake of the tracer represents the presence of active HSV-1. The neuroinflammation occurring in response to HSV-1 infection of the brain can be imaged using the PET tracer *(R)-N*-[^{11}C]-methyl-*N*-(1-methylpropyl)-1-(2-chlorophenyl)isoquinoline-3-carboxamide ([^{11}C]-*(R)*-PK11195) [24]. [^{11}C]-*(R)*-PK11195 is a ligand of the peripheral benzodiazepine receptor (PBR), which is present in the outer mitochondrial membrane in microglia. Activated microglia cells show an increased expression of the PBR and increased binding of [^{11}C]-*(R)*-PK11195 in the brain thus represents the presence of activated microglia cells, i.e. neuroinflammation.

The aim of the present study was to determine if [^{18}F]-FHBG and [^{11}C]-*(R)*-PK11195 PET are valid tools to longitudinally study HSV-1 infection of the brain and the related microglia cell activation in a rat model of HSE.

Material and methods

[^{18}F]-FHBG synthesis

[^{18}F]-FHBG was prepared as described by Alauddin *et al.* [23] with some modifications. A solution of 1 mg N^2-(p-anisyldiphenylmethyl)-9-[(4-tosyl)-3-p-anisyldiphenylmethoxy-methylbutyl]guanine (ABX, Germany) in 0.5 ml of dry acetonitrile (Rathburn Chemicals Ltd, Walkerburn, Scotland) was added to the dry [^{18}F]KF/kryptofix 2.2.2 complex (5 mg K_2CO_3; 15 mg kryptofix) and heated for 30 min at 110°C. Then, 0.4 ml 1M HCl was added and the mixture was heated for 5 min at 90°C in an open vial to allow acetonitrile to evaporate. After cooling, the reaction mixture was neutralized with 1.5 ml 0.1M sodium phosphate buffer (pH 7.2). The reaction mixture was passed through a Waters alumina N seppak to remove unreacted fluoride. The product was purified by HPLC over a Hamilton PRP-1 column (250x10 mm, 10 μm) (Alltech, Breda, The Netherlands) with 7% of ethanol in water as the eluent at a flow rate of 5 ml/min. The HPLC fraction with the same retention time as an authentic reference sample was collected and sterilized over a 0.22 μm Cathivex GS filter. A sample of the product was used for quality control prior to injection. The (radio)chemical purity and specific activity were determined by reversed phase HPLC (Nova-pak C18, 150x3.9 mm, 4 μm, 5% EtOH, 1 ml/min). The presence of unreacted [^{18}F]fluoride was determined by TLC (silica, dichloromethane/methanol:7/3). [^{18}F]-FHBG was obtained in 5-10% yield (corrected for decay) with a specific activity of 22-84 GBq/μmol. The radiochemical purity was always higher than 95%. Unknown impurities were <1 mg/l, kryptofix <10 mg/l and [^{18}F]fluoride <5%.

[^{11}C]-*(R)*-PK11195 synthesis

[^{11}C]-*(R)*-PK11195 was labeled by trapping [^{11}C]-methyl iodide [25] in a solution of 1 mg *(R)*-N-desmethyl PK11195 and 10 mg potassium hydroxide in 300 μl dimethylsulfoxide. The reaction mixture was allowed to react for 1 minute at 40 °C, neutralized with 1M HCl and passed through a 45 μm Millex HV filter. The filtrate was purified by HPLC using a μBondapak C18 column (7.8x300 mm) with acetonitrile/25 mM NaH_2PO_4 (pH 3.5) (55/45) as the eluent (flow 5 ml/min). To

remove the organic solvents from the product, the collected HPLC fraction (retention time 7 min) was diluted with 100 ml of water and passed through an Oasis HLB 30 mg (1 cc) cartridge. The cartridge was washed twice with 8 ml of water and subsequently eluted with 0.7 ml of ethanol and 5 ml of water. The product was sterilized by filtration over a 0.22 μm Millex LG filter. The product was obtained in 33±15% radiochemical yield (corrected for deacy). Quality control was performed by HPLC, using a Novapak C18 column (150x3.9 mm) with acetonitrile/25 mM NaH_2PO_4 (pH 3.5) (60/40) as the eluent at a flow of 1 ml/min. The radiochemical purity was always >95% and the specific activity was 51±18 MBq/nmol.

Animals

Male outbred Wistar-Unilever (SPF) rats (301±33) were obtained from Harlan (Lelystad, The Netherlands). The rats were individually housed in Macrolon cages (38x26x24 cm) on a layer of wood shavings in a room with constant temperature (21±2°C) and fixed, 12-hour light-dark regime. Food (standard laboratory chow, RMH-B, Hope Farms, The Netherlands) and water were available ad libitum. After arrival, the rats where allowed to acclimatize for at least seven days. All experiments were approved by the Animal Ethics Committee of the University of Groningen, The Netherlands.

HSV-1 inoculation

The HSV-1 strain was obtained from a clinical isolate, cultured in Vero-cells and assayed for plaque forming units (PFU) per millilitre. The rats were slightly anaesthetized with 5% isoflurane (Pharmachemie BV, The Netherlands) and inoculated with HSV-1 by the application of 100 μl of phosphate-buffered saline with $1x10^7$ PFU of virus (or less for the rats of the dose-response study) on the nostrils (50 μl per nostril) with a micro pipette. Control rats were treated similarly by the application of 100 μl PBS without virus. Clinical symptoms in all rats were scored daily after the inoculation by the same observer.

PET imaging and ex vivo biodistribution of [^{18}F]-FHBG and [^{11}C]-*(R)*-PK11195

Active HSV-1 and the accompanied activation of microglia cells, was studied in the rat model of herpes encephalitis with [^{18}F]-FHBG and [^{11}C]-*(R)*-PK11195 PET, respectively. The rats were randomly divided into four groups: control rats (control)

scanned with [^{18}F]-FHBG (n=6), rats infected with HSV-1 (HSE) scanned with [^{18}F]-FHBG (n=8), control rats scanned with [^{11}C]-*(R)*-PK11195 (n=5) and HSE rats scanned with [^{11}C]-*(R)*-PK11195 (n=8). The PET scan was acquired when robust clinical signs of infection appeared, which was either on day six or on day seven after the inoculation with HSV-1. The rats were anaesthetized by 5% isoflurane (Pharmachemie BV, The Netherlands) that was mixed with medical air at a flow of 2 ml/min, which was maintained at 2% isoflurane during the PET scan. Following induction of anaesthesia, the rats were positioned in the small animal PET camera (Focus 220, Siemens Medical Solutions USA, Inc.) in transaxial position with their heads in the field of view. A transmission scan of 515 seconds with a Co-57 point source was obtained for the correction of attenuation by tissue. After the transmission scan was completed, the PET tracer [^{18}F]-FHBG (22±9 MBq) or [^{11}C]-*(R)*-PK11195 (65±22 MBq) was injected via the penile vein. Simultaneously with the injection of the PET tracer a dynamic emission scan of 60 min was started. The list-mode data of the emission scans was separated into 4 frames of 15 minutes. Emission sinograms were iteratively reconstructed (OSEM2d, 4 iterations) after being normalized, corrected for attenuation and for decay of radioactivity.

To perform *ex vivo* biodistribution following the PET scan, the rats were sacrificed by extirpation of the heart while under deep anaesthesia. The brain was dissected into several brain areas, peripheral organs were excised and blood was centrifuged to collect a plasma sample. The brain areas, peripheral organs and plasma were weighed and analyzed for the amount of radioactivity, using a gammacounter (LKB Wallac, Turku, Finland). Tracer uptake was expressed as the standardized uptake value (SUV), defined as: [tissue activity concentration(Bq/g))/(injected activity (bq)/rat body weight (g)].

HSV-1 dose response study with longitudinal follow-up: PET with [^{11}C]-*(R)*-PK11195

Inoculation with 1x10^{7} PFU of HSV-1 results in severely ill rats between day 7 to 9 after inoculation. Consequently, rats had to be sacrificed to prevent unnecessary suffering. In order to study the microglia cell activation in response to less severe HSV-1 infection in a longitudinal manner, rats were infected with a lower dose of HSV-1. Therefore, rats were randomly divided into three groups: rats infected with 1x10^{3} PFU of HSV-1 (n=4), rats infected with 1x10^{4} PFU of HSV-1 (n=7) and rats infected with 1x10^{5} PFU of HSV-1 (n=4). [^{11}C]-*(R)*-PK11195 small animal PET scans

were performed on day 7 and 14 after inoculation. The PET scans were performed as described above. After the PET scan on day 14 the rats were sacrificed.

PET image analysis

PET image analysis was performed using the Clinical Applications Packaging Program (CAPP5). Regions of interest were drawn around the bulbus olfactorius, frontal cortex, striatum, parietal/temporal/occipital cortex, brainstem and cerebellum in a template PET scan that was co-registered with the PET scan of interest by image fusion. The uptake of the tracer in these regions of interest was determined in Bq/cm^3, which was converted to SUV's, which was defined as: [tissue activity concentration (MBq/cc)]/[(injected dose (MBq)/body weight (g)]. It was assumed that 1 cm^3 of brain tissue equals 1 gram. The SUV's of the time frames from 30 to 45 minutes after tracer injection were used as a measure for tracer uptake, because from 30 minutes after injection the time-activity curve remains stable over time. Although the *ex vivo* biodistribution was performed at 60 minutes after injection, no differences were found in the [^{11}C]-*(R)*-PK11195 uptake, as obtained from the PET scan, between 30 and 60 minutes after injection.

Statistical analysis

All data are expressed as mean ± standard deviation. Statistical analysis was performed using SPSS for Windows, version 16.0. All between group comparisons were performed using one-way ANOVA.

Results

Clinical symptoms

Clinical symptoms (figure 1) were scored daily after inoculation and categorized into the following clinical scores: (0), no symptoms; (1), ruffled fur and irritated mouth, nose and eyes; (2), behavioral signs, like stress and lethargy, and hunched posture; (3), posterior paralysis and impairment of motor function and (4), severe paralysis, labored breathing or death.

After inoculation with the highest dose, 1x10^7 PFU of HSV-1, the first clinical symptoms in the HSE rats were seen on day four or five after inoculation, followed by

a gradual increase in the severity of the symptoms over time. At day 7 after inoculation an average clinical score of 2.5±0.5 was found.

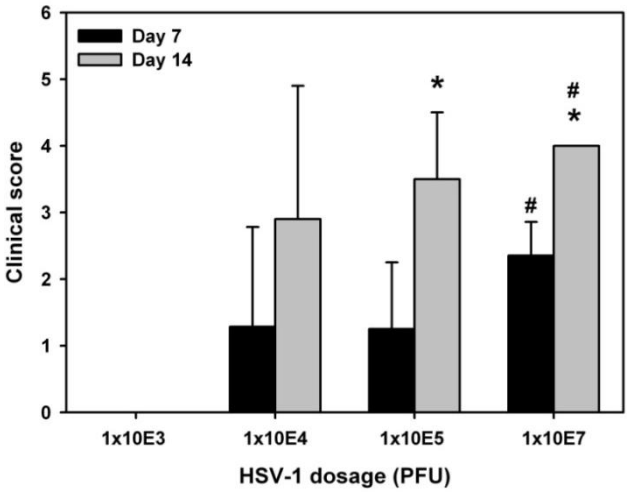

Figure 1 Clinical scores after intranasal inoculation with $1x10^3$, $1x10^4$, $1x10^5$ and $1x10^7$ PFU of HSV-1, on day 7 and 14 after inoculation. The clinical scores represent the following clinical symptoms: (0), no symptoms; (1), ruffled fur and irritated mouth, nose and eyes; (2), behavioral signs, like stress and lethargy, and hunched posture; (3), posterior paralysis and impairment of motor function and (4), severe paralysis, labored breathing or death. *$p<0.01$ for day 14 when compared to day 7 and #$p<0.05$ for $1x10^7$ PFU when compared to $1x10^4$ and $1x10^5$ PFU of HSV-1.

For the HSV-1 dose response study and longitudinal follow up with [^{11}C]-*(R)*-PK11195, rats were inoculated with lower dosages of HSV-1. Rats that were inoculated with $1x10^3$ PFU of HSV-1 did not show any clinical symptoms at both day 7 and 14 after inoculation.

Inoculation with $1x10^4$ PFU of HSV-1 resulted in a clinical score of 1.3±1.5 on day 7 after inoculation, which was significantly lower than the score of the rats inoculated with $1x10^7$ PFU ($p=0.031$). At day 14 after inoculation, five out of the seven rats had to be prematurely sacrificed (meaning a clinical score of 4). The two rats that survived until day 14 did not show any clinical symptoms. No statistically significant difference was found between the clinical score on day 7 (1.3±1.5) and day 14 (2.9±2.0) ($p=0.117$). The clinical score on day 14 was significantly lower when compared to the clinical score of the rats inoculated with $1x10^7$ PFU ($p=0.021$).

Rats inoculated with $1x10^5$ PFU of HSV-1 showed a clinical score of 1.3±1.0 at day 7 after inoculation, which was significantly lower when compared to the score after inoculation with $1x10^7$ PFU of HSV-1 ($p=0.016$). Of the four rats inoculated with $1x10^5$ PFU of HSV-1, one rat survived until day 14 after inoculation. The other three

rats had to be prematurely sacrificed (meaning a clinical score of 4). A statistically significant higher clinical score was found on day 14 (3.5±1.0), when compared to the score on day 7 ($p=0.007$). The clinical score on day 14 after inoculation was significantly lower than the score of the rats infected with $1x10^7$ PFU of HSV-1 ($p=0.035$).

Overall, inoculation with the dosages of $1x10^4$ and $1x10^5$ PFU of HSV-1 resulted in statistically significant lower clinical scores on day 7 and 14 after inoculation when compared to $1x10^7$ PFU of HSV-1. Rats inoculated with $1x10^3$ PFU of HSV-1 did not show any clinical symptoms. In addition, none of the control rats showed any clinical symptoms.

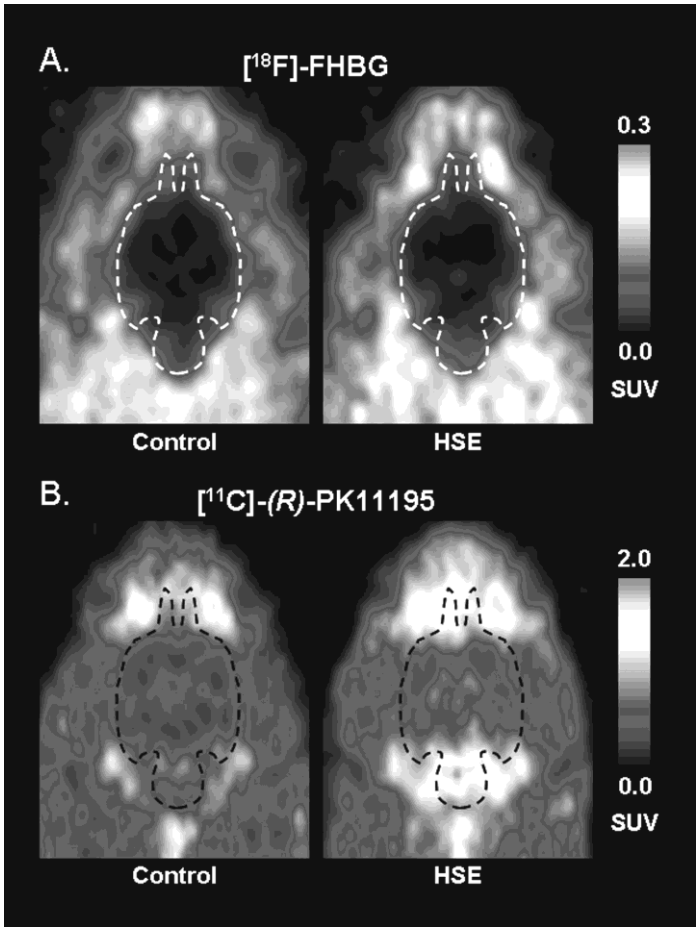

Figure 2 Full-color in appendix. [18F]-FHBG (**A**) and [11C]-*(R)*-PK11195 (**B**) PET images of a control rat (control) and a rat inoculated with $1x10^7$ PFU of HSV-1 (HSE), on 7 after inoculation. The PET images represent tracer uptake between 30 and 45 minutes after injection

Table 1 Quantitative analysis of [18F]-FHBG PET images at day 6 to 7 after inoculation. Data are expressed as standardized uptake values (SUV; mean ± standard deviation) and represent the [18F]-FHBG uptake 30 to 45 minute after tracer injection in control rats (control) and rats infected with 1x10^7 PFU of HSV-1 (HSE).

	Control (n=6)	HSE (n=8)	p-value
Bulbus olfactorius	0.096 ± 0.083	0.074 ± 0.205	0.575
Frontal cortex	0.057 ± 0.060	0.042 ± 0.171	0.625
Striatum	0.037 ± 0.031	0.029 ± 0.141	0.616
P/T/O cortex	0.048 ± 0.030	0.038 ± 0.132	0.505
Brainstem	0.056 ± 0.038	0.048 ± 0.434	0.700
Cerebellum	0.051 ± 0.026	0.047 ± 0.202	0.774

P/T/O, Parietal/Temporal/Occipital

Table 2 *Ex vivo* biodistribution of [18F]-FHBG at day 6 to 7 after inoculation, expressed as standardized uptake values (SUV; mean ± standard deviation), 60 minutes after tracer injection in control rats (control) and rats infected with HSV-1 (HSE).

	Control (n=6)	HSE (n=8)	p-value
Amygdala/Piriform cortex	0.006 ± 0.002	0.025 ± 0.032	0.165
Bulbus olfactorius	0.011 ± 0.002	0.053 ± 0.030	0.004
Cerebellum	0.008 ± 0.001	0.018 ± 0.005	0.001
Cingulate/Frontopolar cortex	0.007 ± 0.002	0.041 ± 0.037	0.047
Entorhinal cortex	0.006 ± 0.002	0.026 ± 0.029	0.138
Frontal cortex	0.005 ± 0.001	0.027 ± 0.021	0.028
Hippocampus	0.006 ± 0.002	0.019 ± 0.015	0.052
Medulla	0.011 ± 0.007	0.024 ± 0.009	0.013
P/T/O cortex	0.006 ± 0.001	0.022 ± 0.014	0.018
Pons	0.009 ± 0.004	0.022 ± 0.011	0.015
Striatum	0.008 ± 0.004	0.030 ± 0.032	0.141
Total Brain	0.008 ± 0.001	0.034 ± 0.029	0.051

P/T/O, Parietal/Temporal/Occipital

[18F]-FHBG PET imaging and ex vivo biodistribution

The [18F]-FHBG PET images (figure 2A) showed a low brain uptake, with no visual differences between control rats and rats infected with 1x10^7 PFU of HSV-1. In addition, quantitative analysis of the PET data did not reveal any differences in [18F]-FHBG uptake between control and HSV-1 infected rats (table 1). In contrast, the *ex vivo* biodistribution study showed a statistically significant increased uptake (SUV) of [18F]-FHBG in the bulbus olfactorius (80%; p=0.004), anterior cingulated/frontopolar

cortex (84%; p=0.047), frontal cortex (81%; p=0.028), parietal/temporal/occipital cortex (75%; p=0.0018), pons (60%; p=0.015), medulla (54%; p=0.013) and cerebellum (53%; p=0.001) of rats infected with HSV-1 as compared to control rats (table 2). [^{18}F]-FHBG uptake as determined by *ex vivo* biodistribution was lower in all brain regions of both control rats and rats infected with HSV-1, when compared to the [^{18}F]-FHBG uptake that was measured by PET imaging.

Table 3 Quantitative analysis [^{11}C]-*(R)*-PK11195 PET images at day 7 and 14 after inoculation. Data are expressed as standardized uptake values (SUV; mean ± standard deviation) and represent the [^{11}C]-*(R)*-PK11195 uptake 30 to 45 minute after tracer injection in control rats and rats infected with 1x10^3, 1x10^4, 1x10^5 or 1x10^7 PFU of HSV-1.

	Control (n=5)	**1x10^3 PFU (n=4/n=4)**	**1x10^4 PFU (n=7/n=2)**	**1x10^5 PFU (n=4/n=1)**	**1x10^7 PFU (n=4/n=1)**
Day 7 after inoculation:					
Bulbus olfactorius	0.83±0.13	1.18±0.13**, #	1.38±0.28**	1.16±0.26*	1.44±0.21**
Frontal cortex	0.44±0.05	0.70±0.02**	0.85±0.19**	0.66±0.03**	0.78±0.17**
Striatum	0.38±0.06	0.49±0.07*	0.54±0.10*	0.51±0.09*	0.59±0.14*
P/T/O cortex	0.40±0.07	0.47±0.07#	0.58±0.17	0.54±0.10	0.67±0.13**
Brainstem	0.56±0.13	0.69±0.08##	1.23±0.76	1.04±0.55	1.55±0.43**
Cerebellum	0.49±0.09	0.61±0.09##	0.88±0.43	0.82±0.33	1.03±0.20**
Day 14 after inoculation:					
Bulbus olfactorius		1.08±0.12	1.50±0.44	0.84	
Frontal cortex		0.70±0.08	1.31±0.63	0.50	
Striatum		0.47±0.04	0.99±0.67	0.48	
P/T/O cortex		0.40±0.03	0.79±0.39	0.53	
Brainstem		0.60±0.02	1.02±0.38	0.67	
Cerebellum		0.51±0.02	0.82±0.20	0.67	

P/T/O, Parietal/Temporal/Occipital; *p<0.05 and **p<0.005 when compared to control rats, #p<0.05 and ##p<0.004 when compared to rats infected with 1x10^7

[^{11}C]-(R)-PK11195 PET imaging and ex vivo biodistribution

Visual examination of the [^{11}C]-*(R)*-PK11195 PET images (figure 2B) showed an increase in [^{11}C]-*(R)*-PK11195 uptake in the caudal brain areas of HSV-1 infected rats at day 7, when compared to control rats. Quantitative PET data analysis showed a significantly higher uptake of [^{11}C]-*(R)*-PK11195 in the bulbus olfactorius (43%;

p<0.001), frontal cortex (44%; p=0.001), striatum (37%; p=0.008), parietal/temporal/occipital cortex (40%; p=0.002), brainstem (64%; p<0.001) and cerebellum (52%; p<0.001) of rats infected with HSV-1, when compared to control rats (table 3).

The *ex vivo* biodistribution (table 4) showed a significantly higher uptake of [^{11}C]-*(R)*-PK11195 in the medulla (53%; p=0.004), pons (62%; p<0.001) and cerebellum (42%; p=0.002) of rats infected with HSV-1, when compared to control rats.

HSV-1 dose response study and longitudinal follow-up: PET with [^{11}C]-(R)-PK11195

The activation of microglia cell was determined with [^{11}C]-*(R)*-PK11195 in the dose response study and longitudinal follow-up of HSV-1 infection of the brain (table 3). Because PET imaging with [^{18}F]-FHBG did not show differences between control and HSV-1 infected rats (in contrast to the *ex vivo* biodistribution) active HSV-1 in the brain could not be studied longitudinally with PET.

Although no clinical symptoms were seen after inoculation with 1x10^3 PFU of HSV-1, a significantly higher uptake of [^{11}C]-*(R)*-PK11195 was found in the bulbus olfactorius (30%; p=0.005), frontal cortex (38%; p<0.001) and striatum (23%; p=0.026) at day 7 after inoculation, when compared to control rats. The increased [^{11}C]-*(R)*-PK11195 uptake that was found at day 7 when compared to control rats, was significantly lower in the bulbus olfactorius (18%; p=0.045), parietal/temporal/occipital cortex (30%; p=0.019), brainstem (55%; p=0.003) and cerebellum (40%; p=0.003), when compared to the [^{11}C]-*(R)*-PK11195 uptake in rats infected with 1x10^7 PFU of HSV-1 at day 7 after inoculation. No differences in [^{11}C]-*(R)*-PK11195 uptake were found between day 7 and 14 in rats inoculated with 1x10^3 PFU of HSV-1.

Inoculation with 1x10^4 PFU of HSV-1, resulted in a significantly higher [^{11}C]-*(R)*-PK11195 uptake in the bulbus olfactorius (40%; p=0.002), frontal cortex (48%; p=0.001) and striatum (31%; p=0.007) at day 7 after inoculation, when compared to control rats. No statistically significant differences were found in [^{11}C]-*(R)*-PK11195 between rats inoculated with 1x10^4 and 1x10^7 PFU of HSV-1 at day 7 after inoculation. For the two rats that survived until day 14 after inoculation, no statistically significant differences were found between day 7 and 14 after inoculation with 1x10^4 PFU of HSV-1. However, one of those two rats showed a 24-63% increase in [^{11}C]-*(R)*-PK11195 uptake, which was clearly visualized with PET (figure 3).

Table 4 *Ex vivo* biodistribution of [^{11}C]-*(R)*-PK11195 at day 6 to 7 after inoculation, expressed as standardized uptake values (SUV; mean ± standard deviation), 60 minutes after tracer injection in control rats (control) and rats infected with HSV-1 (HSE).

	Control (n=5)	HSE (n=8)	p-value
Amygdala/Piriform cortex	0.37 ± 0.11	0.40 ± 0.11	0.590
Bulbus olfactorius	1.20 ± 0.37	1.59 ± 0.51	0.160
Cerebellum	0.51 ± 0.08	0.88 ± 0.19	0.002
Cingulate/Frontopolar cortex	0.31 ± 0.05	0.48 ± 0.20	0.101
Entorhinal cortex	0.33 ± 0.07	0.41 ± 0.12	0.194
Frontal cortex	0.33 ± 0.08	0.40 ± 0.13	0.281
Hippocampus	0.54 ± 0.32	0.41 ± 0.11	0.253
Medulla	0.61 ± 0.12	1.29 ± 0.42	0.004
P/T/O cortex	0.33 ± 0.08	0.40 ± 0.10	0.193
Pons	0.59 ± 0.09	1.54 ± 0.45	0.001
Striatum	0.31 ± 0.06	0.40 ± 0.13	0.222

P/T/O, Parietal/Temporal/Occipital

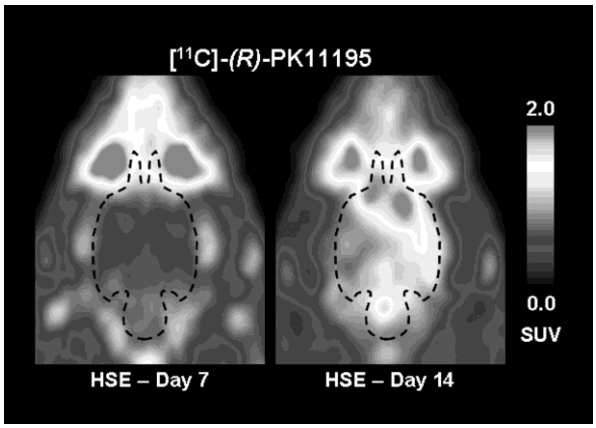

Figure 3 Full-color in appendix. [^{11}C]-*(R)*-PK11195 PET images of one rat that was inoculated with 1x10^4 PFU of HSV-1 that showed the development of severe neuroinflammation in frontal brain areas from day 7 to day 14 after inoculation. The PET images represent tracer uptake between 30 and 45 minutes after injection.

In rats that were inoculated with 1x10^5 PFU, a significantly higher uptake of [^{11}C]-*(R)*-PK11195 was found in the bulbus olfactorius (29%; p=0.048), frontal cortex (33%; p<0.001) and striatum (26%; p=0.044) at day 7 after inoculation, when compared to control rats. One rat survived until day 14 after inoculation and showed a 15-23% increase in [^{11}C]-*(R)*-PK11195 uptake when compared to day 7 after inoculation, with the exception of the bulbus olfactorius and frontal cortex where, respectively, a 41% and 34% decrease was found.

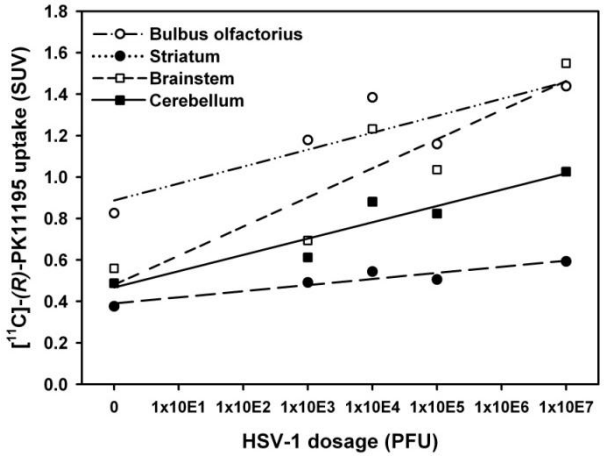

Figure 4 Correlation between the dosages of HSV-1 used for inoculation of the rats and [^{11}C]-*(R)*-PK11195 uptake (SUV) on day 7 after inoculation. The r^2 was 0.77 for the bulbus olfactorius ($p=0.051$, $y=0.89+0.08x$), 0.90 for the striatum ($p=0.015$, $y=0.39+0.03x$), 0.82 for the brainstem ($p=0.034$, $y=0.48+0.14x$) and 0.89 for the cerebellum ($p=0.015$, $y=0.47+0.08x$).

No statistically significant differences in [^{11}C]-*(R)*-PK11195 uptake were found between rats inoculated with $1x10^3$, $1x10^4$ or $1x10^5$ PFU of HSV-1. A positive linear correlation was found between the HSV-1 dosage and the [^{11}C]-*(R)*-PK11195 uptake at day 7 after inoculation. A correlation with an r^2 higher than 0.8 ($p<0.05$) was found for almost all examined brain areas, except for the bulbus olfactorius ($r^2=0.77$, $p=0.051$) and the frontal cortex ($r^2=0.58$, $p=0.137$). The correlations for the bulbus olfactorius, striatum, brainstem and cerebellum are displayed in figure 4. The slope of the linear correlation was the highest for the brainstem (0.14), suggesting that this area is most sensitive for increment of HSV-1 infection.

Taken together, all dosages of HSV-1 induced activation of microglia cells, with the higher dosages ($1x10^4$-$1x10^7$ PFU of HSV-1) resulting in death of 29 to 100% of the rats between day 7 and 14 after inoculation. In the rats that did survive no statistically significant differences in [^{11}C]-*(R)*-PK11195 uptake were found between day 7 and 14 after inoculation.

Discussion

In the present study, we demonstrated that the behavior of HSV-1 in the brain after intranasal inoculation and the activation response of microglia cells could be studied with [^{18}F]-FHBG and [^{11}C]-*(R)*-PK11195, respectively.

Increased uptake of [^{18}F]-FHBG, showing the presence of active HSV-1, was found in the bulbus olfactorius, cerebral cortex, brainstem and cerebellum on day 7 after

inoculation. The presence of HSV-1 in the brain, as shown with [^{18}F]-FHBG, is consistent with previously reported findings [26,27]. Intranasal inoculation of both mice and rats with HSV-1 resulted in the presence of HSV-1 in brain areas along the vomeronasal pathway, including the piriform cortex, entorhinal cortex and the amygdala. In addition, HSV-1 was also found to be present in the principle sensory trigeminal nucleus which is located in the brainstem.

The ability of [^{18}F]-FHBG to detect active HSV-1 in the brain is based on the expression of HSV thymidine kinase by active, replicating HSV-1. HSV thymidine kinase phosphorylates [^{18}F]-FHBG, resulting in trapping of the tracer in brain tissue. Thus increased uptake of [^{18}F]-FHBG indicates the presence of active HSV-1. Theoretically this increase could also be caused by an increased permeability of the blood-brain barrier resulting in an increased tracer influx. However, we have shown with PET that there is no increased influx of PET tracers in the brain of HSE rats, suggesting an intact blood-brain barrier (data will be published elsewhere). In addition, it was shown that the uptake of the less sensitive tracer for viral thymidine kinase, [^{18}F]-FHPG, in the encephalitic brain one hour after tracer injection is due to increased phosphorylation of the tracer and not due to an increase in the permeability of the blood-brain barrier [28]. Thus, increased [^{18}F]-FHBG uptake is probably due to the presence of replicating HSV-1.

Despite the ability of [^{18}F]-FHBG to detect active herpes virus in the brain of rats inoculated with HSV-1 with *ex vivo* biodistribution, the PET images did not reveal an increased [^{18}F]-FHBG uptake. This is probably due to the low brain uptake of [^{18}F]-FHBG and the limited spatial resolution (i.e. 1.35 mm in the center field of view) of the small animal PET camera. Since [^{18}F]-FHBG accumulation in tissues that surrounds the brain and in the ventricular system is much higher than in brain tissue, spill-over effects are likely to occur. In fact, we found that *ex vivo* biodistribution showed lower tracer uptake in brain tissue than PET. Therefore, spill-over likely obscured the differences in brain uptake between control rats and rats infected with HSV-1. However, this does not rule out the use of [^{18}F]-FHBG for imaging active herpes viruses in larger animals or humans as spill-over is less likely to occur.

Microglia cell activation in response to HSV-1 infection of the brain ($1x10^7$ PFU) was found in frontal brain areas, the brainstem and cerebellum, areas where [^{18}F]-FHBG also showed the presence of active HSV-1. Consistent with this finding, it has previously been shown that microglia cell activation followed the expression of HSV-1

antigens in the bulbus olfactorius, brainstem and cerebellum, with approximately one day delay [21].

The peak of the amount of active HSV-1 is present in the brain on day 7 to 9 after intranasal inoculation and is followed by a decrease of active HSV-1 and the supposed establishment of latency at day 14-16 after inoculation [4,22,29]. To prevent death by primary infection with $1x10^7$ PFU of HSV-1, which occurs mostly on day 7 to 9 after inoculation, rats were inoculated with $1x10^3$ to $1x10^5$ PFU of HSV-1. Inoculation with these lower dosages did result in less severe microglia cell activation in the bulbus olfactorius, frontal cortex and striatum on day 7 after inoculation. However, still most rats did not survive until day 14 after inoculation. All rats that were inoculated with $1x10^3$ PFU of HSV-1 survived and did not show changes in activated microglia cells between day 7 and 14 after inoculation, suggesting that there is only mild replication of HSV-1 in the brain in these rats that does not lead to the appearance of severe clinical symptoms or death. The present study showed that [^{11}C]-*(R)*-PK11195 can image microglia cell responses to HSV-1 infection of the brain with a low dosage and can therefore be used to study microglia cell activation longitudinally in animal models for human disease with potential viral involvement. The positive correlation between the HSV-1 dosage used for inoculation and the [^{11}C]-*(R)*-PK11195 uptake in all brain regions showed that [^{11}C]-*(R)*-PK11195 PET is a sensitive tool for imaging of small changes in microglia cell activation in response to different dosages of HSV-1.

Conclusion

Due to spill-over effects [^{18}F]-FHBG is not suitable for PET imaging of HSE in rats. In contrast, PET has proven to be a specific and sensitive tool for monitoring HSV-1 induced activation of microglia cells in rats with herpes simplex encephalitis. Longitudinal follow-up of the activation of microglia cells in response to HSV-1 infection of the brain could be studied using [^{11}C]-*(R)*-PK11195 PET. PET imaging can therefore play an important role in further elucidating the role of herpes viruses and neuroinflammation in neurological diseases, such as herpes simplex encephalitis, schizophrenia and Alzheimer's disease.

Acknowledgements

This study was funded by the Stanley Medical Research Institute, Grant-ID 05-NV-001.

References

1 Kennedy PG, Chaudhuri A. Herpes simplex encephalitis. J.Neurol.Neurosurg.Psychiatry 2002; 73:237-238

2 Whitley RJ, Kimberlin DW. Viral encephalitis. Pediatr.Rev. 1999; 20:192-198

3 Whitley RJ. Herpes simplex encephalitis: adolescents and adults. Antiviral Res. 2006; 71:141-148

4 Klein RJ. The pathogenesis of acute, latent and recurrent herpes simplex virus infections. Arch.Virol. 1982; 72:143-168

5 Kennedy PG. A retrospective analysis of forty-six cases of herpes simplex encephalitis seen in Glasgow between 1962 and 1985. Q.J.Med. 1988; 68:533-540

6 Miller JK, Hesser F, Tompkins VN. Herpes simplex encephalitis. Report of 20 cases. Ann.Intern.Med. 1966; 64:92-103

7 Misra PC, Hay GG. Encephalitis presenting as acute schizophrenia. Br.Med.J. 1971; 1:532-533

8 Dickerson FB, Boronow JJ, Stallings C, Origoni AE, Ruslanova I, Yolken RH. Association of serum antibodies to herpes simplex virus 1 with cognitive deficits in individuals with schizophrenia. Arch.Gen.Psychiatry 2003; 60:466-472

9 Leweke FM, Gerth CW, Koethe D, et al. Antibodies to infectious agents in individuals with recent onset schizophrenia. Eur.Arch.Psychiatry Clin.Neurosci. 2004; 254:4-8

10 Prasad KM, Shirts BH, Yolken RH, Keshavan MS, Nimgaonkar VL. Brain morphological changes associated with exposure to HSV1 in first-episode schizophrenia. Mol.Psychiatry 2007; 12:105-113

11 Shirts BH, Prasad KM, Pogue-Geile MF, Dickerson F, Yolken R, Nimgaonkar VL. Antibodies to cytomegalovirus and Herpes Simplex Virus 1 associated with cognitive function in schizophrenia. Schizophr.Res. 2008; 106:268-274

12 Itzhaki RF, Wozniak MA, Appelt DM, Balin BJ. Infiltration of the brain by pathogens causes Alzheimer's disease. Neurobiol.Aging 2004; 25:619-627

13 Jamieson GA, Maitland NJ, Wilcock GK, Yates CM, Itzhaki RF. Herpes simplex virus type 1 DNA is present in specific regions of brain from aged people with and without senile dementia of the Alzheimer type. J.Pathol. 1992; 167:365-368

14 Cagnin A, Myers R, Gunn RN, et al. In vivo visualization of activated glia by [11C] (R)-PK11195-PET following herpes encephalitis reveals projected neuronal damage beyond the primary focal lesion. Brain 2001; 124:2014-2027

15 Cagnin A, Rossor M, Sampson EL, Mackinnon T, Banati RB. In vivo detection of microglial activation in frontotemporal dementia. Ann.Neurol. 2004; 56:894-897

16 Doorduin J, de Vries EFJ, Willemsen ATM, Dierckx RA, Klein HC. Neuroinflammation in schizophrenic patients: a positron emission tomography study with [11C]-(R)-PK11195. Neuroimage. 2008; 41:T109

17 Groom GN, Junck L, Foster NL, Frey KA, Kuhl DE. PET of peripheral benzodiazepine binding sites in the microgliosis of Alzheimer's disease. J.Nucl.Med. 1995; 36:2207-2210
18 van Berckel BN, Bossong MG, Boellaard R, et al. Microglia Activation in Recent-Onset Schizophrenia: A Quantitative (R)-[(11)C]PK11195 Positron Emission Tomography Study. Biol.Psychiatry 2008; 64:820-822
19 Nakajima K, Kohsaka S. Microglia: neuroprotective and neurotrophic cells in the central nervous system. Curr.Drug Targets Cardiovasc.Haematol.Disord. 2004; 4:65-84
20 Barnett EM, Cassell MD, Perlman S. Two neurotropic viruses, herpes simplex virus type 1 and mouse hepatitis virus, spread along different neural pathways from the main olfactory bulb. Neuroscience 1993; 57:1007-1025
21 Esiri MM, Drummond CW, Morris CS. Macrophages and microglia in HSV-1 infected mouse brain. J.Neuroimmunol. 1995; 62:201-205
22 Marques CP, Hu S, Sheng W, Lokensgard JR. Microglial cells initiate vigorous yet non-protective immune responses during HSV-1 brain infection. Virus Res. 2006;
23 Alauddin MM, Conti PS. Synthesis and preliminary evaluation of 9-(4-[18F]-fluoro-3-hydroxymethylbutyl)guanine ([18F]FHBG): a new potential imaging agent for viral infection and gene therapy using PET. Nucl.Med.Biol. 1998; 25:175-180
24 Doorduin J, de Vries EFJ, Dierckx RA, Klein HC. PET imaging of the peripheral benzodiazepine receptor: monitoring disease progression and therapy response in neurodegenerative disorders. Curr.Pharm.Des 2008; 14:3297-3315
25 Larsen P, Ulin J, Dahlstrom K, Jensen M. Synthesis of [C-11]iodomethane by iodination of [C-11]methane. Appl.Radiat.Isot. 1997; 48:153-157
26 Beers DR, Henkel JS, Schaefer DC, Rose JW, Stroop WG. Neuropathology of herpes simplex virus encephalitis in a rat seizure model. J.Neuropathol.Exp.Neurol. 1993; 52:241-252
27 Mori I, Goshima F, Ito H, et al. The vomeronasal chemosensory system as a route of neuroinvasion by herpes simplex virus. Virology 2005; 334:51-58
28 Buursma AR, de Vries EF, Garssen J, et al. [18F]FHPG positron emission tomography for detection of herpes simplex virus (HSV) in experimental HSV encephalitis. J.Virol. 2005; 79:7721-7727
29 Webb SJ, Eglin RP, Reading M, Esiri MM. Detection of herpes simplex virus antigens in mouse brains by immunoperoxidase staining. A model for human herpes simplex encephalitis. Neuropathol.Appl.Neurobiol. 1989; 15:165-174

Chapter 4

[^{11}C]-DPA-713 and [^{18}F]-DPA-714 as new PET tracers for PBR: a comparison with [^{11}C]-*(R)*-PK11195 in a rat model of herpes encephalitis

Janine Doorduin, Hans C. Klein, Rudi A. Dierckx, Michelle James, Michael Kassiou and Erik F.J. de Vries

Mol Imaging Biol 2009; 11: 386-398

Abstract

Activation of microglia cells plays an important role in neurological diseases. Positron emission tomography (PET) with [^{11}C]-*(R)*-PK11195 has already been used to visualize activated microglia cells in neurological diseases. However, [^{11}C]-*(R)*-PK11195 may not possess the required sensitivity to visualize mild neuroinflammation. In this study we evaluated the PET tracers [^{11}C]-DPA-713 and [^{18}F]-DPA-714 as agents for imaging of activated microglia in a rat model of herpes encephalitis.

Rats were intranasally inoculated with HSV-1. On day six or seven after inoculation, small animal PET studies were performed to compare [^{11}C]-*(R)*-PK11195, [^{11}C]-DPA-713 and [^{18}F]-DPA-714.

Uptake of [^{11}C]-DPA-713 in infected brain areas was comparable to that of [^{11}C]-*(R)*-PK11195, but [^{11}C]-DPA-713 showed lower non-specific binding. Non-specific uptake of [^{18}F]-DPA-714 was lower than that of [^{11}C]-*(R)*-PK11195. In the infected brain, total [^{18}F]-DPA-714 uptake was lower than that of [^{11}C]-*(R)*-PK11195, with comparable specific uptake.

[^{11}C]-DPA-713 may be more suitable for visualizing mild inflammation than [^{11}C]-*(R)*-PK11195. In addition, the fact that [^{18}F]-DPA-714 is an agonist PET tracer opens new possibilities to evaluate different aspects of neuroinflammation. Therefore, both tracers warrant further investigation in animal models and in a clinical setting.

Introduction

Neurological disorders are a significant burden to society world-wide; especially in countries were a growing proportion of the population is over 65 years old [1]. Despite the large difference between neurological disorders, neuroinflammation is involved in both acute pathology, such as stroke and herpes encephalitis, and chronic neurodegenerative diseases, such as Parkinson's and Alzheimer's disease. Although neuroinflammation was found to be involved in neurological disorders, it is still not known when the inflammatory response is beneficial, detrimental or incidental. Nakajima and Kohsaka [2] proposed that neuroinflammation in acute injuries is beneficial, whereas it will lead to neuronal cell death in chronic diseases. When the exact role of neuroinflammation in different neurological disorders is unravelled, this will inevitably lead to early diagnosis, possible therapeutic intervention and improved treatment.

One of the key players in neuroinflammation is the microglia cell, which provides the first line of defence against brain tissue injuries. In the healthy central nervous system, microglia cells continuously survey their microenvironment by rapid extension and extraction of their ramified processes [3,4]. In response to a wide variety of central nervous system insults, microglia cells become activated and change from their ramified state into amoeboid morphology. The activation of microglia cells is accompanied by an increased expression of the peripheral benzodiazepine receptor, an 18 KDa component of a heteromeric complex. The expression of the PBR is low in the healthy brain, but is highly upregulated in neuroinflammation.

Positron emission tomography (PET) is a non-invasive imaging technique that can be used to study the role of neuroinflammation in neurological disorders, using the PBR as a biomarker. PET has already been used in numerous clinical studies to visualize activated microglia cells using the isoquinoline [11C]-*(R)*-PK11195 (*(R)-N*-methyl-*N*-(1-methylpropyl)-1-(2-chlorophenyl)isoquinoline-3-carboxamide) as the tracer. [11C]-*(R)*-PK11195 is a ligand for the PBR. Although [11C]-*(R)*-PK11195 has already been used to image activated microglia cells in, amongst others, stroke [5-8], multiple sclerosis [9-12], herpes encephalitis [13], Parkinson's disease [14,15] and Alzheimer's disease [16-18], it is not an ideal tracer, since it shows low brain uptake and high non-specific binding. Pharmacokinetic modeling of the PET data is complicated and [11C]-*(R)*-PK11195 may not possess the sensitivity to visualize mild neuroinflammation,

which makes it unsuitable for the use in early diagnosis and detection of subtle effects of therapeutic intervention.

Therefore, a more sensitive and specific PET tracer for PBR imaging would be of great interest. Pyrazolopyrimidines display high affinity for the PBR and two compounds from this class have already been radiolabeled for the use in PET. The pyrazolopyrimidines DPA-713 and DPA-714 have higher affinity for the PBR *in vitro* (Ki = 4.7 nM and Ki = 7.0 nM, respectively) than PK11195 (Ki = 9.3 nM) [19-21]. The PBR antagonist DPA-713 was labeled with carbon-11 and evaluated *in vivo* in a healthy baboon [22]. It was concluded that [^{11}C]-DPA-713 is a specific ligand for the PBR and that it may be useful for studying changes in the density of PBR binding sites. In addition, [^{11}C]-DPA-713 exhibited a higher signal-to-noise ratio than [^{11}C]-*(R)*-PK11195 in a rat model of neurodegeneration, which makes it more suitable for quantification of PBR binding sites [23]. The PBR agonist, DPA-714, was labeled with fluorine-18 and demonstrated good uptake in the primate brain and an 8-fold higher uptake in the lesioned striatum of a quinolinic acid lesioned rat model of activated microglia [19,20]. This higher uptake was shown to be selective PBR binding.

Both [^{11}C]-DPA-713 and [^{18}F]-DPA-714 have demonstrated better imaging properties than [^{11}C]-*(R)*-PK11195 in striatum lesioned rats [19,20,23]. However, striatum lesion by injection of a toxic compound requires invasive manipulations to generate an inflammatory response. The aim of this study was to validate these tracers in a different rat model that does not require invasive manipulation and unnatural toxic compounds to evoke neuroinflammation, which may better mimic microglia activation in neurological disorders. Therefore, [^{11}C]-DPA-713 and [^{18}F]-DPA-714 were evaluated in a rat model of herpes encephalitis (HSE) and compared to [^{11}C]-*(R)*-PK11195.

Materials and methods

[^{11}C]-*(R)*-PK11195

[^{11}C]-*(R)*-PK11195 was labeled by trapping [^{11}C]-methyl iodide [24] in a solution of 1 mg *(R)*-N-desmethyl PK11195 and 10 mg potassium hydroxide in 300 µl dimethylsulfoxide. The reaction mixture was allowed to react for 1 minute at 40 °C, neutralized with 1M HCl and passed trhough a 45 µm Millex HV filter. The filtrate was purified by HPLC using a µBondapak C18 column (7.8x300 mm) with acetonitrile/25 mM NaH_2PO_4 (pH 3.5) (55/45) as the eluent (flow 5 ml/min). To

remove the organic solvents from the product, the collected HPLC fraction (retention time 7 min) was diluted with 100 ml of water and passed through an Oasis HLB 30 mg (1 cc) cartridge. The cartridge was washed twice with 10 ml of water and subsequently eluted with 0.7 ml of ethanol and 5 ml of water. The product was sterilized by filtration over a 22 μm Millex LG filter. The product was obtained in 33±15% radiochemical yield (n=11). Quality control was performed by HPLC, using a Novapak C18 column (150x3.9 mm) with acetonitrile/25 mM NaH_2PO_4 (pH 3.5) (60/40) as the eluent at a flow of 1 ml/min. The radiochemical purity was always >95% and the specific activity was 51±18 MBq/nmol.

[11C]-DPA-713 (Compound 2)

For the preparation of *N,N*-diethyl-2-(2-(4-[11C]methoxyphenyl)-5,7-dimethylpyrazolo(1,5-*a*)pyrimidin-3-yl)acetamide (Compound 2, [11C]DPA-713), [11C]-methyl triflate was trapped in a solution of 1 mg *N,N*-diethyl-2-(2-(4-hydroxyphenyl)-5,7-dimethylpyrazolo(1,5-*a*)pyrimidin-3-yl)acetamide (Compound 1) [22] and 2.5 μl 0.5 M NaOH in 0.5 ml of acetonitrile (figure 1). After 5 minutes at 100°C, the reaction mixture was diluted with 0.5 ml of acetonitrile and 1 ml of water and purified by HPLC using a SymmetryPrep C18 column (7μ, 7.8x300 mm) and acetonitrile/0.1 M NaH_2PO_4 (1/1) as the eluent (flow 5 ml/min). The radioactive product with a retention time of 7-8 min was collected. The product was diluted with 100 ml of water and passed through an Oasis HLB 30 mg (1 cc) cartridge. The cartridge was washed twice with 10 ml of water and subsequently eluted with 0.7 ml of ethanol and 5 ml of water. The product was sterilized by filtration over a 22 μm Millex LG filter. The product is obtained in 48±15% radiochemical yield (n=10). Quality control was performed by HPLC, using a Novapak C18 column (150x3.9 mm) with acetonitrile/25 mM NaH_2PO_4 (40/60) as the eluent at a flow of 1 ml/min. The radiochemical purity of [11C]DPA-713 was always >99% and the specific activity was 41±12 MBq/nmol.

N,N-diethyl-2-(2-(4-[2-tosyloxy-1-ethoxy]phenyl)-5,7-dimethylpyrazolo(1,5-a)pyrimidin-3-yl)acetamide (Compound 3)

To a suspension of 42 mg 55% NaH (1.0 mmol) in 15 ml freshly distilled tetrahydrofuran (THF), 100 mg (0.44 mmol) of *N,N*-diethyl-2-(2-(4-hydroxyphenyl)-5,7-dimethylpyrazolo(1,5-*a*)pyrimidin-3-yl)acetamide (Compound 1) [22] was added (figure 1). After the reaction mixture was refluxed for 30 min, a solution of 300 mg

(0.87 mmol) ethyleneglycol ditosylate in 20 ml THF was quickly added to the hot reaction mixture. After another 18 h of refluxing, the reaction flask was cooled on ice and the reaction was quenched by slowly adding 50 ml of water. The mixture was extracted 3 times with 25 ml of dichloromethane. The combined organic layers were washed with 50 ml of water, dried on anhydrous sodium sulfate and filtered. The product was purified by flash column chromatography (silica gel), using 3% methanol in dichloromethane as the eluent. The product was obtained as a light yellow solid in 59% yield (140 mg). ^{1}H-NMR ($CDCl_3$, 200MHz): δ 7.83 (d, 2H, *J* = 8.1 Hz, tosyl), 7.74 (d, 2H, *J* = 8.8 Hz, Ar), 7.35 (d, 2H, *J* = 8.1 Hz, tosyl), 6.86 (d, 2H, *J* = 8.8 Hz, Ar), 6.52 (s, 1H, Ar), 4.39 (t, 2H, *J* = 4.6 Hz, CH_2O), 4.19 (t, 2H, *J* = 4.6 Hz, CH_2O), 3.95 (s, 2H, $CH_2C{=}O$), 3.51 (q, 2H, *J* = 7.1 Hz, CH_2N), 3.40 (q, 2H, *J* = 7.1 Hz, CH_2N), 2.75 (s, 3H, CH_3), 2.58 (s, 3H, CH_3), 2.45 (s, 3H, tosyl), 1.21 (t, 3H, *J* = 7.1 Hz, $CH_2\mathit{CH_3}$), 1.11 (t, 3H, *J* = 7.1 Hz, $CH_2\mathit{CH_3}$).

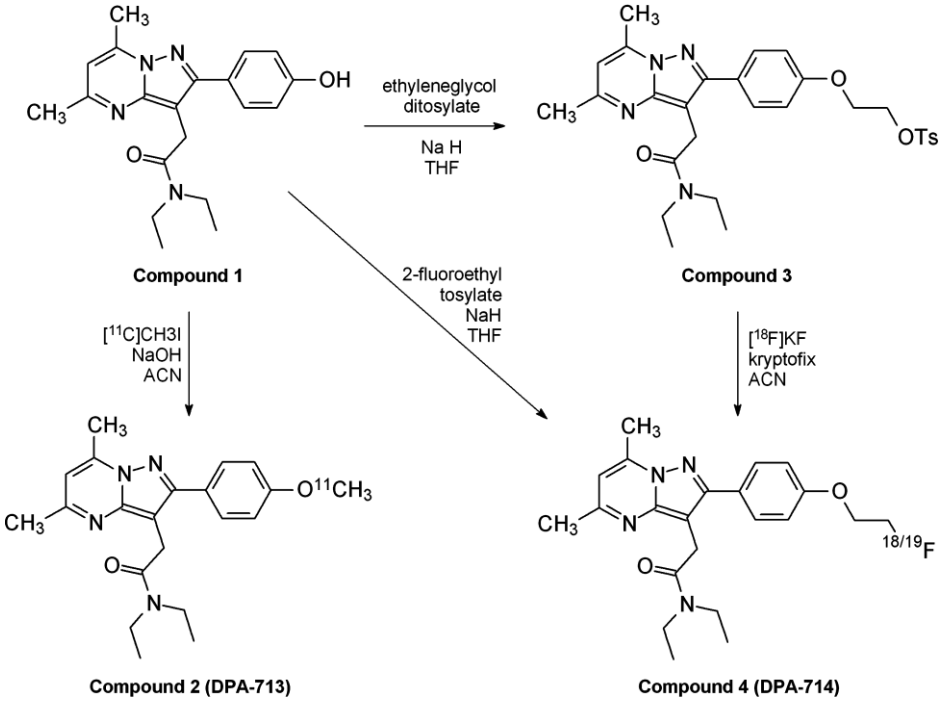

Figure 1 Synthesis of DPA-713 from the labeling precursor compound 1 and DPA-714 from the labeling precursor compound 3. The labeling precursor compound 3 and the reference material for DPA-714 were synthesized from compound 1 using ethyleneglycol ditosylate and 2-fluoroethyltosylate as the alkylating agent, respectively.

N,N-diethyl-2-(2-(4-[2-fluoro-1-ethoxy]phenyl)-5,7-dimethylpyrazolo(1,5-a)pyrimidin-3-yl)acetamide (Compound 4, DPA-714)

Reference material of DPA-714 (Compound 4) was prepared as described for Compound 3, except 2-fluoroethyl tosylate was used as the alkylating agent instead of ethyleneglycol ditosylate (figure 1). Yield: 80% (light yellow solid). ^{1}H-NMR ($CDCl_3$, 200MHz): δ 7.74 (d, 2H, *J* = 8.1 Hz, Ar), 6.99 (d, 2H, *J* = 8.1 Hz, Ar), 6.54 (s, 1H, Ar), 4.77 (dd, 2H, *J* = 2.9 Hz, *J* = 47.6 Hz, CH_2F), 4.26 (dd, 2H, *J* = 2.9 Hz, *J* = 27.5 Hz, CH_2O), 4.05 (s, 2H, $CH_2C{=}O$), 3.51 (q, 2H, *J* = 7.0 Hz, CH_2N), 3.41 (q, 2H, *J* = 7.0 Hz, CH_2N), 2.78 (s, 3H, CH_3), 2.64 (s, 3H, CH_3), 1.23 (t, 3H, *J* = 7.0 Hz, $CH_2\mathit{CH_3}$), 1.12 (t, 3H, *J* = 7.0 Hz, $CH_2\mathit{CH_3}$).

[18F]-DPA-714 ([18F]-Compound 4)

[18F]Fluoride was eluted from a Waters QMA anion exchange cartridge with 5 mg potassium carbonate in 1 ml of water and collected into a vial containing 20 mg kryptofix[2.2.2]. [18F]KF/kryptofix[2.2.2] was dried by azeotropic distillation with acetonitrile at 130°C. A solution of 1 mg Compound 3 in 0.5 ml dry DMF was added to the [18F]KF/kryptofix complex. The reaction mixture was allowed to react for 10 minutes at 100°C. After cooling, the reaction mixture was diluted with water and HPLC eluent (acetonitrile/0.1 M NaH_2PO_4 (45/55)) and passed through an Alumina N seppak to remove the majority of unreacted [18F]fluoride. The product was purified by HPLC using a SymmetryPrep C18 column (7μ, 7.8x300 mm) with acetonitrile/0.1 M NaH_2PO_4 (45/55) as the eluent (flow 5 ml/min). To remove the organic solvents from the product, the collected HPLC fraction (retention time 11 min) was diluted with 15 ml of water and passed through an Oasis HLB 30 mg (1 cc) cartridge. The cartridge was washed with 5 ml of water and subsequently eluted with 0.7 ml of ethanol and 5 ml of water. The product was sterilized by filtration over a 22 μm Millex LG filter. The product was obtained in 17±8% radiochemical yield. Quality control was performed by HPLC, using a Novapak C18 column (150x3.9 mm) with acetonitrile/25 mM NaH_2PO_4 (35/65) as the eluent at a flow of 1 ml/min. The radiochemical purity was >99% and the specific activity was 80±35 MBq/nmol (n=11).

Animals

Male outbred Wistar-Unilever (SPF) rats (weight 287±38 grams) were obtained from Harlan (Lelystad, The Netherlands). The rats were individually housed in Macrolon

cages (38x26x24 cm) on a layer of wood shavings in a room with constant temperature (21±2°C) and fixed, 12-hour light-dark regime. Food (standard laboratory chow, RMH-B, Hope Farms, The Netherlands) and water were available ad libitum. After arrival, the rats where allowed to acclimatize for at least seven days. The rats were randomly divided into nine groups: control rats (control) scanned with either [^{11}C]-*(R)*-PK11195 (n=5), [^{11}C]-DPA-713 (n=5) or [^{18}F]-DPA-714 (n=5), rats infected with HSV-1 (HSE) scanned with either [^{11}C]-*(R)*-PK11195 (n=9), [^{11}C]-DPA-713 (n=9) or [^{18}F]-DPA-714 (n=9) and rats infected with HSV-1 and pretreated with PK11195 (HSE pre-treated with PK11195) scanned with either [^{11}C]-*(R)*-PK11195 (n=4), [^{11}C]-DPA-713 (n=4) or [^{18}F]-DPA-714 (n=4). After PET scanning, the rats were scarified and the *ex vivo* biodistribution of the tracers was determined. The study was approved by the Animal Ethics Committee of the University of Groningen, The Netherlands.

HSV-1 inoculation

The HSV-1 strain was obtained from a clinical isolate, cultured in Vero-cells and assayed for plaque forming units (PFU) per milliliter. The rats were slightly anaesthetized with 5% isoflurane (Pharmachemie BV, The Netherlands) and inoculated with HSV-1 by the application of 100 µl of phosphate-buffered saline with 1x10^{7} PFU of virus on the nostrils (50 µl per nostril) with a micro pipette. Control rats were treated similarly by the application of 100 µl PBS without virus. Clinical symptoms in all rats were scored daily after the inoculation by the same observer.

Immunohistochemistry

Immunohistochemical staining was performed in control and HSV-1 infected rats on day 7 after inoculation. The rats were euthanized, the brains were removed and frozen at -80°C. Coronal brain sections of 10 µm were cut at -18°C using a cryostat (Leica Microsystems, Germany). Sections were collected on slides, vacuum dried, fixated for 20 min in paraformaldehyde (4% in 100 nM PBS) and washed 3 times for 5 min in 100 nM PBS. To block non-specific binding, sections were incubated with 5% normal goat serum in PBS containing 3% triton and washed for 5 min in 100 nM PBS. Sections were incubated overnight at 4°C with the primary antibody (Anti Iba1 Rabbit (1:750), Wako Chemicals, USA). After incubation, sections were washed 3 times for 5 min in 100 nM PBS and incubated for 1 h with the secondary antibody (FITC-conjugated Goat Anti Rabbit IgG (1:250), Jackson ImmunoResearch Laboratories

Inc., USA) in 1% normal goat serum in PBS containing 3% triton. As a negative control, sections were only incubated with the secondary antibody. Subsequently, sections were washed 3 times for 5 min in PBS and mounted with Mowiol Mounting Medium. The fluorescence was examined by using a microscope (Zeiss Axioskop 2, Carl Zeiss Microimaging Inc., Germany) in combination with the Leica Application Suite (Version 2.3.3 R1, Leica, Germany).

PET studies

PET scans were performed when robust clinical signs of infection appeared, which was either on day six or on day seven after the inoculation with HSV-1. The rats were anaesthetized by an intraperitoneal injection of medetomidine (Domitor, Pfizer, The Netherlands, 0.2 mg/kg) and ketamine (Ketanest, Pfizer, The Netherlands, 25 mg/kg), after which the rats were positioned in the small animal PET camera (Focus 220, Siemens Medical Solutions USA, Inc.) in transaxial position with their heads in the field of view. A transmission scan of 515 seconds with a Co-57 point source was obtained for the correction of attenuation by tissue. After the transmission scan was completed, the PET tracer [11C]-*(R)*-PK11195 (65±22 MBq, 0.71±0.48 μg), [11C]-DPA-713 (82±23 MBq, 0.91±0.31 μg) or [18F]-DPA-714 (37±12 MBq, 0.36±0.18 μg) was injected via the penile vein. Simultaneously with the injection of the PET tracer an emission scan of 62 min was started for [11C]-*(R)*-PK11195 and [11C]-DPA-713, and a PET scan of 120 min for [18F]-DPA-714. In the pretreated group, unlabeled PK11195 (Sigma-Aldrich, USA, 5 mg/kg in dimethylsulfoxide at a concentration of 10 mg/ml) was administered via the tail vein 5 minutes prior to injection of the PET tracer.

The list-mode data of the emission scans was separated into 21 frames (8x30, 3x60, 2x120, 2x180, 3x300 and 3x600 seconds) for [11C]-*(R)*-PK11195 and [11C]-DPA-713, and into 28 frames for [18F]-DPA-714 (8x30, 4x60, 3x120, 2x180, 4x300 and 8x600 seconds). Emission sinograms were iteratively reconstructed (OSEM2d, 4 iterations) after being normalized, corrected for attenuation and corrected for decay of radioactivity.

PET image analysis

PET image analysis was performed using the Clinical Applications Packaging Program (CAPP5). Regions of interest were drawn around the bulbus olfactorius, frontal cortex, striatum, parietal/temporal/occipital cortex, brainstem and cerebellum in a

template PET scan that was co-registered with the PET scan of interest by image fusion. The time-activity curves per region of interest were determined in Bq/cm^3 units and converted into Standardized Uptake Values (SUV), defined as: [tissue activity concentration (MBq/g)]/[(injected dose (MBq)/body weight (g)]. It was assumed that 1 cm^3 of brain tissue equals 1 gram. To correct for the activity in plasma, each point on the time-activity curve (SUV) was divided by the *ex-vivo* plasma uptake (SUV) at t=60 minutes for [^{11}C]-*(R)*-PK11195 and [^{11}C]-DPA-713, and at t=120 minutes for [^{18}F]-DPA-714 creating a tissue/plasma ratio.

Ex vivo biodistribution

After the PET scan the rats were sacrificed by extirpation of the heart while under deep anesthesia. The brain was dissected into several brain areas, peripheral organs were excised and blood was centrifuged to collect a plasma sample. The brain areas, peripheral organs and plasma were weighed and analyzed for the amount of radioactivity by using a gammacounter (LKB Wallac, Turku, Finland). Tracer uptake is expressed as the SUV.

To correct for activity of the tracers in plasma, the tissue/plasma ratio was calculated by dividing the uptake (SUV) in the different brain areas by the plasma uptake (SUV), for all rats individually. Subsequently, the PBR specific uptake was calculated for control and HSE rats. The specific uptake was calculated by subtracting the average tissue/plasma ratio of the HSE rats pre-treated with PK11195 from the tissue/plasma ratio of control and HSE rats, for each rat individually.

Statistical analysis

All data are expressed as mean ± standard deviation. Statistical analysis was performed using SPSS for Windows, version 14.0.2. Statistical analysis on differences between the uptake of [^{11}C]-*(R)*-PK11195, [^{11}C]-DPA-713 and [^{18}F]-DPA-714, which were obtained from the PET scan, was performed by one-way ANOVA. Per brain area, a Bonferonni post-hoc test was used to determine if the there were differences in uptake between the PET tracers. For the *ex vivo* biodistribution, statistical analysis on differences in uptake between control rats, HSE rats and HSE rats pre-treated with PK11195 was performed by a one-way ANOVA, using a Bonferonni post-hoc test to compare the three conditions per brain area. Statistical analysis on differences between non-specific and specific uptake of [^{11}C]-*(R)*-PK11195, [^{11}C]-DPA-713 and [^{18}F]-DPA-714 was performed by one-way ANOVA, using a Bonferonni post-hoc test to

compare the uptake of the PET tracers per brain area. The time-activity curves were analyzed with the Repeated Measures General Linear Model of SPSS (version 14.0.2) using a Bonferroni post-hoc test per brain area. Correlations of specific binding in control rats for [11C]-*(R)*-PK11195, [11C]-DPA-713 and [18F]-DPA-714 with [3H]-PK11195 binding as determined by Kurumaji *et al.* [25], were assessed with Pearson's product moment correlation coefficient (r). Significance was reached when the *P* value was <0.05.

Results

Clinical symptoms

Clinical symptoms were scored daily up to seven days post inoculation and categorized into the following clinical scores: (0), no symptoms; (1), ruffled fur and irritated mouth, nose and eyes; (2), behavioral signs, like stress and lethargy, and hunched posture; (3), posterior paralysis and impairment of motor function and (4), severe paralysis, labored breathing or death. The first clinical symptoms in the HSE rats were seen on day four or five after inoculation with HSV-1, after which the severity of the symptoms increased. For both [11C]-*(R)*-PK11195 and [11C]-DPA-713 most rats had a score of 2 at the day of scanning, whereas most rats scanned with [18F]-DPA-714 had a score of 3. The average of the scores (2.44 ± 0.73 for [11C]-*(R)*-PK11195, 2.11 ± 0.78 for [11C]-DPA-713 and 2.67 ± 0.71 for [18F]-DPA-714) did not differ significantly between groups. None of the control rats showed any clinical symptoms.

Immunohistochemistry

At day 7 after inoculation with HSV-1, intense microglial activation was observed in the bulbus olfactorius, cerebellum and brainstem (figure 2). In addition, mild microglial activation was also seen in the frontal cortex and hippocampus of HSV-1 infected rats. The activated microglia cells could be recognized by the rounded shape with short processes, showing that the microglia cells had converted to the macrophage-like state. Microglial activation in the brainstem was observed throughout the whole brainstem and could not be attributed to a specific area. In control rats, only ramified, resting microglia cells were observed in all brain areas.

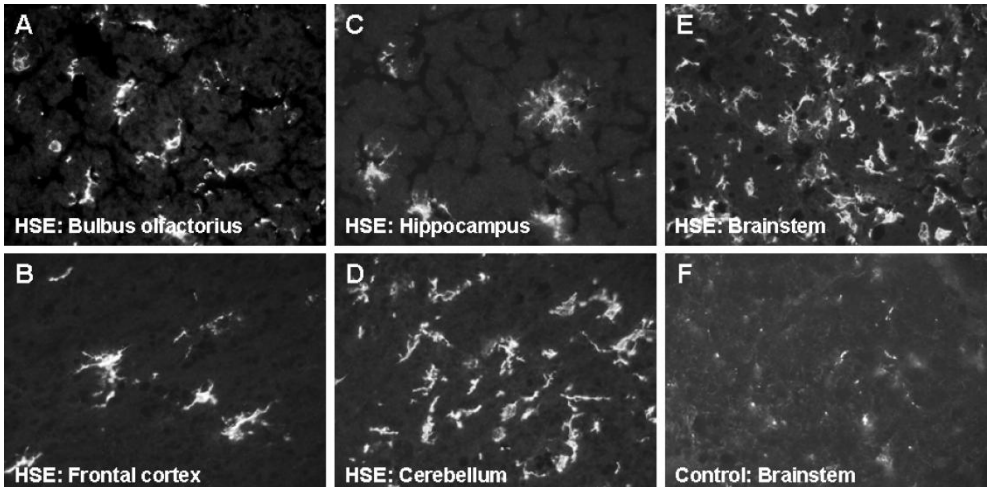

Figure 2 Images (400x) of immunohistochemical staining of microglia cells with Iba, on day 7 after inoculation. For rats infected with HSV-1 (HSE) microglia are shown in the bulbus olfactorius, frontal cortex, hippocampus, cerebellum and brainstem (**A-E**). For control rats only the brainstem (**F**) is shown. The staining in this brain area is representative for the staining in all other brain areas of control rats.

Small animal PET imaging

The standardized uptake values obtained from the last 10 min of the PET scans are displayed in table 1. The uptake of [^{11}C]-(R)-PK11195 in the last 10 min of the scan was significantly higher in the bulbus olfactorius, frontal cortex, parietal/temporal/occipital cortex, cerebellum and brainstem in HSE rats when compared to control rats. The uptake was consistent with the immunohistochemistry data. The [^{11}C]-(R)-PK11195 uptake in the rats pre-treated with PK11195 was significantly decreased in the bulbus olfactorius, cerebellum and brainstem. For [^{11}C]-DPA-713, a significant increase in tracer uptake was found in the brainstem and a non-significant increase in the bulbus olfactorius of HSE rats, as compared to control rats. Also, [^{11}C]-DPA-713 showed a statistically significant reduction in uptake by pre-treatment with PK11195 in the bulbus olfactorius, frontal cortex, parietal/temporal/occipital cortex, cerebellum and brainstem. The uptake of [^{18}F]-DPA-714 derived from the PET scan was found to be non-significantly higher in the bulbus olfactorius and brainstem in HSE rats, as compared to control rats. No effective blocking of [^{18}F]-DPA-714 by pre-treatment with PK11195 was found. The PET scan of [^{18}F]-DPA-714 was 120 min, while the PET scan of both [^{11}C]-*(R)*-PK11195 and [^{11}C]-DPA-713 was 60 min. For comparison, the uptake [^{18}F]-DPA-714

was also determined at 60 min, but no statistically significant differences were found between the uptake of [18F]-DPA-714 at 60 min and 120 min.

Table 1 Standardized uptake values (mean ± SD) obtained from the last 10 minutes of the PET scan of [11C]-*(R)*-PK11195, [11C]-DPA-713 and [18F]-DPA-714 in control rats (control; n=5), rats infected with HSV-1 (HSE; n=9) and rats infected with HSV-1 pre-treated with 5 mg/kg PK11195 5 minutes before tracer injection (HSE + PK11195; n=5). *p<0.05 as compared to control, †p<0.005 as compared to control, ‡p<0.05 as compared to HSE and §p<0.005 as compared to HSE.

	[11C]-(R)-PK11195	[11C]-DPA-713	[18F]-DPA-714
Control:			
Brainstem	0.50 ± 0.11	0.65 ± 0.17	0.51 ± 0.16
Bulbus olfactorius	0.70 ± 0.16	0.74 ± 0.20	0.57 ± 0.18
Cerebellum	0.41 ± 0.06	0.47 ± 0.03	0.39 ± 0.04
Frontal cortex	0.45 ± 0.07	0.44 ± 0.17	0.30 ± 0.10
P/T/O cortex	0.35 ± 0.09	0.41 ± 0.08	0.31 ± 0.05
Striatum	0.29 ± 0.07	0.29 ± 0.06	0.19 ± 0.04
HSE:			
Brainstem	1.52 ± 0.33†	1.23 ± 0.42*	0.84 ± 0.45
Bulbus olfactorius	1.29 ± 0.33†	1.10 ± 0.30	0.82 ± 0.30
Cerebellum	1.02 ± 0.24†	0.82 ± 0.33	0.41 ± 0.22
Frontal cortex	0.74 ± 0.19*	0.60 ± 0.13	0.41 ± 0.18
P/T/O cortex	0.54 ± 0.14*	0.44 ± 0.12	0.32 ± 0.09
Striatum	0.47 ± 0.13	0.34 ± 0.11	0.23 ± 0.06
HSE + PK11195:			
Brainstem	0.76 ± 0.04§	0.27 ± 0.11§	0.44 ± 0.07
Bulbus olfactorius	0.59 ± 0.07§	0.33 ± 0.10§	0.66 ± 0.20
Cerebellum	0.64 ± 0.09‡	0.26 ± 0.07‡	0.48 ± 0.05
Frontal cortex	0.62 ± 0.07	0.27 ± 0.10§	0.46 ± 0.13
P/T/O cortex	0.56 ± 0.06	0.21 ± 0.05*	0.44 ± 0.07*
Striatum	0.61 ± 0.12*	0.20 ± 0.06	0.37 ± 0.09†‡

P/T/O, Parietal/Temporal/Occipital

The time activity curves of the brainstem are displayed in figure 3, to show the kinetics of the tracer over time. These time-activity curves were normalized for activity in plasma because tracer uptake in the brain is dependent on the tracer delivery from plasma. A change in plasma activity concentration due to, for example, pre-treatment with PK11195 can thus influence brain uptake. For plasma activity normalization the uptake (SUV) on each individual time point was divided by the activity in plasma (SUV) as determined *ex vivo* on t=60 for [11C]-*(R)*-PK11195 and [11C]-DPA-713, and on t=120 for [18F]-DPA-714. Post-hoc analysis of the Repeated Measures General

Linear Model revealed that the time-activity curve of [^{11}C]-*(R)*-PK11195 in the brainstem of HSE rats was significantly higher than that of control rats ($p<0.005$) and rats pre-treated with PK11195 ($p<0.005$). For [^{11}C]-DPA-713 the time-activity curve in HSE rats was significantly higher than in the control rats ($p<0.05$) and in rats pre-treated with PK11195 ($p<0.005$). In addition, the uptake of [^{11}C]-DPA-713 over time was significantly reduced by pre-treatment with PK11195, even when compared to control rats ($p<0.05$). No differences in time-activity curves of control, HSE and pre-treated rats were found for [^{18}F]-DPA-714 in the brainstem, although pre-treatment with PK11195 non-significantly reduced the uptake in the brainstem.

Ex-vivo biodistribution: SUV

An *ex vivo* biodistribution study of the three PET tracers was performed to confirm the results of the PET studies. In addition, biodistribution allows investigation of uptake in smaller brain areas than is possible with small animal PET imaging. The *ex vivo* biodistribution, expressed as mean SUV ± SD, was consistent with the results obtained from the PET images. Uptake of [^{11}C]-*(R)*-PK11195 (table 2) in the bulbus olfactorius was increased in HSE rats as compared to control rats (1.59 vs. 1.20), however this increase did not reach statistical significance. A significant increase of [^{11}C]-*(R)*-PK11195 in HSE rats, as compared to control rats, was found in the medulla (1.29 vs. 0.61, $p=0.004$), pons (1.54 vs. 0.59, $p<0.001$) and cerebellum (0.88 vs. 0.51, $p=0.001$). [^{11}C]-*(R)*-PK11195 binding to the PBR was blocked by administration of unlabeled PK11195, resulting in a significantly lower uptake of [^{11}C]-*(R)*-PK11195 in the medulla, pons, cerebellum and bulbus olfactorius.

The *ex vivo* biodistribution of [^{11}C]-DPA-713 is shown in table 3. As was found for [^{11}C]-*(R)*-PK11195, the bulbus olfactorius in HSE rats showed an increase in [^{11}C]-DPA-713 uptake when compared to control rats (1.30 vs. 0.93), but this difference did not reach statistical significance. Uptake in the medulla (1.09 vs. 0.46, $p=0.039$) and the pons (1.12 vs. 0.46, $p=0.004$) of HSE rats was significantly elevated as compared to control rats. This was confirmed by blocking studies. Unlabeled PK11195 significantly reduced [^{11}C]-DPA-713 uptake in the bulbus olfactorius, pons and medulla. The uptake of [^{11}C]-DPA-713 in control rats was on average 26 percent lower ($p<0.005$) than the uptake of [^{11}C]-*(R)*-PK11195, suggesting less non-specific binding. In addition, the brain uptake in PK11195 pre-treated rats was significantly lower for [^{11}C]-DPA-713 than for [^{11}C]-*(R)*-PK11195 ($p<0.005$).

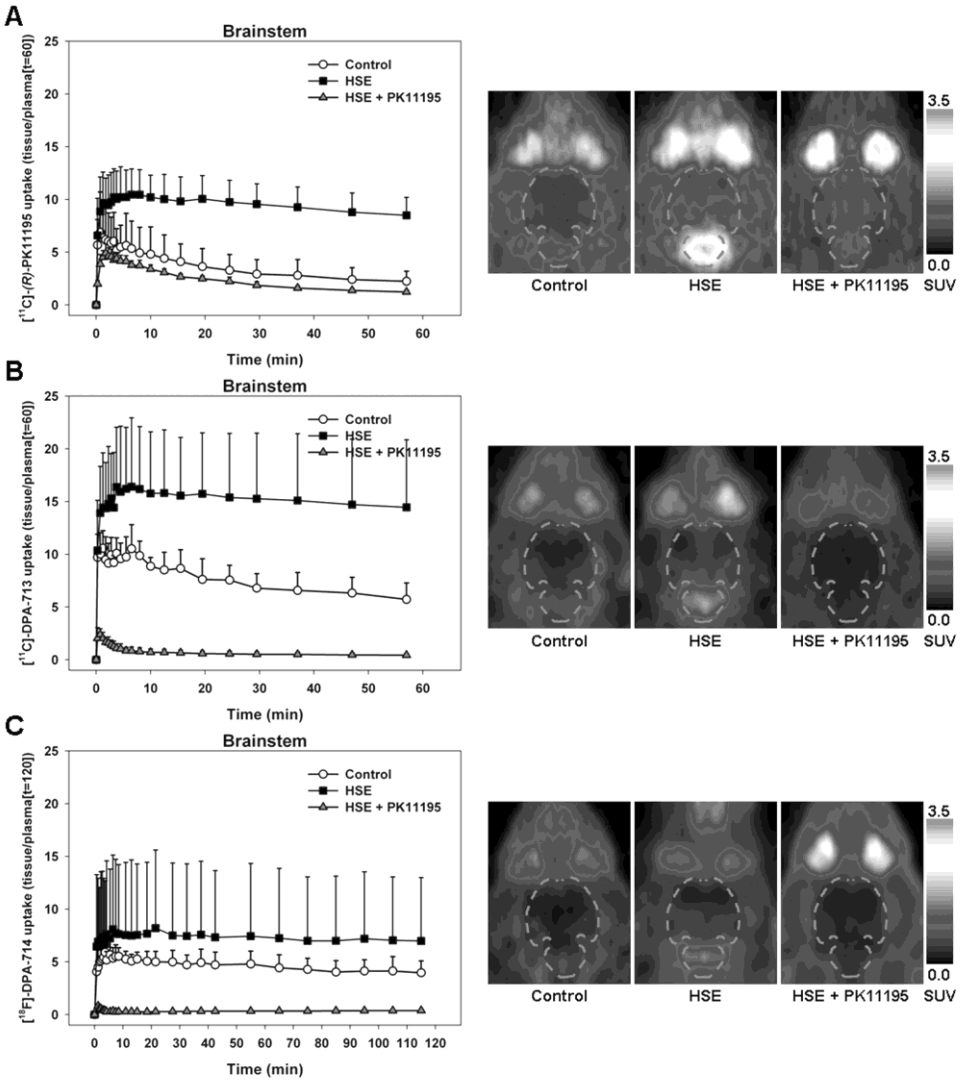

Figure 3 Full-color in appendix. Time-activity curves (left) of the brainstem for [11C]-*(R)*-PK11195 (**A**), [11C]-DPA-713 (**B**) and [18F]-DPA-714 (**C**), and small animal PET images (right) of control rats (control), rats infected with HSV-1 (HSE) and rats infected with HSV-1 injected with 5 mg/kg PK11195 5 minutes before tracer injection (HSE + PK11195). The time-activity curves are expressed as tissue uptake divided by the *ex-vivo* plasma uptake at t=60 for [11C]-*(R)*-PK11195 and [11C]-DPA-713, and at t=120 for [18F]-DPA-714. The small animal PET images display a coronal plane of the rat head at the level of the brainstem, in which the brain is delineated by a dashed line. The images are summed images between 16 and 60 minutes for [11C]-*(R)*-PK11195 and [11C]-DPA-713, and between 12 and 120 minutes for [18F]-DPA-714.

Table 2 Ex vivo biodistribution of [^{11}C]-*(R)*-PK11195, expressed as standardized uptake values (SUV; mean ± SD), 60 minutes after tracer injection in control rats (control; n=5), rats infected with HSV-1 (HSE; n=9) and rats infected with HSV-1 pre-treated with 5 mg/kg PK11195 5 minutes before tracer injection (HSE + PK11195; n=4). *p<0.05 as compared to control, †p<0.005 as compared to control, ‡p<0.05 as compared to HSE and §p<0.005 as compared to HSE.

	Control	HSE	HSE+PK11195
Brain:			
Amygdala/Piriform cortex	0.37 ± 0.11	0.40 ± 0.11	0.49 ± 0.08
Bulbus olfactorius	1.20 ± 0.37	1.59 ± 0.51	0.52 ± 0.06§
Cerebellum	0.51 ± 0.08	0.88 ± 0.19†	0.49 ± 0.07§
Cingulate/Frontopolar cortex	0.31 ± 0.05	0.48 ± 0.20	0.47 ± 0.06
Entorhinal cortex	0.33 ± 0.07	0.41 ± 0.12	0.46 ± 0.07
Frontal cortex	0.33 ± 0.08	0.40 ± 0.13	0.51 ± 0.06
Hippocampus	0.54 ± 0.32	0.41 ± 0.11	0.51 ± 0.05
Medulla	0.61 ± 0.12	1.29 ± 0.42†	0.68 ± 0.07‡
P/T/O cortex	0.33 ± 0.08	0.40 ± 0.10	0.51 ± 0.06*
Pons	0.59 ± 0.09	1.54 ± 0.45†	0.67 ± 0.08§
Striatum	0.31 ± 0.06	0.40 ± 0.13	0.53 ± 0.04*
Peripheral tissues:			
Adrenals	10.49 ± 2.22	10.12 ± 3.01	4.90 ± 0.17*‡
Bone	1.27 ± 0.23	0.95 ± 0.40	0.35 ± 0.06*‡
Lung	6.97 ± 0.63	8.83 ± 3.82	1.11 ± 0.16§
Plasma	0.22 ± 0.05	0.18 ± 0.03	0.56 ± 0.09†§

P/T/O, Parietal/Temporal/Occipital

[^{18}F]-DPA-714 uptake (table 4) in control rats was significantly lower than [^{11}C]-*(R)*-PK11195 uptake (on average 41 percent, p<0.005). Significantly increased uptake of [^{18}F]-DPA-714 was found in the medulla of HSE rats (0.40 vs. 0.81, p=0.004), when compared to control rats, while a non-significant increase in uptake was found in the bulbus olfactorius (0.55 vs. 0.88). No effective blocking of [^{18}F]-DPA-714 uptake was found after administration of unlabeled PK11195.

Ex vivo biodistribution in peripheral organs showed a high uptake of [^{11}C]-*(R)*-PK11195, [^{11}C]-DPA-713 and [^{18}F]-DPA-714 in PBR expressing organs, like the lungs and adrenals. In both the lungs and adrenals, [^{11}C]-*(R)*-PK11195 uptake was effectively blocked by unlabeled PK11195, resulting in a significant reduction in uptake, whereas the uptake of [^{11}C]-DPA-713 and [^{18}F]-DPA-714 was only significantly blocked in the lungs, but not in the adrenals.

Table 3 Ex vivo biodistribution of [11C]-DPA-713, expressed as standardized uptake values (SUV; mean ± SD), 60 minutes after tracer injection in control rats (control; n=5), rats infected with HSV-1 (HSE; n=9) and rats infected with HSV-1 pre-treated with 5 mg/kg PK11195 5 minutes before tracer injection (HSE + PK11195; n=4). *p<0.05 as compared to control, †p<0.005 as compared to control, ‡p<0.05 as compared to HSE and §p<0.005 as compared to HSE.

	Control	HSE	HSE+PK11195
Brain:			
Amygdala/Piriform cortex	0.31 ± 0.09	0.36 ± 0.19	0.24 ± 0.12
Bulbus olfactorius	0.93 ± 0.13	1.30 ± 0.42	0.50 ± 0.35‡
Cerebellum	0.46 ± 0.14	0.70 ± 0.30	0.33 ± 0.19
Cingulate/Frontopolar cortex	0.17 ± 0.04	0.32 ± 0.22	0.40 ± 0.44
Entorhinal cortex	0.20 ± 0.05	0.33 ± 0.19	0.23 ± 0.10
Frontal cortex	0.23 ± 0.16	0.26 ± 0.15	0.25 ± 0.18
Hippocampus	0.55 ± 0.17	0.45 ± 0.23	0.18 ± 0.05*
Medulla	0.46 ± 0.15	1.09 ± 0.53*	0.31 ± 0.17‡
P/T/O cortex	0.20 ± 0.02	0.24 ± 0.10	0.27 ± 0.21
Pons	0.46 ± 0.09	1.12 ± 0.41†	0.28 ± 0.08§
Striatum	0.16 ± 0.02	0.28 ± 0.15	0.18 ± 0.04
Peripheral tissues:			
Adrenals	5.10 ± 1.19	5.75 ± 1.79	8.01 ± 2.35
Bone	0.83 ± 0.24	0.69 ± 0.33	0.48 ± 0.12
Lung	10.68 ± 1.41	13.80 ± 4.14	1.06 ± 0.37†§
Plasma	0.10 ± 0.02	0.09 ± 0.02	0.61 ± 0.10†§

P/T/O, Parietal/Temporal/Occipital

Ex-vivo biodistribution: specific binding

The ex-vivo biodistribution showed an increased binding in HSE rats as compared to controls and a decreased binding after pre-treatment with PK11195, for all three PET tracers. However, plasma levels of the tracer were also found to be different between the three PET tracers and between treatment groups. Since tracer accumulation in the brain is dependent on tracer delivery (and thus tracer concentration) from plasma, the brain uptake was corrected for plasma radioactivity for each rat individually to calculate the tissue/plasma ratio's.

Non-specific binding and specific binding of [11C]-*(R)*-PK11195, [11C]-DPA-713 and [18F]-DPA-714 are displayed in table 5. Non-specific binding was defined as the tissue/plasma ratio of rats pre-treated with PK11195. Specific binding was calculated in control and HSE rats, by subtracting the average tissue/plasma ratio of the HSE rats pre-treated with PK11195 from the tissue/plasma ratio of control and HSE rats, for each rat individually. The rationale behind the definition of specific uptake is that

the uptake in rats pre-treated with PK11195 represents non-specific binding only, whereas the uptake in control and HSE rats is due to both specific and non-specific binding. Non-specific binding was found to be statistical significantly lower in almost all brain areas for both [^{11}C]-DPA-713 and [^{18}F]-DPA-714, when compared to [^{11}C]-*(R)*-PK11195. The specific binding in control rats was found to be significantly higher for [^{11}C]-DPA-713 in the amygdala/piriform cortex, bulbus olfactorius, cerebellum, entorhinal cortex, medulla, parietal/temporal/occipital cortex, pons and striatum, when compared to [^{11}C]-*(R)*-PK11195. For [^{18}F]-DPA-714, the specific uptake in control rats was significantly higher than [^{11}C]-*(R)*-PK11195 uptake in the cingulate/frontopolar cortex, pons and striatum. In addition, specific uptake in HSE rats was found to be significantly higher for [^{11}C]-DPA-713 in the amygdala/piriform cortex, bulbus olfactorius, entorhinal cortex, hippocampus, medulla and parietal/temporal/occipital cortex as compared to [^{11}C]-*(R)*-PK11195. No significant differences in specific binding in HSE rats were found between [^{11}C]-*(R)*-PK11195 and [^{18}F]-DPA-714.

Table 4 Ex vivo biodistribution of [^{18}F]-DPA-714, expressed as standardized uptake values (SUV; mean ± SD), 120 minutes after tracer injection in control rats (control; n=5), rats infected with HSV-1 (HSE; n=9) and rats infected with HSV-1 pre-treated with 5 mg/kg PK11195 5 minutes before tracer injection (HSE + PK11195; n=4). *p<0.05 as compared to control, †p<0.005 as compared to control, ‡p<0.05 as compared to HSE and §p<0.005 as compared to HSE.

	Control	**HSE**	**HSE+PK11195**
Brain:			
Amygdala/Piriform cortex	0.25 ± 0.08	0.41 ± 0.34	0.50 ± 0.17
Bulbus olfactorius	0.55 ± 0.09	0.88 ± 0.30	0.85 ± 0.35
Cerebellum	0.36 ± 0.05	0.41 ± 0.20	0.43 ± 0.08
Cingulate/Frontopolar cortex	0.20 ± 0.02	0.33 ± 0.21	0.45 ± 0.11
Entorhinal cortex	0.20 ± 0.04	0.39 ± 0.32	0.44 ± 0.11
Frontal cortex	0.17 ± 0.02	0.21 ± 0.09	0.40 ± 0.10†§
Hippocampus	0.35 ± 0.25	0.39 ± 0.16	0.48 ± 0.14
Medulla	0.40 ± 0.06	0.81 ± 0.28*	0.45 ± 0.08
P/T/O cortex	0.17 ± 0.02	0.19 ± 0.05	0.38 ± 0.09†§
Pons	0.31 ± 0.02	0.58 ± 0.26	0.43 ± 0.09
Striatum	0.18 ± 0.01	0.32 ± 0.22	0.49 ± 0.18
Peripheral tissues:			
Adrenals	6.75 ± 1.16	6.36 ± 1.48	9.03 ± 2.88
Bone	0.40 ± 0.17	0.50 ± 0.20	0.42 ± 0.12
Lung	16.55 ± 4.53	15.14 ± 4.98	1.49 ± 0.34†§
Plasma	0.13 ± 0.02	0.22 ± 0.34	1.15 ± 0.35†§

P/T/O, Parietal/Temporal/Occipital

Table 5 Non-specific and specific binding of [11C]-*(R)*-PK11195, [11C]-DPA-713 and [18F]-DPA-714. Non-specific binding was defined as the tissue/plasma ratio of HSE rats pre-treated with PK11195 (n=4). The specific binding in control (n=5) and HSE (n=9) rats were calculated by the equations [$control_{tissue/plasma}$–average $pre\text{-}treated_{tissue/plasma}$] and [$HSE_{tissue/plasma}$–average $pre\text{-}treated_{tissue/plasma}$], respectively. *p<0.05 and †p<0.005; specific binding in [11C]-DPA-713 and [18F]-DPA-714 as compared to [11C]-*(R)*-PK11195.

	[11C]-(R)-PK11195	**[11C]-DPA-713**	**[18F]-DPA-714**
Non-specific binding:			
Amygdala/Piriform cortex	0.88 ± 0.05	0.39 ± 0.18*	0.47 ± 0.21*
Bulbus olfactorius	0.94 ± 0.11	0.81 ± 0.53	0.80 ± 0.40
Cerebellum	0.89 ± 0.11	0.53 ± 0.29	0.40 ± 0.12*
Cingulate/Frontopolar cortex	0.85 ± 0.08	0.64 ± 0.67	0.42 ± 0.16
Entorhinal cortex	0.84 ± 0.11	0.38 ± 0.15†	0.41 ± 0.15*
Frontal cortex	0.91 ± 0.07	0.41 ± 0.27*	0.37 ± 0.13*
Hippocampus	0.93 ± 0.10	0.30 ± 0.06†	0.45 ± 0.18†
Medulla	1.23 ± 0.15	0.50 ± 0.26†	0.41 ± 0.13†
P/T/O cortex	0.91 ± 0.10	0.44 ± 0.31*	0.35 ± 0.13*
Pons	1.21 ± 0.10	0.46 ± 0.14†	0.40 ± 0.14†
Striatum	0.97 ± 0.10	0.30 ± 0.04†	0.46 ± 0.21†
Specific binding control:			
Amygdala/Piriform cortex	0.69 ± 0.64	2.62 ± 0.71*	1.44 ± 0.62
Bulbus olfactorius	4.64 ± 2.22	8.28 ± 1.37†	3.43 ± 0.82
Cerebellum	1.50 ± 0.73	3.90 ± 1.20†	2.47 ± 0.82
Cingulate/Frontopolar cortex	0.57 ± 0.26	1.06 ± 0.35	1.12 ± 0.25*
Entorhinal cortex	0.67 ± 0.42	1.62 ± 0.45†	1.20 ± 0.62
Frontal cortex	0.57 ± 0.29	1.85 ± 1.62	0.96 ± 0.35
Hippocampus	1.81 ± 2.26	5.02 ± 1.38	2.37 ± 2.38
Medulla	1.56 ± 0.70	3.93 ± 1.45†	2.76 ± 0.75
P/T/O cortex	0.57 ± 0.31	1.48 ± 0.21*	1.00 ± 0.38
Pons	1.51 ± 0.72	4.05 ± 0.81*	2.07 ± 0.54
Striatum	0.46 ± 0.27	1.22 ± 0.15*	0.95 ± 0.29*
Specific binding HSE:			
Amygdala/Piriform cortex	1.38 ± 0.63	3.87 ± 2.58*	2.14 ± 0.80
Bulbus olfactorius	8.39 ± 3.64	14.44 ± 5.66*	6.89 ± 2.45
Cerebellum	4.36 ± 1.85	7.72 ± 3.68	3.66 ± 2.80
Cingulate/Frontopolar cortex	1.89 ± 1.02	3.23 ± 2.99	1.98 ± 0.47
Entorhinal cortex	1.55 ± 0.71	3.54 ± 2.52*	2.09 ± 0.46
Frontal cortex	1.37 ± 0.59	2.64 ± 2.01	1.30 ± 0.28
Hippocampus	1.44 ± 0.62	4.99 ± 2.88†	3.01 ± 0.79
Medulla	6.21 ± 2.22	12.56 ± 7.11*	7.18 ± 3.90
P/T/O cortex	1.37 ± 0.40	2.44 ± 1.37*	1.24 ± 0.34
Pons	7.77 ± 2.87	12.77 ± 5.39	5.03 ± 3.67
Striatum	1.39 ± 0.98	3.06 ± 2.07	1.80 ± 0.50

P/T/O, Parietal/Temporal/Occipital

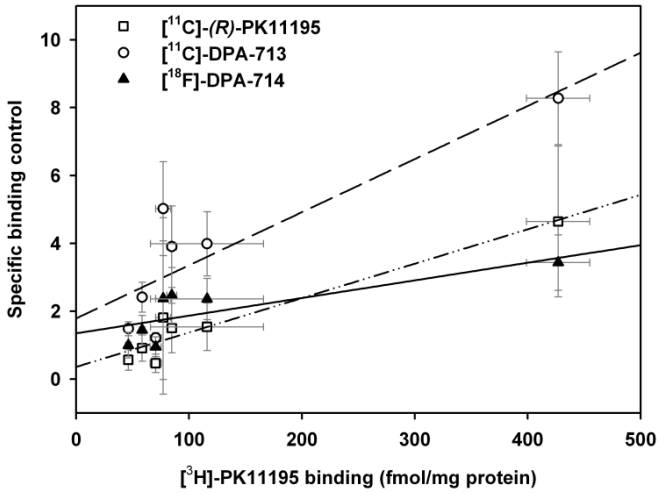

Figure 4 Correlation of specific binding in control rats for [11C]-*(R)*-PK11195, [11C]-DPA-713 and [18F]-DPA-714 with [3H]-PK11195 binding as determined by Kurumaji *et al.* [25]. The R was 0.96 for [11C]-*(R)*-PK11195 (p=0.0006; y=0.36+0.010x), 0.87 for [11C]-DPA-713 (p=0.0116; y=1.79+0.016x) and 0.77 for [18F]-DPA-714 (p=0.0427; y=1.35+0.005x).

The specific binding in control rats showed a good correlation with [3H]-PK11195 binding (figure 4) as was measured by Kurumaji *et al.* [25] for all three PET tracers. The best correlation was found for [11C]-*(R)*-PK11195, that had a R of 0.96 (p=0.0006), followed by [11C]-DPA-713 with a R of 0.87 (p=0.01) and [18F]-DPA-714 with a R of 0.77 (p=0.04). Although the best correlation was found for [11C]-*(R)*-PK11195, the slope of the linear regression was highest for [11C]-DPA-713 (0.016; compared to 0.010 for [11C]-*(R)*-PK11195 and 0.005 for [18F]-DPA-714), which indicates that [11C]-DPA-713 uptake might be most sensitive to changes in PBR expression. Although these results seem to depend on the bulbus olfactorius, which has the highest uptake, the correlation remained good after removal of this data-point from the regression analysis. In addition, the slope of the linear regression remained highest for [11C]-DPA-713.

Discussion

In the present study, the new PBR ligands [11C]-DPA-713 and [18F]-DPA-714 were evaluated in a rat model of herpes encephalitis, using small animal PET imaging. We demonstrated that [11C]-DPA-713 has lower background binding and has the potency to reach higher specific uptake in infected brain tissue than [11C]-*(R)*-PK11195. [18F]-DPA-714 showed low non-specific binding, but also lower specific binding. Data from immunohistochemistry, *in vivo* PET imaging and *ex vivo* biodistribution corresponded nicely for all tracers.

The PBR that is only modestly expressed in the healthy brain is upregulated in microglia cells when they become activated in response to inflammatory stimuli and brain damage. Microglia cells are increasingly associated with neurological diseases, such as Parkinson's disease [15] and multiple sclerosis [9], and are therefore an important target for early diagnosis and detection of the subtle effects of therapeutic intervention. At present, the most widely used PET tracer to visualize activated microglia is the PBR ligand [11C]-*(R)*-PK11195, but this radiotracer may not provide the required sensitivity. The high lipophilicity and high non-specific binding of [11C]-*(R)*-PK11195 result in a low signal-to-noise ratio, which makes detecting mild neuroinflammation or subtle changes due to treatment difficult.

The majority of studies that evaluate new radioligands for the PBR use striatum-lesioned models of neuroinflammation, in which a toxic substance, like quinolinic acid, kainic acid and 6-OH-DOPA, is stereotactically injected into the striatum. The rat model of herpes encephalitis better mimics neurological disorders as it does not involve invasive manipulations, but induces microglia cell activation via a biological process. In addition, HSV-1 is implicated in the etiopathogensis of neurological and psychiatric disorders, like schizophrenia [26] and Alzheimer's disease [26,27] and may be specifically involved in the focal neuroinflammatory processes in these disorders. It has already been shown that HSV-1 invasion of the brain is associated with the activation of microglia cells [13,28,29]. Also in the present study, it was confirmed by immunohistochemical staining that the central nervous system invasion of HSV-1 results in intense microglia activation, in the bulbus olfactorius, frontal cortex, hippocampus, cerebellum and brainstem. The pattern of this microglia activation is consistent with the findings of Barnett *et al.* [30], who showed that intranasal inoculation of mice with HSV-1 resulted in the spread of HSV-1 to the hippocampus, amygdala, midbrain and brainstem via the olfactory bulb. The severe activation of microglia cells in the brainstem may be caused by indirect HSV-1 invasion of the brainstem via the neural pathway from the bulbus olfactorius to the locus coeruleus [30,31] or by direct invasion of the sensory trigeminal nuclei via the main sensory nerve of the face, the trigeminal nerve. In addition, microglia cell activation in the brainstem may also be caused by HSV-1 invasion of the trigeminal nerve, resulting in activation of microglia cells surrounding the anterograde nerve connections [32]. Although the rat model of herpes encephalitis represents a more physiological model of microglia activation, a disadvantage of the model compared to striatum-lesion models, is the variability in the extent of microglia activation. Despite the variation in the extent of microglia cell activation, it was shown that the brainstem was affected in

all rats. One way to reduce some variation in measurement of microglia cell activation would be to compare the different PET tracers in the same rat. However, due to the severity of the disease the degree of microglia cell activation can change quickly within the time period between the PET scans which makes it difficult compare the tracers in the same rat.

The uptake of [^{11}C]-*(R)*-PK11195, [^{11}C]-DPA-713 and [^{18}F]-DPA-714 was determined by both PET scanning and *ex vivo* biodistribution. Uptake values derived from the PET scan were on average higher than the values obtained from *ex vivo* biodistribution, but this difference was statistically not significant. The small difference between both techniques can probably be attributed to tissue kinetics, since the *ex vivo* biodistribution represents a single time point, whereas the values obtained from the PET scan represent an average of 10 minutes. In regions with a high uptake and thus slower washout, like the bulbus olfactorius, this results in PET values lower than the *ex vivo* biodistribution values. For brain regions with lower uptake and faster washout, and thus a larger change within the 10 minutes, this results in PET values that are lower or equal to the *ex vivo* biodistribution values.

In the present study, it was shown that the standardized uptake value of [^{11}C]-DPA-713 is significantly lower in healthy brain tissue as compared to the uptake of [^{11}C]-*(R)*-PK11195. This suggests less non-specific binding. Indeed, pre-treatment with PK11195 showed that [^{11}C]-DPA-713 has lower non-specific binding than [^{11}C]-*(R)*-PK11195. This could be explained by the lower lipophilicity of DPA-713 than that of PK11195 (LogP 2.4 vs. 3.4 [22]). In brain areas in HSV-infected animals where activation of microglia cells was found, [^{11}C]-DPA-713 uptake was comparable to the uptake of [^{11}C]-*(R)*-PK11195. Thus, the lower non-specific binding and comparable uptake in infected areas results in a higher signal-to-noise ratio of [^{11}C]-DPA-713 than of [^{11}C]-*(R)*-PK11195, suggesting that [^{11}C]-DPA-713 is more suitable for the detection of mild neuroinflammation. The results of the present study are consistent with the findings of Boutin *et al.* [23]. In their study, it was also shown that the signal-to-noise ratio of [^{11}C]-DPA-713 is higher than that of [^{11}C]-*(R)*-PK11195, due to a reduced uptake in healthy tissue for [^{11}C]-DPA-713.

In healthy brain tissue, the standardized uptake value of [^{18}F]-DPA-714 is significantly lower than the uptake of both [^{11}C]-*(R)*-PK11195 and [^{11}C]-DPA-713. In addition, the non-specific binding of [^{18}F]-DPA-714 was found to be lower than the non-specific [^{11}C]-*(R)*-PK11195 binding. This suggests that this radiotracer is potentially suitable for visualizing mild neuroinflammation. Although [^{18}F]-DPA-714 is able to visualize

neuroinflammation in our rat model of herpes encephalitis and also in a striatum-lesioned model [19,20], the uptake in infected brain areas is significantly lower as compared to [11C]-*(R)*-PK11195.

Although the standardized uptake value is widely used to display the uptake of tracers, it does not correct for the activity in plasma and thus not for tracer delivery to the brain. This could lead to a wrong interpretation of the data when comparing the tracers in different conditions. Ideally, the binding potential or distribution volume of the tracers should be determined using plasma input on different time points during the scan. However, plasma samples are difficult to obtain, especially in severely ill animals. Therefore, in the present study, the tissue/plasma ratios were calculated from a single *ex vivo* plasma activity measurement. After correction for plasma activity, the specific binding in both control and HSE rats was found to be significantly higher for [11C]-DPA-713 than for [11C]-*(R)*-PK11195. In contrast to [11C]-*(R)*-PK11195, [11C]-DPA-713 is even able to show specific binding to the low basal expression levels of PBR in control rats. In addition, the greater slope of the correlation between tracer uptake and PBR expression (figure 4) suggests that [11C]-DPA-713 is more sensitive for small changes in the amount of PBR as compared to [11C]-*(R)*-PK11195. Thus, this study indicates that [11C]-DPA-713 is more sensitive for visualizing neuroinflammation than [11C]-*(R)*-PK11195.

Although [18F]-DPA-714 showed low non-specific binding, specific binding of [18F]-DPA-714 was much lower than that of [11C]-DPA-713, even after correction for plasma activity. Interestingly, a recent study in a striatum-lesion model showed that the tissue uptake ratio between the control and lesioned striatum was higher for [18F]-DPA-714 than for [11C]-*(R)*-PK11195, with a three times higher binding potential of [18F]-DPA-714 [33]. Moreover, in the present study, [18F]-DPA-714 binding (SUV) in infected brain areas was not effectively blocked by pre-treatment with PK11195, while [18F]-DPA-714 uptake in the striatum-lesion model was inhibited by pre-treatment with PK11195, DPA-713 and DPA-714 [20,22]. The apparent discrepancy between the results of our study and those of the previous studies in the striatum-lesion model might be due to differences in the affinity state of the receptor between both animal models. [18F]-DPA-714 is an agonist of the PBR and an agonist usually binds only to the high affinity state of the receptor. Microglia cell activation in the striatum-lesion model has a more chronic, neurodegenerative character, as microglia cells are mainly involved in removing the debris of the neuronal cells that were destroyed by the chemical compound. In the HSE model, the activated microglia cells are involved in a

more acute response by combating the exogenous pathogen and thus they have a more neuroprotective role. One could speculate that the affinity state of the PBR depends on the neuroprotective or neurodegenerative activity of the microglia cells. The chronically activated (neurodegenerative) microglia cells may contain more PBR in the high affinity state, which would result in better binding of [^{18}F]-DPA-714. If this hypothesis could be confirmed, PBR, agonists like [^{18}F]-DPA-714, may be important radiotracers to visualize an important aspect of neuroinflammation.

Another remarkable finding in this study was that the binding of [^{18}F]-DPA-714 and [^{11}C]-DPA-713 in the adrenals could not be blocked by pre-treatment with PK11195, whereas pre-treatment did block the binding of [^{11}C]-*(R)*-PK11195. For [^{18}F]-DPA-714, similar results were found by James *et al.* [19,20]. This observation suggests the presence of an alternative binding site for DPA-713 and DPA-714 that is predominantly expressed in the adrenals and does not bind PK1115. Whether the alternative binding site in the adrenals could be a hitherto unknown subtype of the PBR, or another receptor remains to be elucidated.

Conclusion

The present results showed that [^{11}C]-DPA-713 is a promising new radioligand for PBR expression in activated microglia due to its low non-specific binding in the brain. This tracer appears to be a more sensitive tool to detect small changes in PBR expression than [^{11}C]-*(R)*-PK11195. To validate superiority of [^{11}C]-DPA-713 over [^{11}C]-*(R)*-PK11195 in quantification of neuroinflammation, clinical studies in neurological diseases that are associated with microglia cell activation are needed. Although there may be differences in the affinity state of the PBR between previous animal models using [^{18}F]-DPA-714 and the present study the fact that this radioligand is an agonist of the PBR may open new possibilities in PET imaging of neuroinflammation, which warrants its further evaluation.

Acknowledgements

The authors thank Namkje Vellinga for her help with the animal experiments. The authors would also like to thank Sietske Welling-Wester and Björge Meijdam of the department of Medical Microbiology of the University of Groningen, The Netherlands for their help with the HSV-1 and Nieske Brouwer of the department of

Medical Physiology of the University of Groningen, The Netherlands for the help with the immunohistochemistry. This study was funded by the Stanley Medical Research Institute, Grant-ID 05-NV-001, and in part by the EC - FP6-project DiMI, LSHB-CT-2005-512146.

References

1 World Health Organization. Neurological disorders; public health challenges.: WHO, 2006

2 Nakajima K, Kohsaka S. Microglia: neuroprotective and neurotrophic cells in the central nervous system. Curr.Drug Targets Cardiovasc.Haematol.Disord. 2004; 4:65-84

3 Davalos D, Grutzendler J, Yang G, et al. ATP mediates rapid microglial response to local brain injury in vivo. Nat.Neurosci. 2005; 8:752-758

4 Nimmerjahn A, Kirchhoff F, Helmchen F. Resting microglial cells are highly dynamic surveillants of brain parenchyma in vivo. Science 2005; 308:1314-1318

5 Gerhard A, Neumaier B, Elitok E, et al. In vivo imaging of activated microglia using [11C]PK11195 and positron emission tomography in patients after ischemic stroke. Neuroreport 2000; 11:2957-2960

6 Gerhard A, Schwarz J, Myers R, Wise R, Banati RB. Evolution of microglial activation in patients after ischemic stroke: a [11C](R)-PK11195 PET study. Neuroimage. 2005; 24:591-595

7 Pappata S, Levasseur M, Gunn RN, et al. Thalamic microglial activation in ischemic stroke detected in vivo by PET and [11C]PK1195. Neurology 2000; 55:1052-1054

8 Ramsay SC, Weiller C, Myers R, et al. Monitoring by PET of macrophage accumulation in brain after ischaemic stroke. Lancet 1992; 339:1054-1055

9 Banati RB, Newcombe J, Gunn RN, et al. The peripheral benzodiazepine binding site in the brain in multiple sclerosis: quantitative in vivo imaging of microglia as a measure of disease activity. Brain 2000; 123:2321-2337

10 Debruyne JC, Versijpt J, Van Laere KJ, et al. PET visualization of microglia in multiple sclerosis patients using [11C]PK11195. Eur.J.Neurol. 2003; 10:257-264

11 Versijpt J, Debruyne JC, Van Laere KJ, et al. Microglial imaging with positron emission tomography and atrophy measurements with magnetic resonance imaging in multiple sclerosis: a correlative study. Mult.Scler. 2005; 11:127-134

12 Vowinckel E, Reutens D, Becher B, et al. PK11195 binding to the peripheral benzodiazepine receptor as a marker of microglia activation in multiple sclerosis and experimental autoimmune encephalomyelitis. J.Neurosci.Res. 1997; 50:345-353

13 Cagnin A, Myers R, Gunn RN, et al. In vivo visualization of activated glia by [11C] (R)-PK11195-PET following herpes encephalitis reveals projected neuronal damage beyond the primary focal lesion. Brain 2001; 124:2014-2027

14 Gerhard A, Pavese N, Hotton G, et al. In vivo imaging of microglial activation with [11C](R)-PK11195 PET in idiopathic Parkinson's disease. Neurobiol.Dis. 2006; 21:404-412

15 Ouchi Y, Yoshikawa E, Sekine Y, et al. Microglial activation and dopamine terminal loss in early Parkinson's disease. Ann.Neurol. 2005; 57:168-175

16 Cagnin A, Brooks DJ, Kennedy AM, et al. In-vivo measurement of activated microglia in dementia. Lancet 2001; 358:461-467
17 Cagnin A, Rossor M, Sampson EL, Mackinnon T, Banati RB. In vivo detection of microglial activation in frontotemporal dementia. Ann.Neurol. 2004; 56:894-897
18 Groom GN, Junck L, Foster NL, Frey KA, Kuhl DE. PET of peripheral benzodiazepine binding sites in the microgliosis of Alzheimer's disease. J.Nucl.Med. 1995; 36:2207-2210
19 James ML, Fulton RR, Vercouille J, et al. DPA-714 a new translocator protein (18kDa) ligand: synthesis, radiofluorination and pharmacological characterisation. Journal of Labelled Compounds and Radiopharmaceuticals 2007; 50, Supplement 1:S25
20 James ML, Fulton RR, Vercoullie J, et al. DPA-714, a new translocator protein-specific ligand: synthesis, radiofluorination, and pharmacologic characterization. J.Nucl.Med. 2008; 49:814-822
21 Selleri S, Bruni F, Costagli C, et al. 2-Arylpyrazolo[1,5-a]pyrimidin-3-yl acetamides. New potent and selective peripheral benzodiazepine receptor ligands. Bioorg.Med.Chem. 2001; 9:2661-2671
22 James ML, Fulton RR, Henderson DJ, et al. Synthesis and in vivo evaluation of a novel peripheral benzodiazepine receptor PET radioligand. Bioorg.Med.Chem. 2005; 13:6188-6194
23 Boutin H, Chauveau F, Thominiaux C, et al. 11C-DPA-713: a novel peripheral benzodiazepine receptor PET ligand for in vivo imaging of neuroinflammation. J.Nucl.Med. 2007; 48:573-581
24 Larsen P, Ulin J, Dahlstrom K, Jensen M. Synthesis of [C-11]iodomethane by iodination of [C-11]methane. Appl.Radiat.Isot. 1997; 48:153-157
25 Kurumaji A, Kaneko K, Toru M. Effects of chronic treatment with haloperidol on [3H]PK 11195 binding in the rat brain and peripheral tissues. Neuropharmacology 1996; 35:1075-1079
26 Steiner J, Mawrin C, Ziegeler A, et al. Distribution of HLA-DR-positive microglia in schizophrenia reflects impaired cerebral lateralization. Acta Neuropathol. 2006; 112:305-316
27 Itzhaki R. Herpes simplex virus type 1, apolipoprotein E and Alzheimer' disease. Herpes. 2004; 11 Suppl 2:77A-82A
28 DeLano RM, Mallery SR. Stress-related modulation of central nervous system immunity in a murine model of herpes simplex encephalitis. J.Neuroimmunol. 1998; 89:51-58
29 Esiri MM, Drummond CW, Morris CS. Macrophages and microglia in HSV-1 infected mouse brain. J.Neuroimmunol. 1995; 62:201-205
30 Barnett EM, Cassell MD, Perlman S. Two neurotropic viruses, herpes simplex virus type 1 and mouse hepatitis virus, spread along different neural pathways from the main olfactory bulb. Neuroscience 1993; 57:1007-1025

31 Mori I, Goshima F, Ito H, et al. The vomeronasal chemosensory system as a route of neuroinvasion by herpes simplex virus. Virology 2005; 334:51-58
32 Banati RB. Visualising microglial activation in vivo. Glia 2002; 40:206-217
33 Chauveau F, van Camp N, Damont A, et al. [18F]DPA-714: a highly promising fluorine-18-labelled tracer for neuroinflammation imaging. World Molecular Imaging Congress 2008

Chapter 5

Evaluation of [^{11}C]-DAA1106 for imaging and quantification of neuroinflammation in a rat model of herpes encephalitis

Janine Doorduin, Hans C. Klein, Johan R. de Jong, Rudi A. Dierckx and Erik F.J. de Vries

Accepted for publication in Nucl Med Biol

Abstract

Many neurological and psychiatric disorders are associated with neuroinflammation. Positron emission tomography (PET) with [^{11}C]-PK11195 can be used to study neuroinflammation in these disorders. However, [^{11}C]-PK11195 may not be sensitive enough to visualize mild neuroinflammation. As a potentially more sensitive PET tracer for neuroinflammation, [^{11}C]-DAA1106 was evaluated in a rat model of herpes encephalitis.

Male Wistar rats were intranasally inoculated with HSV-1 (HSE) or PBS (control). At day 6 or 7 after inoculation, small animal [^{11}C]-DAA1106 PET scans were acquired, followed by *ex vivo* biodistribution. Arterial blood sampling was performed for quantification of uptake.

In HSE rats, a significantly higher *ex vivo*, but not *in vivo*, uptake of [^{11}C]-DAA1106 was found in almost all examined brain areas (24-71%, $p<0.05$), when compared to control rats. Pre-treatment with unlabeled PK11195 effectively reduced [^{11}C]-DAA1106 uptake in HSE rats (54-84%; $p<0.001$). The plasma and brain time-activity curves showed rapid uptake of [^{11}C]-DAA1106 into tissue. The data showed a good fit to the Logan analysis, but could not be fitted with a two-tissue compartment model.

[^{11}C]-DAA1106 showed a high and specific *ex vivo* uptake in the encephalitic rat brain. However, neuroinflammation could not be demonstrated *in vivo* by [^{11}C]-DAA1106 PET. Quantification of the uptake of [^{11}C]-DAA1106 using plasma sampling is not optimal, due to rapid tissue uptake, slow tissue clearance and low plasma activity.

Introduction

Neuroinflammation plays an important role in the pathogenesis and progression of neurological disorders, like Alzheimer's disease and multiple sclerosis [1], but also in psychiatric disorders, like schizophrenia [2,3]. Neuroinflammation is mediated by microglia cells, which are the resident immune cells of the brain. In response to both acute and chronic brain injury, like viral infection or toxicity, microglia cells are activated and change from their normal ramified state into an amoeboid morphology. In the activated state, microglia cells are involved in removal of infectious agents and damaged neuronal tissue. It is not exactly known whether the response of activated microglia cells is beneficial or detrimental, but it is hypothesized that microglia cell activation in acute injury is beneficial, whereas it is detrimental in chronic disease [4]. Because of the importance of microglia cell activation in neurological and psychiatric disorders, it is of great value to gain more insight into microglia cell behavior for better understanding of these disorders and improvement of treatment strategies.

Positron emission tomography (PET) provides the unique opportunity to study physiological processes *in vivo* and can be used for imaging of microglia cell activation. The activation of microglia cells is accompanied by an increased expression of the peripheral benzodiazepine receptor (PBR), which can be used as a biomarker to study activated microglia cells. The PBR is an 18 kDa component of a heteromeric complex that includes a voltage-dependent anion carrier of 32 kDa and an adenine nucleotide carrier of 30 kDa and is located in the outer mitochondrial membrane [5]. The highest levels of the PBR are found in the kidney, lung, heart and hormone secreting tissues [6]. In the healthy human brain, the PBR is mainly expressed in low levels on astrocytes and resting microglia cells [7], although the PBR was also found to be expressed in the muscle cells of small- and medium-sized arteries, in perivascular macrophages, lymphocytes and neutrophils, in the choroid plexus and in the ependyma [8,9]. The highest expression of the PBR in the healthy rat brain tissue was found in the pituitary, bulbus olfactorius, brainstem and cerebellum [10]. Although the exact function of the PBR is unknown, it is thought to be mainly involved in steriodogenesis [11] and mitochondrial function [12]. These functions may be important in controlling neuronal damage [12] and support the accelerated microglia cell proliferation [11], explaining the increased expression of the PBR in activated microglia cells. Although astrocytes, lymphocytes and macrophages were also found to express PBR, activated microglia cells are suggested to be the main source of increase

in PBR expression in neuroinflammation, especially when the blood-brain barrier is intact [7,8,13].

The PBR ligand *(R)*-*N*-methyl-*N*-(1-methylpropyl)-1-(2-chlorophenyl)isoquinoline-3-carboxamide ([^{11}C]-*(R)*-PK11195) is one of the first PET ligands used for imaging of activated microglia cells and showed the presence of activated microglia cells in, amongst others, Alzheimer's disease, Parkinson's disease, Huntington disease and herpes encephalitis (reviewed in [1]). Although [^{11}C]-*(R)*-PK11195 is widely used for imaging of microglia cells, it shows high plasma protein binding and a relatively poor penetration of the blood-brain barrier, which could limit its use for brain imaging [14]. In addition, [^{11}C]-*(R)*-PK11195 shows high levels of non-specific binding, which reduces the signal-to-noise ratio.

Because of the limitations of [^{11}C]-*(R)*-PK11195 it may not possess the required sensitivity to visualize mild neuroinflammation and to detect subtle effects of therapeutic intervention in neurological disorders. Therefore, there is a need for more sensitive and selective PET ligands for the PBR. The aryloxyanilide derivative *N*-(2,5-dimethoxybenzyl)-*N*-(4-fluoro-2-phenoxyphenyl)-acetamide (DAA1106) was found to have a higher affinity (K_i=0.034 nM) for the PBR than PK11195 (K_i=0.766 nM) [15-17] and has proven to be a potent new PET tracer for the imaging of neuroinflammation. Thus far, a PET study has found a higher [^{11}C]-DAA1106 uptake in the inflamed striatum after injection of a toxic compound, when compared to the non-inflamed striatum, but quantification of this effect was not reported [18]. In Alzheimer's disease patients, a significantly increased binding of [^{11}C]-DAA1106 to the PBR was found in various regions, which were more widespread than was found for [^{11}C]-*(R)*-PK11195 [19]. Although it was shown that [^{11}C]-DAA1106 uptake could be quantified in Alzheimer's disease patients and healthy volunteers, using two-tissue compartment modeling [19,20], no studies quantifying [^{11}C]-DAA1106 uptake in rodent models have been reported so far.

In the rat model of herpes encephalitis, intranasal inoculation with the herpes simplex virus type-1 results in the activation of microglia cells in many brain areas, including the bulbus olfactorius, brainstem and cerebellum [21,22]. Because this model does not require invasive manipulations and toxic compounds to evoke neuroinflammation, it may better mimic the activation of microglia cells in human neurological disorders than the unilateral lesion models that are most frequently used to study neuroinflammation. With [^{11}C]-*(R)*-PK11195 it has already been shown that there is an increased activation of microglia cells in the brain of rats with herpes encephalitis,

especially in the bulbus olfactorius (46% increase in [11C]-*(R)*-PK11195 uptake), brainstem (67%) and cerebellum (59%), but also in the cerebral cortex (35%), which was consistent with immunohistochemical evidence for activated microglia cells in these areas [23].

Because [11C]-DAA1106 is potentially a more sensitive PET tracer for imaging of activated microglia cells, the aim of the present study was to evaluate [11C]-DAA1106 for imaging and quantification in the rat model of herpes encephalitis.

Material and methods

[11C]-DAA1106

[11C]-DAA1106 was labeled by trapping [11C]-methyl iodide [24] in a solution of 1 mg of the desmethyl precursor *N*-(5-fluoro-2-phenoxyphenyl)-*N*-(2-hydroxy-5-methoxybenzyl)-acetamide (DAA1123) and 10 µl 10M NaOH in 0.3 ml dimethylformamide. The reaction mixture was allowed to react for 200 seconds at room temperature and neutralized with 0.5 ml H_2O and 1 ml of CH_3CN/0.1M NaH_2PO_4 (55/45). The reaction mixture was then purified by HPLC using a SymmetryPrep C18 column (7.8x300 mm), with CH_3CN/0.1M NaH_2PO_4 (55/45) as the eluent (flow 5 ml/min). To remove the organic solvents from the product, the collected HPLC fraction (retention time 10 min) was diluted with 100 ml of H_2O and passed through an Oasis Seppak cartridge (Waters, Etten-Leur, The Netherlands). The cartridge was washed with 5 ml of water and eluted with 0.8 ml of ethanol and 4.5 ml of H_2O. The product was obtained in 54±25% radiochemical yield. Quality control was performed by HPLC, using a Novapak C18 column (150x3.9 mm) with CH_3CN/H_20 (50/50) as the eluent at a flow of 1.5 ml/min. The radiochemical purity was always >95% and the specific activity was 69±41 MBq/nmol.

Animals

Male outbred Wistar-Unilever (SPF) rats (weight 308±51 grams) were obtained from Harlan (Lelystad, The Netherlands). The rats were individually housed in Macrolon cages (38x26x24 cm) on a layer of wood shavings in a room with constant temperature (21±2°C) and fixed, 12-hour light-dark regime. Food (standard laboratory chow, RMH-B, Hope Farms, The Netherlands) and water were available ad libitum. After arrival, the rats where allowed to acclimatize for at least seven days. The rats were randomly divided into three groups: control rats (control) (n=5), rats infected

with HSV-1 (HSE) (n=7) and rats infected with HSV-1 and pretreated with PK11195 (HSE pre-treated with PK11195) (n=4)). All animals were scanned with [^{11}C]-DAA1106. After PET scanning, the rats were sacrificed and the *ex vivo* biodistribution of the tracers was determined. In an extra group of rats infected with HSV-1 (HSE) (n=2) an arterial catheter was inserted into the femoral artery to allow blood sampling during the [^{11}C]-DAA1106 scan as input function, for pharmacokinetic modeling. The study was approved by the Animal Ethics Committee of the University of Groningen, The Netherlands.

HSV-1 inoculation

A neurovirulent HSV-1 strain was obtained from a human clinical isolate, cultured in Vero-cells and assayed for plaque forming units (PFU) per milliliter. For inoculation, the rats were slightly anaesthetized with 5% isoflurane (Pharmachemie BV, The Netherlands) and 100 µl of phosphate-buffered saline with 1x10^{7} PFU of virus was applied on the nostrils (50 µl per nostril) with a micro pipette. Control rats were treated similarly by the application of 100 µl PBS without virus. Clinical symptoms in all rats were scored daily after the inoculation by the same observer.

PET studies

PET scans were performed when robust clinical signs of infection appeared, which was either on day six or on day seven after the inoculation with HSV-1. The rats were anaesthetized by an intraperitoneal injection of medetomidine (Domitor, Pfizer, The Netherlands, 0.2 mg/kg) and ketamine (Ketanest, Pfizer, The Netherlands, 25 mg/kg), after which the rats were positioned in the small animal PET camera (Focus 220, Siemens Medical Solutions USA, Inc.) in transaxial position with their heads in the field of view. A transmission scan of 515 seconds with a Co-57 point source was obtained for the correction of attenuation and scatter by tissue. After the transmission scan was completed, the PET tracer [^{11}C]-DAA1106 (44±14 MBq, 0.08±0.04 µg) was injected via the penile vein. Simultaneously with the injection of the PET tracer an emission scan of 60 min was started. In the pre-treated group, unlabeled PK11195 (Sigma-Aldrich, USA, 5 mg/kg in dimethylsulfoxide at a concentration of 10 mg/ml) was administered via the tail vein 5 minutes prior to injection of the PET tracer.

The list-mode data of the emission scans were separated into 21 frame sinograms (8x30, 3x60, 2x120, 2x180, 3x300 and 3x600 seconds), which were iteratively

reconstructed (OSEM2d, 4 iterations, 16 subsets) after being normalized and fully corrected for attenuation, scatter, randoms and decay.

Arterial blood sampling

For arterial blood sampling a canula was inserted into the artery femoralis in 2 HSE rats. Rats were anaesthetized by an intraperitoneal injection of medetomidine (Domitor, Pfizer, The Netherlands, 0.2 mg/kg) and ketamine (Ketanest, Pfizer, The Netherlands, 25 mg/kg). After shaving, an incision was made in the skin parallel to the femoral artery. The femoral artery was separated from the femoral vene and temporarily ligated to prevent leakage of blood. A small incision was made in the artery and a canula (0.8 mm o.d.; 0.4 mm i.d.), which was attached to a syringe with heparinized saline, was placed into the artery. The canula was secured to the artery with a suture. After canulation, the rats were positioned in the small animal PET camera with their heads in the field of view. Blood samples of 0.1 ml were taken at 15, 30, 45, 60, 75, 90, 120, 150, 300, 450, 600, 900, 1800 and 3600 seconds after injection. After a blood sample was taken, 0.1 ml of heparinized saline was injected to prevent large changes in blood pressure. The blood samples were centrifuged at 13,000 rpm (15,996 x *g*) for 5 minutes and the activity in plasma was measured with a gammacounter (LKB Wallac, Turku, Finland). The plasma-activity curve was corrected for decay.

PET image analysis

PET image analysis was performed using the Clinical Applications Packaging Program (CAPP5). Regions of interest were drawn around the bulbus olfactorius, frontal cortex, striatum, parietal/temporal/occipital cortex, brainstem and cerebellum in a template PET scan that was co-registered with the PET scan of interest by image fusion. The time-activity curves per region of interest were determined in Bq/cm^3 units and converted into Standardized Uptake Values (SUV), defined as: [tissue activity concentration (Bq/cm^3)]/[injected dose (Bq)/body weight (g)]. It was assumed that 1 cm^3 of brain tissue equals 1 gram.

The time-activity curves of the rats of which arterial blood samples were taken during the scan, were used for pharmacokinetic modeling with software developed in Matlab 7.0. By using the linear models developed by Logan [25] and Patlak [26], it was determined if the binding of [11C]-DAA1106 to the PBR was reversible or irreversible, respectively. In addition, it was determined if the [11C]-DAA1106 time-activity curves

could be fitted to a two-tissue compartment model (K_1-k_4), in order to calculate the binding potential.

Ex vivo biodistribution

After the PET scan the rats were sacrificed by extirpation of the heart while under deep anesthesia. Except for the rats that were used for arterial blood sampling, the brain of the rats was dissected into several areas, peripheral organs were excised and blood was centrifuged to collect a plasma sample. The brain areas, peripheral organs and plasma were weighed and analyzed for the amount of radioactivity by with gammacounter (LKB Wallac, Turku, Finland). Tracer uptake is expressed as the SUV, defined as: [tissue activity concentration (Counts Per Minute/g)]/[injected dose (Counts Per Minute)/body weight (g)].

Statistical analysis

All data are expressed as mean ± standard deviation. Statistical analysis was performed using SPSS for Windows, version 14.0.2. Statistical analysis on differences in the *ex vivo* biodistribution and data obtained from the PET scan were performed by one-way ANOVA with a Bonferroni post hoc test. The time-activity curves were analyzed with the repeated measures general linear model using a Bonferroni post hoc test. Significance was reached when the p value was <0.05.

Results

Clinical symptoms

Clinical symptoms were scored daily up to seven days post inoculation and categorized into the following clinical scores: (0), no symptoms; (1), ruffled fur and irritated mouth, nose and eyes; (2), behavioral signs, like stress and lethargy, and hunched posture; (3), posterior paralysis and impairment of motor function and (4), severe paralysis, labored breathing or death. The first clinical symptoms in the HSE rats were seen on day four or five after inoculation with HSV-1, after which the severity of the symptoms increased. A total of 13 rats were infected with HSV-1, of which 3 had a score of 0, 4 had a score of 1, 4 had a score of 2 and 2 had a score of 4. None of the control rats showed any clinical symptoms (score of 0).

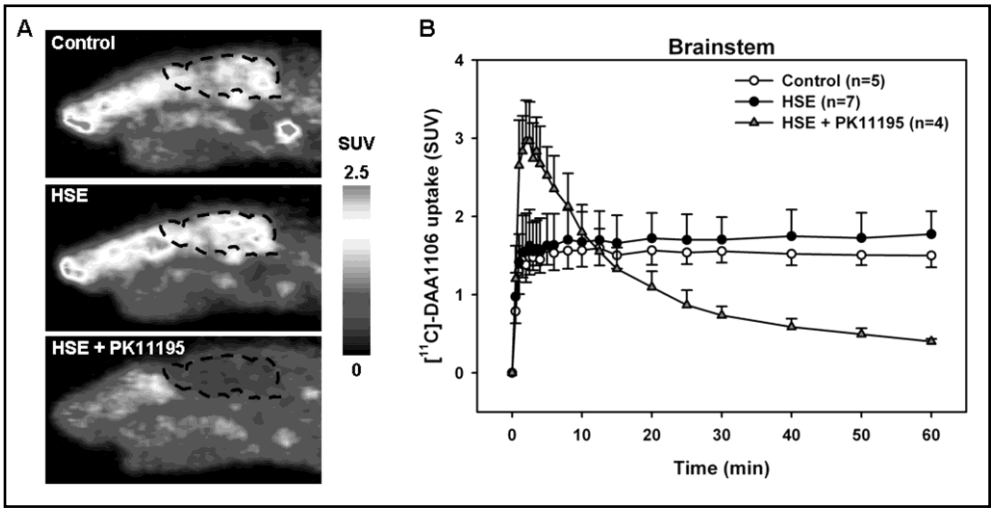

Figure 1 Full-color in appendix. Small animal PET images and time-activity curves of [11C]-DAA1106. **A** Sagittal view of the head of a control rat (control), rat infected with HSV-1 (HSE) and rat infected with HSV-1 pretreated with 5 mg/kg PK11195 (HSE+PK11195), in which the brain is delineated by a dashed line. The images represent tracer uptake between 30 and 60 minutes after injection of [11C]-DAA1106 (44±14 MBq). During the 60 minute small animal PET scan, the rats were anaesthetized with a combination of ketamine (25 mg/kg) and medetomidine (0.2 mg/kg) **B** [11C]-DAA1106 time-activity curves of the brainstem, expressed as standardized uptake values (mean ± standard deviation), of control rats (n=5), HSE rats (n=7) and HSE+PK11195 rats (n=4).

Small animal PET imaging

The [11C]-DAA1106 PET images and time-activity curves in the brainstem, are shown in figure 1. The brainstem is the region with the most intensive microglia cell activation in this model [23]. The images show a high uptake of [11C]-DAA1106 in the brainstem of control rats, when compared to whole brain uptake. In HSE rats, highest uptake of [11C]-DAA1106 can also be seen in the brainstem. Pre-treatment with 5 mg/kg of PK11195 resulted in effective blocking of [11C]-DAA1106 uptake. The time-activity curves show that in control and HSE rats, [11C]-DAA1106 was rapidly taken up by the brain. The uptake remained almost unchanged during the scan time of 60 minutes. Pre-treatment with 5 mg/kg of PK11195 at 5 minutes prior to scanning, resulted in a marked initial increase in brain uptake followed by a gradual decline in uptake during the scan. No statistically significant differences in the time-activity curves were found between control and HSE rats.

Table 1 Brain uptake of [^{11}C]-DAA1106, expressed as standardized uptake values (SUV; mean ± SD), as determined from the last 10 min (50-60 min) of the PET scan of control rats (control), rats infected with HSV-1 (HSE) and rats infected with HSV-1 pretreated with 5 mg/kg PK11195 5 min before [^{11}C]-DAA1106 injection. *p<0.05 as compared to control and HSE, **p≤0.001 as compared to control and HSE

	Control (n=5)	HSE (n=7)	HSE+PK11195 (n=4)
Bulbus olfactorius	1.37 ± 0.14	1.35 ± 0.34	0.89 ± 0.13*
Frontal cortex	1.08 ± 0.05	1.16 ± 0.23	0.53 ± 0.06**
Striatum	0.96 ± 0.04	1.03 ± 0.18	0.43 ± 0.09**
P/T/O cortex	0.97 ± 0.04	1.03 ± 0.15	0.35 ± 0.06**
Cerebellum	1.29 ± 0.10	1.35 ± 0.21	0.39 ± 0.03**
Brainstem	1.50 ± 0.15	1.77 ± 0.29	0.40 ± 0.03**

P/T/O, Parietal/Temporal/Occipital

The standardized uptake values obtained from the last 10 minutes of the PET scan are displayed in table 1. Consistent with the PET images, the highest uptake in control rats was found in the brainstem, followed by the bulbus olfactorius and cerebellum. Uptake in the brainstem, bulbus olfactorius and cerebellum was significantly higher when compared to the other brain areas (20-56%, $p<0.05$). In HSE rats, a significantly higher uptake of [^{11}C]-DAA1106 was found in the brainstem when compared to any other brain area (31-73%, $p<0.05$). High uptake was also found in the bulbus olfactorius and cerebellum. When compared to control rats, the uptake of [^{11}C]-DAA1106 in HSE rats was increased in the brainstem (18%, $p=0.152$), but this was not statistically significant. Pre-treatment of HSE rats with PK11195 resulted in a significantly decreased uptake of [^{11}C]-DAA1106 in all brain areas, when compared to control and HSE rats without pre-treatment (bulbus olfactorius 34-35%, $p<0.05$; any other brain areas 51-77%, $p\leq0.001$). After pre-treatment, the highest uptake was found in the bulbus olfactorius, which was significantly higher when compared to any other brain area (68-155%, $p<0.001$).

Because of the reported high uptake of [^{11}C]-DAA1106 in the lungs [17], one additional control rat was positioned in the small animal PET camera with the lungs in the field of view. [^{11}C]-DAA1106 was rapidly taken up by the lungs (figure 2), with the highest uptake at 30 seconds after injection. Uptake of [^{11}C]-DAA1106 in the lungs was approximately 10-fold higher than uptake in the brain. During the 60 minutes scan, the [^{11}C]-DAA1106 uptake in the lungs decreased by 30%.

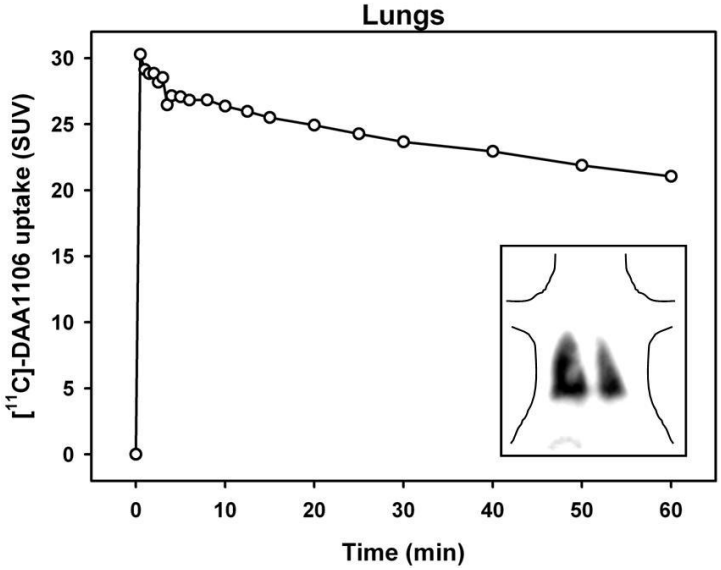

Figure 2 The [11C]-DAA1106 time-activity curve of the lungs of a control rat. The insert represents a coronal plane of the PET image of the rat chest, showing only high uptake in the lungs with no visible uptake in surrounding tissue.

Pharmacokinetic modeling

Brain and plasma time-activity curves are displayed in figure 3a. As mentioned above, [11C]-DAA1106 is rapidly taken up by the brain. The plasma time-activity curves show a small peak in [11C]-DAA1106 activity in plasma and subsequently remained unchanged during the 60 minute scan (SUV of 0.03±0.02). The ratio between brain and plasma uptake of [11C]-DAA1106 activity at 60 minutes was on average 13.

Pharmacokinetic modeling with the [11C]-DAA1106 time-activity curves of the brain showed a good fit to the Logan analysis (figure 3b; r^2 0.99, $p<0.0001$) [25] from 10 minutes after injection, but not to the Patlak analysis [26], suggesting that [11C]-DAA1106 binding is reversible. The distribution volume, as calculated with the Logan analysis, was found to be the highest in the brainstem (42.9±1.0), followed by the cerebellum (34.2±1.8) and the bulbus olfactorius (32.3±0.1). The lowest distribution volume was found in the striatum (26.5±0.2). The distribution volumes correlated well with the average SUV values, as determined from the PET scan ($r^2=0.69$, $p=0.01$). To calculate the binding potential the [11C]-DAA1106 time-activity curves were evaluated with a two-tissue compartment model (K_1-k_4). However, the time-activity curves could not be fitted to the two-tissue compartment model and it was therefore not possible to calculate the binding potential of [11C]-DAA1106.

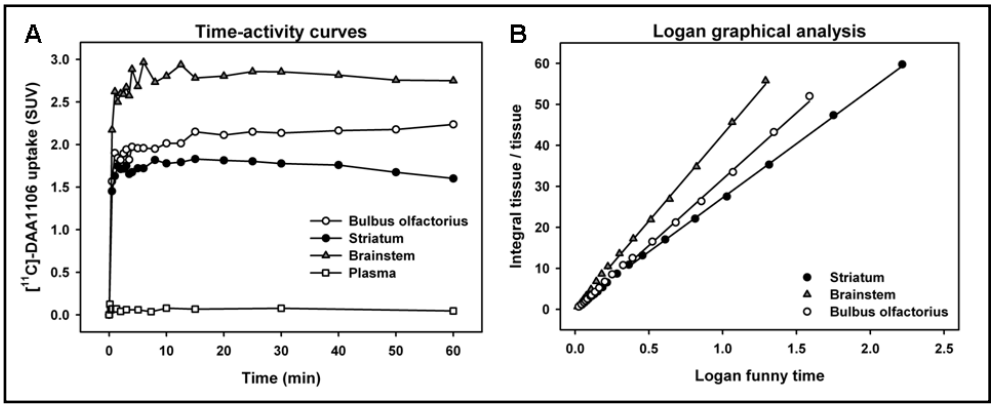

Figure 3 [11C]-DAA1106 time-activity curves and Logan graphical analysis of a HSE rat, of which arterial blood samples were taken during the small animal PET scan. **A** [11C]-DAA1106 time-activity curves of the bulbus olfactorius, striatum, brainstem and plasma, expressed as standardized uptake values. **B** Logan graphical analysis showing a good fit of the bulbus olfactorius, striatum and brainstem, from 10 minutes after injection.

Ex-vivo biodistribution: SUV

For comparison with the results of the PET study, *ex vivo* biodistribution was performed. In addition, *ex vivo* biodistribution allows investigation of brain areas that are too small for small animal PET imaging. The *ex vivo* biodistribution of [11C]-DAA1106 is shown in table 2. In control rats, a significantly higher uptake of [11C]-DAA1106 was found in the bulbus olfactorius, when compared to most other brain areas (15-82%, $p<0.008$), except for the cerebellum ($p=0.130$) and pons ($p=0.170$). High uptake was also found in the medulla, pons and cerebellum.

Intranasal infection with HSV-1, resulted in an increased uptake of [11C]-DAA1106 in all examined brain areas (24-71%), in comparison to control rats. A significantly higher uptake was found in the bulbus olfactorius ($p=0.030$), frontal cortex ($p=0.027$), striatum ($p=0.005$), hippocampus (0.025), entorhinal cortex ($p=0.008$), cerebellum ($p=0.003$), pons ($p=0.001$) and medulla ($p<0.001$). When comparing [11C]-DAA1106 uptake between brain areas in HSE rats, a significantly higher uptake was found in the bulbus olfactorius and medulla when compared to any other brain areas (54-91%, $p<0.005$), except for the cerebellum and pons ($p>0.6$). The standardized uptake values obtained from the last 10 minutes of the PET scan correlated well with the *ex vivo* biodistribution, for both control ($r^2=0.52$, $p<0.0001$) and HSE rats ($r^2=0.54$, $p<0.0001$) (figure 4).

Table 2 *Ex vivo* biodistribution of [11C]-DAA1106, expressed as standardized uptake values (SUV; mean ± SD), 60 min after injection in control rats (control), rats infected with HSV-1 (HSE) and rats infected with HSV-1 pretreated with 5 mg/kg PK11195 5 min before [11C]-DAA1106 injection. *p<0.05 or **p<0.01 as compared to control, ***p<0.001 as compared to control and HSE

	Control (n=5)	HSE (n=7)	HSE+PK11195 (n=4)
Brain:			
Bulbus olfactorius	1.82 ± 0.08	2.55 ± 0.61*	0.84 ± 0.10***
Cingulate/Frontopolar cortex	1.23 ± 0.14	1.64 ± 0.36	0.26 ± 0.03***
Frontal cortex	1.24 ± 0.12	1.66 ± 0.33*	0.29 ± 0.04***
Striatum	1.08 ± 0.07	1.50 ± 0.26**	0.32 ± 0.04***
Hippocampus	1.00 ± 0.07	1.43 ± 0.34*	0.32 ± 0.03***
Amygdala/Piriform cortex	1.08 ± 0.13	1.34 ± 0.23	0.29 ± 0.02***
P/T/O cortex	1.19 ± 0.08	1.55 ± 0.33	0.29 ± 0.03***
Entorhinal cortex	1.18 ± 0.05	1.62 ± 0.30**	0.28 ± 0.03***
Cerebellum	1.57 ± 0.13	2.07 ± 0.27**	0.37 ± 0.04***
Pons	1.57 ± 0.19	2.29 ± 0.30**	0.46 ± 0.10***
Medulla	1.49 ± 0.18	2.55 ± 0.42**	0.53 ± 0.14***
Peripheral organs:			
Heart	20.60 ± 3.47	20.65 ± 4.58	3.79 ± 1.34***
Lungs	61.74 ± 6.80	74.13 ± 19.37	2.22 ± 0.51***
Spleen	16.99 ± 2.42	19.36 ± 5.84	2.34 ± 0.66***
Plasma	0.12 ± 0.04	0.15 ± 0.03	0.70 ± 0.13***

P/T/O, Parietal/Temporal/Occipital

Pre-treatment of HSE rats with PK11195 resulted in a significantly decreased [11C]-DAA1106 uptake when compared to both control (54-79%, p<0.001) and HSE rats (67-84%, p<0.001). Brain area comparison within HSE rats pre-treated with PK11195, revealed a significantly higher [11C]-DAA1106 uptake in the bulbus olfactorius when compared to any other brain area (58-221%, p<0.001).

In peripheral organs, the highest uptake of [11C]-DAA1106 was found in the lungs, followed by the heart and spleen. No differences in uptake were found between control and HSE rats. Pre-treatment with PK11195 resulted in a significantly lower uptake of [11C]-DAA1106 in the organs known to express PBR, including the lungs, heart and spleen (p<0.001). No difference were found between [11C]-DAA1106 plasma uptake in control and HSE rats, while plasma uptake was increased after pre-treatment with PK11195 when compared to both control and HSE rats (p<0.001).

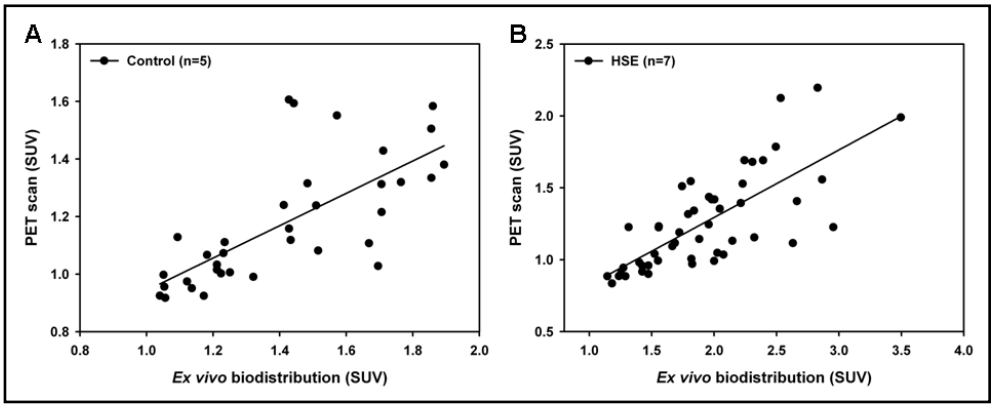

Figure 4 Correlation between the standardized uptake value (SUV) determined *ex vivo* and the standardized uptake value obtained from the PET scan (SUV), for control rats (r^2=0.52, p<0.0001) (**A**) and rats infected with HSV-1 (r^2=0.55, p<0.0001) (**B**).

Discussion

The present study showed that [^{11}C]-DAA1106 binds specifically to the PBR in brain tissue. Distribution of [^{11}C]-DAA1106 in control rats was consistent with in vitro autoradiography studies using [^{3}H]-PK11195 [10] and [^{3}H]-DAA1106 [15]. Highest uptake of [^{11}C]-DAA1106 in the normal rat brain was found in the bulbus olfactorius, followed by the brainstem and cerebellum. In the encephalitic rat brain, a significantly increased *ex vivo* uptake of [^{11}C]-DAA1106 was found in the bulbus olfactorius, frontal cortex, striatum, hippocampus, entorhinal cortex, brainstem and cerebellum. Increased uptake in these brain areas is consistent with viral invasion of the brain via the olfactory epithelium, resulting in the presence of HSV-1 in, amongst others, the bulbus olfactorius, frontal cortex, brainstem and cerebellum [27-29].

Ex vivo uptake of [^{11}C]-DAA1106 in control rats was on average 3-fold higher than the uptake of [^{11}C]-*(R)*-PK11195 [23]. Increased *ex vivo* uptake of [^{11}C]-*(R)*-PK11195 in the encephalitic rat brain was only found in the cerebellum, medulla and pons, while [^{11}C]-DAA1106 uptake was also found in other brain areas, including the cerebral cortex, striatum and hippocampus. The ability of [^{11}C]-DAA1106 to show activation of microglia cells in more brain areas than [^{11}C]-*(R)*-PK11195, is most likely due to the higher affinity of [^{11}C]-DAA1106 for the PBR [15]. A higher binding potential (B_{max}/K_D) of [^{3}H]-DAA1106 was found at the lesion site after traumatic brain injury,

when compared to [3H]-*(R)*-PK11195 [30]. In addition, it was found that [11C]-DAA1106 was retained at greater levels at the site of injury in LPS-lesioned rats, when compared to [11C]-*(R)*-PK11195, as measured with autoradiography and small animal PET [31].

In addition to high affinity binding, [11C]-DAA1106 showed a highly specific binding to the PBR, since pre-treatment with 5 mg/kg of PK11195 resulted in an, on average, 75% decrease in [11C]-DAA1106 brain uptake. Pre-treatment with PK11195 resulted in a high initial peak of [11C]-DAA1106 uptake, as shown by the time-activity curves, which can be explained by reduced binding of [11C]-DAA1106 in peripheral organs. Especially the lungs showed a high [11C]-DAA1106 uptake, which was almost completely blocked by pre-treatment with PK11195.

Although the *ex vivo* biodistribution study showed a significantly increased uptake of [11C]-DAA1106 in several brain areas in the encephalitic rat brain, quantitative analysis of the PET images only showed a small non-significant increased uptake in the brainstem. The discrepancy between *ex vivo* biodistribution and PET images analysis may be attributed to partial volume effects and spillover due to the limited spatial resolution of the PET scanner (1.35 mm FWHM in the center of the field-of-view). Especially partial volume effects can lead to a spread out of high activity to surrounding areas, resulting in an underestimation in the measured [11C]-DAA1106 uptake. This effect may be larger in small brain areas with high activity, surrounded by areas of low activity, i.e. the bulbus olfactorius and brainstem in HSE rats. A previous small animal PET study using rats, visually showed an increased retention of [11C]-DAA1106 in the striatum after local injection of the highly inflammatory LPS (ipsilateral) when compared to the contralateral striatum [31], but the uptake of [11C]-DAA1106 could not be completely blocked by pre-treatment with PK11195. Tracer uptake was only qualitatively analyzed and not compared with *ex vivo* biodistribution. The small animal PET images of the present study also showed an increased uptake at the lesioned sites, when scaling was properly adjusted. This shows that visual analysis of the PET images can be misleading and stresses the necessity of quantification of the uptake. No other small animal PET study, in rodents, has been performed with [11C]-DAA1106 and it is therefore not known if the discrepancy between *ex vivo* biodistribution and quantitative PET analysis is a common finding for [11C]-DAA1106.

Since neuroinflammation can be accompanied by changes in tissue perfusion, which could affect the standardized uptake values, we further explored quantification of

[^{11}C]-DAA1106 uptake by pharmacokinetic modeling. For pharmacokinetic modeling of the uptake of [^{11}C]-DAA1106 in HSE rats, plasma samples were taken from the femoral artery in two rats. The activity in plasma showed a small peak at 15 seconds after injection of [^{11}C]-DAA1106, but remained at a constant level from 30 seconds after injection until the end of the scan. The small initial peak is probably due to a high first pass effect of the tracer in the lungs, which showed high levels of specific uptake of [^{11}C]-DAA1106. Like plasma activity, the time-activity curves of the examined brain areas also showed a constant level of radioactivity over time from 30-60 seconds after injection until the end of the scan. Although the constant level of tracer uptake in the brain suggests that [^{11}C]-DAA1106 irreversibly binds to the PBR, it has been shown that [^{11}C]-DAA1106 can be displaced by DAA1106 and PK11195 [16,31]. The constant high levels of [^{11}C]-DAA1106 in brain tissue may be explained by the 30% decrease in the level of [^{11}C]-DAA1106 in the lungs during the entire scan, suggesting that the lungs serve as a source of constant infusion of [^{11}C]-DAA1106. This may also explain the constant level of plasma activity. The constant low activity in plasma and the constant activity in brain tissue complicated the pharmacokinetic modeling. The time-activity curves showed a good fit to the Logan analysis, showing that the binding of [^{11}C]-DAA1106 to the PBR is reversible. The time-activity curves could not be fitted to a two-tissue compartment model. It was therefore not possible to calculate the binding potential of [^{11}C]-DAA1106. In humans, it has been shown that the binding potential is estimated most reliably using a two-tissue compartment model [20] and was used as an outcome measure in a human study in Alzheimer's disease patients [19]. The plasma time-activity curve of [^{11}C]-DAA1106 in humans showed a higher initial peak in activity, with a more gradual decrease over time. In addition, the plasma time-activity curves in humans were corrected for the presence of radioactive metabolites [20], whereas the rat plasma time-activity curves were not. Because of the high amount of plasma needed to determine the radioactive metabolites, due to the limited counts in the plasma samples, it was not possible to determine the metabolites in the blood samples that were taken in the present study. However, modeling of the time-activity curves that were corrected by an estimate of the percentages of metabolites, by using the percentage of metabolites in plasma of mice that was determined in the study of Zhang et al. [17], did not improve the fit to the two-tissue compartment model. In addition, in study in Alzheimer's disease patients a [^{11}C]-DAA1106 PET scan of 90 minutes was made [19], whereas the [^{11}C]-DAA1106 PET scan in the present study lasted for 60 minutes. It is thus possible that the fit to the two-tissue compartment model is improved by a longer scanning period.

However, the already low plasma levels will be even lower after 90 minutes and therefore not accurate.

Conclusion

[11C]-DAA1106 showed high and specific *ex vivo* uptake in the rat brain, supporting its use in animal models for neurological and psychiatric disorders. However, *in vivo* quantification with PET was complicated, probably due to the limited spatial resolution of the small animal PET scanner. In addition, we showed that reliable quantification using plasma sampling is difficult due to rapid tissue uptake, slow tissue clearance and low plasma activity. [11C]-DAA1106 is therefore not an ideal tracer to perform longitudinal PET studies in small animals to study the role of neuroinflammation in neurological and psychiatric disorders.

Acknowledgements

This study was funded by the Stanley Medical Research Institute, Grant-ID 05-NV-001, and in part by the EC - FP6-project DiMI, LSHB-CT-2005-512146.

References

1 Doorduin J, de Vries EFJ, Dierckx RA, Klein HC. PET imaging of the peripheral benzodiazepine receptor: monitoring disease progression and therapy response in neurodegenerative disorders. Curr.Pharm.Des 2008; 14:3297-3315

2 Doorduin J, de Vries EFJ, Willemsen ATM, Dierckx RA, Klein HC. Neuroinflammation in schizophrenic patients: a positron emission tomography study with [11C]-(R)-PK11195. Neuroimage. 2008; 41:T109-

3 van Berckel BN, Bossong MG, Boellaard R, et al. Microglia Activation in Recent-Onset Schizophrenia: A Quantitative (R)-[(11)C]PK11195 Positron Emission Tomography Study. Biol.Psychiatry 2008; 64:820-822

4 Nakajima K, Kohsaka S. Microglia: neuroprotective and neurotrophic cells in the central nervous system. Curr.Drug Targets Cardiovasc.Haematol.Disord. 2004; 4:65-84

5 Papadopoulos V, Baraldi M, Guilarte TR, et al. Translocator protein (18kDa): new nomenclature for the peripheral-type benzodiazepine receptor based on its structure and molecular function. Trends Pharmacol.Sci. 2006; 27:402-409

6 Gavish M, Bachman I, Shoukrun R, et al. Enigma of the peripheral benzodiazepine receptor. Pharmacol.Rev. 1999; 51:629-650

7 Venneti S, Wang G, Nguyen J, Wiley CA. The positron emission tomography ligand DAA1106 binds with high affinity to activated microglia in human neurological disorders. J.Neuropathol.Exp.Neurol. 2008; 67:1001-1010

8 Cosenza-Nashat M, Zhao ML, Suh HS, et al. Expression of the translocator protein of 18 kDa by microglia, macrophages and astrocytes based on immunohistochemical localization in abnormal human brain. Neuropathol.Appl.Neurobiol. 2009; 35:306-328

9 Turkheimer FE, Edison P, Pavese N, et al. Reference and target region modeling of [11C]-(R)-PK11195 brain studies. J.Nucl.Med. 2007; 48:158-167

10 Kurumaji A, Kaneko K, Toru M. Effects of chronic treatment with haloperidol on [3H]PK 11195 binding in the rat brain and peripheral tissues. Neuropharmacology 1996; 35:1075-1079

11 Papadopoulos V, Lecanu L, Brown RC, Han Z, Yao ZX. Peripheral-type benzodiazepine receptor in neurosteroid biosynthesis, neuropathology and neurological disorders. Neuroscience 2006; 138:749-756

12 Casellas P, Galiegue S, Basile AS. Peripheral benzodiazepine receptors and mitochondrial function. Neurochem.Int. 2002; 40:475-486

13 Banati RB, Myers R, Kreutzberg GW. PK ('peripheral benzodiazepine')--binding sites in the CNS indicate early and discrete brain lesions: microautoradiographic detection of [3H]PK11195 binding to activated microglia. J.Neurocytol. 1997; 26:77-82

14 Bartels AL, Willemsen AT, Doorduin J, de Vries EF, Dierckx RA, Leenders KL. [(11)C]-PK11195 PET: Quantification of neuroinflammation and a monitor of anti-inflammatory treatment in Parkinson's disease? Parkinsonism.Relat Disord. 2009;

15 Chaki S, Funakoshi T, Yoshikawa R, et al. Binding characteristics of [3H]DAA1106, a novel and selective ligand for peripheral benzodiazepine receptors. Eur.J.Pharmacol. 1999; 371:197-204

16 Maeda J, Suhara T, Zhang MR, et al. Novel peripheral benzodiazepine receptor ligand [11C]DAA1106 for PET: an imaging tool for glial cells in the brain. Synapse 2004; 52:283-291

17 Zhang MR, Kida T, Noguchi J, et al. [(11)C]DAA1106: radiosynthesis and in vivo binding to peripheral benzodiazepine receptors in mouse brain. Nucl.Med.Biol. 2003; 30:513-519

18 Venneti S, Wagner AK, Wang G, et al. The high affinity peripheral benzodiazepine receptor ligand DAA1106 binds specifically to microglia in a rat model of traumatic brain injury: implications for PET imaging. Exp.Neurol. 2007; 207:118-127

19 Yasuno F, Ota M, Kosaka J, et al. Increased binding of peripheral benzodiazepine receptor in Alzheimer's disease measured by positron emission tomography with [11C]DAA1106. Biol.Psychiatry 2008; 64:835-841

20 Ikoma Y, Yasuno F, Ito H, et al. Quantitative analysis for estimating binding potential of the peripheral benzodiazepine receptor with [(11)C]DAA1106. J.Cereb.Blood Flow Metab 2007; 27:173-184

21 Esiri MM, Drummond CW, Morris CS. Macrophages and microglia in HSV-1 infected mouse brain. J.Neuroimmunol. 1995; 62:201-205

22 Marques CP, Hu S, Sheng W, Lokensgard JR. Microglial cells initiate vigorous yet non-protective immune responses during HSV-1 brain infection. Virus Res. 2006;

23 Doorduin J, Klein HC, Dierckx RA, James M, Kassiou M, de Vries EFJ. [(11)C]-DPA-713 and [(18)F]-DPA-714 as New PET Tracers for TSPO: A Comparison with [(11)C]-(R)-PK11195 in a Rat Model of Herpes Encephalitis. Mol.Imaging Biol. 2009; DOI: 10.1007/s11307-009-0211-6-

24 Larsen P, Ulin J, Dahlstrom K, Jensen M. Synthesis of [C-11]iodomethane by iodination of [C-11]methane. Appl.Radiat.Isot. 1997; 48:153-157

25 Logan J. Graphical analysis of PET data applied to reversible and irreversible tracers. Nucl.Med.Biol. 2000; 27:661-670

26 Patlak CS, Blasberg RG. Graphical evaluation of blood-to-brain transfer constants from multiple-time uptake data. Generalizations. J.Cereb.Blood Flow Metab 1985; 5:584-590

27 Beers DR, Henkel JS, Schaefer DC, Rose JW, Stroop WG. Neuropathology of herpes simplex virus encephalitis in a rat seizure model. J.Neuropathol.Exp.Neurol. 1993; 52:241-252

28 Doorduin J, Klein HC, Dierckx RA, de Vries EFJ. Herpes simplex encephalitis in rats: a positron emission tomography study with [18F]-FHBG, [11C]-(R)-PK11195 and [18F]-FDG. Neuroimage. 2008; 41:T110

29 Mori I, Goshima F, Ito H, et al. The vomeronasal chemosensory system as a route of neuroinvasion by herpes simplex virus. Virology 2005; 334:51-58

30 Venneti S, Wang G, Wiley CA. The high affinity peripheral benzodiazepine receptor ligand DAA1106 binds to activated and infected brain macrophages in areas of synaptic degeneration: implications for PET imaging of neuroinflammation in lentiviral encephalitis. Neurobiol.Dis. 2008; 29:232-241

31 Venneti S, Lopresti BJ, Wang G, et al. A comparison of the high-affinity peripheral benzodiazepine receptor ligands DAA1106 and (R)-PK11195 in rat models of neuroinflammation: implications for PET imaging of microglial activation. J.Neurochem. 2007; 102:2118-2131

Chapter 6

HSV-1 infection of the brain affects the behavioral and dopaminergic response to ketamine

Janine Doorduin, Erik F.J. de Vries, Fokko J. Bosker, Johan A. den Boer, Rudi A. Dierckx and Hans C. Klein

Submitted for publication

Abstract

Dopaminergic and glutamatergic neurotransmission, as well as their interaction, were found to be disturbed in schizophrenia. Herpes viruses have been proposed to play a role in the etiology of schizophrenia and may be responsible for the disturbed neurotransmission. The aim of the present study was therefore to study the effects of herpes virus infection on dopaminergic and glutamatergic neurotransmission, using positron emission tomography (PET).

Rats were intranasally inoculated with the herpes simplex virus type 1 (HSV-1) or PBS (control). Open field and prepulse inhibition (PPI) studies were performed at day -1 pre-inoculation and on day 2 and 4 post-inoculation. Ketamine or saline was administered from day 0 to 4 post-inoculation. PET was used to study neuroinflammation with [^{11}C]-PK11195 and dopamine release with [^{11}C]-raclopride, at day 5 post-inoculation.

HSV-1 infection of the brain resulted in significantly increased exploration and rearing, but did not affect PPI. Administration of ketamine significantly decreased exploration and rearing in HSV-1 infected rats only. Ketamine did not affect PPI. Neuroinflammation was found in the bulbus olfactorius, frontal cortex, striatum, thalamus and brainstem of HSV-1 infected rats. Administration of ketamine did not affect neuroinflammation in control and HSV-1 infected rats. [^{11}C]-Raclopride binding was increased by ketamine in HSV-1 infected rats, but not affected by HSV-1 infection or ketamine alone.

HSV-1 infection and the corresponding neuroinflammation may play a role in the disturbances in dopaminergic and glutamatergic neurotransmission that were seen in schizophrenia. Additional research is necessary to further unravel to role of HSV-1 in the interaction between dopaminergic and glutamatergic neurotransmission.

Introduction

Schizophrenia is a chronic, disabling brain disease that affects approximately 1% of the human population world-wide [1] and typically has its onset during adolescence and early adulthood. The symptoms of schizophrenia are classified into positive symptoms (i.e. psychosis), such as hallucinations and delusions, negative symptoms, such as social withdrawal and flattened emotion, cognitive symptoms and mood symptoms. Although the exact etiology of schizophrenia is unknown, evidence suggests that several neurotransmitter systems are involved in eliciting the clinical symptoms, of which dopamine and glutamate have received the most attention.

Dopamine was the first neurotransmitter that was thought to be involved in schizophrenia, since positive symptoms could be caused by dopamine enhancing drugs, such as amphetamine and cocaine, [2] and reduced by antipsychotic drugs that block dopamine D_2 receptors [3]. It is nowadays proposed that the positive symptoms are due to hyperactivity of the mesolimbic dopamine system (from the ventral tegmental area to the nucleus accumbens), involving D_2 receptors, and that the negative, cognitive and mood symptoms are due to a hypoactivity of the mesocortical dopamine system (from the ventral tegmental area to the prefrontal cortex), involving D_1 receptors [4-7].

Besides dopamine, glutamate has also been suggested to play a role in schizophrenia. This was based on the finding that antagonists of the glutamate *N*-methyl-*D*-aspartate (NMDA) receptor, such as phencyclidine and ketamine, caused symptoms in healthy volunteers that mimic the positive, negative and cognitive symptoms of schizophrenia [8,9]. In schizophrenic patients, NMDA receptor antagonists increased the symptoms that these patients were already experiencing. These finding suggests that hypofunction of NMDA receptors plays a role in schizophrenia. However, it has also been proposed that hyperactivity of glutamatergic neurons in several brain areas, including the prefrontal cortex, plays a role in schizophrenia. This was, amongst others, based on the finding that NMDA antagonists increased glutamate levels in the striatum and prefrontal cortex [10].

Both dopaminergic and glutamatergic disturbances have been hypothesized to play an important role in schizophrenia, but these disturbances might be related. Glutamatergic projections from the prefrontal cortex to the ventral tegmental area have been suggested to exert an excitatory influence on the mesocortical dopamine system and an inhibitory influence on the mesolimbic dopamine system [11]. NMDA

receptor hypofunction, i.e. reduced glutamatergic neurotransmission, would then results in a decreased mesocortical and an increased mesolimbic dopaminergic neurotransmission, resulting in the negative and positive symptoms of schizophrenia, respectively [12].

Although dopaminergic and glutamatergic neurotransmission, and their interaction, may play a role in schizophrenia, it remains to be elucidated what triggers the dysfunction of these neurotransmitters systems. Genetic and environmental factors may be responsible for the development of schizophrenia and therefore dopaminergic and glutamatergic dysfunction. Related to the involvement of environmental factors, it has been hypothesized that herpes viruses play a role in schizophrenia [13]. Herpes viruses are a family of large DNA viruses, of which eight types are known to cause disease in humans [14]. Schizophrenic patients were found to have an increase in the serum antibodies against herpes viruses, when compared to healthy controls, although negative findings have also been reported [13]. Serum antibodies to both the herpes simplex virus type-1 (HSV-1) and the cytomegalovirus (CMV) were associated with cognitive deficits in schizophrenic patients [15,16], and brain morphological changes with exposure to HSV-1 [17,18]. HSV-1 infection of the brain, resulting in herpes encephalitis, results in changes in consciousness, confusion and psychosis, which resembles the positive symptoms seen in schizophrenia [19,20].

Since herpes viruses were hypothesized to play a role in schizophrenia, it would be of interest to determine whether herpes virus infection of the brain could be responsible for dopaminergic and glutamatergic dysfunction. In mice, it has been shown that intracerebral injection of HSV-1 resulted in an increase in the concentration of whole brain homovanillic acid (HVA), the main metabolite of dopamine [21,22]. In addition, it was found that acute infection of rabbits with HSV-1 by corneal inoculation, resulted in dopaminergic activation, whereas chronic infection decreased dopaminergic neurotransmission [23,24]. To our knowledge, there are no studies that report if HSV-1 infection affects glutamatergic neurotransmission.

Of interest is that HSV-1 infection causes a neuroinflammatory response, characterized by the activation of microglia cells, which are the resident macrophages of the brain, and astrocytes. Both activated microglia cells and astrocytes have shown to be involved in the kynurenine pathway of tryptophan. When the immune response is mediated by activated microglia cells, the degradation of tryptophan results in the formation of the NMDA agonist quinolinic acid, while mediation of the immune response by astrocytes results in the formation of the NMDA antagonist kynurenic

acid [25]. Neuroinflammation, whether or not caused by HSV-1 infection, may thus affect glutamatergic transmission and consequently dopaminergic transmission.

Dopaminergic and glutamatergic neurotransmission may directly or indirectly be affected by HSV-1 infection of the brain, resulting in the symptoms of schizophrenia. The aim of the present study was therefore to study the effect of HSV-1 infection on dopaminergic and glutamatergic neurotransmission, in a rat model of HSV-1 encephalitis. Dopaminergic neurotransmission was studied using positron emission tomography (PET) with [^{11}C]-raclopride, which binds to the dopamine D_2/D_3 receptor. To study glutamatergic neurotransmission, the HSV-1 infected rats were injected with the NMDA antagonist ketamine. With [^{11}C]-raclopride, it has been shown that ketamine enhanced the amphetamine induced dopamine release in the striatum [26]. We hypothesized that HSV-1 infection would affect dopaminergic neurotransmission and that this would be enhanced by ketamine administration.

In addition to [^{11}C]-raclopride PET, [^{11}C]-PK11195 PET was used to study the activation of microglia cells in response to HSV-1 infection and ketamine administration. [^{11}C]-PK11195 is a ligand of the peripheral benzodiazepine receptor, which expression is increased in activated microglia cells.

In addition to the PET study, the behavior of the rats was studied in an open field and prepulse inhibition test. In the open field test, the rats are exposed to a novel environment, which is commonly used to test exploration based anxiety (i.e. locomotion and emotion). PPI is used to measure sensorimotor gating in the central nervous system, which refers to the regulation of transmission of sensory information to a motor system to prevent flooding of sensory information. The principle of PPI is that the magnitude of the reaction to a startling stimulus, such as sound, is decreased when it is immediately preceded by a weaker non-startling prestimulus. In schizophrenic patients, PPI is diminished or absent [27] and ketamine was also found to cause a disruption in PPI in rats [28]. Like for [^{11}C]-raclopride, it was hypothesized that ketamine enhanced the HSV-1 induced behavioral changes.

Material and methods

Animals

Male outbred Wistar-Unilever (SPF) rats (279±29 gram) were obtained from Harlan (Lelystad, The Netherlands). The rats were individually housed in Macrolon cages

(38x26x24 cm) on a layer of wood shavings in a room with constant temperature (21±2°C) and fixed, 12-hour light-dark regime (light phase from 7:00–19:00 hours). Food (standard laboratory chow, RMH-B, Hope Farms, The Netherlands) and water were available ad libitum. After arrival, the rats where allowed to acclimatize for at least seven days. During acclimatization and the entire study, all rats were handled daily. All experiments were approved by the Animal Ethics Committee of the University of Groningen, The Netherlands.

Study design

The rats were randomly divided into four groups: control rats (control), which were administered with saline (n=8) or ketamine (n=6), and rats inoculated with HSV-1 (HSE), which were administered with saline (n=8) or ketamine (n=6). After acclimatization, the study started with the open field and prepulse inhibition (PPI) studies on day -1 (figure 1). On day 0 the rats were inoculated with HSV-1 (HSE) or PBS (control) and the open field and PPI tests were repeated on day 2 and 4 post-inoculation. On day 5 post-inoculation, [^{11}C]-PK11195 and [^{11}C]-raclopride PET scans were made. The first administration with saline or ketamine was on day 0 (at 1 hour post-inoculation), where after saline or ketamine was administered daily until day 4. All studies were performed between 8:00-12:00 hours, in the light phase of the rats.

HSV-1 inoculation

The HSV-1 strain was obtained from a clinical isolate, cultured in Vero-cells and assayed for plaque forming units (PFU) per milliliter. On day 0, the rats were slightly anaesthetized with 5% isoflurane (Pharmachemie BV, The Netherlands) and inoculated with HSV-1 by the application of 100 µl of phosphate-buffered saline with 1x10^7 PFU of virus on the nostrils (50 µl per nostril) with a micro pipette. Control rats were treated similarly by the application of 100 µl PBS without virus. Clinical symptoms in all rats were scored daily post- inoculation by the same observer.

Drugs and administration

Ketamine (Ketanest-S®, 5 mg/ml) was obtained from Pfizer B.V. (Capelle a/d IJssel, The Netherlands). The rats were once daily administered with ketamine (16 mg/kg) or saline, from day 0 to 4 post-inoculation. On day 2 and 4, when the open field and PPI tests were carried out, ketamine or saline was administrated before the open field test

to obtain a direct effect on behavior in addition to the daily (subchronic) administration of ketamine.

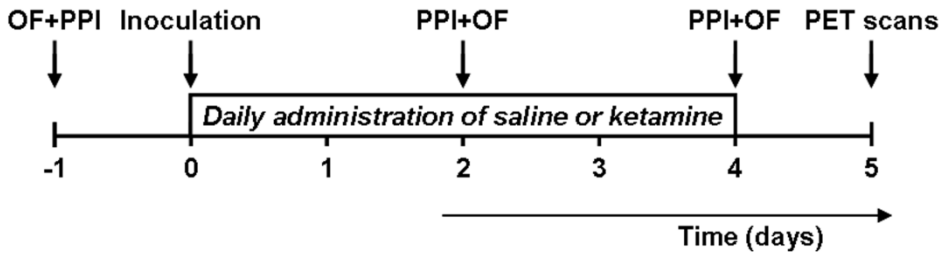

Figure 1 Study design. Rats were inoculated with HSV-1 or PBS at day 0. Open field (OF) and prepulse inhibition (PPI) studies were carried out at day -1 pre-inoculation and at day 2 and day 4 post-inoculation. A [^{11}C]-PK11195 small animal PET scan was performed on day 5 post-inoculation. Administration of saline or ketamine started at day 0 and finished at day 4 post-inoculation.

Open field test

Open field tests on day -1 pre-inoculation and at day 2 and day 4 post-inoculation, were carried out in the light phase of the cycle. The open field tests on day 2 and day 4 post-inoculation were started at 15 minutes after administration of saline or ketamine. The open field consisted of a circular black arena with a diameter of 1 m. The rats were placed into the open field near the wall and behavior was recorded for 8 minutes using a video tracking system (Ethovision 1.96, Noldus Information Technology, Wageningen, The Netherlands). The total distance moved and the frequencies of grooming, exploration and rearing were analyzed.

Prepulse inhibition test

Prepulse inhibition (PPI) tests on day -1 pre-inoculation and at day 2 and day 4 post-inoculation, were carried out in the light phase of the cycle. The PPI tests at day 2 and day 4 post-inoculation started at 40 minutes after administration of saline and ketamine, which was 17 minutes after the open field study was finished. The PPI test was performed using a TSE Startle Response Measuring System. The rats were placed in a small cage (270x100x125 mm) to restrict movement and exploratory behavior. This cage was placed on a transducer platform in the sound-attenuating startle box.

The acoustic stimuli, generated by high-quality and high-linearity speakers, were presented to the rat from both sides of the cages.

After the rats were placed in the startle box, they were allowed to acclimatize for a period of 5 min with a background noise of 70 dB. The PPI test consisted of four different trials: startle pulse alone (SP, 120 dB sound for 40 ms), prepulse alone (PP, 85 dB sound for 20 ms), startle pulse preceded by the prepulse (PP+SP, 85 dB sound for 20 ms followed after 100 ms by 120 dB sound for 40 ms) and nothing (70 dB background noise). Each of the four different trails was presented to the rats 8 times. In addition, the test started with an extra of 3 consecutive SP trials. These extra trials were presented first in order to achieve a relatively stable level of response to the SP trails, since habituation of the reaction is thought to only occur within the first presentations of SP.

The primary outcome measure of the PPI test was the startle response magnitude that was used to calculate the PPI, using the following equation: 100-[100*(mean PP+SP/mean SP)].

PET study

[^{11}C]-PK11195 [29] and [^{11}C]-raclopride [30] were synthesized as described previously. [^{11}C]-PK11195 and [^{11}C]-raclopride PET scans were performed at day 5 post-inoculation, between 8:00-12:00 hours and 13:00-17:00 hours, respectively. There was always more than two hours (3.5±1.2 hours) between the start of the PET scans to allow for decay of [^{11}C]-PK11195. For each PET scan, the rats were anaesthetized by 5% isoflurane (Pharmachemie BV, The Netherlands) that was mixed with medical air at a flow of 2 ml/min, after which anesthesia was maintained with 2% isoflurane. Following induction of anesthesia, the rats were positioned in the small animal PET camera (Focus 220, Siemens Medical Solutions USA, Inc.) in transaxial position with their heads in the field of view. A transmission scan of 515 seconds with a Co-57 point source was obtained for the correction of attenuation by tissue. After the transmission scan was completed, the PET tracer [^{11}C]-PK11195 (42±12 MBq) or [^{11}C]-raclopride (31±16 MBq) was injected via the penile vein. Simultaneously with the injection of the PET tracer a dynamic emission scan of 60 min was started.

The list-mode data of the emission scans was separated into 21 frames (8x30, 3x60, 2x120, 2x180, 3x300 and 3x600 seconds). Emission sinograms were iteratively reconstructed (OSEM2d, 4 iterations) after being normalized, corrected for attenuation and decay of radioactivity.

PET image analysis was performed using the Clinical Applications Packaging Program (CAPP5). Regions of interest were drawn around the bulbus olfactorius, frontal cortex, striatum, thalamus, parietal/temporal/occipital cortex, midbrain, brainstem and cerebellum in a template PET scan that was co-registered with the PET scan of interest by image fusion.

For [^{11}C]-PK11195, the uptake in these regions of interest in the last 10 min of the PET scan was determined in Bq/cm^3 and converted into the standardized uptake value (SUV), which was defined as: [tissue activity concentration (MBq/g)]/[(injected dose (MBq)/body weight (g)]. It was assumed that 1 cm^3 of brain tissue equals 1 gram.

For [^{11}C]-raclopride the time-activity curves were used to calculate the binding potential (BP) with a reference tissue model, using software developed in Matlab 7.1 (Mathworks, Natick, Massachusets). In the reference tissue model, the BP can be calculated without arterial plasma input, by using the time-activity curve of a reference tissue that is devoid of the target receptor, as the input. Because D_2-receptors are not expressed in the cerebellum, this region was chosen as a reference region to calculate the BP in the bulbus olfactorius, frontal cortex, striatum, thalamus, parietal/temporal/occipital cortex, midbrain and brainstem.

Statistics

All data are expressed as mean ± standard deviation. Statistical analysis was performed using SPSS for Windows, version 14.0.2. Statistical analysis on the clinical scores was performed with a one-way ANOVA with a Tukey post hoc test to assess group difference on a given day. The pre-inoculation open field data (day -1) was analyzed using a one-way ANOVA with a Tukey post hoc test. Statistical analysis of open field data on day 2 and 4 post-inoculation was performed with a univariate general linear model, with day -1 as a covariate. Day -1 was used as a covariate to correct for individual differences already present before inoculation. The PPI data, the [^{11}C]-PK11195 uptake and the [^{11}C]-raclopride BP were analyzed using a one-way ANOVA with a Tukey post hoc test. Significance for all tests was reached when the p value was <0.05.

Results

Clinical symptoms

Clinical symptoms (figure 2) were scored daily up to five days post inoculation and categorized into the following clinical scores: (0), no symptoms; (1), ruffled fur and irritated mouth, nose and eyes; (2), behavioral signs, like stress and lethargy, and hunched posture; (3), posterior paralysis and impairment of motor function and (4), severe paralysis, labored breathing or death. For rats inoculated with HSV-1 and treated with saline, the first clinical symptoms appeared on day 2 post-inoculation, while the first clinical symptoms in HSV-1 infected rats treated with ketamine were seen on day 4 post-inoculation. In both the rats that received a daily administration of saline and ketamine, the severity of the clinical symptoms increased gradually over time. No statistically significant differences were found between rats that were administered with saline or ketamine. None of the control rats showed any clinical symptoms.

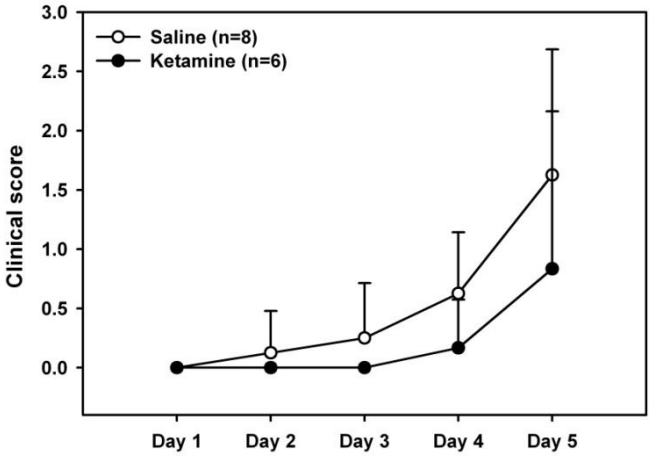

Figure 2 Clinical scores of rats inoculated with HSV-1 on day 1 to day 5 post-inoculation, that received a daily administration of saline (n=8) or ketamine (n=6) from day 1 up until day 4 post-inoculation. The clinical scores represent the following symptoms: (0), no symptoms; (1), ruffled fur and irritated mouth, nose and eyes; (2), behavioral signs, like stress and lethargy, and hunched posture; (3), posterior paralysis and impairment of motor function and (4), severe paralysis, labored breathing or death.

Open field test

The results of the open field tests, which were performed on day -1 pre-inoculation and day 2 and day 4 post-inoculation, are displayed in figure 3. No statistically significant differences between groups on day -1 pre-inoculation were found between

any of the examined behavioral parameters. To correct for the default behavior on day -1 pre-inoculation, statistical analysis on day 2 and day 4 post-inoculation was performed using day -1 as a covariate.

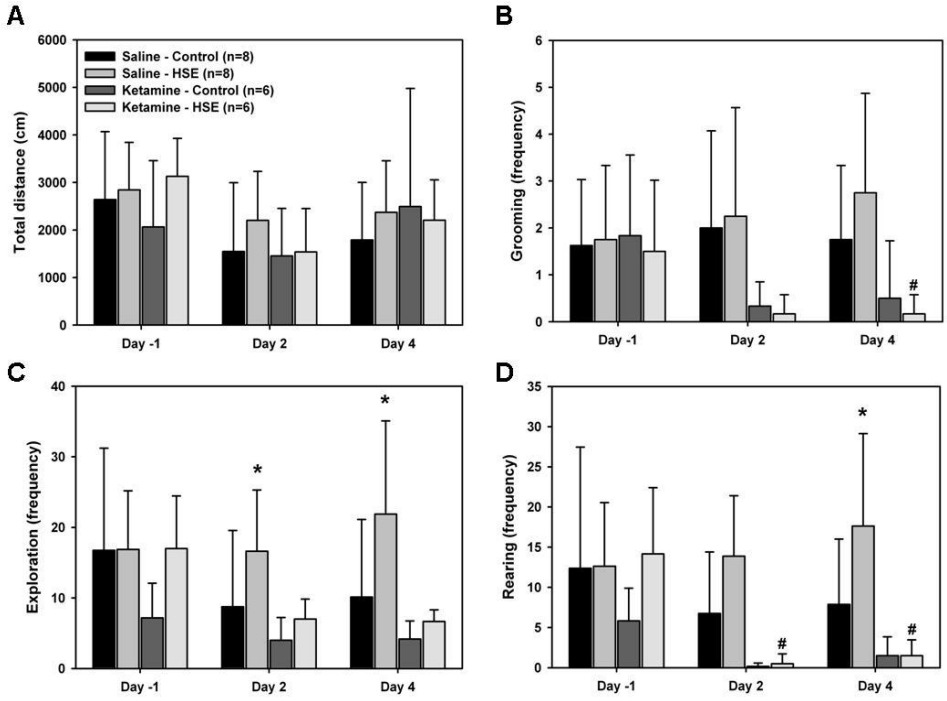

Figure 3 Open field study. The total distance (**A**), the frequency of grooming (**B**), the frequency of exploration (**C**) and the frequency of rearing (**D**) during 8 minute exposure to the open field, on day -1 pre-inoculation and day 2 and 4 post-inoculation of rats inoculated with PBS (control) or HSV-1 (HSE). Rats were administered daily with saline or ketamine from the day of inoculation (day 0) up until day 4 post-inoculation. Data are presented as mean ± standard deviation. *$p<0.05$ in HSV-1 infected rats when compared to the corresponding control rats and #$p<0.05$ in rats that were administered with ketamine when compared to the corresponding rats that were administered with saline.

No statistically significant differences in the total distance moved were found between any of the examined groups. No effect of HSV-1 infection on the frequency of grooming was found on day 2 and 4 post-inoculation. Ketamine did not affect the frequency of grooming on day 2 post-inoculation, but on day 4 post-inoculation, a statistically significant lower frequency of grooming was found in HSV-1 infected rats

that were administered with ketamine, when compared to HSV-1 infected rats administered with saline (0.2±0.4 vs. 2.8±2.1, p=0.037). The frequency of grooming in control rats was not significantly affected by ketamine.

When compared to control rats, a significantly higher frequency of exploration was found for HSV-1 infected rats, when administered with saline, on both day 2 (16.6±8.7 vs. 8.8±10.8, p=0.030) and day 4 (21.9±13.2 vs. 10.1±11.0, p=0.008) post-inoculation. Ketamine did not significantly affect the frequency of exploration on day 2 and day 4 post-inoculation.

The frequency of rearing was statistically significantly higher in HSV-1 infected rats that were administered with saline, when compared to control rats administered with saline (17.6±11.5 vs. 7.9±8.1, p=0.006), on day 4 post-inoculation. In HSV-1 infected rats, administration of ketamine statistically significantly decreased the frequency of rearing, when compared to administration of saline on both day 2 (0.5±1.2 vs. 13.9±7.5, p<0.001) and day 4 (1.5±2.0 vs. 17.6±11.5, p<0.001) post-inoculation. Ketamine did not significantly affect the frequency of rearing in control rats.

Prepulse inhibition test

For the prepulse inhibition test, the difference between day -1 pre-inoculation and day 4 post-inoculation were calculated as follows: (day -1/day 4)*100% (figure 4). Regarding prepulse inhibition, no statistically significant differences were found between any of the examined groups. When looking at the startle pulse when preceded by the prepulse, the difference between day -1 pre-inoculation and day 4 was statistically significantly higher for HSV-1 infected rats when administered with ketamine, when compared to saline (110±40% vs. 51±18%, p=0.025). No statistically significant differences were found for the startle pulse alone.

PET study

The images of the [^{11}C]-PK11195 PET study are displayed in figure 5. In HSV-1 infected rats, increased uptake was mainly seen in the caudal brain areas, when compared to control rats, after both saline and ketamine administration. For quantification of the [^{11}C]-PK11195 uptake, the standardized uptake values (SUV) were calculated (table 1). In HSV-1 infected rats, a statistically significant increase in uptake of [^{11}C]-PK11195 was found in the bulbus olfactorius (46%, p=0.001), frontal cortex (36%, p=0.002), striatum (24%, p=0.011), thalamus (34%, p=0.001), parietal/occipital/temporal cortex (21%, p=0.039) and brainstem (46%, p=0.017),

when compared to control rats, after administration of saline. In rats that were administered with ketamine, a statistically significant increased uptake was found only in the bulbus olfactorius (34%, p=0.012) and the frontal cortex (32%, p=0.013) of HSV-1 infected rats, when compared to control rats. Administration of ketamine alone did not affect [^{11}C]-PK11195 uptake, since no statistically significant differences were found between control and HSE rats (p>0.9) that were administered with saline or ketamine.

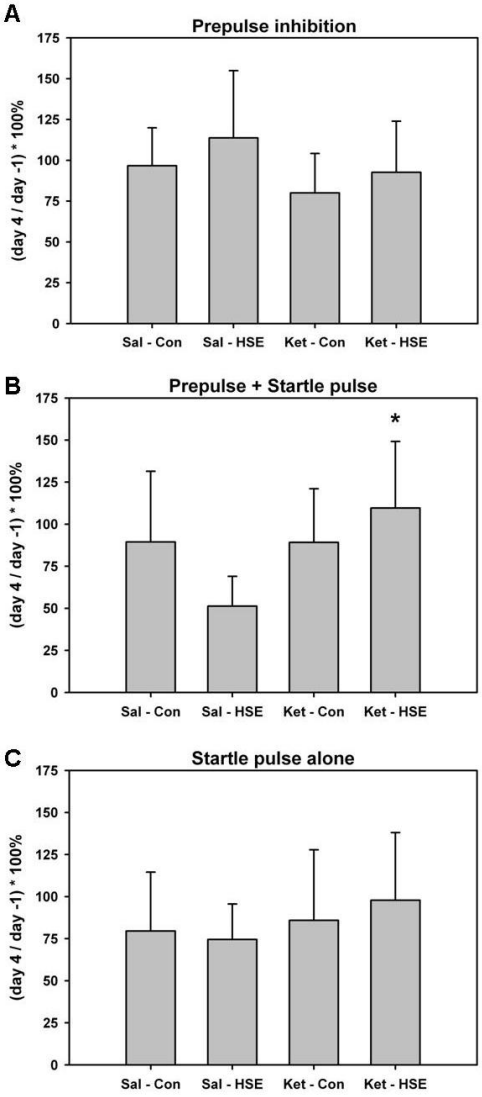

Figure 4 Prepulse inhibition study. The difference between prepulse inhibition (**A**), prepulse + startle pulse (**B**) and startle pulse alone (**C**) on day -1 pre-inoculation and day 4 post-inoculation of rats inoculated with PBS (Con) or HSV-1 (HSE). Rats were administered with saline (Sal) or ketamine (Ket) from the day of inoculation (day 0) up until day 4 post-inoculation. The difference was calculated as follows: (day 4/day -1)*100%. Data are presented as mean ± standard deviation. *p<0.05 when compared to the corresponding rats that were administered with saline.

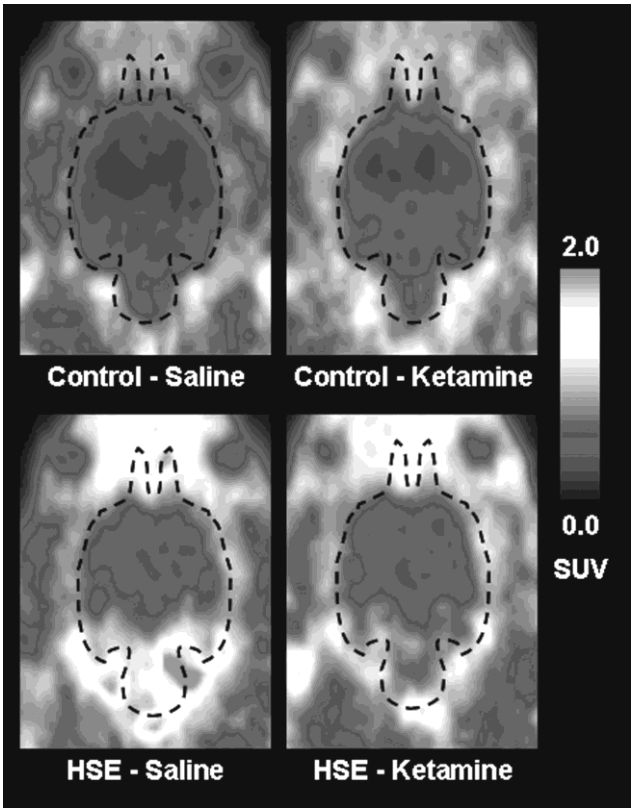

Figure 5 Full-color in appendix. [^{11}C]-PK11195 small animal PET images of control rats (control) and rats inoculated with HSV-1 (HSE), that received a daily administration of saline or ketamine, on day 5 after inoculation. The images display a coronal plane of the rat head at the level of the brainstem, in which the brain is delineated by a dashed line. The images represent brain uptake between 15 and 60 minutes after injection.

Table 1 [^{11}C]-PK11195 uptake in control rats (control) and rats inoculated with HSV-1 (HSE), administered with either saline or ketamine, on day 5 post-inoculation. The values represent the standardized uptake value (SUV, mean ± standard deviation) from the last 10 minutes of the 60 minute small animal PET scan. *p<0.05 and **p<0.005 when compared to the corresponding control

	Saline		Ketamine	
	Control (n=7)	**HSE (n=7)**	**Control (n=6)**	**HSE (n=6)**
Bulbus olfactorius	0.82±0.09	1.19±0.18**	0.86±0.09	1.16±0.21*
Frontal cortex	0.49±0.07	0.67±0.07**	0.48±0.04	0.63±0.11*
Striatum	0.40±0.05	0.50±0.07*	0.40±0.03	0.47±0.04
Thalamus	0.31±0.06	0.41±0.04**	0.33±0.03	0.40±0.04
P/T/O cortex	0.40±0.05	0.48±0.07*	0.44±0.04	0.47±0.06
Midbrain	0.34±0.09	0.36±0.06	0.36±0.05	0.41±0.04
Brainstem	0.46±0.07	0.67±0.19*	0.48±0.07	0.60±0.09
Cerebellum	0.48±0.05	0.54±0.09	0.53±0.06	0.52±0.05

P/T/O, Parietal/Temporal/Occipital

Table 2 [^{11}C]-Raclopride binding potential (mean ± standard deviation) in control rats (control) and rats inoculated with HSV-1 (HSE), administered with either saline or ketamine, on day 5 post-inoculation. *p<0.05 when compared to saline-control

	Saline		Ketamine	
	Control (n=7)	**HSE (n=7)**	**Control (n=6)**	**HSE (n=6)**
Bulbus olfactorius	0.44± 0.17	0.50± 0.17	0.52±0.07	0.64± 0.09
Frontal cortex	0.51± 0.16	0.67± 0.27	0.62±0.15	0.84± 0.21*
Striatum	1.11± 0.26	1.27± 0.32	1.32±0.11	1.43± 0.11
Thalamus	0.45± 0.10	0.47± 0.13	0.46±0.06	0.54± 0.06
P/T/O cortex	0.20± 0.07	0.24± 0.08	0.20±0.05	0.27± 0.06
Midbrain	0.39± 0.09	0.45± 0.10	0.42±0.05	0.49± 0.10
Brainstem	0.30± 0.20	0.39± 0.08	0.42±0.06	0.43± 0.11
Cerebellum	0.44± 0.17	0.50± 0.17	0.52±0.07	0.64± 0.09

P/T/O, Parietal/Temporal/Occipital

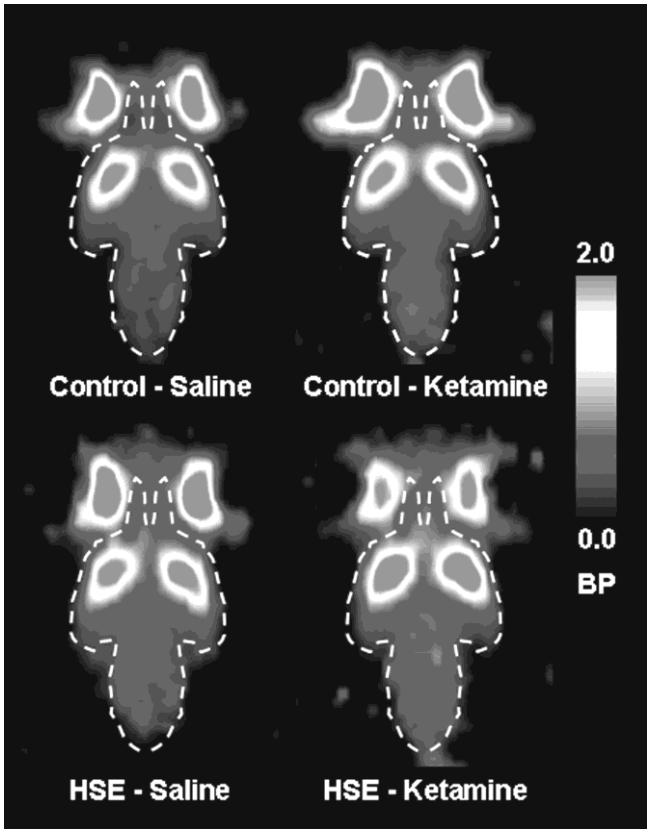

Figure 6 Full-color in appendix. Small animal binding potential (BP) images of the [^{11}C]-raclopride binding potential of control rats (control) and rats inoculated with HSV-1 (HSE), which received a daily administration of saline or ketamine, on day 5 after inoculation. The images display a coronal plane of the rat head at the level of the brainstem, in which the brain is delineated by a dashed line.

The [^{11}C]-raclopride BP images are displayed in figure 6. The highest BP of [^{11}C]-raclopride can be seen in the striatum, consistent with the highest density of D_2 receptors in this area. The [^{11}C]-raclopride BP values of all examined brain areas are displayed in table 2. Both infection with HSV-1 and administration of ketamine did not statistically significantly affect the [^{11}C]-raclopride BP. The combination of HSV-1 infection and ketamine administration did, however, cause a statistically significant increase in the [^{11}C]-raclopride BP in the frontal cortex (65%, $p=0.046$), when compared to control rats that were administered with saline.

Discussion

Disturbances in dopaminergic and glutamatergic neurotransmission, as well as their interaction, have been proposed to play an important role in schizophrenia. Environmental factors, such as herpes viruses, may be the cause of these disturbances. In the present study, it was therefore determined if HSV-1 infection of the brain affects dopaminergic and glutamatergic neurotransmission, as well as the behavioral response. It was found that HSV-1 infection significantly increased the frequency of exploration and rearing, but did not affect PPI and [^{11}C]-raclopride binding. Administration of ketamine significantly decreased the frequency of exploration and rearing, and increased [^{11}C]-raclopride binding, in HSV-1 infected rats only. These finding suggests that HSV-1 infection results in changes in dopaminergic and/or glutamatergic transmission that are inhibited by administration of ketamine.

The intranasal inoculation with HSV-1 resulted in the development of clinical symptoms within two days post-inoculation, with an increase in severity over time. HSV-1 typically infects brain areas along the vomeronasal pathway, such as the prefrontal cortex, piriform cortex, entorhinal cortex and the amygdala, as well as the principle sensory trigeminal nucleus which is located in the brainstem [31,32]. Activation of microglia cells, as shown by [^{11}C]-PK11195, was found in the bulbus olfactorius, frontal cortex, striatum, thalamus and brainstem, which was consistent with the presence of HVS-1 in these areas. Administration of ketamine (16 mg/kg) did not cause activation of microglia cells in control rats, suggesting that this dose of ketamine used did not cause neuronal damage. Higher dosages of ketamine (80-140 mg/kg) were found to increase the number of activated microglia cells [33]. In HSV-1 infected rats, ketamine did not affect the activation of microglia cells either. This does, however, not exclude that ketamine affects the expression of pro- and/or anti-

inflammatory cytokines. It has been shown that ketamine inhibited the expression of pro-inflammatory cytokines (tumor necrosis factor-alpha and nitric oxide) by microglia cells that were activated by bacterial lipoplysaccharide [34,35].

HSV-1 infection of the brain resulted in an increased frequency of exploration and rearing, but did not change the total distance that was travelled in the open field. This suggests that HSV-1 infection of the brain did not affect locomotion per se, but increased hyperactive and stereotype behavior, as shown by a continuous repetition of exploration and rearing behavior. This was consisted with the increase in motor activity of HSV-1 infected rats in their home cage that was found by Ben Hur *et al.* [36,37], although in that study rearing was not reported separately from general motor activity. While HSV-1 infection did cause hyperactivity and stereotype behavior in the open field, PPI inhibition was not affected by HSV-1 infection. Since the present study investigated for the first time the effect of acute HSV-1 infection on PPI, the negative finding could not be compared to other data. It has, however, been shown that postnatal HSV-1 infection reduced PPI in the adult rat, when infection occurred at postnatal day 2 [38]. This could be explained by the interference of HSV-1 with brain development, which was not the case in the present study.

The hyperactivity and stereotype behavior in HSV-1 infected rats may represent behavior relevant to the positive symptoms of schizophrenia, rather than the negative, cognitive and mood symptoms, and could be mediated by increased mesolimbic dopaminergic neurotransmission. However, no changes in the dopamine D_2 receptor binding of [^{11}C]-raclopride were found. This is in accordance with earlier studies, in which HSV-1 infection of the mice brain was found to cause an increase in the whole brain concentration of the main metabolite of dopamine, homovanillic acid (HVA), but did not affect dopamine concentration [22]. In addition, no change was found in the amount or affinity of dopamine D_1 and D_2 receptors in the striatum of HSV-1 infected rabbits. These findings suggest that there is an increase in the dopamine metabolism, without affecting concentrations in dopamine. This could explain the hyperactivity and stereotype behavior found in the presents study, without changes in D_2 receptor binding. While dopamine was thought to mediate the hyperactivity and stereotypy in HSV-1 infected rats, PPI inhibition was not affected. PPI involves a complex brain circuitry, involving the frontal cortex, limbic system, basal ganglia and pons, and is thought to be mainly mediated by dopaminergic neurotransmission at the dopamine D_2 receptor. The absence of PPI inhibition is therefore in agreement with the lack of changes in D_2 receptor binding.

The HSV-1 induced hyperactivity and stereotypy were significantly reduced after ketamine administration. A similar trend was seen in control rats, but this was not statistically significant. The reduction of activity and stereotypy in HSV-1 infected rats was accompanied by an increase in the binding of [^{11}C]-raclopride, in the frontal cortex. Glutamate could play a role in the observed HSV-1 induced behavioral changes and [^{11}C]-raclopride binding.

In this study, we found that ketamine reduced the HSV-1 induced hyperactivity and stereotypy, which is in contrast with the generally reported hyperactivity after administration of ketamine. In addition, ketamine did not induce hyperactivity in control rats. The discrepancy could be related to the treatment protocol. Because of the possible effects of ketamine on HSV-1 infection, a subchronic treatment protocol was chosen, in which rats were treated with ketamine during the entire disease process. In the majority of the studies that show hyperactivity, behavioral tests were performed immediately after a single injection of ketamine in control rats, while open field behavior in the present study was studied at 15 minutes after injection. It has been shown that injection of control rats with 16 mg/kg of ketamine, resulted in a statistically significant increase in open field locomotion that persisted until 25 minutes after injection, after which it normalized to pre-treatment levels of locomotion [39]. This was not found in the present study, despite the same dose of ketamine was used. Chronic administration may thus have different effects on activity. Indeed, both subchronic (5 days) [40] and chronic (90 days) [41] ketamine administration did not affect activity in control rats. In addition, it has been reported in control rats that chronic administration with the NMDA antagonist PCP caused a decrease in dopamine release in the prefrontal cortex, while dopamine is increased after a single injection of PCP [42]. This could explain the lack of ketamine induced hyperactivity in control rats and the decrease in activity and stereotypy that was found in the present study, as well as the increased binding of [^{11}C]-raclopride in the prefrontal cortex of HSV-1 infected rats, due to a decrease in dopamine release. This increased binding of [^{11}C]-raclopride could be an indirect effect of ketamine administration, since the [^{11}C]-raclopride PET scan was performed 1 day after the last ketamine administration.

However, it still remains to be elucidated why these effects were found in HSV-1 infected rats, but not in control rats. Perhaps the enhancement of glutamatergic neurotransmission by activated microglia cells plays a role. Activated microglia cells were found to induce glutamate production, via pro-inflammatory cytokines. In

addition, pro-inflammatory cytokines caused an increase in the expression of indoleamine dioxygenase (IDO) in activated microglia cells, which results in an increased degradation of tryptophan into the NMDA agonist quinolinic acid. Ketamine administration blocks the NMDA receptor and may therefore interfere with the quinolinic acid induced glutamatergic hyperfunction, resulting in reduced activity and stereotypy, as well as reduced dopamine in the prefrontal cortex. In addition, it was found that ketamine inhibits the expression of pro-inflammatory cytokines by microglia, resulting in reduced expression of IDO. Although disturbances in glutamatergic neurotransmission, and consequently, dopaminergic neurotransmission by HSV-1 induced activation of microglia cells were found, the exact mechanism needs to be further elucidated. The results do, however, suggest that HSV-1 induced activation of microglia cells induce changes in dopaminergic and glutamatergic neurotransmission.

Conclusion

Ketamine reduced the HSV-1 induced hyperactivity and stereotypy and affected dopaminergic neurotransmission in HSV-1 infected rats. HSV-1 infection and the corresponding activation of microglia cells may thus play a role in the disturbances in dopaminergic and glutamatergic neurotransmission that were seen in schizophrenia. However, the relation between dopaminergic and glutamatergic neurotransmission is complex, as well as the role in HSV-1 infection on this relation. Thus although the presents study indicated, for the first time, that HSV-1 may play a role in the disturbances in dopaminergic and glutamatergic neurotransmission, additional research is necessary. Especially direct measurements of dopamine and glutamate release may be of particular interest.

Acknowledgement

This study was funded by the Stanley Medical Research Institute, Grant-ID 05-NV-001

References

1 World Health Organization. Neurological disorders; public health challenges.: WHO, 2006

2 Lieberman JA, Kane JM, Alvir J. Provocative tests with psychostimulant drugs in schizophrenia. Psychopharmacology (Berl) 1987; 91:415-433

3 Seeman P, Lee T. Antipsychotic drugs: direct correlation between clinical potency and presynaptic action on dopamine neurons. Science 1975; 188:1217-1219

4 Abi-Dargham A, Moore H. Prefrontal DA transmission at D1 receptors and the pathology of schizophrenia. Neuroscientist. 2003; 9:404-416

5 Davis KL, Kahn RS, Ko G, Davidson M. Dopamine in schizophrenia: a review and reconceptualization. Am.J.Psychiatry 1991; 148:1474-1486

6 Goldman-Rakic PS, Muly EC, III, Williams GV. D(1) receptors in prefrontal cells and circuits. Brain Res.Brain Res.Rev. 2000; 31:295-301

7 Howes OD, Kapur S. The dopamine hypothesis of schizophrenia: version III--the final common pathway. Schizophr.Bull. 2009; 35:549-562

8 Krystal JH, D'Souza DC, Mathalon D, Perry E, Belger A, Hoffman R. NMDA receptor antagonist effects, cortical glutamatergic function, and schizophrenia: toward a paradigm shift in medication development. Psychopharmacology (Berl) 2003; 169:215-233

9 Luby ED, Cohen BD, Rodenbaum G, Gottlieb JS, Kelley R. Study of a new schizophrenomimetic drug; sernyl. AMA.Arch.Neurol.Psychiatry 1959; 81:363-369

10 Moghaddam B, Adams B, Verma A, Daly D. Activation of glutamatergic neurotransmission by ketamine: a novel step in the pathway from NMDA receptor blockade to dopaminergic and cognitive disruptions associated with the prefrontal cortex. J.Neurosci. 1997; 17:2921-2927

11 Carlsson A, Waters N, Carlsson ML. Neurotransmitter interactions in schizophrenia--therapeutic implications. Biol.Psychiatry 1999; 46:1388-1395

12 Laruelle M, Kegeles LS, Abi-Dargham A. Glutamate, dopamine, and schizophrenia: from pathophysiology to treatment. Ann.N.Y.Acad.Sci. 2003; 1003:138-158

13 Yolken R. Viruses and schizophrenia: a focus on herpes simplex virus. Herpes. 2004; 11 Suppl 2:83A-88A

14 Murray, P. K., Rosenthal, K. S., Kobayasi, G. S., and Pfaller, M. A. Medical Microbiology. St. Louis: C.V. Mosby, 2002

15 Dickerson FB, Boronow JJ, Stallings C, Origoni AE, Ruslanova I, Yolken RH. Association of serum antibodies to herpes simplex virus 1 with cognitive deficits in individuals with schizophrenia. Arch.Gen.Psychiatry 2003; 60:466-472

16 Shirts BH, Prasad KM, Pogue-Geile MF, Dickerson F, Yolken R, Nimgaonkar VL. Antibodies to cytomegalovirus and Herpes Simplex Virus 1 associated with cognitive function in schizophrenia. Schizophr.Res. 2008; 106:268-274
17 Pandurangi AK, Pelonero AL, Nadel L, Calabrese VP. Brain structure changes in schizophrenics with high serum titers of antibodies to herpes virus. Schizophr.Res. 1994; 11:245-250
18 Prasad KM, Shirts BH, Yolken RH, Keshavan MS, Nimgaonkar VL. Brain morphological changes associated with exposure to HSV1 in first-episode schizophrenia. Mol.Psychiatry 2007; 12:105-113
19 Torrey EF, Peterson MR. The viral hypothesis of schizophrenia. Schizophr.Bull. 1976; 2:136-146
20 Whitley RJ. Herpes simplex encephalitis: adolescents and adults. Antiviral Res. 2006; 71:141-148
21 Lycke E, Roos BE. Effect on the monoamine-metabolism of the mouse brain by experimental Herpes simplex infection. Experientia 1968; 24:687-689
22 Lycke E, Roos BE. Influence of changes in brain monoamine metabolism on behaviour of herpes simplex-infected mice. J.Neurol.Sci. 1974; 22:277-289
23 Paivarinta MA, Marttila RJ, Rinne JO, Rinne UK. Decrease in mesencephalic dopamine autoreceptors in experimental herpes simplex encephalitis. J.Neural Transm.Gen.Sect. 1992; 89:71-80
24 Paivarinta MA, Marttila RJ, Rinne JO, Rinne UK. Dopaminergic neurotransmission in chronic herpes simplex virus brain infection in rabbits. J.Neural Transm.Gen.Sect. 1993; 93:205-212
25 Muller N, Schwarz M. Schizophrenia as an inflammation-mediated dysbalance of glutamatergic neurotransmission. Neurotox.Res. 2006; 10:131-148
26 Kegeles LS, Abi-Dargham A, Zea-Ponce Y, et al. Modulation of amphetamine-induced striatal dopamine release by ketamine in humans: implications for schizophrenia. Biol.Psychiatry 2000; 48:627-640
27 Braff DL, Geyer MA, Swerdlow NR. Human studies of prepulse inhibition of startle: normal subjects, patient groups, and pharmacological studies. Psychopharmacology (Berl) 2001; 156:234-258
28 Swerdlow NR, Bakshi V, Waikar M, Taaid N, Geyer MA. Seroquel, clozapine and chlorpromazine restore sensorimotor gating in ketamine-treated rats. Psychopharmacology (Berl) 1998; 140:75-80
29 Doorduin J, Klein HC, Dierckx RA, James M, Kassiou M, de Vries EFJ. [(11)C]-DPA-713 and [(18)F]-DPA-714 as New PET Tracers for TSPO: A Comparison with [(11)C]-(R)-PK11195 in a Rat Model of Herpes Encephalitis. Mol.Imaging Biol. 2009; DOI: 10.1007/s11307-009-0211-6-

30 Ehrin E, Farde L, de Paulis T, et al. Preparation of 11C-labelled Raclopride, a new potent dopamine receptor antagonist: preliminary PET studies of cerebral dopamine receptors in the monkey. Int.J.Appl.Radiat.Isot. 1985; 36:269-273
31 Beers DR, Henkel JS, Schaefer DC, Rose JW, Stroop WG. Neuropathology of herpes simplex virus encephalitis in a rat seizure model. J.Neuropathol.Exp.Neurol. 1993; 52:241-252
32 Mori I, Goshima F, Ito H, et al. The vomeronasal chemosensory system as a route of neuroinvasion by herpes simplex virus. Virology 2005; 334:51-58
33 Nakki R, Nickolenko J, Chang J, Sagar SM, Sharp FR. Haloperidol prevents ketamine- and phencyclidine-induced HSP70 protein expression but not microglial activation. Exp.Neurol. 1996; 137:234-241
34 Chang Y, Lee JJ, Hsieh CY, Hsiao G, Chou DS, Sheu JR. Inhibitory effects of ketamine on lipopolysaccharide-induced microglial activation. Mediators.Inflamm. 2009; 2009:705379-
35 Shibakawa YS, Sasaki Y, Goshima Y, et al. Effects of ketamine and propofol on inflammatory responses of primary glial cell cultures stimulated with lipopolysaccharide. Br.J.Anaesth. 2005; 95:803-810
36 Ben Hur T, Cialic R, Itzik A, Barak O, Yirmiya R, Weidenfeld J. A novel permissive role for glucocorticoids in induction of febrile and behavioral signs of experimental herpes simplex virus encephalitis. Neuroscience 2001; 108:119-127
37 Ben Hur T, Itzik A, Barak O, et al. Immunization with a nonpathogenic HSV-1 strain prevents clinical and neuroendocrine changes of experimental HSV-1 encephalitis. J.Neuroimmunol. 2004; 152:5-10
38 Engel JA, Zhang J, Bergstrom T, et al. Neonatal herpes simplex virus type 1 brain infection affects the development of sensorimotor gating in rats. Brain Res. 2000; 863:233-240
39 Imre G, Fokkema DS, den Boer JA, Ter Horst GJ. Dose-response characteristics of ketamine effect on locomotion, cognitive function and central neuronal activity. Brain Res.Bull. 2006; 69:338-345
40 Becker A, Grecksch G. Ketamine-induced changes in rat behaviour: a possible animal model of schizophrenia. Test of predictive validity. Prog.Neuropsychopharmacol.Biol.Psychiatry 2004; 28:1267-1277
41 Lannes B, Micheletti G, Warter JM, Kempf E, Di Scala G. Behavioural, pharmacological and biochemical effects of acute and chronic administration of ketamine in the rat. Neurosci.Lett. 1991; 128:177-181
42 Jentsch JD, Roth RH. The neuropsychopharmacology of phencyclidine: from NMDA receptor hypofunction to the dopamine hypothesis of schizophrenia. Neuropsychopharmacology 1999; 20:201-225

Chapter 7

Inhibition of HSV-1 induced behavioral changes and microglia cell activation by antipsychotics

Janine Doorduin, Hans C. Klein, Rudi A. Dierckx, Willem A. Nolen and Erik F.J. de Vries

Submitted for publication

Abstract

Schizophrenia is a severe and chronic brain disease with unknown etiology. It is hypothesized that viral brain infections play a role in schizophrenia. In line with this hypothesis, the present study investigated whether antipsychotics can reduce virus induced activation of microglia cells (neuroinflammation) and behavioral changes in a rat model of herpes encephalitis.

Rats were intranasally inoculated with the herpes simplex virus type 1 (HSV-1). Open field behavior was assessed at day -1 pre-inoculation and on day 2 and 4 post-inoculation. To determine the effect of antipsychotics, clozapine or risperidone was administered from day 0 to day 4 post-inoculation. Positron emission tomography was used to study activated microglia cells with [^{11}C]-PK11195 and dopamine D_2 receptors with [^{11}C]-raclopride at day 5 post-inoculation.

Inoculation with HSV-1 resulted in significantly increased open field exploration on day 4 post-inoculation, but did not significantly change locomotion, anxiety and arousal. Activated microglia cells were found in the brainstem, frontal and cortical brain areas of HSV-1 infected rats. Treatment with clozapine and risperidone resulted in inhibition of microglia cell activation and inhibition of increased exploration in HSV-1 infected rats. [^{11}C]-Raclopride binding was not affected by HSV-1 infection or treatment with antipsychotics.

Behavioral changes and microglia cell activation in response to HSV-1 infection of the brain were inhibited by the antipsychotics clozapine and risperidone, while no effect of D_2 binding was found. Additional research on the role of HSV-1 and the accompanied microglia cell activation as potential targets for the treatment of schizophrenia seems justified.

Introduction

Schizophrenia is a severe brain disease that affects approximately 1% of the world's population [1]. The symptoms of schizophrenia usually have its onset during adolescence or early adulthood and are classified into positive symptoms, such as hallucinations and delusions, negative symptoms, such as social withdrawal and flattened emotion, cognitive symptoms and mood symptoms. To reduce symptoms, schizophrenic patients are in general treated with antipsychotic drugs. The typical (classical) antipsychotic drugs were the first drugs used in the treatment of schizophrenia and were effective in reducing the positive symptoms of schizophrenia, primarily by blocking dopamine receptors. The reduction of symptoms by typical antipsychotics has led, amongst others, to the hypothesis that dopamine is one of the major neurotransmitter systems involved in schizophrenia. Starting with the discovery of clozapine as an antipsychotic drug that not only reduced the positive symptoms, but also the negative, cognitive and mood symptoms, several new atypical antipsychotic drugs have been introduced, including olanzapine and risperidone. The increased effectiveness of the atypical antipsychotic drugs is attributed to the fact that they do not only block dopamine receptors, but also bind to a variety of other neurotransmitter receptors. Amongst others, this suggested the involvement of these neurotransmitter systems in schizophrenia.

Despite extensive research, including studies involving the variety of neurotransmitter systems, the exact etiology remains unknown. Genetic and environmental factors are thought to be responsible for the development of schizophrenia and therefore the deficits in neurotransmission. Related to the environmental factors, it has been hypothesized that herpes viruses play a role in the etiology of schizophrenia [2]. Herpes viruses are a family of large DNA viruses, of which eight types are known to cause disease in humans [3]. Schizophrenic patients were found to have an increase in the serum antibodies against the herpes simplex virus type-1 (HSV-1) and the cytomegalovirus (CMV) [2], which were associated with cognitive deficits in schizophrenic patients [4,5]. In addition, brain morphological changes were associated with exposure to HSV-1 [6,7]. In addition, treatment of CMV positive schizophrenic patients with the anti-viral drug valaciclovir resulted in a reduction in the overall schizophrenic symptoms (positive, negative and cognitive) [8]. HSV-1 may be of particular interest because either reactivation of latent HSV-1 in the trigeminal ganglion or primary infection with HSV-1 can result in herpes encephalitis, mainly involving the temporal lobe and limbic structures. Consequently, patients with herpes

encephalitis present with changes in consciousness, confusion and can also reveal psychosis in the prodromal phase [9-11].

A consequence of HSV-1 infection of the brain is the development of a neuroinflammatory response, characterized by the presence of activated microglia cells. In patients with a herpes encephalitis, caused by HSV-1, activated microglia cells were found beyond the primary focal lesion, which persisted many months after anti-viral treatment [12]. In rats infected with HSV-1, we and others have showed widespread activation of microglia cells in brain areas infected with HSV-1 [13-15]. Herpes virus infection of the brain is thus accompanied by the activation of microglia cells and if herpes viruses do indeed play a role in schizophrenia, a neuroinflammatory response is expected in schizophrenic patients. Indeed, activated microglia cell were found to be present in the post-mortem schizophrenic brain [16], In addition, functional imaging studies with positron emission tomography (PET) have shown a global activation of microglia cells in first-episodes schizophrenic patients [17] and a focal, hippocampal activation of microglia cells in psychotic schizophrenic patients [18].

Related to herpes virus infection of the brain and the accompanied activation of microglia cells, it has been suggested that neuroleptic drugs have antiviral and anti-inflammatory properties. The neuroleptic drug chlorpromazine, used to treat schizophrenia patients, was found to reduce HSV-1 activity [19]. *In vitro* studies on the effect of antipsychotic drugs on inflammation, showed that risperidone and haloperidol were found to inhibit the production of pro-inflammatory cytokines by microglia cells treated with interferon-γ [20]. In addition, olanzapine was also found to reduce the production of nitric oxide by lipopolysaccharide-stimulated microglia cells [21].

Based on the proposed role of herpes virus infections and neuroinflammation in schizophrenia, we hypothesized that antipsychotic drugs may in part improve schizophrenic symptoms by reducing neuroinflammatory processes. Therefore we investigated the effect of antipsychotic drugs on HSV-1 induced behavioral changes and neuroinflammation in a rat model of HSV-1 encephalitis. In this model rats are intranasally inoculated with HSV-1, resulting in transport of the virus from the olfactory epithelium towards the brain. This causes a direct and controlled dissemination of HSV-1 within the brain, involving brain areas that correspond to the frontal, orbital and temporal cortices in humans [13,22]. Behavioral studies in rats infected with HSV-1 showed the presence of learning impairment [23] and an increase

in motor activity and aggression [24]. Inoculation of 2-day old pups with HSV-1 resulted in impairment in sensorimotor gating at adulthood [25], which has also been found to be impaired in schizophrenic patients [26].

To study behavior in HSV-1 infected rats, we exposed the rats to an open field arena to study locomotion and exploratory behavior. Activation of microglia cells was determined using PET, with the tracer [^{11}C]-PK11195. [^{11}C]-PK11195 is a ligand of the peripheral benzodiazepine receptor that is overexpressed in activated microglia cells and can therefore be used as a marker for imaging of neuroinflammation. To investigate the effect of antipsychotics on HSV-1 induced behavior and neuroinflammation, rats were treated with the atypical antipsychotics clozapine and risperidone. Clozapine and risperidone are the most commonly used antipsychotics in treatment of schizophrenia patients and were found to bind to different neurotransmitter receptors. While clozapine has moderate affinity for most neurotransmitter receptors, including dopaminergic and serotonergic receptor, risperidone has a higher affinity for mainly the dopaminergic D_2 and serotonergic $5HT_{2A}$ receptor. With respect to the different affinity for the dopaminergic D_2 and the importance of dopamine in schizophrenia, the effect of HSV-1 infection of the brain and the treatment with antipsychotics on dopamine D_2 receptors was studied using the D_2 receptor ligand [^{11}C]-raclopride PET as well.

Material and methods

[^{11}C]-PK11195

[^{11}C]-PK11195 was labeled by trapping [^{11}C]-methyl iodide [27] in a solution of 1 mg N-desmethyl-PK11195 and 10 mg potassium hydroxide in 300 µl dimethylsulfoxide. The reaction mixture was allowed to react for 1 minute at 40 °C, neutralized with 1M HCl and passed through a 45 µm Millex HV filter. The filtrate was purified by HPLC using a µBondapak C18 column (7.8x300 mm) with acetonitrile/25 mM NaH_2PO_4 (pH 3.5) (55/45) as the eluent (flow 5 ml/min). To remove the organic solvents from the product, the collected HPLC fraction (retention time 7 min) was diluted with 100 ml of water and passed through an Oasis HLB 30 mg (1 cc) cartridge. The cartridge was washed twice with 10 ml of water and subsequently eluted with 0.7 ml of ethanol and 5 ml of water. The product was sterilized by filtration over a 0.20 µm Millex LG filter. The product was obtained in 20-70% radiochemical yield. Quality control was performed by HPLC, using a Novapak C18 column (150x3.9 mm) with

acetonitrile/25 mM NaH_2PO_4 (pH 3.5) (60/40) as the eluent at a flow of 1 ml/min. The radiochemical purity was always >95% and the specific activity was 25-100 MBq/nmol.

[^{11}C]-Raclopride

[^{11}C]-Raclopride was labeled by trapping [^{11}C]-methyl iodide [27] in a solution of 1 mg desmethylraclopride and 1.4 mg sodium hydroxide in 300 µl dimethylsulfoxide. The reaction mixture was allowed to react for 4 minute at 80 °C. After the reaction, the product was purified by HPLC using a µBondapak C18 column (7.8x300 mm) with acetonitrile/10 mM H_3PO_4 (30/70) as the eluent (flow 5 ml/min). To remove the organic solvents from the product, the collected HPLC fraction (retention time 8 min) was diluted with 100 ml of water and passed through an Oasis HLB 200 mg cartridge. The cartridge was washed twice with 8 ml of water and subsequently eluted with 0.8 ml of 1% H_3PO_4 in ethanol and 8 ml of phosphate buffer (pH 7.2). The product was sterilized by filtration over a 0.20 µm Millex LG filter. Quality control was performed by HPLC, using a µBondapak C18 column (300x3.9 mm) with acetonitrile/10 mM H_3PO_4 (30/70) as the eluent at a flow of 1 ml/min. The radiochemical purity was always >95% and the specific activity was 40-100 MBq/nmol.

Animals

Male outbred Wistar-Unilever (SPF) rats (272±30 gram) were obtained from Harlan (Lelystad, The Netherlands). The rats were individually housed in Macrolon cages (38x26x24 cm) on a layer of wood shavings in a room with constant temperature (21±2°C) and fixed, 12-hour light-dark regime (light phase from 7:00–19:00 hours). Food (standard laboratory chow, RMH-B, Hope Farms, The Netherlands) and water were available ad libitum. After arrival, the rats were allowed to acclimatize for at least seven days. During acclimatization and during the entire study all rats were handled daily. All experiments were approved by the Animal Ethics Committee of the University of Groningen, The Netherlands.

Study design

The rats were randomly divided into six groups: control rats (control) treated with either saline (n=8), clozapine (n=6) or risperidone (n=5) and rats inoculated with HSV-1 (HSE) treated with either saline (n=8), clozapine (n=6) or risperidone (n=6).

After acclimatization, the study started with an open field experiment on day -1 (figure 1). On day 0, the rats were inoculated with HSV-1 (HSE) or PBS (control) and the open field experiment was repeated on day 2 and 4 post-inoculation. On day 5 post-inoculation, a [^{11}C]-PK11195 and a [^{11}C]-raclopride PET scan were made. Treatment with saline, clozapine or risperidone started on day 0 (at 1 hour post-inoculation) and the last dose was given on day 4. The rats were sacrificed on day 6 post-inoculation to prevent severe discomfort due to HSV-1 infection of the brain. The experiments were performed between 8:00-12:00 hours, with exception of the [^{11}C]-raclopride PET scan that was performed between 13:00-17:00 hours.

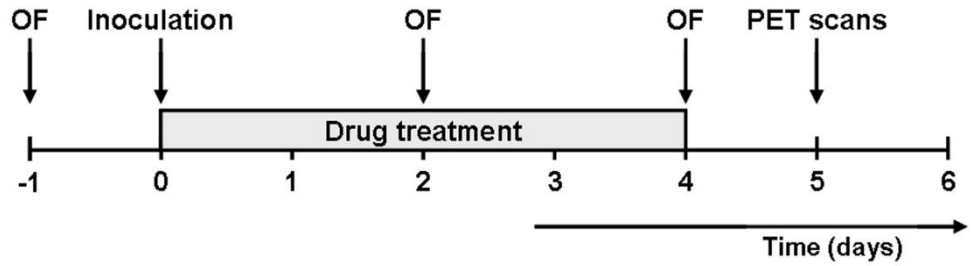

Figure 1 Study design. Rats were inoculated with HSV-1 or PBS at day 0. Open field (OF) experiments were carried out on day -1 pre-inoculation and on day 2 and day 4 post-inoculation. [^{11}C]-PK11195 and [^{11}C]-raclopride small animal PET scans were performed on day 5 post-inoculation. Drug treatment (saline, clozapine and risperidone) started on day 0 and finished on day 4 post-inoculation.

HSV-1 inoculation

The HSV-1 strain was obtained from a clinical isolate, cultured in Vero-cells and assayed for plaque forming units (PFU) per milliliter. On day 0, the rats were slightly anaesthetized with 5% isoflurane (Pharmachemie BV, The Netherlands) and inoculated with HSV-1 by application of 100 µl of phosphate-buffered saline with 1x10^{7} PFU of virus on the nostrils (50 µl per nostril) with a micro pipette. Control rats were treated similarly by application of 100 µl PBS without virus. Clinical symptoms in all rats were scored daily post-inoculation by the same observer.

Drugs and treatment

Clozapine was obtained from Sigma-Aldrich Inc (Saint Louis, Missouri, USA) and risperidone was obtained from MP Biomedicals (Irvine, California, USA). Clozapine

and risperidone were dissolved in a minimal volume of 0.1 M HCl and diluted with saline. The pH was adjusted to 6-7 with 0.1 M NaOH. The final concentration was 4.3 mg/ml for clozapine and 0.35 mg/ml for risperidone. The solutions were made freshly prior to injection.

Rats were treated once daily with clozapine (10 mg/kg/day i.p.) or risperidone (0.5 mg/kg/day i.p.) from day 0 until day 4 post-inoculation. Control rats were treated similarly with saline. On day 2 and 4, when the open field experiments were carried out, drug treatment was 1 hour after the open field experiment.

Open field experiment

Open field experiments on day -1 pre-inoculation and day 2 and day 4 post-inoculation, were carried out in the light phase of the daily cycle. The open field consisted of a circular black arena with a diameter of 1 m. The rats were placed into the open field near the wall and behavior was recorded for 8 minutes using a video tracking system (Ethovision 1.96, Noldus Information Technology, Wageningen, The Netherlands).

The total distance moved was analyzed as a measure of locomotion, the frequency of rearing as a measure of exploration and the frequency of grooming as a measure of arousal. To measure anxiety, the open field area was subdivided into three circular zones with diameters of 0.33, 0.66 and 1 meter with the centre of the zones in the centre of the open field. The total distance moved in the zone in the centre of the open field (with the diameter of 0.33 m) was used as a reciprocal measure of anxiety (i.e. a high total distance moved in the centre of the open field corresponds to low anxiety).

PET experiment

[^{11}C]-PK11195 and [^{11}C]-raclopride PET scans were performed on day 5 post-inoculation, between 8:00-12:00 hours and 13:00-17:00 hours, respectively. There was always more than two hours (3.5±1.2 hours) between the start of the PET scans to allow for decay of [^{11}C]-PK11195. For each PET scan the rats were anaesthetized by 5% isoflurane (Pharmachemie BV, The Netherlands) that was mixed with medical air at a flow of 2 ml/min, after which anesthesia was maintained with 2% isoflurane. Following induction of anesthesia, the rats were positioned in the small animal PET camera (Focus 220, Siemens Medical Solutions USA, Inc.) in transaxial position with

their heads in the field of view. A transmission scan of 515 seconds with a Co-57 point source was obtained for the correction of attenuation by tissue. After the transmission scan was completed, the PET tracer [^{11}C]-PK11195 (44±16 MBq) or [^{11}C]-raclopride (35±16 MBq) was injected via the penile vein. Simultaneously with the injection of the PET tracer a dynamic emission scan of 60 min was started.

The list-mode data of the emission scans was separated into 21 frames (8x30, 3x60, 2x120, 2x180, 3x300 and 3x600 seconds). Emission sinograms were iteratively reconstructed (OSEM2d, 4 iterations) after being normalized, corrected for attenuation and decay of radioactivity.

PET image analysis

PET image analysis was performed using the Clinical Applications Packaging Program (CAPP5). Regions of interest were drawn around the bulbus olfactorius, frontal cortex, striatum, thalamus, parietal/temporal/occipital cortex, midbrain, brainstem and cerebellum in a template PET scan that was co-registered with the PET scan of interest by image fusion. For [^{11}C]-PK11195, the uptake in these regions of interest in the last 10 min of the PET scan was determined in Bq/cm^3 and converted into the standardized uptake value (SUV), which was defined as: [tissue activity concentration (MBq/cm^3)]/[(injected dose (MBq)/body weight (g)]. It was assumed that 1 cm^3 of brain tissue equals 1 gram.

For [^{11}C]-raclopride the time-activity curves were used to calculate the binding potential (BP) with a reference tissue model, using software developed in Matlab 7.1 (Mathworks, Natick, Massachusets). In the reference tissue model, the BP can be calculated without arterial plasma input, using the time-activity curve of a reference tissue that is devoid of the target receptor as the input. Because D_2-receptors are not expressed in the cerebellum, this region was chosen as a reference region to calculate the BP in the bulbus olfactorius, frontal cortex, striatum, thalamus, parietal/temporal/occipital cortex, midbrain and brainstem.

Statistics

All data are expressed as mean ± standard deviation. Statistical analysis was performed using SPSS for Windows, version 14.0.2.

Statistical analysis on the clinical scores was performed with a one-way ANOVA with a LSD post hoc test to assess group difference on a given day. The pre-inoculation open field data on locomotion, exploration, arousal and anxiety on day -1 was

analyzed using a one-way ANOVA with a LSD post hoc test. For locomotion on day 2 and 4 post-inoculation, analysis was performed with a univariate general linear model, with locomotion on day -1 as a covariate. Day -1 was used as a covariate to correct for individual differences in locomotion already present before inoculation. For exploration, arousal and anxiety on day 2 and day 4 post-inoculation, analysis was performed using a univariate general linear model with as covariates the exploration, arousal and anxiety on day-1 respectively, and the locomotion on the corresponding day (i.e. locomotion on day 2 was used as a covariate for analysis of behavior on day 2). Day -1 was used as a covariate for the same reason as mentioned for locomotion, being that it allows correction for individual differences. Locomotion can be a confounder in the other behavioral outcome measures and was therefore used as a covariate in the analysis of the other behavioral outcome measures. The [^{11}C]-PK11195 uptake and the binding potential of [^{11}C]-raclopride were analyzed using a one-way ANOVA with a LSD post hoc test. Significance for all tests was reached when the p value was <0.05.

Results

Clinical symptoms

Clinical symptoms (figure 2) were scored daily until day 6 post-inoculation and categorized into the following clinical scores: (0), no symptoms; (1), ruffled fur and irritated mouth, nose and eyes; (2), behavioral signs, like stress and lethargy, and hunched posture; (3), posterior paralysis and impairment of motor function and (4), severe paralysis, labored breathing or death. The first clinical symptoms were seen on day 2 post-inoculation, in HSE rats treated with saline. For risperidone and clozapine treated HSE rats, the first clinical symptoms were seen on day 4 and 5 post-inoculation, respectively. At day 4 post-inoculation, a significantly lower clinical sore was found in HSE rats treated with clozapine, when compared to HSE rats treated with saline (0.0 vs. 0.63 ± 0.52, $p=0.011$). A lower clinical score was also found in HSE rats treated with risperidone, when compared to HSE rats treated with saline, but this was not statistically significant (0.17 ± 0.41 vs. 0.63 ± 0.52, $p=0.099$). None of the control rats showed any clinical symptoms.

In the HSE rats treated with saline, there was a gradual increase in the clinical score from day 2 to day 6 post-inoculation. In contrast, in HSE rats treated with clozapine and risperidone, there was a delayed, but more rapid, increase in clinical symptoms

from day 4, the last day of treatment, to day 6 post-inoculation. No differences were found between the clinical scores of HSE rats treated with saline (2.13±1.25), clozapine (2.17±1.83) and risperidone (2.50±0.55) on day 6 post-inoculation. Thus, the antipsychotics clozapine and risperidone delayed the onset of clinical symptoms, but could not prevent them.

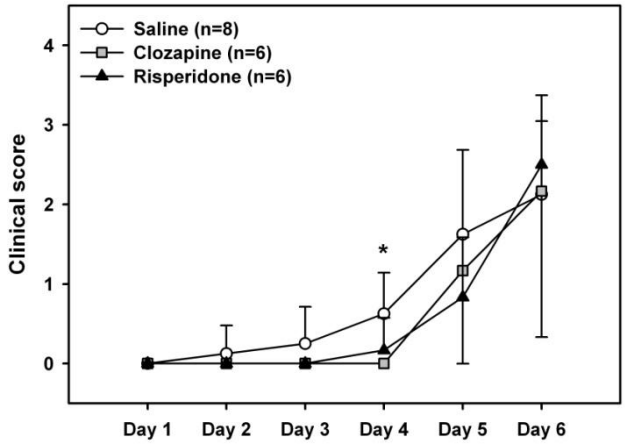

Figure 2 Clinical scores of rats inoculated with HSV-1 on day 1 to day 6 post-inoculation, that were treated with either saline (n=8), clozapine (n=6) or risperidone (n=6) from day 1 until day 4 post-inoculation. The clinical scores represent the following symptoms: (0), no symptoms; (1), ruffled fur and irritated mouth, nose and eyes; (2), behavioral signs, like stress and lethargy, and hunched posture; (3), posterior paralysis and impairment of motor function and (4), severe paralysis, labored breathing or death. *$p<0.05$ for saline treated rats, when compared to clozapine treated rats at day 4 post-inoculation.

Open field experiment

The results of the open field experiments, that were performed on day -1 pre-inoculation and on day 2 and 4 post-inoculation, are displayed in figure 3. The total distance moved in the open field was used as a measure of locomotion. No differences in locomotion between groups were found on day -1 pre-inoculation. Statistical analysis of day 2 and 4 post-inoculation were performed with day -1 as a covariate to correct for variance pre-inoculation. No statistically significant differences between groups were found on day 2. On day 4 post-inoculation, locomotion was statistically significantly decreased by treatment with clozapine in HSE rats, when compared to saline treatment (1250±405 vs. 2370±1085, $p=0.018$).

The total distance moved in the centre of the open field, the frequency of rearing and the frequency of grooming were analyzed as a measure of anxiety (i.e. a high total

distance moved in the centre of the open field corresponds to low anxiety), exploration and arousal, respectively. No group differences for anxiety, exploration and arousal were found on day -1 pre-inoculation. Because locomotion on day 2 or day 4 post-inoculation can affect anxiety, exploration and arousal on the corresponding days, locomotion was used as a covariate. In addition, anxiety, exploration and arousal on day -1 pre-inoculation, can affect the behavior on day 2 and day 4 post-inoculation. Therefore, anxiety, exploration or arousal on day -1 pre-inoculation, were also used as a covariate in the statistical analysis on day 2 and day 4.

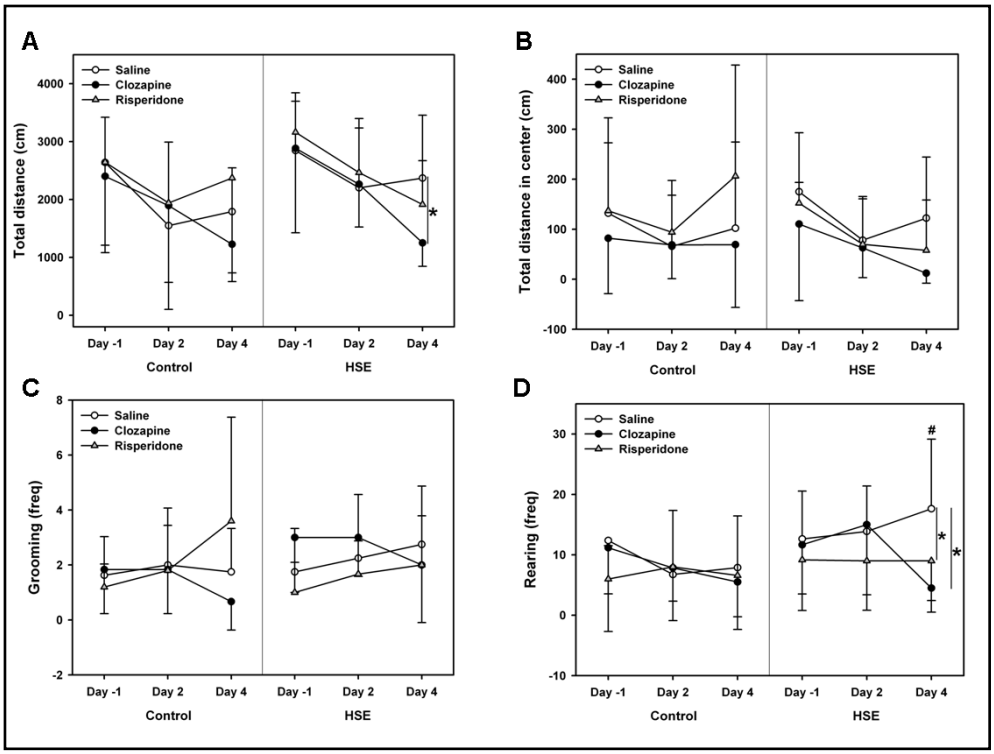

Figure 3 Open field experiment. The total distance (**A**), total distance in the center of the open field (**B**), the frequency of grooming (**C**) and the frequency of rearing (**D**) during 8 minute exposure to the open field, on day -1 pre-inoculation and day 2 and 4 post-inoculation with PBS (control) or HSV-1 (HSE). Rats were treated with saline, clozapine or risperidone from the day of inoculation (day 0) until day 4 post-inoculation. Data are presented as mean ± standard deviation, *$p<0.05$ between different treatment groups on the same day and #$p<0.001$ for saline treated HSE rats, when compared to saline treated control rats.

HSV-1 inoculation, did not affect exploration (i.e. frequency of rearing) on day 2 post-inoculation. However, a statistically significant increase in exploration (i.e. frequency of rearing) was found for HSE rats treated with saline on day 4 post-inoculation, when compared to control rats treated with saline (18±12 vs. 8±8, p=0.005). This increased exploration in HSE rats on day 4 post-inoculation was statistically significantly reduced by treatment with clozapine (5±2 vs. 18±12, p=0.008) and risperidone (9±9 vs. 18±12, p=0.033), when compared to saline treatment. No effect of treatment on exploration was found in control rats.

In summary, HSE rats showed an increase in exploration, which was inhibited by treatment with clozapine and risperidone. Locomotion was decreased by clozapine, while anxiety and arousal were not affected by HSV-1 infection or clozapine and risperidone treatment.

[^{11}C]-PK11195 PET

The [^{11}C]-PK11195 PET images of control and HSE rats, treated with saline, clozapine or risperidone, are displayed in figure 4. The PET images showed low [^{11}C]-PK11195 brain uptake in control rats, which was not affected by treatment with clozapine and risperidone. In HSE rats treated with saline, visual analysis of the PET images showed an increased [^{11}C]-PK11195 uptake when compared to control rats treated with saline, mainly in the bulbus olfactorius and brainstem. This increased uptake was inhibited by treatment with clozapine or risperidone. To quantify the uptake of [^{11}C]-PK11195, the SUV from the last 10 minutes of the PET scan was calculated for all examined brain areas (table 1). In saline treated rats, a statistically significant increased [^{11}C]-PK11195 uptake was found in the bulbus olfactorius ($p<0.001$), frontal cortex ($p=0.001$), striatum ($p=0.013$), parietal/occipital/temporal cortex ($p=0.020$) and brainstem ($p=0.019$) of HSE rats, when compared to control rats. Treatment with clozapine or risperidone prevented the increase in [^{11}C]-PK11195 uptake in HSE rats and consequently the brain uptake in these groups resembled the uptake in saline treated control rats. In HSE rats treated with clozapine, a statistically significant increased [^{11}C]-PK11195 uptake only remained in the brainstem ($p=0.013$), when compared to control rats treated with clozapine. In addition, pre-treatment of HSE rats with clozapine statistically significantly reduced the [^{11}C]-PK11195 uptake in the bulbus olfactorius ($p=0.012$), when compared to saline treated HSE rats. For risperidone treated rats, a statistically significant higher [^{11}C]-PK11195 uptake in HSE rats only remained in the striatum ($p=0.011$), when compared to control rats.

Treatment with clozapine and risperidone did not affect the [11C]-PK11195 uptake in sham inoculated rats.

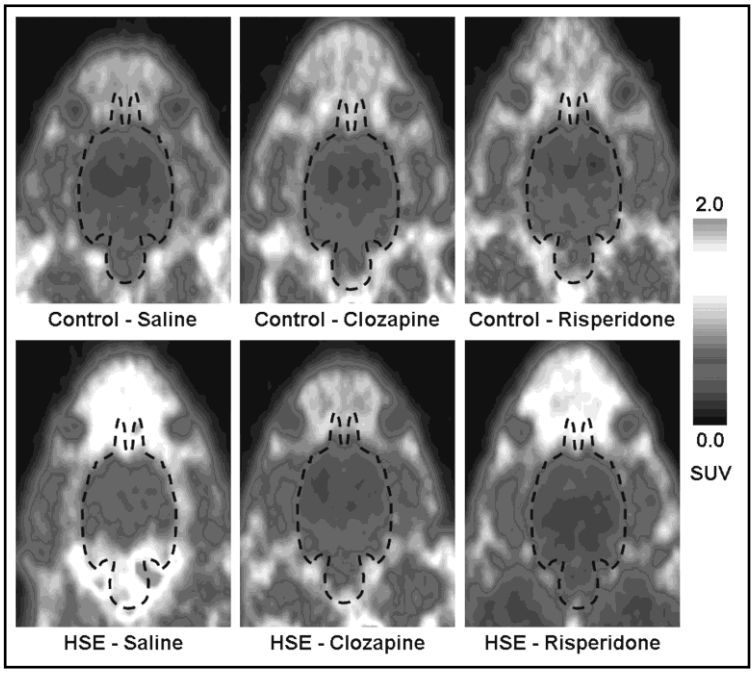

Figure 4 Full-color in appendix. [11C]-PK11195 small animal PET images of control rats (control) and rats inoculated with HSV-1 (HSE), treated with saline, clozapine or risperidone, on day 5 after inoculation. The images display a coronal plane of the rat head at the level of the brainstem, in which the brain is delineated by a dashed line. The images represent brain uptake between 15 and 60 minutes after injection.

Table 1 [11C]-PK11195 brain uptake in control rats (control) and rats inoculated with HSV-1 (HSE), treated with either saline, clozapine or risperidone, on day 5 after inoculation. The values represent the standardized uptake value (SUV, mean ± standard deviation) from the last 10 minutes of the 60 minute small animal PET scan. *p<0.05 or **p<0.005 as compared to control

	Saline		Clozapine		Risperidone	
	Cntrl (n=7)	**HSE (n=7)**	**Cntrl (n=6)**	**HSE (n=6)**	**Cntrl (n=4)**	**HSE (n=5)**
Bulbus olf	0.82±0.09	1.19±0.18**	0.90±0.18	0.91±0.15	1.01±0.22	1.03±0.13
Frontal ctx	0.49±0.07	0.67±0.07**	0.55±0.14	0.53±0.15	0.54±0.12	0.59±0.07
Striatum	0.40±0.05	0.50±0.07*	0.41±0.07	0.43±0.06	0.40±0.03	0.47±0.03*
Thalamus	0.31±0.06	0.41±0.04**	0.32±0.07	0.39±0.03	0.33±0.07	0.41±0.06
P/T/O ctx	0.40±0.05	0.48±0.07*	0.43±0.05	0.47±0.02	0.41±0.05	0.50±0.08
Midbrain	0.34±0.09	0.36±0.06	0.36±0.05	0.40±0.07	0.37±0.09	0.42±0.12
Brainstem	0.46±0.07	0.67±0.19*	0.45±0.08	0.59±0.09*	0.38±0.12	0.57±0.20
Cerebellum	0.48±0.05	0.54±0.09	0.49±0.06	0.56±0.07	0.51±0.15	0.49±0.13

Cntrl, control, P/T/O; Parietal/Temporal/Occipital

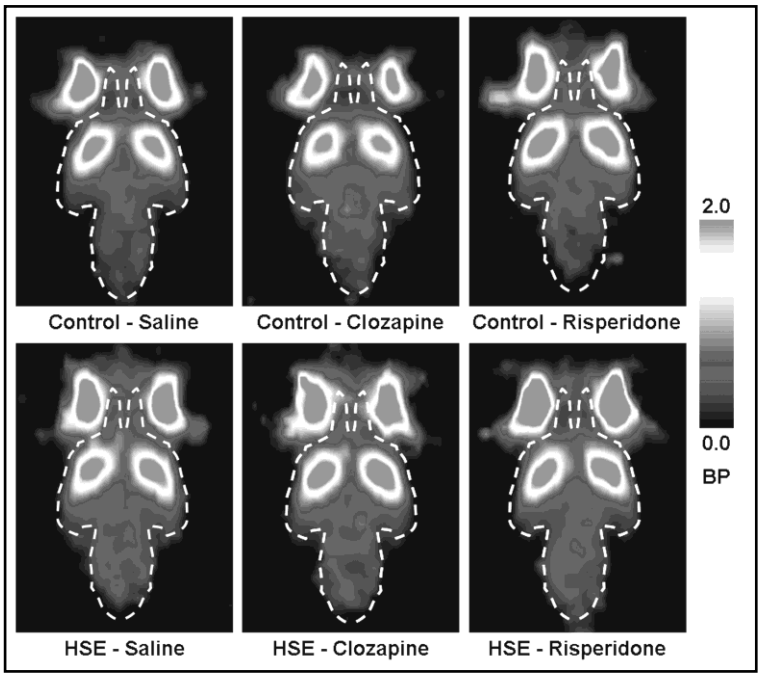

Figure 5 Full-color in appendix. Small animal PET images of the [11C]-raclopride binding potential (BP) of control rats (control) and rats inoculated with HSV-1 (HSE), treated with saline, clozapine or risperidone, on day 5 after inoculation. The images display a coronal plane of the rat head at the level of the brainstem, in which the brain is delineated by a dashed line.

Table 2 [11C]-Raclopride brain uptake in control rats (control) and rats inoculated with HSV-1 (HSE), treated with either saline, clozapine or risperidone, on day 5 after inoculation. The values represent the binding potential (BP, mean ± standard deviation) of [11C]-raclopride.

	Saline		Clozapine		Risperidone	
	Cntrl (n=6)	**HSE (n=6)**	**Cntrl (n=5)**	**HSE (n=5)**	**Cntrl (n=3)**	**HSE (n=4)**
Bulbus olf	0.44±0.17	0.50±0.17	0.51±0.07	0.48±0.09	0.51±0.14	0.37±0.09
Frontal ctx	0.51±0.16	0.67±0.27	0.74±0.10	0.68±0.20	0.57±0.11	0.66±0.03
Striatum	1.11±0.26	1.27±0.32	1.33±0.10	1.29±0.22	1.26±0.15	1.30±0.14
Thalamus	0.45±0.10	0.47±0.13	0.54±0.06	0.48±0.08	0.44±0.07	0.41±0.03
P/T/O ctx	0.20±0.07	0.24±0.08	0.26±0.06	0.23±0.04	0.19±0.06	0.20±0.04
Midbrain	0.39±0.09	0.45±0.10	0.48±0.08	0.48±0.07	0.39±0.02	0.41±0.03
Brainstem	0.30±0.20	0.39±0.08	0.41±0.07	0.46±0.09	0.35±0.04	0.38±0.06
Cerebellum	0.44±0.17	0.50±0.17	0.51±0.07	0.48±0.09	0.51±0.14	0.37±0.09

Cntrl, control, P/T/O; Parietal/Temporal/Occipital cortex

[11C]-Raclopride PET

The [11C]-raclopride BP images (figure 5) showed the highest BP in the striatum, consistent with the distribution of dopamine D_2-recepors in the brain. No differences

between control and HSE rats, treated with either saline, clozapine or risperidone could be demonstrated.

The values of the BP were statistically significantly higher in the striatum, when compared to all other brain areas ($p<0.005$), but no differences in BP were found between control and HSE rats, treated with saline, clozapine or risperidone. In addition, no differences between any of the groups were found for the influx of [^{11}C]-raclopride (K_1/k_1) into or the efflux of [^{11}C]-raclopride (k_2) out of brain tissue.

Discussion

The present study showed that HSV-1 infection of the brain induced activation of microglia cells and specific behavioral changes in the rat. Treatment with the atypical antipsychotics clozapine and risperidone inhibited both the behavioral changes and the activation of microglia cells. To the best of our knowledge, this is the first study that showed that atypical antipsychotics can inhibit activation of microglia cells and HSV-1 induced behavioral changes, *in vivo*.

The presence of activated microglia cells, as measured with [^{11}C]-PK11195 PET, that was found in the frontal brain areas, cortical brain areas and in the brainstem at day 5 post-inoculation, was consistent with the presence of infectious virus and activation of microglia cells in these areas, as reported in literature [22,28,29]. The inhibition of HSV-1 induced activation of microglia cells by clozapine and risperidone implies a novel mechanism of action of these drugs. It has been shown that global activation of microglia cells is present in the grey matter in recent-onset schizophrenic patients [17] and that focal activation of microglia cells appeared to be a feature of schizophrenia-related psychosis [18]. Thus, efficacy of antipsychotic treatment may in part be explained by the anti-inflammatory properties of these drugs. Indeed, it has been shown *in vitro* that typical and atypical antipsychotic drugs inhibited the expression of pro-inflammatory cytokines by LPS and IFN-γ induced activation of microglia cells [20,21,30,31].

The outcome measure of the effect of antipsychotic treatment in HSV-1 infected rats was the activation of microglia cells, which was inhibited by clozapine and risperidone. However, one could argue that antipsychotic treatment inhibited viral replication and thus HSV-1 infection of the brain, resulting in a prevention of microglia cell activation. However, the appearance of clinical symptoms after clozapine and risperidone treatment was terminated, suggested that viral infection of the brain was

only temporarily suppressed, if not at all. Antipsychotic treatment was effective in suppressing the clinical symptoms in HSV-1 infected rats up to day 4 post-inoculation, but was not effective in preventing the symptoms at day 5 and 6 post-inoculation. If treatment with clozapine and risperidone would have prevented viral replication, the severe clinical symptoms at day 6 post-inoculation would most likely not have occurred, because the viral entry of the brain would have been prevented. Thus, clozapine and risperidone appear to exert their protective effect predominantly by the suppression of the activation of microglia cells.

Important questions that rise from the findings of the present study are how HSV-1 induced activation of microglia cells caused increased exploratory behavior and what the mechanism is behind inhibition of microglia cell activation by clozapine and risperidone. The occurrence of behavioral changes could be related to dopaminergic neurotransmission. The increased exploratory behavior was consistent with the increased locomotor activity that was observed in HSV-1 infected rats in their home cage, especially between day 4 and 5 after inoculation [24]. Changes in locomotor activity are often used to assess rodent models for schizophrenia and the effect of treatment with antipsychotics, and can be attributed to an increase in the action of dopamine at both the D_1 and D_2 receptors [32]. In psychostimulant rodent models, the amphetamine induced increase in dopamine caused an increase in locomotion and rearing in the open field [33,34]. Based on the behavioral data of the present study and the resemblance of this behavior with amphetamine induced behavioral changes, dopamine seems to be involved. Indeed, it has been shown that acute HSV-1 infection of the brain caused an increase in dopamine release [35,36], while chronic HSV-1 infection may cause a decrease in dopaminergic activation [37]. Although dopamine may play a role in HSV-1 induced behavioral changes, it was shown in the present study that there were no changes in the binding potential of [^{11}C]-raclopride in HSV-1 infected rats, suggesting there are no changes in the expression of D_2 receptors or release of dopamine. However, it should be noted that [^{11}C]-raclopride PET was performed one day after the last behavioral test and termination of drug treatment. Consequently, any changes in dopaminergic activity could have been normalized in this period of time.

The inhibition of the activation of microglia cells may be due to binding of clozapine and risperidone to the variety of neurotransmitter receptors that are expressed on microglia cells [38] or to inhibition of pro-inflammatory cytokines that are involved in progression of the activation of microglia cells. Clozapine and risperidone were found

to bind with different affinity to different neurotransmitter receptors, which could explain why clozapine was found to more effective in inhibiting HSV-1 induced behavioral changes and activation of microglia cells than risperidone. However, to give a definite answer to the question how HSV-1 infection of the brain and the accompanied microglia cell activation affects behavior and what the mechanism is behind inhibition by antipsychotics, as well as the difference between antipsychotics, further research is necessary.

Conclusion

The increase in exploratory behavior and the microglia cell activation in response to HSV-1 infection of the brain are inhibited by the atypical antipsychotics clozapine and risperidone. The present study implies a novel mechanism of action of clozapine and risperidone, which is to inhibit HSV-1 induced behavioral changes by reducing microglia cell activation in the brain. Additional research on the role of HSV-1 and the accompanied microglia cell activation as a potential target for the treatment of schizophrenia is warranted.

Acknowledgement

This study was funded by the Stanley Medical Research Institute, Grant-ID 05-NV-001.

References

1 World Health Organization. Neurological disorders; public health challenges.: WHO, 2006

2 Yolken R. Viruses and schizophrenia: a focus on herpes simplex virus. Herpes. 2004; 11 Suppl 2:83A-88A

3 Murray, P. K., Rosenthal, K. S., Kobayasi, G. S., and Pfaller, M. A. Medical Microbiology. St. Louis: C.V. Mosby, 2002

4 Dickerson FB, Boronow JJ, Stallings C, Origoni AE, Ruslanova I, Yolken RH. Association of serum antibodies to herpes simplex virus 1 with cognitive deficits in individuals with schizophrenia. Arch.Gen.Psychiatry 2003; 60:466-472

5 Shirts BH, Prasad KM, Pogue-Geile MF, Dickerson F, Yolken R, Nimgaonkar VL. Antibodies to cytomegalovirus and Herpes Simplex Virus 1 associated with cognitive function in schizophrenia. Schizophr.Res. 2008; 106:268-274

6 Pandurangi AK, Pelonero AL, Nadel L, Calabrese VP. Brain structure changes in schizophrenics with high serum titers of antibodies to herpes virus. Schizophr.Res. 1994; 11:245-250

7 Prasad KM, Shirts BH, Yolken RH, Keshavan MS, Nimgaonkar VL. Brain morphological changes associated with exposure to HSV1 in first-episode schizophrenia. Mol.Psychiatry 2007; 12:105-113

8 Dickerson FB, Boronow JJ, Stallings CR, Origoni AE, Yolken RH. Reduction of symptoms by valacyclovir in cytomegalovirus-seropositive individuals with schizophrenia. Am.J.Psychiatry 2003; 160:2234-2236

9 Kennedy PG. A retrospective analysis of forty-six cases of herpes simplex encephalitis seen in Glasgow between 1962 and 1985. Q.J.Med. 1988; 68:533-540

10 Miller JK, Hesser F, Tompkins VN. Herpes simplex encephalitis. Report of 20 cases. Ann.Intern.Med. 1966; 64:92-103

11 Misra PC, Hay GG. Encephalitis presenting as acute schizophrenia. Br.Med.J. 1971; 1:532-533

12 Cagnin A, Myers R, Gunn RN, et al. In vivo visualization of activated glia by [11C] (R)-PK11195-PET following herpes encephalitis reveals projected neuronal damage beyond the primary focal lesion. Brain 2001; 124:2014-2027

13 Doorduin J, Klein HC, Dierckx RA, de Vries EFJ. Herpes simplex encephalitis in rats: a positron emission tomography study with [18F]-FHBG, [11C]-(R)-PK11195 and [18F]-FDG. Neuroimage. 2008; 41:T110-

14 Esiri MM, Drummond CW, Morris CS. Macrophages and microglia in HSV-1 infected mouse brain. J.Neuroimmunol. 1995; 62:201-205

15 Marques CP, Hu S, Sheng W, Lokensgard JR. Microglial cells initiate vigorous yet non-protective immune responses during HSV-1 brain infection. Virus Res. 2006;

16 Steiner J, Mawrin C, Ziegeler A, et al. Distribution of HLA-DR-positive microglia in schizophrenia reflects impaired cerebral lateralization. Acta Neuropathol. 2006; 112:305-316
17 van Berckel BN, Bossong MG, Boellaard R, et al. Microglia Activation in Recent-Onset Schizophrenia: A Quantitative (R)-[(11)C]PK11195 Positron Emission Tomography Study. Biol.Psychiatry 2008; 64:820-822
18 Doorduin J, de Vries EFJ, Willemsen ATM, Dierckx RA, Klein HC. Neuroinflammation in schizophrenic patients: a positron emission tomography study with [11C]-(R)-PK11195. Neuroimage. 2008; 41:T109-
19 Patou G, Crow TJ, Taylor GR. The effects of psychotropic drugs on synthesis of DNA and the infectivity of herpes simplex virus. Biol.Psychiatry 1986; 21:1221-1225
20 Kato T, Monji A, Hashioka S, Kanba S. Risperidone significantly inhibits interferon-gamma-induced microglial activation in vitro. Schizophr.Res. 2007; 92:108-115
21 Hou Y, Wu CF, Yang JY, et al. Effects of clozapine, olanzapine and haloperidol on nitric oxide production by lipopolysaccharide-activated N9 cells. Prog.Neuropsychopharmacol.Biol.Psychiatry 2006; 30:1523-1528
22 Beers DR, Henkel JS, Schaefer DC, Rose JW, Stroop WG. Neuropathology of herpes simplex virus encephalitis in a rat seizure model. J.Neuropathol.Exp.Neurol. 1993; 52:241-252
23 Beers DR, Henkel JS, Kesner RP, Stroop WG. Spatial recognition memory deficits without notable CNS pathology in rats following herpes simplex encephalitis. J.Neurol.Sci. 1995; 131:119-127
24 Ben Hur T, Cialic R, Itzik A, Barak O, Yirmiya R, Weidenfeld J. A novel permissive role for glucocorticoids in induction of febrile and behavioral signs of experimental herpes simplex virus encephalitis. Neuroscience 2001; 108:119-127
25 Engel JA, Zhang J, Bergstrom T, et al. Neonatal herpes simplex virus type 1 brain infection affects the development of sensorimotor gating in rats. Brain Res. 2000; 863:233-240
26 Parwani A, Duncan EJ, Bartlett E, et al. Impaired prepulse inhibition of acoustic startle in schizophrenia. Biol.Psychiatry 2000; 47:662-669
27 Larsen P, Ulin J, Dahlstrom K, Jensen M. Synthesis of [C-11]iodomethane by iodination of [C-11]methane. Appl.Radiat.Isot. 1997; 48:153-157
28 Barnett EM, Cassell MD, Perlman S. Two neurotropic viruses, herpes simplex virus type 1 and mouse hepatitis virus, spread along different neural pathways from the main olfactory bulb. Neuroscience 1993; 57:1007-1025
29 Mori I, Goshima F, Ito H, et al. The vomeronasal chemosensory system as a route of neuroinvasion by herpes simplex virus. Virology 2005; 334:51-58
30 Bian Q, Kato T, Monji A, et al. The effect of atypical antipsychotics, perospirone, ziprasidone and quetiapine on microglial activation induced by interferon-gamma. Prog.Neuropsychopharmacol.Biol.Psychiatry 2008; 32:42-48

31 Zheng LT, Hwang J, Ock J, Lee MG, Lee WH, Suk K. The antipsychotic spiperone attenuates inflammatory response in cultured microglia via the reduction of proinflammatory cytokine expression and nitric oxide production. J.Neurochem. 2008; 107:1225-1235

32 Plaznik A, Stefanski R, Kostowski W. Interaction between accumbens D1 and D2 receptors regulating rat locomotor activity. Psychopharmacology (Berl) 1989; 99:558-562

33 Jennings WA, Jr. Effect of DL-amphetamine on open-field behaviors in the rat. Psychol.Rep. 1968; 22:345-346

34 Schiorring E. An open field study of stereotyped locomotor activity in amphetamine-treated rats. Psychopharmacology (Berl) 1979; 66:281-287

35 Lycke E, Roos BE. Influence of changes in brain monoamine metabolism on behaviour of herpes simplex-infected mice. J.Neurol.Sci. 1974; 22:277-289

36 Neeley SP, Cross AJ, Crow TJ, Johnson JA, Taylor GR. Herpes simplex virus encephalitis. Neuroanatomical and neurochemical selectivity. J.Neurol.Sci. 1985; 71:325-337

37 Paivarinta MA, Marttila RJ, Rinne JO, Rinne UK. Dopaminergic neurotransmission in chronic herpes simplex virus brain infection in rabbits. J.Neural Transm.Gen.Sect. 1993; 93:205-212

38 Pocock JM, Kettenmann H. Neurotransmitter receptors on microglia. Trends Neurosci. 2007; 30:527-535

Chapter 8

P-glycoprotein activity in the rat brain is affected by HSV-1 induced neuroinflammation and antipsychotic treatment: implication in treatment resistant schizophrenia

Janine Doorduin, Erik F.J. de Vries, Rudi A. Dierckx and Hans C. Klein

Submitted for publication

Abstract

Schizophrenia is a chronic and disabling brain disease, with a high percentage (20-40%) of patients being resistant to antipsychotic treatment. The drug efflux transporter P-glycoprotein (P-gp) might play a role in treatment resistance. Neuroinflammation was recently shown to be present in schizophrenic patients and may influence P-gp activity or expression and thus treatment resistance. The aim of this study was to determine, in a rat model of herpes encephalitis, if neuroinflammation and antipsychotic drugs affected P-gp activity. Rats were intranasally inoculated with the herpes simplex virus type-1 (HSV-1) on day 0. Rats were treated with saline, clozapine or risperidone from day 0 until day 4 post-inoculation. Positron emission tomography with [^{11}C]-verapamil was used to study the activity of P-gp at the blood-brain barrier at day 6 post-inoculation. Plasma and tissue time-activity curves were used to calculate the [^{11}C]-verapamil distribution volume.

Inoculation with HSV-1 resulted in a decrease of the [^{11}C]-verapamil distribution volume in the brainstem and cerebellum (-22 and -21%, $p<0.05$), when compared to control rats. Clozapine further decreased the [^{11}C]-verapamil distribution volume in the brainstem (-6%, $p<0.05$), while risperidone increased the distribution volume of [^{11}C]-verapamil in the parietal/temporal/occipital cortex and in the cerebellum (15 and 16%, $p<0.05$), when compared to saline treatment.

HSV-1 induced neuroinflammation was found to increase the activity of P-gp at the blood-brain barrier. Clozapine further increased P-gp activity, whereas risperidone treatment counteracted the effect of HSV-1 on P-gp function. These results encourage future studies in schizophrenic patients to elucidate the role of neuroinflammation, antipsychotic treatment and P-gp in treatment resistance in schizophrenia.

Introduction

Schizophrenia is a chronic and disabling brain disease that affects about 1% of the population world-wide [1]. Although many antipsychotic drugs can be used to treat schizophrenia patients, between 20 and 40% of the patients are resistant to antipsychotic treatment [2]. Although treatment resistant patients show a considerable clinical heterogeneity and the causes of resistance are likely to be multifactorial [3], the drug efflux transporter P-glycoprotein (P-gp) might play an important role in treatment resistance in schizophrenia.

P-gp is the product of the multidrug resistance 1 (MDR1) gene and is expressed in healthy tissues, including intestine, liver, kidney and the blood-brain barrier (BBB), but also in cancer cells [4]. P-gp is an efflux pump that protects the brain and other vital tissues from harmful substances. Many pharmacological agents that are used to treat cancer and brain diseases, like epilepsy and schizophrenia, are substrates of P-gp, resulting in reduced treatment efficacy. The activity and expression of P-gp is influenced by a variety of factors, including drugs, glutamate and also gene polymorphisms [5]. In addition, neuroinflammation has been shown to regulate the activity and expression of P-gp at the BBB, which is possibly mediated by pro-inflammatory cytokines [6]. *In vivo* and *ex vivo* studies have shown conflicting results on the effect that neuroinflammation can have on activity and expression of P-gp [7-10]. Possibly, this effect depends on the time and nature of neuroinflammation (e.g. acute vs. chronic).

It has been shown that (recent-onset) schizophrenia is associated with global neuroinflammation [11-13] and that focal neuroinflammation is a feature of schizophrenia related psychosis [14]. Neuroinflammation may increase P-gp activity or expression at the BBB in a subpopulation of schizophrenic patients, which could explain treatment resistance in schizophrenia.

P-gp activity can be determined using positron emission tomography (PET) as a non-invasive imaging technique. The P-gp substrate [^{11}C]-verapamil has frequently been used as a PET ligand for measuring P-gp activity [15]. P-gp activity can be quantified by pharmacokinetic modeling. It has recently been shown that [^{11}C]-verapamil pharmacokinetics are well described by a two-tissue compartment model or Logan analysis without correction for radioactive metabolites [16].

To study the role of neuroinflammation on P-gp activity at the BBB, we used a rat model of herpes encephalitis. Intranasal inoculation with HSV-1 results in invasion of

the brain by HSV-1, causing herpes encephalitis which is accompanied by severe neuroinflammation [17]. This model does not require invasive manipulations and toxic compounds to evoke neuroinflammation, which may lead to changes in the permeability of the blood brain barrier. Because P-gp might play a role in treatment resistance to antipsychotics, it is also of interest to study the effect of antipsychotics on P-gp activity. *In vitro*, the atypical antipsychotics clozapine and risperidone were both found to have affinity for P-gp, with risperidone having the highest affinity [18-20]. To study the indirect effect of atypical antipsychotics on P-gp activity, rats were subchronically treated with clozapine and risperidone until 48 hours before the PET study. Thus, the aim of the present study was to determine the effect of neuroinflammation and treatment with clozapine or risperidone on the activity of P-gp at the BBB.

Material and methods

Animals

Male outbred Wistar-Unilever (SPF) rats (264±26 gram) were obtained from Harlan (Lelystad, The Netherlands). The rats were individually housed in Macrolon cages (38x26x24 cm) on a layer of wood shavings in a room with constant temperature (21±2°C) and fixed, 12-hour light-dark regime (light phase from 7:00–19:00 hours). Food (standard laboratory chow, RMH-B, Hope Farms, The Netherlands) and water were available ad libitum. After arrival, the rats were randomly divided into six groups: control rats (control) treated with either saline (n=6), clozapine (n=6) or risperidone (n=5) and rats inoculated with HSV-1 (HSE) treated with either saline (n=5), clozapine (n=4) or risperidone (n=5), and allowed to acclimatize for at least seven days. All experiments were approved by the Animal Ethics Committee of the University of Groningen, The Netherlands.

HSV-1 inoculation

The HSV-1 strain was obtained from a clinical isolate, cultured in Vero-cells and assayed for plaque forming units (PFU) per milliliter. On day 0, the rats were slightly anaesthetized with 5% isoflurane (Pharmachemie BV, The Netherlands) and inoculated with HSV-1 by application of 100 µl of phosphate-buffered saline with $1x10^7$ PFU of virus in the nostrils (50 µl per nostril) with a micropipette. Control rats

were treated similarly by application of 100 µl PBS without virus. Clinical symptoms in all rats were scored daily post-inoculation by the same observer.

Drugs and treatment

Clozapine was obtained from Sigma-Aldrich Inc (Saint Louis, Missouri, USA) and risperidone was obtained from MP Biomedicals (Irvine, California, USA). Clozapine and risperidone were dissolved in a minimal volume of 0.1 M HCl, and diluted with saline. The pH was adjusted to 6-7 with 0.1 M NaOH. The final concentration was 4.3 mg/ml for clozapine and 0.35 mg/ml for risperidone, and the total injection volume was 0.3-0.7 ml. The solutions were freshly made prior to injection.

Rats were treated with clozapine (10 mg/kg/day i.p.) or risperidone (0.5 mg/kg/day i.p.) from day 0 until day 4 post-inoculation. Control rats were treated similarly with saline. It was expected that five days of treatment in rats is sufficient to induce changes in P-gp activity.

[^{11}C]-Verapamil PET

[^{11}C]-Verapamil was synthesized as described previously [21]. After synthesis, [^{11}C]-verapamil was formulated in ethanol/water (10/90). The radiochemical purity was always >99% and the specific activity was always > 4000 GBq/mmol.

Small animal PET scans were performed on day 6 post-inoculation, at least 48 hours after the last drug treatment. To allow for arterial blood sampling during the PET scan, a canula was inserted in the femoral artery prior to the PET scan. After canulation, the rats were positioned in the small animal PET camera (Focus 220, Siemens Medical Solutions USA, Inc.) in transaxial position with their heads in the field of view. A transmission scan of 515 seconds with a Co-57 point source was obtained for the correction of attenuation by tissue. After the transmission scan was completed, the PET tracer [^{11}C]-verapamil (63±16 MBq) was injected via the penile vein. Simultaneously with the injection of the PET tracer a dynamic emission scan of 3600 seconds was started. Blood samples of 0.1 ml were taken at 15, 30, 45, 60, 75, 90, 120, 150, 300, 450, 600, 900, 1800 and 3600 seconds after injection. After a blood sample was taken, 0.1 ml of heparinized saline was injected into the artery to prevent large changes in blood pressure. The blood samples were centrifuged at 130,000 rpm (15,996 x *g*) for 5 minutes and the activity in plasma was measured using a gammacounter (LKB Wallac, Turku, Finland). The plasma-activity curve was corrected for decay.

The list-mode data of the emission scan was separated into 21 frame sinograms (8x30, 3x60, 2x120, 2x180, 3x300 and 3x600 seconds), which were iteratively reconstructed (OSEM2d, 4 iterations, 16 subsets) after being normalized and corrected for attenuation, scatter, randoms and decay.

PET image analysis

PET image analysis was performed using the Clinical Applications Packaging Program (CAPP5). Regions of interest were drawn around the bulbus olfactorius, frontal cortex, striatum, thalamus, parietal/temporal/occipital cortex, midbrain, brainstem and cerebellum in a template PET scan that was co-registered with the PET scan of interest by image fusion. The time-activity curves of these regions of interest were used for kinetic modeling using software developed in Matlab 7.1 (Mathworks, Natick, Massachusets). The Logan analysis [22] was used to calculate the distribution volume (DV) of [^{11}C]-verapamil using arterial plasma as the input.

Statistical analysis

All data are expressed as mean ± standard deviation. Statistical analysis was performed using SPSS for Windows, version 14.0.2. Statistical analysis on the clinical symptoms, [^{11}C]-verapamil DV and [^{11}C]-verapamil influx (k_1) were performed by one-way ANOVA with a LSD post hoc test. Significance was reached when the p value was ≤ 0.05.

Results

Clinical symptoms

Clinical symptoms (figure 1) were scored daily up to six days post inoculation and categorized into the following clinical scores: (0), no symptoms; (1), ruffled fur and irritated mouth, nose and eyes; (2), behavioral signs, like stress and lethargy, and hunched posture; (3), posterior paralysis and impairment of motor function and (4), severe paralysis, labored breathing or death. For rats inoculated with HSV-1 and treated with saline, the first clinical symptoms appeared on day 2 post-inoculation. The severity of the clinical symptoms increased gradually over time and at day 6 post-inoculation most rats (60%) had a clinical score of 3. For the HSV-1 inoculated rats that were treated with clozapine and risperidone a delay in the onset of clinical

symptoms was found. The first clinical symptoms in these rats were seen at day 5 post-inoculation, which is one day after the last treatment (at day 4). Of the clozapine treated rats, 50% did not shown any clinical symptoms at day 6 post-inoculation, while 60% of the risperidone treated rats had a clinical score of 2. No statistically significant differences were found in the averages of the clinical scores in saline (2.0±1.4), clozapine (1.3±1.5) and risperidone (2.6±0.5) treated rats on day 6 post-inoculation. None of the control rats showed any clinical symptoms.

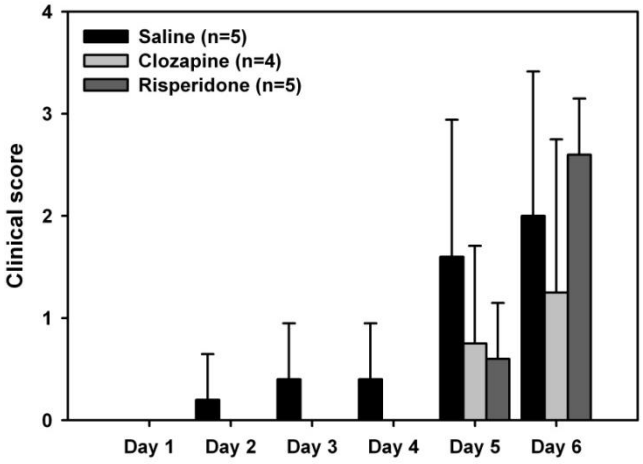

Figure 1 Clinical scores of rats inoculated with HSV-1 on day 1 to day 6 post-inoculation that were treated with either saline (n=5), clozapine (n=4) or risperidone (n=5) from day 1 until day 4 post-inoculation. The clinical scores represent the following symptoms: (0), no symptoms; (1), ruffled fur and irritated mouth, nose and eyes; (2), behavioral signs, like stress and lethargy, and hunched posture; (3), posterior paralysis and impairment of motor function and (4), severe paralysis, labored breathing or death.

Distribution volume of [^{11}C]-verapamil

The images of the [^{11}C]-verapamil DV are displayed in figure 2. The images show low brain uptake, due to efflux of [^{11}C]-verapamil by P-gp, with no visual differences between any of the examined groups. The whole brain DV of [^{11}C]-verapamil is displayed in figure 3 and the DV of [^{11}C]-verapamil in the focal brain regions of interest is displayed in table 1.

HSV-1 infection of the brain resulted in a decrease in the whole brain [^{11}C]-verapamil DV (-15%, p=0.050). In addition to a global decrease in whole brain [^{11}C]-verapamil DV, a statistically significant focal decrease in the [^{11}C]-verapamil DV was found in the cerebellum (-22%, p=0.013) and in the brainstem (-21%, p=0.013).

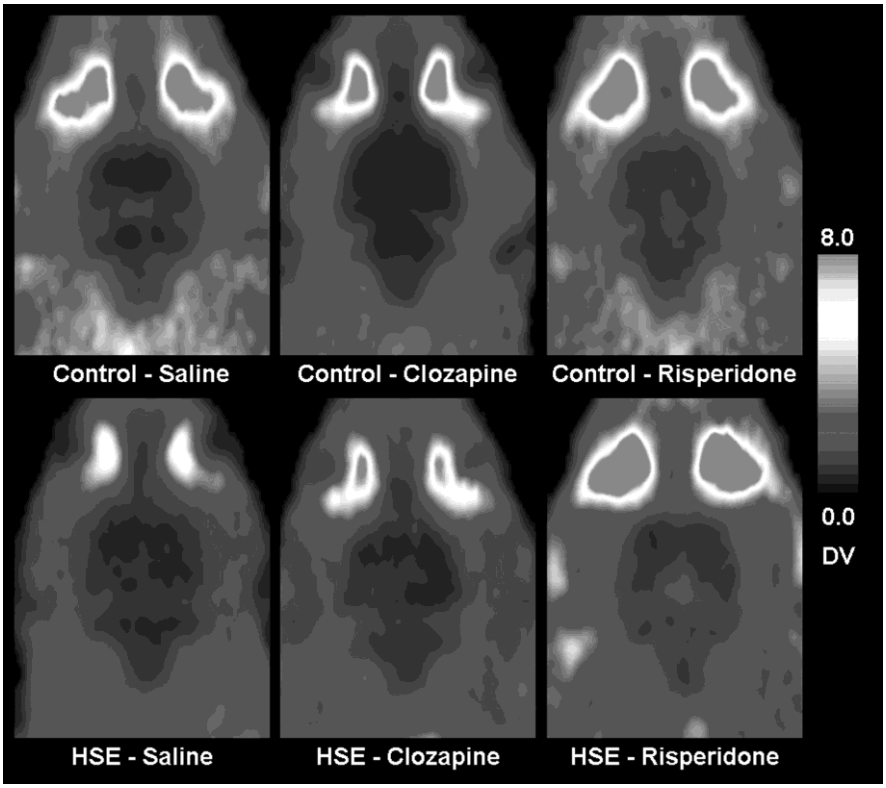

Figure 2 Full-color in appendix. Small animal PET images of the [^{11}C]-verapamil distribution volume (DV) on day 6 post-inoculation in control rats (control) and rats inoculated with HSV-1 (HSE) that were treated with saline, clozapine or risperidone from day 0 until day 4 post-inoculation. The images display a coronal plane of the rat head, at the level of the brainstem.

Treatment of control rats with clozapine resulted in a statistically significant decrease in the whole brain [^{11}C]-verapamil DV (-15%, p=0.036), when compared to saline treatment. A statistically significant focal decrease in [^{11}C]-verapamil DV after clozapine treatment was found in the brainstem (-16%, p=0.040), when compared to saline treated rats. Risperidone treatment did not significantly alter whole brain [^{11}C]-verapamil DV (p=0.146). However, a statistically significant focal increase in DV was found in the parietal/temporal/occipital cortex (15%, p=0.029) and in the cerebellum (16%, p=0.026), when compared to saline treated rats.

In clozapine treated rats, no significant differences in the [^{11}C]-verapamil DV were found between control rats and rats inoculated with HSV-1, either in the whole brain

or in individual brain regions. In the risperidone treated rats, whole brain [^{11}C]-verapamil DV was not different between the rats inoculated with HSV-1 and control rats (p=0.062). However, a statistically significant focal decrease in DV was observed in the parietal/temporal/occipital cortex (-18%, p=0.013) and the cerebellum (-28%, p=0.001) of HSV-1 infected rats, as compared to control rats.

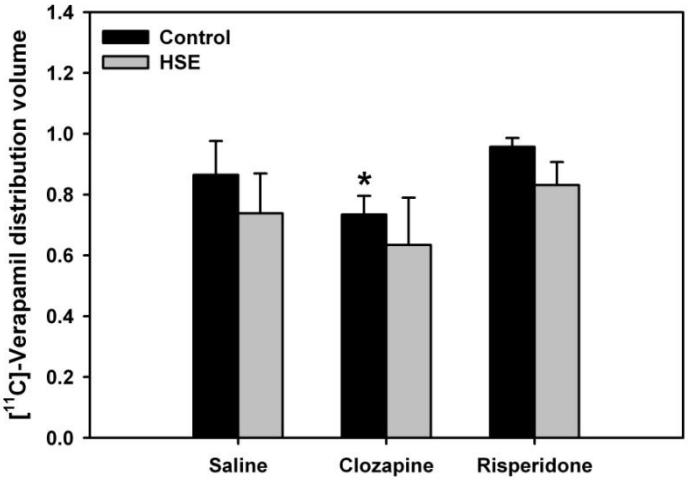

Figure 3 The whole brain distribution volume of [^{11}C]-verapamil on day 6 post-inoculation in control rats (control) and rats inoculated with HSV-1 (HSE), that were treated with saline, clozapine or risperidone from day 0 up until day 4 post-inoculation. Data are presented as mean ± standard deviation. *p<0.05 when compared to control rats.

Table 1 Distribution volume of [^{11}C]-verapamil on day 6 post-inoculation in control rats (control) and rats inoculated with HSV-1 (HSE), that were treated with saline, clozapine or risperidone from day 0 up until day 4 post-inoculation. Data are presented as mean ± standard deviation. *p<0.05 when compared to control rats, **p<0.005 when compared to control rats and #p<0.05 when compared to saline treated rats.

	Saline		Clozapine		Risperidone	
	Cntrl (n=6)	**HSE (n=5)**	**Cntrl (n=6)**	**HSE (n=4)**	**Cntrl (n=5)**	**HSE (n=5)**
Bulbus olf	1.14±0.12	1.00±0.34	0.96 ± 0.12	0.79±0.20	1.14±0.02	1.14±0.19
Frontal ctx	0.99±0.20	0.91±0.24	0.78 ± 0.12	0.68±0.24	1.01±0.22	1.05±0.14
Striatum	0.78±0.22	0.68±0.15	0.60 ± 0.05	0.57±0.19	0.81±0.12	0.73±0.10
Thalamus	0.67±0.09	0.55±0.12	0.59 ± 0.09	0.46±0.18	0.71±0.08	0.60±0.09
P/T/O ctx	0.87±0.13	0.74±0.14	0.76 ± 0.07	0.63±0.15	1.02±0.04#	0.84±0.07*
Midbrain	0.70±0.12	0.60±0.09	0.60 ± 0.03	0.56±0.13	0.82±0.04	0.72±0.14
Cerebellum	0.94±0.10	0.74±0.11*	0.83 ± 0.18	0.67±0.13	1.12±0.10#	0.81±0.11**
Brainstem	0.95±0.11	0.75±0.10*	0.79 ± 0.14#	0.70±0.13	1.06±0.10	0.92±0.14#

Contrl, control; P/T/O, Parietal/Temporal/Occipital

Influx (k_1) of [^{11}C]-verapamil

The DV of [^{11}C]-verapamil is dependent on both the influx (k_1) of [^{11}C]-verapamil into brain tissue and the P-gp related efflux (k_2) from the brain. Changes in the influx of [^{11}C]-verapamil, due to for example changes in the permeability of the BBB, could explain the change in [^{11}C]-verapamil DV. In the present study, however, no statistically significant differences in the whole brain k_1 were found between control rats and rats infected with HSV-1 treated with saline (0.26±0.12 vs. 0.19±0.11, p=0.490). When compared to saline treatment, clozapine treatment did not affect the k_1 of [^{11}C]-verapamil in control (0.26±0.12 vs. 0.22±0.02, p=0.676) or HSE rats (0.19±0.11 vs. 0.14±0.07, p=0.611). Risperidone treatment, when compared to saline treatment did not change the k_1 of [^{11}C]-verapamil in control (0.32±0.16 vs. 0.26±0.12, p=0.586) or HSE rats (0.34±0.36 vs. 0.19±0.11, p=0.211). In addition to the findings in whole brain k_1 of [^{11}C]-verapamil, no statistically significant differences were found in the k_1 of [^{11}C]-verapamil in the focal regions of interest, in saline and clozapine treated rats. In contrast, risperidone treatment caused a statistically significant increase in k_1 in the parietal/temporal/occipital cortex (p=0.011) of rats infected with HSV-1, when compared to saline treated rats.

Discussion

Since 20 to 40% of the schizophrenic patients were found to be resistant to antipsychotic treatment, it is of importance to gain more insight into the mechanism behind treatment resistance in order to improve treatment strategies. We hypothesized that neuroinflammation, which is proposed to play a role in schizophrenia, has a role in regulating P-gp activity.

In the present study, we have demonstrated that HSV-1 infection caused increased P-gp activity at the BBB, in particular in the brainstem and cerebellum. Recently, we have shown that neuroinflammation in the rat model of herpes encephalitis is most pronounced in these brain areas [23]. The change in P-gp activity in these brain areas is therefore most likely caused by the presence of HSV-1 induced neuroinflammation. Because it has been shown that schizophrenia is associated with neuroinflammation, treatment resistance may thus be caused by neuroinflammation induced changes in P-gp activity. The increased P-gp activity due to neuroinflammation is consistent with previous findings related to the effect of pro-inflammatory cytokines on P-gp expression. It has recently been shown *in vitro* that the pro-inflammatory cytokine

tumor-necrosis factor alpha increased P-gp activity and expression [7,10]. In contrast, it has also been reported that the intraventricular injection of lipopolysaccharide resulted in a decrease in *in vivo* P-gp expression [8]. As already mentioned by Miller *et al.* [9], it is plausible that the first response to pro-inflammatory cytokines is a decrease in P-gp activity, whereas the delayed response could cause an increase in P-gp activity and expression. Although a dynamic regulation of the P-gp expression by pro-inflammatory cytokines in time seems likely, the time span may vary between different *in vitro* and *in vivo* models.

Because P-gp is suggested to play a role in resistance to antipsychotic treatment, it is of interest to study the effect of antipsychotics on P-gp activity. It has been shown that antipsychotics, including clozapine and risperidone, have affinity for P-gp [18-20], resulting in a decreased treatment efficacy. However, to our knowledge, it has not been studied if chronic treatment with antipsychotics influences P-gp activity. In the present study, we have shown that clozapine treatment of healthy control rats increased P-gp activity in some brain areas. This suggests that clozapine can eventually induce resistance in the normal brain. In treatment resistant schizophrenic patients, however, the atypical antipsychotic drug clozapine was found to be most effective. In contrast to clozapine, risperidone decreased the activity of P-gp, suggesting that risperidone could increase treatment efficacy. It remains to be elucidated how clozapine and risperidone affect P-gp activity, however, increased P-gp activity may be due to increased P-gp expression. The expression of P-gp is under regulation of nuclear receptors (e.g. steroid and xenobiotic receptors) that can bind many different ligands, thereby affecting P-gp activity [5]. Binding of antipsychotics to these nuclear receptors may thus explain the antipsychotic induced changes in P-gp activity.

Taken that a neuroinflammatory response in schizophrenic patients is in part responsible for treatment resistance, it is especially of interest to know the effects of antipsychotics on P-gp activity or expression during a neuroinflammation. Both neuroinflammation and clozapine increased the activity of P-gp at the BBB and these effects were shown to be additive. Treatment of HSV-1 infected rats with risperidone resulted in no net change in P-gp activity, when compared to saline treated control rats, showing that risperidone was effective in inhibiting the increase in P-gp activity induced by neuroinflammation.

Although we have found an effect of neuroinflammation and antipsychotics on the P-gp activity at the BBB, one could argue that the found change in [^{11}C]-verapamil DV is related to changes in [^{11}C]-verapamil metabolism. It was, however, shown by

Lubberink *et al.* [16] that the [^{11}C]-verapamil time-activity curve was well described by a two-tissue compartment model or Logan analysis without metabolite correction. In addition, the last treatment with clozapine and risperidone was 48 hours before the [^{11}C]-verapamil PET scan, and given the half-life of clozapine and risperidone of 2 to 4 hours in rats, it seems unlikely that the metabolism of clozapine and risperidone affected the formation of [^{11}C]-verapamil metabolites.

Conclusion

HSV-1 induced neuroinflammation was found to increase P-gp activity at the BBB. Because neuroinflammation is suggested to play a role in schizophrenia, this is of great interest with respect to treatment resistance in schizophrenic patients. The HSV-1 induced increase in P-gp activity was augmented by the atypical antipsychotic clozapine, but was antagonized by risperidone. Increasing knowledge on treatment resistance in schizophrenia is of importance for improving treatment strategies. These findings may therefore promote further research on the role of P-gp and neuroinflammation in treatment resistant schizophrenia in a clinical setting.

Acknowledgement

This study was funded by the Stanley Medical Research Institute, Grant-ID 05-NV-001.

References

1 World Health Organization. Neurological disorders; public health challenges.: WHO, 2006

2 Essock SM, Hargreaves WA, Covell NH, Goethe J. Clozapine's effectiveness for patients in state hospitals: results from a randomized trial. Psychopharmacol.Bull. 1996; 32:683-697

3 Hellewell JS. Treatment-resistant schizophrenia: reviewing the options and identifying the way forward. J.Clin.Psychiatry 1999; 60 Suppl 23:14-19

4 Cordon-Cardo C, O'Brien JP, Boccia J, Casals D, Bertino JR, Melamed MR. Expression of the multidrug resistance gene product (P-glycoprotein) in human normal and tumor tissues. J.Histochem.Cytochem. 1990; 38:1277-1287

5 Loscher W, Potschka H. Drug resistance in brain diseases and the role of drug efflux transporters. Nat.Rev.Neurosci. 2005; 6:591-602

6 McRae MP, Brouwer KL, Kashuba AD. Cytokine regulation of P-glycoprotein. Drug Metab Rev. 2003; 35:19-33

7 Bauer B, Hartz AM, Miller DS. Tumor necrosis factor alpha and endothelin-1 increase P-glycoprotein expression and transport activity at the blood-brain barrier. Mol.Pharmacol. 2007; 71:667-675

8 Goralski KB, Hartmann G, Piquette-Miller M, Renton KW. Downregulation of mdr1a expression in the brain and liver during CNS inflammation alters the in vivo disposition of digoxin. Br.J.Pharmacol. 2003; 139:35-48

9 Miller DS, Bauer B, Hartz AM. Modulation of P-glycoprotein at the blood-brain barrier: opportunities to improve central nervous system pharmacotherapy. Pharmacol.Rev. 2008; 60:196-209

10 Yu C, Kastin AJ, Tu H, Waters S, Pan W. TNF activates P-glycoprotein in cerebral microvascular endothelial cells. Cell Physiol Biochem. 2007; 20:853-858

11 Bayer TA, Buslei R, Havas L, Falkai P. Evidence for activation of microglia in patients with psychiatric illnesses. Neurosci.Lett. 1999; 271:126-128

12 Radewicz K, Garey LJ, Gentleman SM, Reynolds R. Increase in HLA-DR immunoreactive microglia in frontal and temporal cortex of chronic schizophrenics. J.Neuropathol.Exp.Neurol. 2000; 59:137-150

13 van Berckel BN, Bossong MG, Boellaard R, et al. Microglia Activation in Recent-Onset Schizophrenia: A Quantitative (R)-[(11)C]PK11195 Positron Emission Tomography Study. Biol.Psychiatry 2008; 64:820-822

14 Doorduin J, de Vries EFJ, Willemsen ATM, Dierckx RA, Klein HC. Neuroinflammation in schizophrenic patients: a positron emission tomography study with [11C]-(R)-PK11195. Neuroimage. 2008; 41:T109-

15 Elsinga PH, Franssen EJ, Hendrikse NH, et al. Carbon-11-labeled daunorubicin and verapamil for probing P-glycoprotein in tumors with PET. J.Nucl.Med. 1996; 37:1571-1575

16 Lubberink M, Luurtsema G, van Berckel BN, et al. Evaluation of tracer kinetic models for quantification of P-glycoprotein function using (R)-[11C]verapamil and PET. J.Cereb.Blood Flow Metab 2007; 27:424-433

17 Doorduin J, Klein HC, Dierckx RA, de Vries EFJ. Herpes simplex encephalitis in rats: a positron emission tomography study with [18F]-FHBG, [11C]-(R)-PK11195 and [18F]-FDG. Neuroimage. 2008; 41:T110-

18 Boulton DW, DeVane CL, Liston HL, Markowitz JS. In vitro P-glycoprotein affinity for atypical and conventional antipsychotics. Life Sci. 2002; 71:163-169

19 El Ela AA, Hartter S, Schmitt U, Hiemke C, Spahn-Langguth H, Langguth P. Identification of P-glycoprotein substrates and inhibitors among psychoactive compounds--implications for pharmacokinetics of selected substrates. J.Pharm.Pharmacol. 2004; 56:967-975

20 Wang JS, Zhu HJ, Markowitz JS, Donovan JL, DeVane CL. Evaluation of antipsychotic drugs as inhibitors of multidrug resistance transporter P-glycoprotein. Psychopharmacology (Berl) 2006; 187:415-423

21 Wegman TD, Maas B, Elsinga PH, Vaalburg W. An improved method for the preparation of [11C]verapamil. Appl.Radiat.Isot. 2002; 57:505-507

22 Logan J. Graphical analysis of PET data applied to reversible and irreversible tracers. Nucl.Med.Biol. 2000; 27:661-670

23 Doorduin J, Klein HC, Dierckx RA, James M, Kassiou M, de Vries EFJ. [(11)C]-DPA-713 and [(18)F]-DPA-714 as New PET Tracers for TSPO: A Comparison with [(11)C]-(R)-PK11195 in a Rat Model of Herpes Encephalitis. Mol.Imaging Biol. 2009; DOI: 10.1007/s11307-009-0211-6

Chapter 9

Neuroinflammation in schizophrenia related psychosis: a positron emission tomography study

Janine Doorduin, Erik F.J. de Vries, Antoon T.M. Willemsen, Jan Cees de Groot, Rudi A. Dierckx and Hans C. Klein

J Nucl Med 2009; 50: 1801-1807

Abstract

Schizophrenia is a chronic and disabling brain disease characterized by psychotic episodes, with unknown etiology. It is suggested that neuroinflammation plays a role in the pathophysiology of schizophrenia. Neuroinflammation is characterized by the activation of microglia cells, which show an increase in the expression of the peripheral benzodiazepine receptor. The isoquinoline [^{11}C]-*(R)*-PK11195 [*(R)-N*-[^{11}C]-methyl-*N*-(1-methylpropyl)-1-(2-chlorophenyl)isoquinoline-3-carboxamide)] is peripheral benzodiazepine receptor ligand that can be used for imaging of activated microglia cells, and thus neuroinflammation, with positron emission tomography. We hypothesized that neuroinflammation would be more profound in schizophrenic patients during psychosis and it was therefore investigated whether neuroinflammation is present in patients within the schizophrenia-spectrum that were in a psychotic phase.

Seven patients within the schizophrenia spectrum that were recovering from psychosis were included. Recovering psychosis was defined by a score of 5 or more on one item of the positive scale of the PANSS, or a score of 4 on two items. The patients were compared to eight age-matched healthy volunteers. Dynamic PET scans of 60 minutes were acquired after injection of [^{11}C]-*(R)*-PK11195. All subjects underwent a T1- and T2-weighted MRI scan, which were visually examined for abnormalities and used for anatomical coregistration in data-analysis. The PET data was analyzed with a two-tissue compartment model to calculate the binding potential, using the metabolite corrected plasma curve as input.

A significantly higher binding potential of [^{11}C]-*(R)*-PK11195, indicative of neuroinflammation, was found in the hippocampus of schizophrenic patients, when compared to healthy volunteers (2.07 ± 0.42 vs. 1.37 ± 0.30; $p=0.004$). A non-significant 30% higher [^{11}C]-*(R)*-PK11195 binding potential was found in the whole brain grey matter of schizophrenic patients. The MRI images did not reveal any visual abnormalities.

The present study suggests that focal neuroinflammation may play an important role in schizophrenia during psychosis.

Introduction

Schizophrenia is a chronic, disabling brain disease accompanied by psychosis with positive symptoms, such as hallucinations and delusions. Despite considerable research, the exact etiology of psychosis remains unknown. Disturbances in immune mechanisms are thought to play an important role in psychosis of schizophrenia [1]. Although these disturbances in immune mechanisms were mainly found in peripheral blood and in cerebrospinal fluid, they are hypothesized to derive from inflammatory processes in the central nervous system. Indeed, there is evidence from post-mortem studies that schizophrenia is associated with an increased number of activated microglia cells.

Microglia cells are the predominant population of macrophages in the brain and are responsive to injury or infection of brain tissue. In healthy brain tissue, microglia cells have a ramified morphology, characterized by long processes that continuously survey the microenvironment [2]. In response to brain injury or infection, microglia cells change from the ramified morphology into a reactive or amoeboid form. Activated microglia cells, characteristic of neuroinflammation, are involved in the removal of the infectious agents and irreversibly damaged brain tissue. However, in neurological disorders this process runs out of control, resulting in chronic microglia cell activation, which has a detrimental effect. Although neuroinflammation has been shown to play a major role in many neurodegenerative diseases, such as multiple sclerosis, Parkinson's disease and Alzheimer's disease [3], there is only limited and ambiguous data on the presence of neuroinflammation in psychiatric diseases like schizophrenia.

Post-mortem studies in schizophrenic patients have demonstrated the presence of activated microglia cells in the brain. However, the results of these studies are inconsistent. Some studies showed increased density of microglia cells in a subpopulation of schizophrenic patients [4,5], but other studies could not provide evidence for such an increase [6,7]. This might be explained by the differences in markers used for microglia cells and the differences in brain regions that were examined.

Thus far, the majority of the findings supporting the presence of neuroinflammation in schizophrenia are derived from post-mortem studies in a limited number of brain areas without the specific selection of patients with psychosis. Positron emission tomography (PET) provides the opportunity to study the presence of

neuroinflammation in psychotic patients non-invasively. In neuroinflammation, activated microglia cells exhibit an increase in the expression of peripheral benzodiazepine receptors (PBR) in the outer mitochondrial membrane. The PET tracer [^{11}C]-*(R)*-PK11195 (*(R)*-*N*-[^{11}C]-methyl-*N*-(1-methylpropyl)-1-(2-chlorophenyl)isoquinoline-3-carboxamide) is an antagonist of the PBR and binding of [^{11}C]-*(R)*-PK11195 to the PBR can be used to visualize neuroinflammation. [^{11}C]-*(R)*-PK11195 has already been used to show the presence of neuroinflammation in neurological diseases, like Parkinson's disease, Alzheimer's disease, multiple sclerosis and herpes encephalitis (reviewed in [3]. A recent study also showed a general increase in whole brain grey matter binding of [^{11}C]-*(R)*-PK11195 in schizophrenia patients within the first 5 years of disease onset [8]. No specific foci of neuroinflammation were observed. We hypothesized that microglia cells would be more active in schizophrenic patients during psychosis. In the present study, we investigated whether [^{11}C]-*(R)*-PK11195 could demonstrate the presence of neuroinflammation in patients within the schizophrenia-spectrum that were in a psychotic phase.

Material and methods

Subjects

Ten patients were recruited from local psychiatric hospitals based on the following inclusion criteria: 1) fulfilling DSM-IV criteria for the schizophrenia-spectrum (295.xx and 298.xx); 2) psychosis, i.e. a total score of 14 or higher on the positive scale of the positive and negative symptoms scale (PANSS) and at least a score of five on one item or a score of four on two items of the positive scale of the PANSS; 3) age above eighteen; 4) no use of benzodiazepines within 3 half-lives (on average 1-2 weeks) of the benzodiazepines before the start of the study and 5) ability to provide written informed consent. Healthy volunteers, matched for age and gender, were recruited by advertisement and were included if they had 1) no personal history of psychiatric disorders; 2) no family history of psychiatric disorders in their first-degree relatives and 3) no presence of inflammation as measured by C-reactive protein (CRP) (i.e. CRP <0.5 mg/L). Exclusion criteria for all subjects were 1) concomitant or past severe medical conditions; 2) substance abuse; 3) the use of non-steroidal anti-inflammatory drugs (NSAID) or paracetamol; 4) pregnancy and 5) the presence of irremovable magnetic materials in and/or on the body. Classification of diagnoses was performed by an experienced psychiatrist (HCK) using the Schedule for Clinical

Assessment in Neuropsychiatry Version 2 (SCAN2, World Health Organization). Psychopathology in patients was assessed with the PANSS by trained psychiatric nurses.

Of the 20 included subjects, three patients and two healthy volunteers were excluded. One patient withdrew from the study after the MRI scan was performed, so no [^{11}C]-*(R)*-PK11195 PET scan was made. A second patient had too much head movement during the MRI scan and consequently the MRI scan could not be used for normalization of the PET data. A third patient had enlarged ventricles within the physiological range, which hampered normalization of the PET scan. Of two healthy volunteers the PET scan was not performed because the arterial catheter could not be placed. No healthy volunteers were excluded due to elevated CRP.

The study was approved by the medical ethical committee of the University Medical Center Groningen. All subjects provided written informed consent after receiving a complete description of the study.

Radiochemistry

[^{11}C]-*(R)*-PK11195 was labeled by trapping [^{11}C]-methyl iodide in a solution of 1 mg *(R)*-N-desmethyl-PK11195 and 10 mg potassium hydroxide in 300 µl dimethylsulfoxide. The reaction mixture was allowed to react for 1 minute at 40 °C, neutralized with 1M HCl and passed through a 45 µm Millex HV filter. The filtrate was purified by HPLC using a µBondapak C18 column (7.8x300 mm) with acetonitrile/25 mM NaH_2PO_4 (pH 3.5) (55/45) as the eluent (flow 5 ml/min). To remove the organic solvents from the product, the collected HPLC fraction (retention time 7 min) was diluted with 100 ml of water and passed through an Oasis HLB 30 mg (1 cc) cartridge. The cartridge was washed twice with 10 ml of water and subsequently eluted with 1 ml of ethanol and 8 ml of water. The product was sterilized by filtration over a 0.20 µm Millex LG filter. The product was obtained in 36±12% radiochemical yield (n=16). Quality control was performed by HPLC, using a Novapak C18 column (150x3.9 mm) with acetonitrile/25 mM NaH_2PO_4 (pH 3.5) (60/40) as the eluent at a flow of 1 ml/min. The radiochemical purity was always >95% and the specific activity was 89±58 GBq/µmol. No differences were found between the injected dose in healthy volunteers (398±38 MBq) and patients (398±61) (p=0.995). The injected mass was slightly higher in patients as compared to healthy volunteers (1.9±1.5 mg/L vs. 0.7±0.4 mg/L, p=0.051), due to a lower specific activity in patients (56±42 GBq/µmol vs. 112±58 GBq/µmol, p=0.053).

PET protocol

An arterial catheter was inserted in the radial artery after testing for collateral circulation with the Allen test and injection of 1% lidocaine (Fresenius Kabi Nederland BV, 's Hertogenbosch, The Netherlands) for local anesthesia. In the other arm, a venous catheter was inserted in the antebrachial vein. Positron emission tomography imaging was performed with the ECAT EXACT HR+ camera (Siemens, Knoxville, Tenessee). Head movement was minimized with a head-restraining adhesive band and a neuroshield was used to minimize the interference of radiation from the subject's body. A 60-min emission scan in 3D-mode was performed, starting simultaneously with the intravenously injection of [^{11}C]-*(R)*-PK11195. The tracer was injected at a speed of 0.5 ml/sec (total volume of 8.3 ml).

After radiotracer injection, arterial blood radioactivity was continuously monitored with an automated sampling system (Veenstra Instruments, Joure, The Netherlands). Five extra blood samples were collected at 10, 20, 30, 45 and 60 min after [^{11}C]-*(R)*-PK11195 injection to determine the amount of radioactivity in blood and plasma to calibrate the sampling system. The arterial blood samples that were collected at 20, 45 and 60 min after [^{11}C]-*(R)*-PK11195 injection were also used for metabolite analysis. These blood samples were centrifuged at 3000 *g* for 3 min and 1.5 ml plasma was collected. Then 2 ml of acetonitrile (Rathburn Chemicals Ltd, Walkerburn, Scotland) was added to the plasma to precipitate plasma proteins. The plasma samples were shaken on a vortex mixer for 30 s and centrifuged at 3000 *g* for 5 min. A volume of 1 ml of the supernatant was injected into a HPLC system, consisting of a Waters 590 HPLC-pump (Waters Corporation, Milford, USA) and an Alltima 5μm RP-C_{18} column (250x10.0 mm I.D.) (Alltech, Laarne, Belgium). The mobile phase consisted of a mixture of 69.5% of acetonitrile (Rathburn Chemicals Ltd, Walkerburn, Scotland), 30% water (Fresenius Kabi, Sevres, France) and 0.5% of triethylamine (Merck, Haarlem, The Netherlands). The flow-rate was set at 5.0 ml/min and samples were collected at time intervals of 30 s. The collected samples were counted for radioactivity using a gamma-counter (LKB Wallac, Turku, Finland).

MRI

All subjects underwent a magnetic resonance imaging (MRI) of the brain using a 3 Tesla Intera MRI scanner (Philips, Best, The Netherlands) obtaining transaxial 3D-T1 gradient echo (repetition time (RT) 25 ms, echo time (ET) 4.6 ms, field of view (FOV) 256x160x204 mm, matrix 265 x 265, slice thickness 2.0 mm, 160 slices, 1 average, α=

30º), 3D-T1 turbo gradient echo (RT 7.5 ms, ET 3.2 ms, FOV 260x160x232.14 mm, matrix 265 x 265, slice thickness 1.0 mm, 160 slices, 1 average, α= 8º), dual echo (RT 3000 ms, ET 26.7 and 120 ms, inversion time (IT) 2800 ms, FOV 220x150x175.31 mm, matrix 265 x 265, slice thickness 3.0 mm, 50 slices, 1 averages, α= 90º) and T2-FLAIR weighted images (RT 11000 ms, ET 100 ms, IT 2800 ms, FOV 220x150x175.31 mm, matrix 265 x 265, slice thickness 3.0 mm, 50 slices, 2 averages, α= 90º) aligned with the AC-PC (anterior commissure-posterior commissure) plane. The 3D-T1 gradient echo weighted MRI images were used to align to the PET image for normalization. The MRI images of all subjects were visually examined for structural abnormalities and neuroinflammation by an experienced neuroradiologist (JCdeG).

Data-analysis

Attenuation correction was performed with the separate ellipse algorithm. Images were reconstructed by filtered back projection in 21 successive frames of increasing duration (6x 10 sec, 2x 30 sec, 3x 1 min, 2x 2min, 2x 3 min, 3x 5min, 3x 10 min). The first two minutes of the PET scan were summed to create an image that resembles a perfusion image, which was used to align the MRI image to the corresponding PET image using Statistical Parametric Mapping (SPM2) software. The aligned MRI image was normalized to the SPM2 MRI template. The normalization was then applied to each individual frame of the PET image. A limited number of brain regions of interest in the neuroinflammatory process were a-priori selected for comparison between psychotic patients and healthy volunteers. [^{11}C]-*(R)*-PK11195 time-activity curves of the frontal, occipital, temporal and parietal lobe, basal ganglia, hippocampus and cerebellum were created using an automated region of interest (ROI) tool. In addition, time-activity curves of the midbrain and brainstem were created using manually drawn ROIs. The time-activity curves were used for kinetic modeling using software developed in Matlab 7.1 (Mathworks, Natick, Massachusets). The individual delay was calculated to correct for the delay in radioactivity measurements in blood, caused by the distance between the subject and the automated sampling system. Two-tissue compartment modeling (figure 1) was used to calculate the K_1-k_4 using the metabolite corrected plasma curve as an input function, correction for the individual delay and an individually fixed blood volume, which was the median of the blood volume of all areas determined using two-tissue compartment modeling with a free blood volume. The fixed instead of the free blood volume was chosen because it provides a more

stable measurement of K_1-k_4. The binding potential was defined as k_3/k_4 and was calculated for each ROI individually.

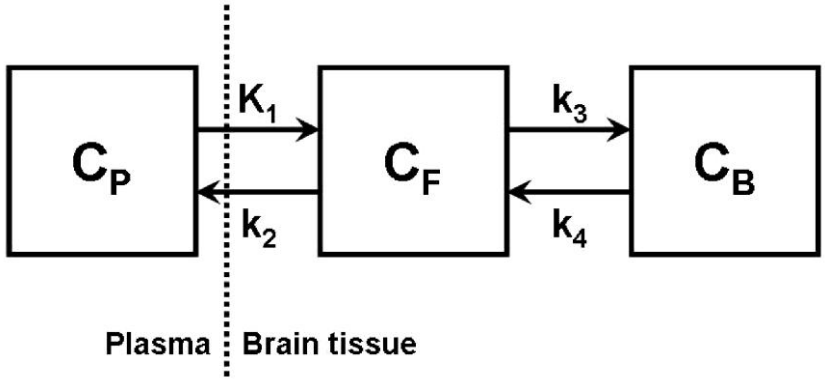

Figure 1 Two-tissue compartment model to describe the kinetics of [^{11}C]-*(R)*-PK11195. Influx of [^{11}C]-*(R)*-PK11195 from plasma (C_P) to brain tissue is described by K_1 and the efflux of from brain tissue to plasma is described by k_2. In brain tissue, [^{11}C]-*(R)*-PK11195 can be either free (C_F) or bound to the peripheral benzodiazepine receptor (C_B). Binding to the receptor is described by k_3 and since [^{11}C]-*(R)*-PK11195 binds reversibly to the PBR, it can return to the free compartment, as described by k_4. The binding potential is defined as k_3/k_4.

Statistics

Statistical analysis was performed with SPSS 16.0. One-way ANOVA was used to determine group differences between the tracer and subject characteristics, and whole brain grey matter binding potential. Statistical analysis on the binding potentials in the examined brain regions was performed using a multivariate general linear model, with the whole brain grey matter binding potential as a covariate to correct for global [^{11}C]-*(R)*-PK11195 uptake. To correct for multiple comparisons, the p-value threshold was defined according to Bonferroni. Therefore, 0.05 was divided by the number of brain regions (n=10) resulting in a significance threshold of 0.005. Correlations between the score on the positive scale of the PANSS and binding potentials were assessed with Pearson's product moment correlation coefficient (r) and were assumed to be significant when $p<0.05$.

Results

Subjects

Subject characteristics are displayed in table 1. The diagnostic SCAN interview confirmed that all patients fit within the DSM-IV criteria of schizophrenia spectrum disorders. Five patients were diagnosed as schizophrenia of the paranoid type, and two patients as having a brief psychotic disorder not otherwise specified. Six patients were scanned within 2 months after onset of a psychotic episode and 1 patient was chronically symptomatic. The number of lifetime psychotic episodes ranged from 1 to 4. The average score on the positive scale of the PANSS was 20±3, on the negative scale 17±5 and on the global scale 37±7. No significant differences were found between the age of patients (31±7) and healthy volunteers (27±6) (p=0.124).

Table 1 Subject characteristics

Subject No.	M/F	Age	DSM-IV	Onset 1st psych	No. of psych	Positive PANSS	Negative PANSS	Global PANSS	Anti-psychotic
Healthy volunteers									
1	F	27	–	–	–	–	–	–	–
2	F	39	–	–	–	–	–	–	–
3	F	23	–	–	–	–	–	–	–
4	M	23	–	–	–	–	–	–	–
5	M	24	–	–	–	–	–	–	–
6	M	22	–	–	–	–	–	–	–
7	M	30	–	–	–	–	–	–	–
8	M	27	–	–	–	–	–	–	–
Patients									
1	M	28	295.30	21	4	20	21	40	Olanzapine
2	M	42	298.90	26	2	20	10	28	Zuclopentixol
3	F	40	295.30	40	1	19	18	37	Olanzapine
4	M	28	295.30	26	1	18	19	42	Haloperidol
5	M	31	295.30	29	1	21	19	37	Risperidone
6	M	28	295.30	20	2	25	20	47	Risperidone
7	M	22	298.90	20	2	15	9	30	Risperidone

M, male; F, female; DSM, diagnostic and statistical manual of mental disorders; Psych, psychoses; PANSS, positive and negative syndrome scale

[11C]-(R)-PK11195 PET

A strong significantly higher [11C]-*(R)*-PK11195 binding potential was found in the hippocampus of patients when compared to healthy volunteers (2.07±0.42 vs. 1.37±0.30; p=0.004) (table 2). The whole brain grey (figure 2) and white matter binding potential of [11C]-*(R)*-PK11195 were respectively 30% higher (1.99±0.64 vs. 1.54±0.41; p=0.122) and 20% higher (2.18±0.70 vs. 1.73±0.51; p=0.180) in patients than in healthy volunteers, but this difference did not reach statistical significance. A non-significant focal increase of [11C]-*(R)*-PK11195 binding potential was found in the midbrain (2.63±0.40 vs. 1.68±0.60; p=0.014), basal ganglia (1.82±0.59 vs. 1.39±0.28; p=0.017), pons (2.85±1.42 vs. 1.54±0.32; p=0.027) and cerebellum (1.45±0.48 vs. 1.11±0.22; p=0.040) of patients when compared to healthy volunteers. No statistically significant differences were found in the influx of [11C]-*(R)*-PK11195 (K_1) in any of the examined brain areas between patients and healthy volunteers. In patients a significantly higher efflux (k_2) of [11C]-*(R)*-PK11195 was found in all examined brain areas when compared to healthy volunteers (p<0.005).

No correlations were found between the total score on the positive, negative and global scale of the PANSS with both the whole brain grey matter and hippocampal binding potential. Age, the total number of psychotic episodes, the onset of the first psychotic episode and the duration of the psychotic episodes were not correlated to the [11C]-*(R)*-PK11195 binding potential.

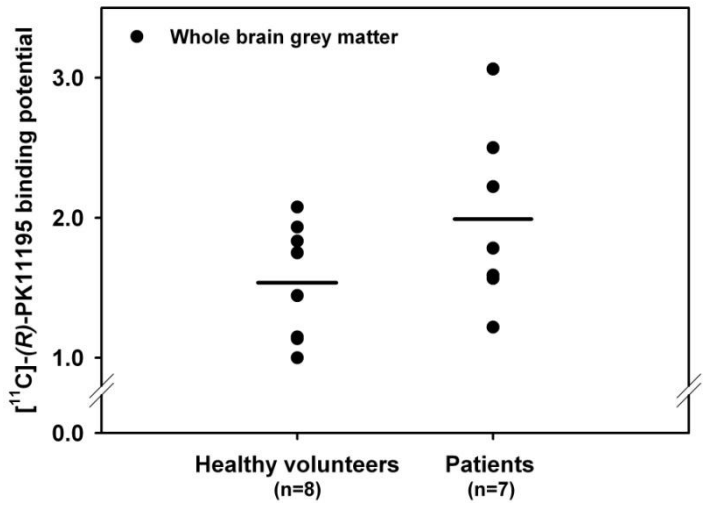

Figure 2 Binding potential of [11C]-*(R)*-PK11195 in the whole brain grey matter. Each dot represents an individual subject and the horizontal lines represent the mean values.

Table 2 Binding potentials of [^{11}C]-*(R)*-PK11195 (average ± standard deviation). Statistical analysis was performed using a multivariate general linear model, with whole brain grey matter as a covariate. *p<0.005

	Healthy volunteers	Patients	p-value
Frontal lobe	1.76 ± 0.75	2.08 ± 0.76	0.459
Occipital lobe	1.83 ± 1.20	1.93 ± 0.74	0.892
Temporal lobe	1.28 ± 0.34	1.64 ± 0.56	0.079
Parietal lobe	1.77 ± 0.93	2.28 ± 1.22	0.720
Basal Ganglia	1.39 ± 0.28	1.82 ± 0.59	0.017
Thalamus	1.61 ± 1.44	1.49 ± 0.35	0.742
Hippocampus	1.37 ± 0.30	2.07 ± 0.42	0.004*
Midbrain	1.68 ± 0.60	2.63 ± 0.40	0.014
Cerebellum	1.11 ± 0.22	1.45 ± 0.48	0.040
Pons	1.54 ± 0.32	2.85 ± 1.42	0.027

MRI

Visual examination of the MRI scans by an experienced neuroradiologist did not show any gross structural abnormalities in either patients or controls. Especially, no white matter lesions, indicative of neuroinflammation, were found.

Discussion

In the present study, we have shown a statistically significant increased binding potential of [^{11}C]-*(R)*-PK11195 in the hippocampus of psychotic patients as compared to healthy volunteers, indicating the presence of neuroinflammation. To our knowledge, this is the first study that reveals the presence of neuroinflammation in a focal area in living patients during psychosis. The presence of focal neuroinflammation in the hippocampus was accompanied by a non-significant increase in the whole brain grey and white matter [^{11}C]-*(R)*-PK11195 binding potential.

In a recent study, Van Berckel *et al.* [8] showed a small increase in whole brain grey matter binding potential of [^{11}C]-*(R)*-PK11195 in stable schizophrenic patients, with no reported focal increase. This is in line with the hypothesis of our study that focal neuroinflammation is a feature of psychosis and not necessarily present in stable schizophrenic patients. The focal neuroinflammation may evolve into a more widespread process in time. Increased focal neuroinflammation during psychosis is an

important pathological finding. The neuroinflammation found in the hippocampus may reflect exceptional vulnerability of this region during psychosis.

The relation between schizophrenia and neuroinflammation was shown in several post-mortem studies, showing an increase in the number of activated microglia cells [4,5,7], but other studies failed to show differences in the presence of activated microglia cells between the brain of schizophrenic patients and control subjects [6,9-11]. Steiner *et al.* [6] could not find support for the presence of activated microglia cells in schizophrenia, but two patients that died from suicide during acute psychosis showed highly elevated microglia cell activation. In a subsequent study, Steiner *et al.* [12] found a significantly increased density of activated microglia cells in the dorsolateral prefrontal cortex, nucleus accumbens and mediodorsal thalamus of six schizophrenic patients that committed suicide during acute psychosis as compared to ten non-suicidal schizophrenic patients. A non-significant increased density of activated microglia cells was found in the hippocampus. No differences in the density of activated microglia cells were found between non-suicidal schizophrenic patients and healthy volunteers. Although suicidal behavior may be linked to other regions of focal neuroinflammation, these results are consistent with the findings in the present study that focal neuroinflammation occurs predominately during psychosis.

Neuroinflammation is characterized by the activation of microglia cells, however, activated astrocytes also play an important role in the neuroinflammatory process [13]. Like in activated microglia cells, the expression of the PBR is also increased in activated astrocytes [14-16]. Increased [^{11}C]-*(R)*-PK11195 can therefore represent activated microglia cells and/or astrocytes. To date, the cell type that is responsible for the increased uptake of [^{11}C]-*(R)*-PK11195, and thus the increased expression of the PBR in neurological disorders, is not exactly known. However, many studies are performed to unravel the contribution of activated microglia cells and/or astrocytes to the PBR mediated [^{11}C]-*(R)*-PK11195 uptake. It has been shown that the contribution is dependent on the phase of activation of microglia cells and astrocytes [14] and on the type of lesion that is investigated. For example, in facial nerve axotomy, only microglia cells were responsible for the [^{11}C]-*(R)*-PK11195 signal [17], whereas in a toxic lesion of the hippocampus an increase in PBR expression was found in both microglia cells and astrocytes [18]. However, it cannot be excluded that the increased [^{11}C]-*(R)*-PK11195 binding potential found in this study is due to activated astrocytes only, unrelated to a neuroinflammatory process. The calcium binding protein S100B, which is primarily expressed by activated astrocytes, was found to be increased in

serum and plasma of schizophrenic patients without damage to neurons and astrocytes [19]. However, since it is not known if S100B expressing astrocytes also show an increase in PBR expression, and since it has been suggested that S100B contributes to neuroinflammation by activation of microglia cells [20], additional research is necessary to unravel the exact mechanism behind S100B expression in schizophrenia. Taken together, regardless of activated microglia cells and/or astrocytes being responsible for the increased expression in the PBR, the focal increased [^{11}C]-*(R)*-PK11195 in schizophrenia most likely represents a neuroinflammatory process.

In the present study, neuroinflammation was found in the hippocampus. Hippocampal pathology in schizophrenia is abundantly reported in the literature. MRI studies showed a decrease in hippocampal size in schizophrenic patients, even in prodromal and first-episode patients showing that it is not secondary to treatment [21,22]. Despite the reported decrease in hippocampal volume, there is no evidence for a change in the total number of neurons in the hippocampus of schizophrenia [23,24]. More likely, the morphology of the hippocampal neurons in schizophrenia is altered with respect to parameters such as size, shape and organization [25]. The involvement of microglia cells in hippocampal pathology is hitherto unknown.

The marked increase in [^{11}C]-*(R)*-PK11195 binding potential in the hippocampus suggests that neuroinflammation plays an important role in schizophrenia, especially during psychosis, and provides a potential target for therapy. In fact, it was shown that both patients with an acute exacerbation of schizophrenia [26] and chronic schizophrenic patients [27] that were treated with the cyclooxygenase-2 inhibitor celecoxib in addition to treatment with risperidone, had a significantly greater improvement on the PANSS than the patients that were treated with risperidone alone. In addition, the broad spectrum tetracycline antibiotic minocycline, was found to be beneficial as an add-on treatment in schizophrenia, in both an open label study [28] and a double-blind placebo controlled study [29]. Besides celecoxib and mincocycline, addition of aspirin to regular antipsychotic treatment over a period of three months was also found to substantially reduce the symptoms of schizophrenia when compared to patients that were treated with antipsychotics only [30]. Thus the anti-inflammatory drugs celecoxib, minocycline and aspirin can improve the symptoms of schizophrenia, most likely due to inhibition of pro-inflammatory cytokines. These results are in agreement with the presence of a neuroinflammatory process in schizophrenia.

Because all patients were taking antipsychotic medication during the period in which the [^{11}C]-*(R)*-PK11195 PET scan was performed, there is a possibility that the medication influenced the microglia cell activation. *In vitro* studies on the effect of antipsychotic drugs on microglia cells show that they decrease the neurotoxic molecules released by activated microglia cells. Both risperidone and haloperidol were found to inhibit the production of nitric oxide, the expression of inducible nitric oxide synthase and the production of pro-inflammatory cytokines by microglia cells treated with interferon-γ [31]. Olanzapine was also found to have anti-inflammatory properties, since the production of nitric oxide by lipopolysaccharide-stimulated microglia cells was reduced by pre-treatment with olanzapine [32]. In addition to the *in vitro* studies, we have recently shown that both clozapine and risperidone inhibited the activation of microglia cells in a rat model of herpes simplex encephalitis, while chronic treatment with clozapine and risperidone of healthy rats did not cause activation of microglia cells (data will be published elsewhere). Thus antipsychotic drugs most likely affect neuroinflammation in such a way that they decrease the microglia cell activation rather than cause activation of the microglia cells.

In addition to antipsychotics, all patients have used benzodiazepines. Because benzodiazepines were found to have affinity for the PBR, the patients had to stop with the use of benzodiazepines at minimal 3 half-lives (on average 1-2 weeks) of the benzodiazepines before the start of the study, to prevent a direct effect on the binding of [^{11}C]-*(R)*-PK11195. It can, however, not been ruled out that treatment with benzodiazepines affected the expression of the PBR. Most studies on benzodiazepines and other PBR ligands, such as Ro5-4864 and PK11195, indicate a neuroprotective effects of these ligands [33]. Wilms *et al.* [34] have shown that midazolam, clonazepam and diazepam interfered with the *in vitro* synthesis and release of pro-inflammatory cytokines by microglia cells. *In vivo*, it has been shown that diazepam protected against neuronal death in the hippocampus after transient forebrain ischemia [35]. Benzodiazepines, like antipsychotic, thus rather decreased neuroinflammation then being responsible for the increased [^{11}C]-*(R)*-PK11195 binding potential in the hippocampus. However, additional research on the role of both antipsychotics and benzodiazepines is necessary to determine their (protective) role in neuroinflammation.

Conclusion

The present study in patients within the schizophrenia spectrum suggests the presence of focal neuroinflammation in the hippocampus, during psychosis. This focal neuroinflammation was not accompanied by structural abnormalities. Which cell type is responsible for the increased [^{11}C]-*(R)*-PK11195 binding potential and how neuroinflammation is related to psychosis in schizophrenia, remains to be elucidated. Therefore, future studies are needed for further evaluation of the role of focal neuroinflammation during psychosis and the feasibility of anti-inflammatory drugs to treat the disease.

Acknowledgement

We would like to thank Rixt Elgersma and the nurse staff of Lentis Winschoten, The Netherlands for accompanying the patients. This study was funded by the Stanley Medical Research Institute, Grant-ID 05-NV-001.

References

1 Muller N, Schwarz MJ. A psychoneuroimmunological perspective to Emil Kraepelins dichotomy: schizophrenia and major depression as inflammatory CNS disorders. Eur.Arch.Psychiatry Clin.Neurosci. 2008; 258:97-106

2 Nimmerjahn A, Kirchhoff F, Helmchen F. Resting microglial cells are highly dynamic surveillants of brain parenchyma in vivo. Science 2005; 308:1314-1318

3 Doorduin J, de Vries EFJ, Dierckx RA, Klein HC. PET imaging of the peripheral benzodiazepine receptor: monitoring disease progression and therapy response in neurodegenerative disorders. Curr.Pharm.Des 2008; 14:3297-3315

4 Bayer TA, Buslei R, Havas L, Falkai P. Evidence for activation of microglia in patients with psychiatric illnesses. Neurosci.Lett. 1999; 271:126-128

5 Radewicz K, Garey LJ, Gentleman SM, Reynolds R. Increase in HLA-DR immunoreactive microglia in frontal and temporal cortex of chronic schizophrenics. J.Neuropathol.Exp.Neurol. 2000; 59:137-150

6 Steiner J, Mawrin C, Ziegeler A, et al. Distribution of HLA-DR-positive microglia in schizophrenia reflects impaired cerebral lateralization. Acta Neuropathol. 2006; 112:305-316

7 Wierzba-Bobrowicz T, Lewandowska E, Lechowicz W, Stepien T, Pasennik E. Quantitative analysis of activated microglia, ramified and damage of processes in the frontal and temporal lobes of chronic schizophrenics. Folia Neuropathol. 2005; 43:81-89

8 van Berckel BN, Bossong MG, Boellaard R, et al. Microglia Activation in Recent-Onset Schizophrenia: A Quantitative (R)-[(11)C]PK11195 Positron Emission Tomography Study. Biol.Psychiatry 2008; 64:820-822

9 Arnold SE, Trojanowski JQ, Gur RE, Blackwell P, Han LY, Choi C. Absence of neurodegeneration and neural injury in the cerebral cortex in a sample of elderly patients with schizophrenia. Arch.Gen.Psychiatry 1998; 55:225-232

10 Falke E, Han LY, Arnold SE. Absence of neurodegeneration in the thalamus and caudate of elderly patients with schizophrenia. Psychiatry Res. 2000; 93:103-110

11 Kurumaji A, Wakai T, Toru M. Decreases in peripheral-type benzodiazepine receptors in postmortem brains of chronic schizophrenics. J.Neural Transm. 1997; 104:1361-1370

12 Steiner J, Bielau H, Brisch R, et al. Immunological aspects in the neurobiology of suicide: elevated microglial density in schizophrenia and depression is associated with suicide. J.Psychiatr.Res. 2008; 42:151-157

13 Chavarria A, Alcocer-Varela J. Is damage in central nervous system due to inflammation? Autoimmun.Rev. 2004; 3:251-260

14 Chen MK, Guilarte TR. Translocator protein 18 kDa (TSPO): molecular sensor of brain injury and repair. Pharmacol.Ther. 2008; 118:1-17

15 Itzhak Y, Baker L, Norenberg MD. Characterization of the peripheral-type benzodiazepine receptors in cultured astrocytes: evidence for multiplicity. Glia 1993; 9:211-218
16 Raghavendra Rao VL, Dogan A, Bowen KK, Dempsey RJ. Traumatic brain injury leads to increased expression of peripheral-type benzodiazepine receptors, neuronal death, and activation of astrocytes and microglia in rat thalamus. Exp.Neurol. 2000; 161:102-114
17 Banati RB, Myers R, Kreutzberg GW. PK ('peripheral benzodiazepine')--binding sites in the CNS indicate early and discrete brain lesions: microautoradiographic detection of [3H]PK11195 binding to activated microglia. J.Neurocytol. 1997; 26:77-82
18 Kuhlmann AC, Guilarte TR. Cellular and subcellular localization of peripheral benzodiazepine receptors after trimethyltin neurotoxicity. J.Neurochem. 2000; 74:1694-1704
19 Steiner J, Bielau H, Bernstein HG, Bogerts B, Wunderlich MT. Increased cerebrospinal fluid and serum levels of S100B in first-onset schizophrenia are not related to a degenerative release of glial fibrillar acidic protein, myelin basic protein and neurone-specific enolase from glia or neurones. J.Neurol.Neurosurg.Psychiatry 2006; 77:1284-1287
20 Rothermundt M, Peters M, Prehn JH, Arolt V. S100B in brain damage and neurodegeneration. Microsc.Res.Tech. 2003; 60:614-632
21 Pantelis C, Velakoulis D, McGorry PD, et al. Neuroanatomical abnormalities before and after onset of psychosis: a cross-sectional and longitudinal MRI comparison. Lancet 2003; 361:281-288
22 Wright IC, Rabe-Hesketh S, Woodruff PW, David AS, Murray RM, Bullmore ET. Meta-analysis of regional brain volumes in schizophrenia. Am.J.Psychiatry 2000; 157:16-25
23 Heckers S, Heinsen H, Geiger B, Beckmann H. Hippocampal neuron number in schizophrenia. A stereological study. Arch.Gen.Psychiatry 1991; 48:1002-1008
24 Walker MA, Highley JR, Esiri MM, et al. Estimated neuronal populations and volumes of the hippocampus and its subfields in schizophrenia. Am.J.Psychiatry 2002; 159:821-828
25 Harrison PJ. The hippocampus in schizophrenia: a review of the neuropathological evidence and its pathophysiological implications. Psychopharmacology (Berl) 2004; 174:151-162
26 Muller N, Riedel M, Scheppach C, et al. Beneficial antipsychotic effects of celecoxib add-on therapy compared to risperidone alone in schizophrenia. Am.J.Psychiatry 2002; 159:1029-1034
27 Akhondzadeh S, Tabatabaee M, Amini H, Ahmadi Abhari SA, Abbasi SH, Behnam B. Celecoxib as adjunctive therapy in schizophrenia: a double-blind, randomized and placebo-controlled trial. Schizophr.Res. 2007; 90:179-185

28 Miyaoka T, Yasukawa R, Yasuda H, Hayashida M, Inagaki T, Horiguchi J. Minocycline as adjunctive therapy for schizophrenia: an open-label study. Clin.Neuropharmacol. 2008; 31:287-292

29 Levkovitz Y, Mendlovic S, Issaki S, Braw Y, Levkovitch-Verbin H, Gal G. Minocycline ameliorates negative symptoms and cognitive deficits in early-phase schizophrenia: a double-blind, randomized placebo-controlled study. Schizophr.Res. 2008; 98 (suppl 1):14-

30 Laan W. Anti-inflammatory drugs and psychosis.: University of Utrecht, 2008

31 Kato T, Monji A, Hashioka S, Kanba S. Risperidone significantly inhibits interferon-gamma-induced microglial activation in vitro. Schizophr.Res. 2007; 92:108-115

32 Hou Y, Wu CF, Yang JY, et al. Effects of clozapine, olanzapine and haloperidol on nitric oxide production by lipopolysaccharide-activated N9 cells. Prog.Neuropsychopharmacol.Biol.Psychiatry 2006; 30:1523-1528

33 Papadopoulos V, Lecanu L. Translocator protein (18 kDa) TSPO: An emerging therapeutic target in neurotrauma. Exp.Neurol. 2009;

34 Wilms H, Claasen J, Rohl C, Sievers J, Deuschl G, Lucius R. Involvement of benzodiazepine receptors in neuroinflammatory and neurodegenerative diseases: evidence from activated microglial cells in vitro. Neurobiol.Dis. 2003; 14:417-424

35 Sarnowska A, Beresewicz M, Zablocka B, Domanska-Janik K. Diazepam neuroprotection in excitotoxic and oxidative stress involves a mitochondrial mechanism additional to the GABAAR and hypothermic effects. Neurochem.Int. 2009; 55:164-173

Chapter 10

Imaging herpes virus activity in the central nervous system of schizophrenic patients

Janine Doorduin, Erik F.J. de Vries, Antoon T.M. Willemsen, Rudi A. Dierckx and Hans C. Klein

Submitted for publication

Abstract

Schizophrenia is a chronic, disabling brain disease with unknown etiology. Herpes viruses have been implicated in the etiology of schizophrenia and antibodies against herpes viruses were found to be associated with schizophrenia. In the present study, positron emission tomography (PET) with [^{18}F]-FHBG, a tracer for the viral thymidine kinase, was used to study the presence of active herpes viruses in the brain of schizophrenic patients during psychosis.

Eight schizophrenic patients were included for [^{18}F]-FHBG PET. Patients were assigned to a mildly or severely affected group, based on psychosis and memory as measured with the positive and negative syndrome scale and 15-word test, respectively.

The metabolic rate of [^{18}F]-FHBG in the temporal lobe of the severely affected group was 50% higher ($p<0.05$) than in the mildly affected group. No differences were found in any other brain region. No increased influx of [^{18}F]-FHBG was found, indicating that the higher metabolic rate is due to an increased phosphorylation of [^{18}F]-FHBG by the viral thymidine kinase.

The increased metabolic rate of [^{18}F]-FHBG in the temporal lobe of schizophrenic patients experiencing severe psychosis, suggests the focal presence of active herpes viruses. Additional studies are needed to confirm viral presence and to specify which of the herpes viruses are present in the schizophrenic brain.

Introduction

Schizophrenia is a chronic, disabling brain disease with unknown etiology. It has been suggested that herpes viruses play a role in schizophrenia [1-4]. An important characteristic of these viruses is that they establish latency in the central nervous system after primary infection. Both primary infection and reactivation of herpes viruses may sporadically result in herpes encephalitis, mostly caused by the herpes simplex virus type-1 (HSV-1) [5].

Post-mortem studies found the presence of herpes viruses in the brain, but there was no difference in herpes virus levels between schizophrenic patients and healthy volunteers [6,7]. However, these studies do not give any insight in whether the viruses were latent or actively replicating. Interestingly, herpes encephalitis patients may initially present with symptoms that resemble psychosis associated with schizophrenia [8,9]. It is possible that psychosis in schizophrenia represents a mild form of herpes encephalitis only caused by herpes viruses in an active state. We aimed to explore the hypothesis that active herpes viruses are present in the brain of schizophrenic patients during a psychotic and impaired cognitive state.

Imaging techniques like positron emission tomography (PET) provide the opportunity to study functional processes in patients. The PET tracer 9-(4-[^{18}F]-fluoro-3-hydroxymethylbutyl)guanine ([^{18}F]-FHBG) is a radiolabelled analog of the antiviral pro-drug penciclovir. After entering the cell, [^{18}F]-FHBG can phosphorylated by a viral thymidine kinase (or a viral analogue), which results in trapping of [^{18}F]-FHBG inside the cell (figure 1). Viral thymidine kinase is only expressed in active, replicating viruses, thus only in infected cells trapping of [^{18}F]-FHBG can occur. Human thymidine kinase has high substrate specificity and does not phosphorylate the antiviral drug. [^{18}F]-FHBG can be phosphorylated by HSV-1, HSV-2, Varicella-Zoster virus (VZV) [10], Epstein-Barr virus (EBV) [11], cytomegalovirus (CMV) [12] and possibly human herpes virus-6 (HHV-6). [^{18}F]-FHBG was already evaluated as a PET tracer for imaging of viral thymidine kinase in transduced tumor cells [13] and for imaging of herpes simplex encephalitis in rats [14]. [^{18}F]-FHBG was found to be a suitable PET tracer to image HSV thymidine kinase, but it has not been used to study replicating viruses in the CNS of schizophrenic patients. In the present study, it was determined if active herpes viruses could be detected with [^{18}F]-FHBG PET in the brain of schizophrenia patients during a psychotic episode.

Methods

Chemicals

All chemicals were purchased from commercial suppliers and used without further purification.

[^{18}F]-FHBG

A solution of 1 mg N^2-(p-anisyldiphenylmethyl)-9-[(4-tosyl)-3-p-anisyldiphenylmethoxy-methylbutyl]guanine (ABX, Germany) in 0.5 ml of dry acetonitrile was added to dry [^{18}F]KF/kryptofix 2.2.2 complex (5 mg K_2CO_3; 15 mg kryptofix) and heated for 30 min at 110°C. Then, 0.4 ml 1M HCl was added and the mixture was heated for 5 min at 90°C in an open vial to allow evaporation of acetonitrile. After cooling, the reaction mixture was neutralized with 1.5 ml 0.1M sodium phosphate buffer (pH 7.2). The reaction mixture was passed through a Waters alumina N seppak to remove unreacted fluoride. The product was purified by HPLC over a Hamilton PRP-1 column (250x10 mm, 10 μm) (Alltech, The Netherlands) with 7% of ethanol in water as the eluent at a flow rate of 5 ml/min. The HPLC fraction with the same retention time as an authentic reference sample was collected and sterilized over a Cathivex GS filter. A sample of the product was used for quality control prior to injection. The (radio)chemical purity and specific activity were determined by reversed phase HPLC (Nova-pak C18, 150x3.9 mm, 4 μm, 5% EtOH, 1 ml/min). The presence of unreacted [^{18}F]fluoride was determined by TLC (silica, dichloromethane/methanol:7/3). [^{18}F]-FHBG was obtained in 5-10% yield with a specific activity of 22-84 GBq/μmol. The radiochemical purity was always higher than 95%. Unknown impurities were <1 mg/l , kryptofix <10 mg/l and [^{18}F]fluoride <5%.

Patients

Eight patients were recruited from psychiatric services based on the following inclusion criteria: 1) fulfilling DSM-IV criteria for schizophrenia (295.xx); 2) active psychosis (i.e. a minimum score of four on two items of the positive PANSS (positive and negative syndrome scale) [15] or a five or higher on one item; 3) age above eighteen; 4) ability to provide written informed consent. Exclusion criteria were 1) concomitant severe medical conditions; 2) substance abuse; 3) pregnancy and 4) use of anti-viral drugs. Patients were a-priori divided in severely and mildly affected groups

based on severity of psychosis and memory disorder. An increased risk for the presence of active herpes viruses was expected in patients with the most severe psychosis and memory disturbances, i.e. severely affected patients. The severely affected group consisted of patients with a score on the positive item of the PANSS higher than $^1/_3$ of the total score of 49, or of patients that scored below $^1/_2$ of the total score on the 15-word test (i.e. half of the total score of 120 on immediate recall, delayed recall and recognition). Because a memory disorder can be secondary to disturbances in attention, patients also underwent a continuous performance test (CPT) to test their sustained attention. The PANSS, 15-word test and CPT were taken by trained psychiatric nurses. Antibodies against the herpes viruses that phosphorylate [^{18}F]-FHBG were determined using enzyme immunoassay.

A-priori division of patients into severely and mildly affected groups was preferred over inclusion of healthy volunteers, because no brain uptake of [^{18}F]-FHBG was found in healthy volunteers [16].

The study was approved by the medical ethical committee of the University Medical Center Groningen. All patients provided written informed consent after detailed description of the study.

15-word test

Patients listened to a total of 15 words that were read aloud by the investigator, after which the patient was asked to repeat as many words as possible (immediate recall, representing short-term memory). This was repeated four times. After 15-30 minutes the patients were asked to repeat all the words that he/she still remembered, without hearing the words again (delayed recall, representing long-term memory). The test was ended by the investigator reading aloud a list of 30 words of which half of the words were from the list in the 15-word test. For each of the 30 words the patient had to indicate if the word was either present or not present in the list of the 15-word test (word recognition).

Continuous performance test

The test randomly presented numbers between 0 and 9 at the centre of the monitor at a constant rate of 1000 ms, with the number visible for 100 ms. The patients had to respond to the target number (7), by pressing a button, when it was preceded by the cue number (3). A total of 600 numbers with 90 targets were presented over 11

minutes. Outcome measurements were the reaction time and the sensitivity index (d'), which measures the ability of the patients to discriminate the target stimuli from the non-target stimuli.

PET protocol

A catheter was inserted in the radial artery after testing for collateral circulation and injection of 1% lidocaine for local anesthesia. In the other arm, a catheter was inserted in the antebrachial vein. PET was performed with the ECAT EXACT HR+ camera (Siemens, Tenessee). Head movement was minimized with a head-restraining adhesive band and a neuroshield was used to attenuate radiation from the subject's body. A 60-min emission scan in 3D-mode was performed, starting simultaneously with the intravenously injection of [^{18}F]-FHBG (411±17 MBq) at a speed of 0.5 ml/sec (total volume of 8.3 ml).

After injection, arterial blood radioactivity was continuously monitored with an automated sampling system (Veenstra Instruments, The Netherlands). An amount of 5 extra blood samples were collected at 10, 20, 30, 45 and 60 min after [^{18}F]-FHBG injection to determine the amount of radioactivity in blood and plasma. In the arterial blood samples that were collected at 20 and 60 min after [^{18}F]-FHBG injection, the fraction of intact tracer in plasma was also determined. Therefore, these blood samples were centrifuged at 3000 g for 3 min. Then 40 µl of 70% perchloric acid was added to 1.5 ml plasma. The plasma was mixed for 30 s and centrifuged at 3000 g for 5 min. After filtration over a Millex HV 45µm filter, a volume of 1 ml of the supernatant was injected into a HPLC system, consisting of a Waters 590 HPLC-pump (Waters Corporation, USA) and µBondapak C18 column (300x7.8 mm, 5 µm) (Alltech, The Netherlands). The mobile phase consisted of a mixture of 8% of acetonitrile in water. The flow-rate was set at 3.0 ml/min and samples were collected at time intervals of 30 s. The collected samples were counted for radioactivity using a gamma-counter (LKB Wallac, Finland).

PET data-analysis

Attenuation correction was performed with the separate ellipse algorithm. Images were reconstructed by filtered back projection in 21 successive frames of increasing duration (6x 10 sec, 2x 30 sec, 3x 1 min, 2x 2min, 2x 3 min, 3x 5min, 3x 10 min). Time-activity curves of the frontal, occipital, temporal and parietal lobe, thalamus, basal ganglia and cerebellum were created using manually drawn regions of interest

and used for kinetic modelling with software developed in Matlab 7.1 (Mathworks, Massachusets). Patlak analysis [17] was used to calculate the metabolic rate (K_i, i.e. the amount of phosphorlylated tracer in relation to the amount of tracer that has been available in plasma, defined as $(K_1*k_3)/(k_2+k_3)$), using a fixed blood volume of 3% (figure 1). The influx of [^{18}F]-FHBG into the brain was determined using two-compartment modeling with a fixed blood volume of 3% and an individual delay.

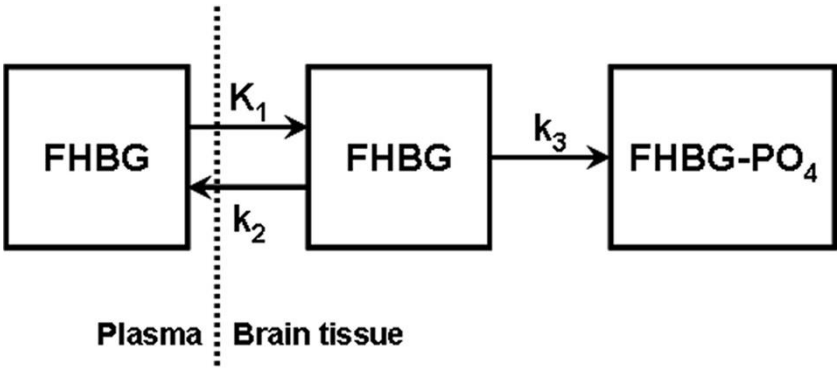

Figure 1 Two-tissue compartment model to describe the kinetics of FHBG. Influx of FHBG_from plasma to brain tissue is described by K_1 and the efflux of from brain tissue to plasma is described by k_2. In brain tissue, FHBG can be phosphorylated into FHBG-phosphate (FHBG-P) in cells expressing viral thymidine kinase, resulting in trapping of FHBG-P in these cells (k_3).

Statistical analysis

Statistical analysis was performed with SPSS 16.0. Correlations between the score on the PANSS, 15-word test and CPT, were assessed with Pearson's product moment correlation coefficient (r). To determine the differences between the averages of the metabolic rate in severely and mildly affected groups, one-way ANOVA was used. Correlations and differences were considered to be significant when $p<0.05$.

Results

Patient characteristics

A total number of 8 psychotic patients (5 male and 3 female) were included (table 1). All patients were diagnosed as having schizophrenia (DSM-IV: 295.xx). The age of the patients was 42±13 (n=8) (mean ± standard deviation), with the onset of

schizophrenia at an average age of 22±5 (n=8). All patients were recruited during psychosis and were using benzodiazepines and/or anti-psychotics in the period of the [18F]-FHBG scan. One patient (patient number 8) was diagnosed as having herpes encephalitis at the age of 13. At the age of 30, this patient experienced the first appearance of paranoid psychosis.

The presence of antibodies against the herpes viruses that phosphorylate [18F]-FHBG are displayed in table 1. All patients had antibodies against one or more herpes viruses.

Table 1 Patient characteristics

			Psychoses			
Pat#	**Sex**	**Age**	**Onset**	**Total**	**Medication**	**Antibodies**
1	M	44	22	6	Oxazepam	VZV, HHV-6
2	M	37	19	5	Risperidone, Diazepam, Venlafaxine	VZV, HHV-6
3	M	47	42	1	Risperidone, Diazepam	HSV-1, EBV, HHV-6
4	F	61	22	10	Zuclopentixol, Oxazepam, Lormetazepam, Esomeprazol, Amitriptyline, Temazepam	HSV-1, VZV, EBV, HHV-6
5	M	30	13	1	Risperidone, Oxazepam, Temazepam	HHV-6
6	F	58	54	2	-	HSV-1, VZV, HHV-6
7	F	28	27	1	Olanzapine, Oxazepam, Temazepam	HSV-1, HSV-2, VZV, EBV, HHV-6
8	M	30	27	1	Olanzapine, Valproic acid, Lamotrigine	HSV-1, HHV-6

M, male; F, female; VZV, Varicella-Zoster virus; HHV-6, human herpes virus 6; HSV-1, herpes simplex virus type-1; EBV, Epstein-Barr virus; HSV-2, herpes simplex virus type-2

The average score on the positive scale of the PANSS was 18±4 (n=8) (table 2), 22±6 (n=8) on the negative scale and 43±8 (n=8) on the global scale. The patients with a score on the positive item of the PANSS higher than $^1/_3$ of the total score of 49, i.e. 16.3, where assigned to the severely affected group. The severely affected group regarding psychosis included patient number 2, 4, 6 and 8. The average score on the immediate recall in the 15-word test was 27±10 (n=8), on the delayed recall 3.8±2.8 (n=8) and on the recognition 27±3 (n=8). No correlations were found between immediate and delayed recall, and the scores on both items did not correlate to either of the items on the PANSS ($p>0.1$). The score on recognition showed a significantly negative correlation to the score on the positive scale of the PANSS ($r=0.87$; $p=0.005$), but not to the negative ($r=0.20$; $p=0.628$) and the global scale of the

PANSS (r=0.30; p=0.478). No correlation was found between the immediate recall, delayed recall and recognition in the 15-word test and the d' on the CPT (p>0.1), suggesting that the memory disturbances are not secondary to attention deficits. Patients that had a score lower than $^1/_2$ of the total score on the 15-word test, which is a score of 60, were assigned to the severely affected group for memory disorder (i.e. patient 2, 4, 6 and 8). These were the same patients as the patients assigned to the severely affected group of psychosis.

Table 2 Patient scores on the PANSS, the 15-word test and the continuous performance test

	PANSS			15 WT				CPT	
Pat#	**Pos**	**Neg**	**Global**	**Imm. recall**	**Del. recall**	**Recognition**	**Total score**	**RT (ms)**	**d'**
1	14	25	33	34	2	30	66	636	2.1
2	23	28	42	23	2	22	47	648	1.7
3	16	24	51	27	6	29	62	744	2.5
4	20	30	53	12	2	28	42	377	0.6
5	16	11	41	43	8	30	81	692	2.1
6	24	23	52	15	2	22	39	833	0.6
7	12	19	32	27	7	29	63	639	2.7
8	19	15	39	33	1	24	58	622	4.2

Pos, positive; Neg, negative; 15 WT, 15-word test; Imm., immediate; Del., delayed; CPT, continuous performance test; RT, reaction time

[^{18}F]-FHBG PET

The [^{18}F]-FHBG images showed low brain uptake (figure 2). No radioactive metabolites were found in plasma at 20 and 60 minutes after the injection of [^{18}F]-FHBG (data not shown). Two-tissue compartment modeling revealed a low influx of [^{18}F]-FHBG into brain tissue (K_1 = 0.022±0.018) (n=8). No differences in the influx were found between the severely and mildly affected group (p>0.200). A significantly higher metabolic rate was found in the temporal lobe of the severely affected group when compared to the mildly affected group ($3.9x10^{-4}$±$1.0x10^{-4}$ vs. $5.9x10^{-4}$±$1.1x10^{-4}$, p=0.035) (table 3). The increased metabolic rate of [^{18}F]-FHBG could not be attributed to a single herpes virus.

In the patient that had herpes encephalitis at the age of 13 (patient 8), no significant deviation in influx or metabolic rate of [^{18}F]-FHBG was found in any of the examined brain areas, when compared to the severely and mildly affected groups.

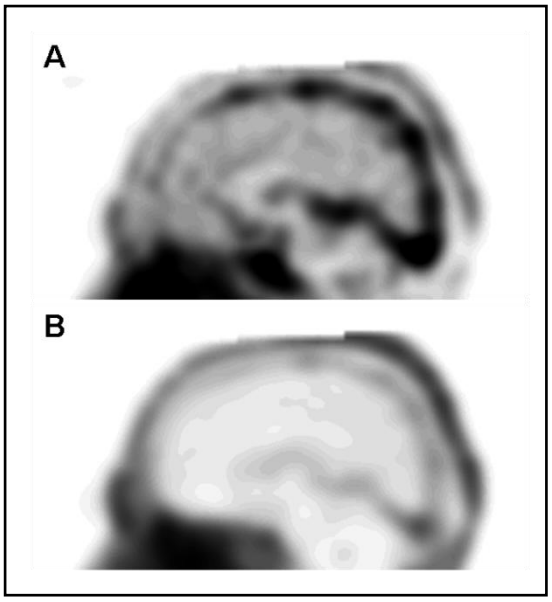

Figure 2 Sagittal view of the [18F]-FHBG PET images. **A** Summation of the first 2 min of the PET scan. **B** Summation of the last 55 min of the PET scan.

Table 3 Metabolic rate, as determined by Patlak analysis. Averages ± standard deviation of patients groups based on the severity of psychosis and memory disorder.

	Mildly affected (n=4)	Severely affected (n=4)	p-value
Frontal lobe	6.9E-04 ± 2.3E-04	6.6E-04 ± 3.4E-04	n.s.
Parietal lobe	4.9E-04 ± 1.2E-04	3.6E-04 ± 1.7E-04	n.s.
Occiptal lobe	3.7E-04 ± 1.7E-04	5.4E-04 ± 6.0E-05	n.s.
Temporal lobe	3.8E-04 ± 1.0E-04	5.9E-04 ± 1.1E-04	0.035
Thalamus	3.7E-04 ± 1.8E-04	3.8E-04 ± 1.4E-04	n.s.
Basal ganglia	4.2E-04 ± 1.9E-04	4.7E-04 ± 1.1E-04	n.s.
Cerebellum	5.2E-04 ± 2.9E-04	3.0E-04 ± 1.7E-04	n.s.

n.s., non-significant

Discussion

In the present study, a significantly higher metabolic rate of [18F]-FHBG was found in the temporal lobe of severely affected patients, based on severity of psychosis and memory deficit. Herpes viruses that are hypothesized to play a role in the etiology of schizophrenia have thus far only been found in post-mortem brains, in undefined

latent or active state. This [^{18}F]-FHBG PET study provided the first evidence of the presence of active herpes viruses in living schizophrenic patients.

The increased metabolic rate of [^{18}F]-FHBG in the temporal lobe suggests the presence of active herpes viruses. However, the metabolic rate is a function of the influx of [^{18}F]-FHBG (K_1), the efflux (k_2) and the phosphorylation (k_3) ($[K_1*k_3]/[k_2+k_3]$) and consequently an increased metabolic rate could also be caused by an increased [^{18}F]-FHBG influx. Since no differences were found in the influx, the increased metabolic rate is due to increased phosphorylation the thymidine kinase of active herpes viruses.

The finding of an increased metabolic rate of [^{18}F]-FHBG in the temporal lobe is consistent with the involvement of this brain area in schizophrenia. The temporal lobe is involved in, amongst others, memory and the processing of both auditory and visual information, which is disturbed in schizophrenia, especially during psychosis [18]. The severely affected group in the present study showed a high score on the positive item of the PANSS and memory disturbances, consistent with the involvement of the temporal lobe in psychosis in schizophrenia. In addition, HSV-1, VZV and EBV infection of the brain was found to mainly involve the temporal lobe [19,20]. Interestingly, we recently found evidence for an increased activation of microglia cells, indicative of neuroinflammation, in the hippocampus of schizophrenic patients during psychosis [21]. Since the hippocampus is part of the temporal lobe, the presence of active herpes viruses in the temporal lobe can be responsible for the observed neuroinflammation.

The activity of herpes viruses in the temporal lobe may cause psychosis and memory disturbances in the severely affected patients. However, it is important to keep in mind that the viral hypothesis of schizophrenia may only account for a subgroup of the patients and that the presence of active virus alone may not be sufficient for the development of schizophrenia.

Conclusion

The increased metabolic rate of [^{18}F]-FHBG in the temporal lobe of schizophrenic patients experiencing severe psychosis, suggests the presence of active herpes viruses and supports the viral hypothesis of schizophrenia. Additional studies are needed to confirm the presence of the active herpes viruses and to specify which herpes virus is present in the schizophrenic brain.

Acknowledgement

The authors thank Dr. Robert Yolken of the Stanley Division of Developmental Neurovirology, John Hopkins Medicine, Baltimore for determining viral antibodies and the Stanley Medical Research Institute (Grant-ID 05-NV-001) for funding for this study.

Reference List

1 Dickerson FB, Boronow JJ, Stallings C, Origoni AE, Ruslanova I, Yolken RH. Association of serum antibodies to herpes simplex virus 1 with cognitive deficits in individuals with schizophrenia. Arch.Gen.Psychiatry 2003; 60:466-472

2 Leweke FM, Gerth CW, Koethe D, et al. Antibodies to infectious agents in individuals with recent onset schizophrenia. Eur.Arch.Psychiatry Clin.Neurosci. 2004; 254:4-8

3 Prasad KM, Shirts BH, Yolken RH, Keshavan MS, Nimgaonkar VL. Brain morphological changes associated with exposure to HSV1 in first-episode schizophrenia. Mol.Psychiatry 2007; 12:105-113

4 Shirts BH, Prasad KM, Pogue-Geile MF, Dickerson F, Yolken R, Nimgaonkar VL. Antibodies to cytomegalovirus and Herpes Simplex Virus 1 associated with cognitive function in schizophrenia. Schizophr.Res. 2008; 106:268-274

5 Whitley RJ, Kimberlin DW. Viral encephalitis. Pediatr.Rev. 1999; 20:192-198

6 Carter GI, Taylor GR, Crow TJ. Search for viral nucleic acid sequences in the post mortem brains of patients with schizophrenia and individuals who have committed suicide. J.Neurol.Neurosurg.Psychiatry 1987; 50:247-251

7 Taller AM, Asher DM, Pomeroy KL, et al. Search for viral nucleic acid sequences in brain tissues of patients with schizophrenia using nested polymerase chain reaction. Arch.Gen.Psychiatry 1996; 53:32-40

8 Torrey EF, Peterson MR. The viral hypothesis of schizophrenia. Schizophr.Bull. 1976; 2:136-146

9 Whitley RJ. Herpes simplex encephalitis: adolescents and adults. Antiviral Res. 2006; 71:141-148

10 Earnshaw DL, Bacon TH, Darlison SJ, Edmonds K, Perkins RM, Vere Hodge RA. Mode of antiviral action of penciclovir in MRC-5 cells infected with herpes simplex virus type 1 (HSV-1), HSV-2, and varicella-zoster virus. Antimicrob.Agents Chemother. 1992; 36:2747-2757

11 Bacon TH, Boyd MR. Activity of penciclovir against Epstein-Barr virus. Antimicrob.Agents Chemother. 1995; 39:1599-1602

12 Zimmermann A, Michel D, Pavic I, et al. Phosphorylation of aciclovir, ganciclovir, penciclovir and S2242 by the cytomegalovirus UL97 protein: a quantitative analysis using recombinant vaccinia viruses. Antiviral Res. 1997; 36:35-42

13 Alauddin MM, Conti PS. Synthesis and preliminary evaluation of 9-(4-[18F]-fluoro-3-hydroxymethylbutyl)guanine ([18F]FHBG): a new potential imaging agent for viral infection and gene therapy using PET. Nucl.Med.Biol. 1998; 25:175-180

14 Doorduin J, Klein HC, Dierckx RA, de Vries EFJ. Herpes simplex encephalitis in rats: a positron emission tomography study with [18F]-FHBG, [11C]-(R)-PK11195 and [18F]-FDG. Neuroimage. 2008; 41:T110-

15 Kay SR, Fiszbein A, Opler LA. The positive and negative syndrome scale (PANSS) for schizophrenia. Schizophr.Bull. 1987; 13:261-276
16 Yaghoubi S, Barrio JR, Dahlbom M, et al. Human pharmacokinetic and dosimetry studies of [(18)F]FHBG: a reporter probe for imaging herpes simplex virus type-1 thymidine kinase reporter gene expression. J.Nucl.Med. 2001; 42:1225-1234
17 Patlak CS, Blasberg RG. Graphical evaluation of blood-to-brain transfer constants from multiple-time uptake data. Generalizations. J.Cereb.Blood Flow Metab 1985; 5:584-590
18 Heckers, G and Goff, D. C. Neural circuitry and signaling in schizophrenia. In: Brain circuitry and signaling in psychiatry. American Psychiatric Publishing, Inc., 2002; 67-98
19 Berger JR, Houff S. Neurological complications of herpes simplex virus type 2 infection. Arch.Neurol. 2008; 65:596-600
20 Vince A, Lepej SZ, Kurelac I, et al. Virological and immunological characteristics of fatal Epstein-Barr virus mononucleosis in a 17-year-old Caucasian male presenting with meningoencephalitis and hemophagocytic syndrome. J.Neurovirol. 2007; 13:389-396
21 Doorduin J, de Vries EFJ, Willemsen ATM, Dierckx RA, Klein HC. Neuroinflammation in schizophrenic patients: a positron emission tomography study with [11C]-(R)-PK11195. Neuroimage. 2008; 41:T109

Chapter 11

Using nuclear medicine to unravel the etiology of schizophrenia: a focus on herpes viruses

Janine Doorduin, Erik F.J. de Vries and Hans C. Klein

In preparation

Schizophrenia is a chronic and disabling brain disease that affect approximately 1% of the human population worldwide [1]. The symptoms of schizophrenia are classified into positive symptoms, such as delusions and hallucinations, negative symptoms, such as social withdrawal and flattened emotion, cognitive symptoms and mood symptoms. Despite extensive research, it is not known what causes schizophrenia or how the causative factors lead to the clinical symptoms. Environmental factors are thought to play a role in the etiology of schizophrenia, causing schizophrenia only in individuals with a genetic predisposition. Related to the environmental factors, viruses have been proposed to be involved in the etiology of schizophrenia.

Herpes viruses, large DNA viruses of which eight types are known to cause disease in humans, are most frequently associated with schizophrenia. These viruses have the ability to establish latency in the human body after primary infection. Reactivation of these viruses can occur due to a variety of factors at any point in life. However, the concept of herpes virus latency is complex and not fully understood. The sites in the human body where herpes viruses were found to establish latency include lymphocytes, monocytes and neuronal ganglions, depending on the type of herpes virus, but it has been proposed that these viruses also establish latency within the brain. Reactivation of these viruses within the brain causes neuronal damage, which could lead to the clinical symptoms resembling those of schizophrenia. The herpes simplex virus type-1 (HSV-1) is the most common cause of viral encephalitis that mainly involves the temporal lobe and limbic structures. HSV-1 encephalitis patients present with changes in consciousness, confusion and can also reveal psychosis similar to that in the prodromal phase of schizophrenia [2]. Imaging studies with positron emission tomography (PET) and single photon emission computed tomography (SPECT) studies have shown hyperperfusion of the affected brain areas in early HSV-1 encephalitis, which was followed by progressive hypoperfusion [3,4]. In addition, a neuroinflammatory process beyond the primary focal lesion has been found in HSV-1 encephalitis patients, using PET [5]. Although HSV-1 encephalitis usually is an acute necrotizing encephalitis, mild forms of encephalitis have also been reported [6]. Schizophrenia was hypothesized by us to represent a mild form of herpes encephalitis.

The challenge in unraveling the role of herpes viruses in schizophrenia is to provide direct evidence for this hypothesis. Up to date, the only attempt to provide direct evidence for the presence of herpes viruses in the schizophrenic brains was by studying post-mortem brains [7]. The majority of these studies could not detect herpes viruses in the brain and in those who could, no differences were found between

healthy controls and schizophrenic patients. The negative results of these studies can be attributed to the attempt to detect herpes viruses many years after onset of schizophrenia. In addition, post-mortem studies in general do not discriminate between latent and actively replicating herpes viruses.

In order to further elucidate the role of herpes viruses in schizophrenia, non-invasive imaging techniques, such as PET and SPECT, can be of value for providing both indirect and direct evidence. Indirect evidence for the role of herpes viruses in schizophrenia could be obtained by imaging of processes in the brain that are influenced by the presence of herpes viruses. Imaging of neuroinflammation could be used to measure viral activity indirectly. Neuroinflammation is characterized by the presence of activated microglia cells, which show an increased expression of the peripheral benzodiazepine receptor (PBR). The PET tracer [^{11}C]-PK11195 is a PBR ligand and has been used to study neuroinflammation in many neurological diseases and could also be used for monitoring of disease progression and therapy response [8]. Recently, [^{11}C]-PK11195 PET showed the presence of global neuroinflammation in recent-onset schizophrenic patients, when compared to healthy volunteers [9]. In this study, patients were not experiencing psychosis at the time of the PET scan. However, with the viral hypothesis in mind it seems plausible that a viral infection of the brain causes focal neuroinflammation, especially during psychosis. Therefore, a [^{11}C]-PK11195 PET study was performed in schizophrenic patients that were scanned during psychosis [10]. Consistent with our hypothesis, focal neuroinflammation was found to be present in the hippocampus of schizophrenic patients, which is of particular interest in relation to the preference of HSV-1 to infect the temporal lobe and limbic structures. Although the presence of neuroinflammation does not provide evidence for a viral infection in the schizophrenic brain, it can be used as a tool to monitor treatment response in future studies. If the detected neuroinflammation is indeed caused by the presence of active herpes viruses, anti-viral treatment could be effective in reducing neuroinflammation.

In order to study the role of herpes viruses in schizophrenia directly, the availability of a PET tracer that images a specific characteristic of replicating herpes viruses or herpes virus infection is essential. The PET tracer 9-(4-[^{18}F]-fluoro-3-hydroxymethylbutyl)guanine ([^{18}F]-FHBG) and others were originally developed as imaging agents for monitoring of gene therapy with the HSV thymidine kinase reporter gene. [^{18}F]-FHBG is the radiolabelled analogue of the antiviral pro-drug penciclovir. The antiviral properties of penciclovir are based on the expression of viral

thymidine kinase (or a viral analogue) by active, replicating viruses. [^{18}F]-FHBG, like penciclovir, is phosphorylated by the viral thymidine kinase and remains trapped in the infected cell, allowing for localized imaging and quantification of viral activity. It is important to know that the endogenous human thymidine kinase has high substrate specificity and does not phosphorylate [^{18}F]-FHBG. Since penciclovir treatment was found to be effective against six out of the eight types of herpes viruses, these herpes viruses can likely be imaged with [^{18}F]-FHBG. It was recently shown in a rat model of herpes encephalitis that [^{18}F]-FHBG was suitable for the *ex vivo* detection of HSV-1 infection of the brain [11].

The finding that [^{18}F]-FHBG could detect active herpes viruses in the rat brain led to the start of a human study in schizophrenic patients [12]. In a first approach, schizophrenic patients were studied that were a priori divided into mildly and severely affected group, based on severity of psychosis and memory disorder. An important aspect of this study was that these patients were scanned during active psychosis. Based on the similarity between HSV-1 induced psychosis in herpes encephalitis and psychosis related to schizophrenia, it was hypothesized that if herpes viruses are present in the schizophrenic brain they would be more active during severe psychosis. Indeed, a significantly higher phosphorylation rate of [^{18}F]-FHBG was found in the temporal lobe of severely affected schizophrenic patients (as based on the PANSS and memory impairment), when compared to mildly affected patient. Interestingly, neuroinflammation was particularly found in the hippocampus, which is a part of the temporal lobe. The increased phosphorylation rate of [^{18}F]-FHBG could not be attributed to a single herpes virus, but the result of the [^{18}F]-FHBG study suggests the presence of active herpes viruses and supports the viral hypothesis of schizophrenia. Although [^{18}F]-FHBG suggests the presence of active herpes viruses in the temporal lobe of schizophrenic patients, its brain uptake is on general low and it is therefore a far from ideal tracer for brain imaging.

Despite the evidence that supports the viral hypothesis of schizophrenia that was provided by PET, further research is necessary to elucidate the exact role of herpes viruses in schizophrenia. Only then treatment strategies can be improved. Because PET and SPECT are non-invasive imaging techniques used for studying functional processes in the body, they can play an important role in providing further evidence for the viral hypothesis of schizophrenia. In addition, PET can be used for studying other psychiatric or neurological disorders in which neuroinflammation and/or viruses are hypothesised to play a role, such as depression, bipolar disorder and

Alzheimer's disease. With [^{18}F]-FHBG and [^{11}C]-PK11195 PET a first step was taken in providing evidence for the viral hypothesis of schizophrenia. However, the PET tracers that were used to study a viral infection in the human CNS have substantial limitations and future studies therefore require the development of new PET tracers with better image characteristics. These can include new PET tracers for imaging of neuroinflammation that are more sensitive than [^{11}C]-PK11195, which are already receiving a lot of attention, or for imaging of other aspects of the neuroinflammatory response to viral infection, like cyclooxygenase-2 and cytokine expression. Important for providing direct evidence of infection are PET traces for viral thymidine kinase with better access to the CNS or that target different processes of viral replication. Many PET and SPECT studies on schizophrenia are nowadays focussed on the imaging of neurotransmitter systems that are implicated in schizophrenia. Among these, imaging of dopaminergic neurotransmission has received the most attention, since dopamine is proposed to play an important role in schizophrenia. PET and SPECT tracers have been developed for imaging of dopamine synthesis (e.g. [^{18}F]-DOPA), the dopamine transporter (e.g. [^{123}I]-FP-CIT), dopamine D_2 (e.g. [^{11}C]-raclopride, [^{123}I]-IBZM) and D_1 (e.g. [^{11}C]-SCH-23390) receptors [13,14]. While glutamatergic neurotransmission is also thought to be disturbed in schizophrenia, there is no suitable PET or SPECT tracer for imaging glutamatergic neurotransmission, yet. Imaging of dopaminergic and glutamatergic, as well as serotonergic, GABA-ergic and other, neurotransmitters system can also be of importance in unravelling the role of herpes viruses in schizophrenia. Especially when neurotransmitter disturbances can be linked to the presence of viruses or neuroinflammatory processes in the brain.

Thus, future research is necessary to provide additional and conclusive evidence for the viral hypothesis of schizophrenia. PET can be of great importance in these future studies, especially if more potent PET tracers for imaging viruses and viral processes in the CNS can be developed.

References

1 World Health Organization. Neurological disorders; public health challenges.: WHO, 2006

2 Kennedy PG. A retrospective analysis of forty-six cases of herpes simplex encephalitis seen in Glasgow between 1962 and 1985. Q.J.Med. 1988; 68:533-540

3 Launes J, Nikkinen P, Lindroth L, Brownell AL, Liewendahl K, Iivanainen M. Diagnosis of acute herpes simplex encephalitis by brain perfusion single photon emission computed tomography. Lancet 1988; 1:1188-1191

4 Tanaka M, Uesugi M, Igeta Y, Kondo S, Sun X, Hirai S. Luxury perfusion phenomenon in acute herpes simplex virus encephalitis. Ann.Nucl.Med. 1995; 9:43-45

5 Cagnin A, Myers R, Gunn RN, et al. In vivo visualization of activated glia by [11C] (R)-PK11195-PET following herpes encephalitis reveals projected neuronal damage beyond the primary focal lesion. Brain 2001; 124:2014-2027

6 Klapper PE, Cleator GM, Longson M. Mild forms of herpes encephalitis. J.Neurol.Neurosurg.Psychiatry 1984; 47:1247-1250

7 Yolken R. Viruses and schizophrenia: a focus on herpes simplex virus. Herpes. 2004; 11 Suppl 2:83A-88A

8 Doorduin J, de Vries EFJ, Dierckx RA, Klein HC. PET imaging of the peripheral benzodiazepine receptor: monitoring disease progression and therapy response in neurodegenerative disorders. Curr.Pharm.Des 2008; 14:3297-3315

9 van Berckel BN, Bossong MG, Boellaard R, et al. Microglia Activation in Recent-Onset Schizophrenia: A Quantitative (R)-[(11)C]PK11195 Positron Emission Tomography Study. Biol.Psychiatry 2008; 64:820-822

10 Doorduin J, de Vries EFJ, Willemsen ATM, Dierckx RA, Klein HC. Neuroinflammation in schizophrenic patients: a positron emission tomography study with [11C]-(R)-PK11195. Neuroimage. 2008; 41:T109-

11 Doorduin J, Klein HC, Dierckx RA, de Vries EFJ. Herpes simplex encephalitis in rats: a positron emission tomography study with [18F]-FHBG, [11C]-(R)-PK11195 and [18F]-FDG. Neuroimage. 2008; 41:T110-

12 Doorduin J, de Vries EFJ, Willemsen ATM, Dierckx RA, Klein HC. Imaging herpes virus activity in the central nervous system of schizophrenic patients. Submitted 2009;

13 Elsinga PH, Hatano K, Ishiwata K. PET tracers for imaging of the dopaminergic system. Curr.Med.Chem. 2006; 13:2139-2153

14 Hall H, Farde L, Halldin C, Hogberg T, Larsson S, Sedvall G. Imaging of dopamine receptors using PET and SPECT. Neurochem.Int. 1992; 20 Suppl:329S-333S

Chapter 12

Summary

Introduction

Schizophrenia is a chronic and disabling brain disease that affects approximately 1% of the human population world-wide. Usually, the onset of the disease is between 16 and 25 years of age. The symptoms of schizophrenia can be classified into positive symptoms (i.e. the presence of abnormal behavior), such as hallucinations and delusions, and negative symptoms (i.e. the absence of normal behavior), such as social withdrawal and flattened emotion. Many structural and functional abnormalities have been reported in schizophrenic patients, including reduced brain volume and disturbed dopaminergic and glutamatergic neurotransmission. Although the exact etiology of the disease is unknown, it is thought that environmental factors are responsible for the development of schizophrenia especially in individuals with a genetic predisposition. It is hypothesized that viruses play a role in the etiology of schizophrenia, in particular the family of herpes viruses. Evidence that supports the role of herpes viruses in schizophrenia has been found, but this is still inconclusive. Besides herpes viruses, it has been proposed that immune mechanisms are involved in schizophrenia. Activation of microglia cells, indicative of neuroinflammation, has been found in the schizophrenic brain, which could have been caused by virus infection.

Driven by the viral hypothesis of schizophrenia, it was aimed to further study the role of herpes viruses in schizophrenia, using the non-invasive imaging technique positron emission tomography (PET). The behavioral and functional consequences of herpes virus infection in rats were studied, and it was determined if neuroinflammation and active herpes viruses could be detected in the brain of schizophrenic patients.

PET for imaging of neuroinflammation and active herpes viruses

The application of PET for imaging of neuroinflammation and herpes viruses was studied in rats first. The first PET tracer used for imaging of neuroinflammation is [^{11}C]-PK11195. It has long been the only PET tracers used for human application. Imaging of neuroinflammation is based on the activation of microglia cells, characteristic of neuroinflammation, and the accompanied increase in expression of the peripheral benzodiazepine receptor (PBR). [^{11}C]-PK11195 is a ligand of the PBR and can therefore be used for imaging of neuroinflammation. Review of the literature regarding the imaging of the PBR with PET revealed several promising new PET tracers for this purpose, including [^{11}C]-DAA1106, [^{11}C]-PBR28 and [^{11}C]-DPA713.

Although these new PET tracers are potentially more sensitive for PBR imaging, [^{11}C]-PK11195 is still predominately used in human studies. With [^{11}C]-PK11195 it has been shown that many neurological disorders, such as dementia, Parkinson syndromes, multiple sclerosis and encephalitis, are associated with an increased expression of the PBR and thus neuroinflammation. In addition, it has been shown that anti-inflammatory drugs reduce the activation of microglia cells. The PBR can therefore be an important target for monitoring of disease progress and therapy response.

Intranasal inoculation of rats with the herpes simplex virus type-1, which is one of the herpes viruses most likely involved in schizophrenia, results in severe herpes encephalitis (i.e. infection of the brain). This rat model of herpes encephalitis can be used to study the behavioral and functional consequences of herpes virus infection, but was first used to evaluate if active herpes viruses and neuroinflammation could be imaged with [^{11}C]-PK11195 and [^{18}F]-FHBG, respectively. Imaging of herpes viruses in the brain is based on the expression of viral thymidine kinase, only expressed in active herpes viruses, which phosphorylates [^{18}F]-FHBG, resulting in trapping of [^{18}F]-FHBG in the infected cell. Increased *ex vivo* uptake of [^{18}F]-FHBG was found in brain areas know in literature to be infected by HSV-1, showing that the presence of herpes viruses in these areas can in principle be detected with this tracer. Due to limited spatial resolution of the small animal PET camera used, [^{18}F]-FHBG could not be used for imaging of herpes virus infection in rats, but this does not rule out its use in human studies. [^{11}C]-PK11195 PET showed the presence of neuroinflammation in the HSV-1 infected brain areas, also when rats were infected with lower dosages to reduce the severity of symptoms due to HSV-1 infection. [^{11}C]-PK11195 was thus shown to be suitable for imaging of neuroinflammation in HSV-1 infected rats.

Because [^{11}C]-PK11195 exhibits some unfavorable properties for PET imaging, resulting in a poor signal of noise ratio, improved PET tracers are needed to image mild neuroinflammation. The new PET tracers [^{11}C]-DPA713, [^{18}F]-DPA714 and [^{11}C]-DAA1106 were therefore evaluated for imaging of neuroinflammation in the rat model of herpes encephalitis and compared to [^{11}C]-PK11195. All PET tracers were able to detect the presence of neuroinflammation in the encephalitic brain. [^{18}F]-DPA714 was not found to be superior to [^{11}C]-PK11195. Since this PET tracer is the only agonist known to be developed for imaging of the PBR and was shown to be superior to [^{11}C]-PK11195 in another animal model, application of [^{18}F]-DPA714 may lead to new possibilities for imaging of neuroinflammation. While [^{11}C]-DAA1106 showed higher uptake in comparison to [^{11}C]-PK11195, which was highly specific,

neuroinflammation could only be revealed *ex vivo* and not by PET imaging, which could again be related to limited spatial resolution of the small animal PET camera. In addition, quantification of [^{11}C]-DAA1106 uptake using plasma sampling and pharmacokinetic modeling was complicated by the fast plasma clearance. [^{11}C]-DAA1106 is therefore not ideal for imaging of neuroinflammation in rats. In contrast to [^{18}F]-DPA714 and [^{11}C]-DAA1106, [^{11}C]-DPA713 showed better properties for imaging then [^{11}C]-PK11195. While the uptake in the healthy brain was lower, the uptake in the infected brain was higher than [^{11}C]-PK11195 uptake. [^{11}C]-DPA713 is therefore a promising new PET tracer for imaging of (mild) neuroinflammation, although human studies are needed to validate its superiority over [^{11}C]-PK11195.

Behavioral and functional consequences of HSV-1 infection

The effect of HSV-1 infection of the brain on behavior and brain function was studied in relation to ketamine, antipsychotic treatment and therapy resistance. Dopaminergic and glutamatergic neurotransmission are disturbed in schizophrenic patients. It was therefore hypothesized that viral infection of the brain, and the corresponding neuroinflammation, could cause these disturbances in neurotransmission. The effect of ketamine, an antagonist of the glutamatergic NMDA-receptor, on behavior and dopaminergic neurotransmission in HSV-1 infected rats was studied. In addition, it was studied if ketamine affected neuroinflammation. Open field and prepulse inhibition were used for behavioral assessment and [^{11}C]-raclopride PET was used to study dopaminergic neurotransmission. HSV-1 infection was found to increase exploratory behavior in the open field, but did not affect prepulse inhibition and dopaminergic neurotransmission. Interestingly, it was found that ketamine only significantly affected behavior and dopaminergic neurotransmission in HSV1-1 infected rats, but not in control rats. Ketamine did not cause or affect neuroinflammation. The exact mechanism behind the relation between HSV-1 induced neuroinflammation, glutamatergic neurotransmission and dopaminergic neurotransmission remains to be elucidated.

The majority of the schizophrenic patients are treated with antipsychotics. If the viral hypothesis is valid, antipsychotics would be able to reduce the effects of herpes infection. The effect of the commonly used and effective atypical antipsychotics clozapine and risperidone on behavior, HSV-1 induced neuroinflammation and dopaminergic neurotransmission was therefore investigated. Behavior was studied in

the open field, while [11C]-PK11195 and [11C]-raclopride PET were used to study neuroinflammation and dopaminergic neurotransmission, respectively. HSV-1 was found to increase exploratory behavior in the open field, which was inhibited by treatment with both clozapine and risperidone. In addition, clozapine and risperidone treatment inhibited HSV-1 induced neuroinflammation. Dopaminergic neurotransmission was not affected by either HSV-1 infection or treatment with clozapine or risperidone. The results imply that clozapine and risperidone could reduce the symptoms in schizophrenic patients by reducing activation of microglia cells. Additional research is, however, necessary to determine the role of HSV-1 and neuroinflammation in schizophrenia and its treatment strategies.

Although antipsychotics are used to treat the majority of the schizophrenic patients, 20 to 40% of the patients are resistant to antipsychotic treatment. P-glycoprotein (P-gp) is a drug efflux pump that is, amongst others, located in the blood-brain barrier to protect the brain from harmful substances. As a consequence, drugs for treatment of neurological disorders are also removed from the brain by P-gp, including antipsychotics. P-gp might thus play an important role in treatment resistance in schizophrenia. Neuroinflammation is thought to affect P-gp activity and it was therefore determined if HSV-1 induced neuroinflammation affected P-gp activity. In addition, the effect of clozapine and risperidone treatment on P-gp activity was determined. The PET tracer [11C]-verapamil, a substrate of P-gp, was used to determine P-gp activity. HSV-1 infection caused an increase in P-gp activity in the blood-brain barrier, which was thought to be related to the presence of neuroinflammation. In addition, clozapine increased P-gp activity, whereas risperidone decreased P-gp activity in healthy rats. In HSV-1 infected rats, clozapine further increased the neuroinflammation induced increase in P-gp activity. Risperidone inhibited the increase in P-gp activity caused by neuroinflammation. Since HSV-1 infection and the corresponding neuroinflammation are suggested to play a role in schizophrenia, they may explain treatment resistance. In addition, clozapine and risperidone may influence treatment efficacy. In order to improve treatment strategies in schizophrenia, these findings need to be further explored.

Human PET studies on neuroinflammation and herpes viruses

While the studies in the rat model of herpes encephalitis show that herpes viruses and the corresponding neuroinflammation might be associated with different aspects of

schizophrenia, the ultimate goal is to provide direct evidence for the involvement in schizophrenic patients. First, it was studied if neuroinflammation could be detected in schizophrenic patients, with [^{11}C]-PK11195 PET. It was hypothesized that neuroinflammation would be more profound in schizophrenic patients during psychosis. We have found a significantly increased binding of [^{11}C]-PK11195 in the hippocampus of schizophrenic patients when compared to healthy volunteers, which was accompanied by a non-significant increase in whole brain grey matter binding. This showed, for the first time, the presence of focal neuroinflammation in schizophrenic patients during psychosis. The results warranted further research to reveal the cause of the focal neuroinflammation and on the feasibility of treatment with anti-inflammatory drugs.

The results of the finding of focal neuroinflammation in the hippocampus of schizophrenic patients, encouraged us to determine if the presence of active herpes viruses could be responsible for the neuroinflammation. To this purpose, a [^{18}F]-FHBG study was performed in schizophrenic patients, which were scanned during psychosis. Patients were a-priori divided into mildly- and severely affected groups, based on psychosis and memory. A significantly higher metabolic rate of [^{18}F]-FHBG was found in the temporal lobe of severely affected schizophrenic patients, when compared to mildly affected patients. This increased metabolic rate was due to the presence of active herpes viruses, although it could not be determined which type of herpes virus was responsible for the increased metabolic rate. The finding of herpes viruses in the temporal lobe is consistent with the finding of neuroinflammation in the hippocampus, because the hippocampus is part of the temporal lobe. Herpes viruses in the temporal lobe may this be responsible for psychosis and memory disturbances in schizophrenic patients.

Although we have found evidence for the role of viruses in schizophrenia using PET, further research is necessary to elucidate the exact role of herpes viruses in schizophrenia. PET can play an important role in this, because it allows for non-invasive imaging and thus longitudinal follow-up and evaluation of treatment response. However, this requires development of new PET tracers for imaging of neuroinflammation, also for other targets than the PBR, and for imaging of active herpes viruses.

Chapter 13

Future perspectives

The studies that were performed in this thesis aimed to provide evidence for the involvement of herpes viruses and neuroinflammation in schizophrenia. The most important findings are that PET showed the presence of neuroinflammation and active herpes viruses in the brain of psychotic schizophrenic patients. In addition, it was found that HSV-1 can influence the relation between the dopaminergic and glutamatergic neurotransmission, and that antipsychotics inhibit HSV-1 induced neuroinflammation. Herpes viruses and neuroinflammation may thus play an important role in schizophrenia and may be responsible for the functional disturbances in schizophrenic patients. Further research is, however, necessary to further elucidate the role of herpes viruses in schizophrenia.

Most importantly, it first needs to be confirmed that herpes viruses do play a role in schizophrenia. This would mean to find conclusive evidence for the presence of viruses in the brain of schizophrenic patients. Although a first attempt was made with PET using [^{18}F]-FHBG, this PET tracer was not found to be ideal due to low penetration of the blood-brain barrier. As already discussed in chapter 11, improved PET tracers for imaging of active herpes viruses would be of great value. It could then be determined if active herpes viruses are present in the brain of recent onset schizophrenic patients and the activity could be followed longitudinally. In addition, it allows for evaluation of treatment response. Other PET tracers have been developed for imaging of viral thymidine kinase, of which especially [^{18}F]-FEAU was shown to have a higher affinity than [^{18}F]-FHBG [1]. However, [^{18}F]-FEAU also showed low penetration of the blood-brain barrier and is therefore not ideal for brain imaging [2]. More lipophilic PET tracers for viral thymidine kinase or for other specific characteristics of active herpes viruses need to be developed.

Another approach for finding evidence for the role of herpes viruses in schizophrenia is based on anti-viral treatment. It has been shown that treatment of schizophrenic patients that were positive for cytomegalovirus, with the anti-viral drug valacyclovir improved symptoms [3]. In this approach, the treatment response could also been monitored with PET, although not (yet) directly by determining herpes virus activity. Since neuroinflammation was found to be present in the schizophrenic brain and hypothesized to be caused by herpes viruses, PET imaging of neuroinflammation could be used for treatment evaluation. If herpes viruses are responsible for the neuroinflammation, anti-viral treatment should hypothetically decrease neuroinflammation, which can be imaged with [^{11}C]-PK11195. Based on the results of the studies in these thesis, we will perform a study in which schizophrenic patients will

be treated with valacyclovir. The treatment response will be monitored with [^{11}C]-PK11195 PET.

Although [^{11}C]-PK11195 is well established for imaging of neuroinflammation, it showed a low signal-to-noise ratio. This suggests that [^{11}C]-PK11195 is not sensitive enough to visualize mild inflammation [4]. As discussed in chapter 2, new PET tracer for imaging of neuroinflammation are being developed that are potentially more sensitive than [^{11}C]-PK11195. Since neuroinflammation was found to be involved in many neurological diseases, PET can play a role in the early detection of these diseases, as well as evaluation of treatment. In chapter 4 it was shown that [^{11}C]-DPA713 is potentially more sensitive and therefore more suitable for imaging of neuroinflammation. Interestingly, [^{18}F]-DPA714 was not found to be more sensitive than [^{11}C]-PK11195 in the rat model of herpes simplex encephalitis, but was found to have a 3-fold higher binding potential in the striatum were neuroinflammation was induced by injection of a toxic compound [5]. [^{18}F]-DPA714 is a the only full agonist PET tracer for the PBR and agonists are known to usually bind to the receptor in a high affinity state. This suggests that the nature of neuroinflammation, which might be more acute in the herpes simplex model and chronic in the striatum lesioned model, causes different PBR expression. Although little is known about this phenomenon, this could lead to development of PET tracers that specifically image different aspects of neuroinflammation. These PET tracers could then be used to further evaluate the role of herpes viruses and neuroinflammation in schizophrenia. Although many of the newly developed PET tracers have shown to be suitable for imaging in rats, the ability to detect neuroinflammation in patients remains to be determined.

When new PET tracers for herpes viruses and neuroinflammation have been shown to be useful in human studies, the role of herpes viruses and neuroinflammation in schizophrenia could be established. These tracers could, however, also been used to determine the role of herpes viruses and neuroinflammation in other diseases. Herpes viruses have also been implicated in Alzheimer's disease [6], in which neuroinflammation was also found to play an important role. While many neurological and neurodegenerative disease have been shown to be associated with neuroinflammation, its role is psychiatric diseases has received much less attention. Besides schizophrenia, neuroinflammation may also been present in, for example, patients with depression or bipolar disorder. If neuroinflammation will also be found to be involved in these psychiatric disorders, this may lead to more understanding and improved treatment.

As mentioned before, it is of great importance to develop new PET tracers in order to provide evidence for the role of herpes viruses and also neuroinflammation in schizophrenia. If it can be shown that herpes viruses do indeed play a role in the etiology of schizophrenia, there are many questions that remain to be answered, like 'Are all cases of schizophrenia caused by herpes viruses?', 'Are other viruses or infectious agents also involved?', 'Why do herpes viruses not cause schizophrenia in all infected individuals?' and 'What is the mechanism behind viral infection and the symptoms seen?'. While the first question is probably the easiest to answer, because it only requires screening of schizophrenic patients, it can initially complicate the search for evidence for the role of herpes viruses. While the involvement of other infectious agents need to be proven first, it is possible that infectious agents in general cause schizophrenia and not one agent in particular. Because herpes viruses are present in the majority of individuals in the human population, theoretically all individuals should develop schizophrenia when herpes viruses are shown to be involved in its etiology. A genetic predisposition may explain why not all infected individuals develop schizophrenia. Indeed, it has been shown that an association between genetic polymorphisms and herpes viruses increased the risk for schizophrenia [7].

In order to answer the last question that was proposed, animal studies are great importance. When infecting rats or mice with herpes viruses, the consequences on brain function can directly be measured. With this approach, it was shown in chapter 6 that HSV-1 infection in rats could influence dopaminergic and glutamatergic neurotransmission, as well as the expression of P-gp (chapter 8). In these studies the rats had a severe HSV-1 encephalitis which complicated the longitudinal follow-up due to death of the rats. Although in this model the effects of HSV-1 on brain function could well be studied, the infection does not compare to the mild HSV-1 infection that was proposed in schizophrenia. In addition, severe encephalitis does not occur in schizophrenic patients. Infection with less HSV-1 could lead to longer survival and the establishment of latency, better mimicking the human situation. Brain function, as well as behavioral function and treatment effects could then be studied longitudinally.

In conclusion, herpes viruses are proposed to play an important role in the etiology of schizophrenia and could be responsible for the functional changes found in the schizophrenic brain. Schizophrenia is, however, a complex disease and we are still far from finding the exact etiology or even a cure. PET can play an important role in finding evidence for the involvement of herpes viruses as well as in defining the role

of neuroinflammation in schizophrenia. We have taken a first step in using PET in order to determine the presence of active herpes viruses in schizophrenic patients. The development of PET tracers with improved image properties is, however, needed. When in the future the role of herpes viruses in schizophrenia can be proven with absolute certainty, this can greatly improve the treatment outcome for schizophrenic patients.

References

1 Buursma AR, Rutgers V, Hospers GA, Mulder NH, Vaalburg W, de Vries EF. 18F-FEAU as a radiotracer for herpes simplex virus thymidine kinase gene expression: in-vitro comparison with other PET tracers. Nucl.Med.Commun. 2006; 27:25-30

2 Miyagawa T, Gogiberidze G, Serganova I, et al. Imaging of HSV-tk Reporter gene expression: comparison between [18F]FEAU, [18F]FFEAU, and other imaging probes. J.Nucl.Med. 2008; 49:637-648

3 Dickerson FB, Boronow JJ, Stallings CR, Origoni AE, Yolken RH. Reduction of symptoms by valacyclovir in cytomegalovirus-seropositive individuals with schizophrenia. Am.J.Psychiatry 2003; 160:2234-2236

4 Bartels AL, Willemsen AT, Doorduin J, de Vries EF, Dierckx RA, Leenders KL. [(11)C]-PK11195 PET: Quantification of neuroinflammation and a monitor of anti-inflammatory treatment in Parkinson's disease? Parkinsonism.Relat Disord. 2009;

5 Chauveau F, Van Camp N, Dolle F, et al. Comparative evaluation of the translocator protein radioligands 11C-DPA-713, 18F-DPA-714, and 11C-PK11195 in a rat model of acute neuroinflammation. J.Nucl.Med. 2009; 50:468-476

6 Itzhaki R. Herpes simplex virus type 1, apolipoprotein E and Alzheimer' disease. Herpes. 2004; 11 Suppl 2:77A-82A

7 Kim JJ, Shirts BH, Dayal M, et al. Are exposure to cytomegalovirus and genetic variation on chromosome 6p joint risk factors for schizophrenia? Ann.Med. 2007; 39:145-153

Chapter 14

Samenvatting

Inleiding

Schizofrenie is een chronische en ernstige psychiatrische aandoening die wordt gekenmerkt door abnormale gedachten en verstoord gedrag. De eerste beschrijving van schizofrenie dateert uit het begin van de twintigste eeuw toen Emil Kraeplin de aandoening 'dementia praecox' noemde. Hij dacht namelijk dat schizofrenie begon tijdens de vroege kinderjaren en uiteindelijk leidde tot geestelijk verval. Toen later bleek dat schizofrenie ook begon op latere leeftijd en niet per se geestelijk verval tot gevolg had, stelde Eugen Bleuler de naam schizofrenie voor. Omdat schizofrenie letterlijk 'gespleten geest' betekent, wordt er vaak ten onrechte gedacht dat schizofreniepatiënten meerdere persoonlijkheden hebben.

Ongeveer 1% van de totale bevolking wereldwijd leidt aan schizofrenie en over het algemeen openbaren de eerst symptomen van schizofrenie zich tussen de 16 en 25 jaar. Schizofrenie wordt gekenmerkt door de zogenaamde positieve en negatieve symptomen. Symptomen zijn positief wanneer deze niet aanwezig zijn in een gezond persoon, zoals het hebben van hallucinaties en waanbeelden, maar ook het niet helder kunnen ordenen van gedachtegangen. Positieve symptomen zijn meestal niet continu aanwezig, maar komen voor in periodes die dagen tot maanden kunnen duren. Deze perioden van positieve symptomen wordt ook wel psychosen genoemd. Negatieve symptomen komen juist wel voor in een gezond persoon, maar ontbreken in schizofrenie patiënten. Voorbeelden zijn het terugtrekken uit de samenleving, afgevlakte emotie en het gebrek aan spontaan denken. Over het algemeen worden schizofrenie patiënten behandeld met antipsychotica. De eerste antipsychotica die werden ontwikkeld hadden voornamelijk effect op de positieve symptomen, maar de moderne antipsychotica zorgen ook voor een verbetering van de negatieve symptomen. De symptomen van schizofrenie kunnen worden behandeld, maar een schizofreniepatiënt kan niet worden genezen.

Hoewel er veel onderzoek wordt gedaan naar schizofrenie, is het niet bekend wat de ziekte veroorzaakt. Er zijn wel aanwijzingen voor veranderingen in de structuur en de functie van de hersenen. Het is bijvoorbeeld aangetoond dat bepaalde hersengebieden kleiner zijn in schizofrenie patiënten dan in gezonde personen. Ook zijn er veranderingen gevonden in systemen in de hersenen die met behulp van bepaalde stoffen (neurotransmitters) zorgen voor communicatie tussen verschillende hersengebieden. De eerste neurotransmitter waarvan gedacht werd dat die een belangrijke rol speelt bij schizofrenie was dopamine. De rede hiervoor was dat drugs

die er voor zorgden dat er meer dopamine in de hersenen aanwezig was, zoals cocaïne, psychotische verschijnselen veroorzaakten en omdat antipsychotica die dopamine juist verlaagden, de symptomen verminderden. In navolging van dopamine, werd later ook aangetoond dat glutamate een rol speelt in schizofrenie omdat drugs die glutamate in de hersenen verhoogden, zoals ketamine, ook leidden tot psychotische verschijnselen.

Hoewel zowel veranderingen in de structuur van de hersenen als in dopamine en glutamate een belangrijke rol spelen bij schizofrenie, zullen ze waarschijnlijk niet de oorzaak zijn. Met betrekking tot de oorzaak wordt er gedacht dat bepaalde factoren in de omgeving schizofrenie veroorzaken, maar dan alleen in personen die daar een genetische aanleg voor hebben. Een van de omgevingsfactoren waarvan wordt verondersteld dat deze een belangrijke rol spelen in schizofrenie, zijn herpes virussen. De groep van herpes virussen bestaat uit acht typen virussen waarvan bekend is dat deze mensen kunnen infecteren. De meeste bekende herpes virussen zijn waarschijnlijk het herpes simplex virus type-1 (HSV-1), die de veroorzaker is van de koortslip, en het Varicella-Zoster virus (VZV), die waterpokken veroorzaakt. Vooral HSV-1 is interessant met betrekking tot schizofrenie. Ongeveer 80% van de bevolking wereldwijd is besmet met HSV-1 en heel af en toe kan HSV-1 een infectie veroorzaken in de hersenen. Dit leidt dan tot een ernstige ontsteking in de hersenen (een encefalitis) die in de meeste gevallen leidt tot de dood, wanneer er niet wordt behandeld. Eén van eerste symptomen van een herseninfectie met HSV-1 is een psychose die lijkt op de psychose die wordt gezien bij schizofrenie.

Er zijn een aantal studies uitgevoerd die laten zien dat er een relatie is tussen schizofrenie en herpes virussen. De meeste van deze studies hebben gekeken naar antistoffen tegen herpes virussen in het bloed van schizofreniepatiënten en hebben laten zien dat deze hoger zijn dan in gezonde personen. Tevens is er aangetoond dat er een relatie is tussen de ernst van schizofrenie en de hoeveelheid van deze antistoffen in het bloed. Behandeling van schizofreniepatiënten die antistoffen hadden tegen een bepaald herpesvirus, het cytomegalovirus, met een medicijn tegen dat virus, leidde tot een vermindering van de symptomen. Studies naar de hersenen van overleden schizofreniepatiënten hebben de aanwezigheid van herpes virussen echter niet kunnen aantonen.

Naast herpes virussen zijn er ook aanwijzingen dat schizofreniepatiënten een ontsteking in hersenen hebben, die de symptomen veroorzaakt. Bij een ontsteking in de hersenen spelen microglia cellen een belangrijke rol. Microglia cellen komen alleen voor in de hersenen en zijn belangrijk voor de eerste afweer tegen ziekteverwekkers

die de hersenen binnen zijn gedrongen. In de gezonde hersenen zijn microglia cellen in rust en tasten ze met lange uitlopers continu de omgeving af. Bij een verandering in de omgeving, doordat bijvoorbeeld binnengedrongen ziekteverwekkers schade hebben veroorzaakt aan de hersenen, worden de microglia cellen actief en gaan naar de schade toe. Geactiveerde microglia cellen trekken hun uitlopers in en ruimen het beschadigd hersenweefsel op. Het ontstekingsproces is dan in gang gezet en ook ander type cellen worden geactiveerd om de hersenen te beschermen. Een aantal studies hebben in de hersenen van schizofrenie patiënten een toename gevonden van geactiveerde microglia. Dit zou veroorzaakt kunnen zijn door herpes virussen, maar dat is nooit aangetoond.

Doel van het proefschrift

Het doel van de studies, die zijn uitgevoerd in dit proefschrift, was om verder uit te zoeken wat de rol is van herpes virussen in schizofrenie. Globaal zijn er daarom drie aspecten onderzocht: als eerste is er uitgezocht wat de gevolgen zijn van een herpes virus infectie in ratten, voor het gedrag van ratten en de functie van de hersenen. Daarnaast is er bepaald of schizofrenie patiënten een ontsteking in de hersenen hebben of dat er herpes virussen aanwezig zijn.

Voor bovengenoemde onderzoeken is gebruik gemaakt van positron emissie tomografie (PET). PET is een techniek die wordt gebruikt voor het afbeelden van bepaalde processen die zich in het lichaam afspelen, zoals activatie van microglia cellen. Hiervoor wordt een stof die een rol speelt bij dit bepaalde proces radioactief gemerkt met een zogenoemde radioactieve isotoop. In het geval van geactiveerde microglia cellen wordt de stof PK11195 gemerkt met het radioactieve isotoop koolstof-11 (^{11}C), zodat een PET tracer wordt gevormd. De radioactieve isotoop is onstabiel en zal uiteen vallen, waarbij 2 gammadeeltjes vrijkomen (straling). Wanneer de PET tracer, [^{11}C]-PK11195, wordt geïnjecteerd in bijvoorbeeld een schizofrenie patiënt, zal deze binden aan geactiveerde microglia cellen. De gammadeeltjes (straling) die dan worden afgestaan door [^{11}C]-PK11195, kunnen worden waargenomen door de PET camera. Met behulp van computers wordt dan uiteindelijk uit alle waargenomen gammastraling een afbeelding gemaakt, waarin dan precies kan worden gezien waar in de hersenen zich geactiveerde microglia cellen bevinden. Door verschillende PET tracers te gebruiken kunnen hele verschillende processen in het lichaam worden afgebeeld, zonder dat er geopereerd hoeft te worden.

Afbeelden van ontsteking in de hersenen en actief herpes virus

Als eerste werd bepaald of PET kon worden gebruikt voor het afbeelden van ontsteking in de hersenen. [^{11}C]-PK11195 was de eerste PET tracer die werd gebruikt voor het afbeelden van ontsteking in de hersenen. Een overzicht van de literatuur *(hoofdstuk 2)* laat zien dat er een aantal veelbelovende alternatieve PET tracers zijn ontwikkeld voor het afbeelden van ontsteking in de hersenen, waaronder [^{11}C]-DAA1106, [^{11}C]-PBR28 en [^{11}C]-DPA713. Ondanks deze alternatieve PET tracers, worden de meeste studies in mensen nog steeds uitgevoerd met [^{11}C]-PK11195, en is met deze PET tracer ontsteking in de hersenen aangetoond in vele neurologische aandoeningen, waaronder dementie, de ziekte van Parkinson, multiple sclerose en virale encefalitis. Omdat vele neurologische aandoeningen zijn geassocieerd met een ontsteking in de hersenen, kan PET een belangrijke rol spelen bij het vervolgen van zowel de aandoening als de behandeling.

Als voorbereiding op de studies in schizofrenie patiënten, is er in ratten bepaald of [^{11}C]-PK11195 en [^{18}F]-FHBG geschikt zijn voor het afbeelden van, respectievelijk, geactiveerde microglia cellen en herpes virussen *(hoofdstuk 3)*. Hiervoor werd gebruik gemaakt van ratten met een herpes encefalitis, veroorzaakt door infectie met HSV-1. In de hersengebieden waarvan het bekend is dat deze worden geïnfecteerd door HSV-1 werd zowel een verhoogde opname van [^{18}F]-FHBG als van [^{11}C]-PK11195 gevonden. De resultaten lieten zien dat [^{18}F]-FHBG en [^{11}C]-PK11195 zouden kunnen worden gebruikt voor de studies in schizofrenie patiënten.

Zoals al eerder genoemd zijn er een aantal veelbelovende alternatieven voor [^{11}C]-PK11195 als het gaat om het afbeelden van ontsteking in de hersenen. De rede dat deze nieuwe PET tracers worden ontwikkeld is dat [^{11}C]-PK11195 een aantal nadelige eigenschappen bezit. Omdat [^{11}C]-PK11195 naast de binding aan microglia cellen (het signaal) ook aan veel andere cellen en stoffen in de hersenen bindt (de ruis), is de verhouding tussen het signaal en de ruis slecht, waardoor milde ontstekingen misschien niet goed kunnen worden afgebeeld met [^{11}C]-PK11195. We hebben daarom in ratten met een herpes encefalitis bepaald of de nieuwe PET tracers [^{11}C]-DPA713, [^{18}F]-DPA714 en [^{11}C]-DAA1106 gevoeliger waren dan [^{11}C]-PK11195 *(hoofdstuk 4 en 5)*. [^{11}C]-DPA713 en [^{11}C]-DAA1106 waren beide gevoeliger voor het afbeelden van ontsteking in de hersenen, maar [^{11}C]-DAA1106 had weer andere nadelen voor het gebruik van deze tracer in PET studies. Omdat de ruis van [^{11}C]-DPA713 lager was dan die van [^{11}C]-PK11195 en het signaal hoger, lijkt deze PET

tracer een zeer geschikt alternatief. Het zal dan in een studie in mensen moeten worden bevestigd of dit daadwerkelijk zo is. Hoewel [^{18}F]-DPA714 niet gevoeliger was dan [^{11}C]-PK11195, kan het wel interessant zijn om deze PET tracer verder te bestuderen omdat het waarschijnlijk andere eigenschappen van ontsteking kan afbeelden dan [^{11}C]-PK11195.

De gevolgen van HSV-1 infectie op gedrag en hersenfunctie

De gevolgen van HSV-1 infectie op gedrag en hersenfunctie werden bestudeerd in relatie tot ketamine en antipsychotica, en resistentie tegen behandeling met antipsychotica. Omdat de dopamine- en glutamaatsystemen verstoord zijn bij schizofrenie, zou het kunnen dat een infectie met HSV-1 deze verstoringen veroorzaakt. Er is daarom bepaald wat het effect is van het toedienen van ketamine, die een toename in glutamate veroorzaakt, op gedrag en dopamine in HSV-1 geïnfecteerde ratten *(hoofdstuk 6)*. Er is ook bepaald of ketamine invloed had op ontsteking in de hersenen. De ratten, die waren geïnfecteerd met HSV-1, waren actiever dan de gezonde ratten, maar lieten geen verandering zien in dopamine receptor binding. Het toedienen van ketamine resulteerde in een afname in de activiteit van de ratten, maar alleen wanneer ze waren geïnfecteerd met HSV-1 en niet in de gezonde ratten. Ook is gevonden dat alleen de combinatie van HSV-1 infectie en ketamine het dopaminesysteem beïnvloedt. Ketamine had geen effect op ontsteking in de hersenen. De resultaten suggereren dat HSV-1 geïnfecteerde ratten gevoeliger zijn voor het effect van ketamine en dat er daarom voornamelijk een relatie is tussen dopamine en glutamate in ratten met een HSV-1 infectie.

De meeste schizofreniepatiënten worden behandeld met antipsychotica. Omdat virussen worden verondersteld een rol te spelen in schizofrenie, zou de behandeling van HSV-1 geïnfecteerde ratten met antipsychotica de gevolgen van HSV-1 infectie kunnen verminderen. Twee veelgebruikte antipsychotica zijn clozapine en risperidone en het effect van behandeling met deze antipsychotica op gedrag, ontsteking in de hersenen en dopamine is onderzocht *(hoofdstuk 7)*. HSV-1 geïnfecteerde ratten waren actiever dan de gezonde ratten en zowel clozapine als risperidone remde de toename van actief gedrag. Tevens remden clozapine en risperidone de ontsteking in de hersenen veroorzaakt door HSV-1 infectie. Dopamine receptor binding werd niet beïnvloed door HSV-1 infectie, clozapine en risperidone. De resultaten van deze studie suggereren dat het verbeteren van de symptomen in schizofreniepatiënten door

clozapine en risperidone deels verklaard kan worden door het remmen van ontsteking in de hersenen.

Hoewel schizofreniepatiënten over het algemeen worden behandeld met antipsychotica, is ongeveer 20 tot 40% van de patiënten immuun tegen deze behandeling. In de hersenen is een barrière aanwezig tussen het bloed en de hersenen om te voorkomen dat bijvoorbeeld schadelijke stoffen de hersenen binnen komen. In deze barrière is een pomp aanwezig, de P-glycoproteine (P-gp) pomp, die er voor zorgt dat schadelijke stoffen die toch de hersenen binnen dringen, er direct weer uit worden gepompt. Een nadeel van deze pomp is dat ook medicijnen, zoals antipsychotica, deels de hersenen worden uitgepompt en daarom hun werk niet goed kunnen doen. Dit resulteert dan in resistentie tegen de behandeling. Er wordt verondersteld dat een ontsteking in de hersenen P-gp beïnvloedt. Omdat ook wordt gedacht dat een ontsteking in de hersenen een rol speelt in schizofrenie, is er in ratten bepaald of een ontsteking veroorzaakt door HSV-1 de activiteit van P-gp beïnvloedt *(hoofdstuk 8)*. Tevens is er gekeken of clozapine en risperidone de P-gp activiteit kunnen beïnvloeden. Er is aangetoond dat ontsteking in de hersenen een toename veroorzaakt in de activiteit van P-gp, wat dus zou kunnen leiden tot resistentie tegen behandeling. Ook is er gevonden dat clozapine de activiteit van P-gp verhoogt, terwijl risperidone de activiteit verlaagt. Wanneer HSV-1 geïnfecteerde ratten werden behandeld met clozapine veroorzaakte dit een extra toename van de P-gp activiteit. Risperidone remde de HSV-1 geïnduceerde toename in P-gp activiteit. Clozapine en risperidone lijken dus te beïnvloeden of de behandeling efficiënt is. Meer onderzoek is echter nodig om uiteindelijk de behandeling van schizofreniepatiënten te kunnen verbeteren.

PET studies in schizofrenie patiënten

Hoewel er aanwijzingen zijn dat een infectie met HSV-1 en de daaraan gerelateerde ontsteking in de hersenen betrokken is bij verschillende eigenschappen van schizofrenie, is het uiteindelijke doel bewijs te leveren voor de herpes virussen en ontsteking in schizofreniepatiënten. Met [^{11}C]-PK11195 PET is er aangetoond dat er inderdaad een ontsteking in de hersenen van psychotische schizofrenie patiënten aanwezig is, in tegenstelling tot in gezonde personen *(hoofdstuk 9)*. Deze ontsteking werd gevonden in een hersengebied genaamd de hippocampus en ging samen met lichte ontsteking in de gehele hersenen. Het is de eerste keer dat er in de hersenen van

schizofrenie patiënten een locale ontsteking is aangetoond. Aanvullend onderzoek is nodig om te bepalen wat de oorzaak is van deze ontsteking en ook om te bepalen of medicijnen tegen ontsteking de symptomen van schizofrenie wellicht kunnen verbeteren.

Door het vinden van een ontsteking in de hersenen van schizofrenie werden we aangemoedigd om te bepalen of herpes virussen de oorzaak zouden kunnen zijn van de ontsteking. Daarom werd een [^{18}F]-FHBG studie uitgevoerd in schizofrenie patiënten *(hoofdstuk 10)*. Voorafgaande aan de studie werden de patiënten ingedeeld in een groep met een mild ziektebeeld en een groep met een ernstig ziektebeeld, afhankelijk van de mate van psychose en verstoring van geheugen. Een hogere opname van [^{18}F]-FHBG werd gevonden in de temporale hersenschors van patiënten met een ernstig ziektebeeld, in vergelijking tot de patiënten met een mild ziektebeeld. Dit duidt op de aanwezigheid van een actief herpes virus in dit hersengebied, hoewel het type herpes virus niet kon worden bepaald. Het is interessant om te weten dat de temporale hersenschors een belangrijke rol speelt bij psychose en geheugen, en dat de hippocampus, waar ontsteking is gevonden, in de temporale hersenschors ligt. De aanwezigheid van herpes virussen zouden dus een rol kunnen spelen in schizofrenie en voornamelijk tijdens de psychose.

Conclusie

De resultaten van de studies in dit proefschrift hebben aanvullend bewijs geleverd voor een rol van herpes virussen in schizofrenie. De belangrijkste bevindingen waren dat er met PET is aangetoond dat in psychotische schizofrenie patiënten een ontsteking en actieve herpes virussen aanwezig waren. Tevens is er gevonden dat HSV-1 de relatie tussen dopamine en glutamate kan beïnvloeden, en dat antipsychotica de ontsteking als gevolg van HSV-1 infectie remmen. Herpes virussen en een ontsteking in de hersenen kunnen dus een belangrijke rol spelen in schizofrenie en kunnen de oorzaak zijn voor de verstoring van de hersenfunctie in schizofrenie patiënten. Aanvullend onderzoek is echter nodig om verder uit zoeken wat de precieze rol van herpes virussen in schizofrenie is.

Dankwoord

Er wordt wel eens gezegd "Time flies when you're having fun" en dat geldt zeker wanneer ik terugkijk op mijn 4 jaar promotieonderzoek. Ik heb er altijd enorm veel plezier in gehad en de jaren vlogen dan ook (helaas) zo voorbij. Diegenen die de hoofdstukken al hebben doorgelezen, alvorens te zijn toegekomen aan het dankwoord, kunnen hopelijk beamen dat het onderzoek tot mooie resultaten heeft geleid (en daar ben ik best trots op), maar het moet gezegd worden: ik heb hier en daar toch wel wat hulp gehad bij het voorbereiden, uitvoeren en opschrijven van alle studies. Ik wil daarom alvast iedereen bedanken die, op welke manier dan ook, een bijdrage heeft geleverd aan de totstandkoming van dit proefschrift. In de hoop niemand te vergeten, wil ik een aantal mensen in het bijzonder bedanken.

Allereerst wil ik mijn copromotoren Dr. Erik de Vries en Dr. Hans Klein bedanken. Volgens mij kan een promovendus zich geen betere copromotoren wensen. Erik, ik kon echt altijd bij je terecht voor vragen en problemen, en ook wanneer er weer eens een tracer moest worden gemaakt voor mij. Jouw kritische kijk op de studies, resultaten en manuscripten hebben me altijd goed tot nadenken gezet en ik heb er veel van geleerd. Als iemand snel manuscripten nakijkt ben jij het wel, en ik heb dat altijd erg fijn gevonden.

Hans, ook bij jou kon ik altijd terecht en je was al bijna even snel met het leveren van commentaar op mijn manuscripten. Jouw enthousiasme voor onderzoek heeft mij zeker aangestoken, evenals je 'wilde' ideeën (en dat zijn vaak wel de leukste). We hebben daar dan ook interessante wetenschappelijke discussies over gehad. Je was altijd positief wanneer het ging om nieuwe studies en resultaten, en dat heb ik altijd erg gewaardeerd.

Naast mijn copromotoren wil ik natuurlijk mijn promotor Prof. Dr. Rudi Dierckx bedanken. Rudi, je hebt altijd veel interesse getoond in mijn onderzoek en ik vond het fijn dat je ook altijd de tijd had om (soms op het laatste moment) mijn manuscripten te beoordelen. Je hebt ontzettend veel kennis en ervaring met onderzoek doen en daar heb ik veel van geleerd. Bedankt ook voor de mogelijkheid om als post-doc nieuw onderzoek te mogen gaan doen.

De leden van de beoordelingscommissie, Prof. Dr. Kurt Audenaert, Prof. Dr. Erik Boddeke en Prof. Dr. Peter van Rijk, wil ik bedanken voor het lezen en beoordelen van mijn proefschrift.

Tja, en waar ga je dan verder als er nog zoveel mensen te bedanken zijn. Maar laat ik (logischerwijze) beginnen bij de afdeling Nucleaire Geneeskunde en Moleculaire Beeldvorming (NGMB). Ik wil in ieder geval iedereen bedanken voor de gezellige tijd (vooral in de koffiekamer…).

De eerste twee jaar van mijn promotieonderzoek heb ik doorgebracht op 'de kamer van 6' (tegenwoordig vergaderruimte), samen met Bertha, Hilde, Lizette, Bram en Oliver. Er werd natuurlijk altijd hard gewerkt, maar we hebben het ook heel gezellig gehad, dus bedankt daarvoor. De verhuizing naar een andere kamer bracht mij een verdieping hoger, waar ik Ines gezelschap ging houden, later bijgestaan door Leila, Anna en Valentina. Girls, we had (and still have) a lot of fun in our 'kippenhok'. Of course we also worked hard and shared the ups and downs of research (and for the downs… the chocolate Fridays did help a lot). Thank you for being such nice roommates and friends, and good luck with your theses, you may need it. Silvana, hoewel jij helaas niet bij ons op de kamer zat (maar ver weg werd verstopt…), geldt natuurlijk hetzelfde voor jou. Bedankt voor alle gezellige gesprekken (ik herinner me ook nog een erg leuk sinterklaasgedicht) en jij ook succes met je proefschrift.

Het grootste deel van de studies in mijn proefschrift zijn uitgevoerd met behulp van proefdieren. Tijdens mijn eerste stapjes in het uitvoeren van dierstudies met PET tracers werd ik bijgestaan door Aren. Dus Aren, bedankt voor al je hulp bij de dierstudies en de DEC aanvragen, en ook voor het beantwoorden van al mijn vragen. Mijn eerste dierstudies waren nog alleen biodistributie studies, maar al snel kwam toen de microPET. Johan (dJ), jij stond altijd klaar bij al mijn problemen met de microPET (in het begin zijn we er zeker wel een paar tegen gekomen…) en je hebt mij echt veel geholpen met al je denkwerk en conversieprogramma's. Big thanks. En nu ik het toch over de microPET heb, Jürgen ik wil jou bedanken voor alle tijd die je hebt gestopt in het plannen van de studies en al die keren dat je me hebt geholpen met het canuleren en samplen van de ratten.

Voor alle (dier)studies moesten er, als vanzelfsprekend, elke keer weer tracers worden gemaakt. Ik kan iedereen op het lab daarom niet genoeg bedanken voor al die keren dat er [^{11}C]-PK11195, [^{11}C]-verapamil of [^{11}C]-raclopride voor mij werd gemaakt. Bram, ik kan me niet herinneren dat jij de [^{11}C]-PK11195 synthese ooit hebt laten mislukken… Bedankt voor elke keer een mooie opbrengst en de gezellige tijd in het lab. Hilde en Bertha, jullie hebben ook zo vaak tracers voor me gemaakt en vrijwel altijd met succes. Bedankt voor jullie gezelligheid, hulp en inzet. Peet, Chantal en Michel, jullie heb ik wat minder vaak aan het werk gezet, maar daarom zijn jullie niet

minder belangrijk geweest. Jitze, hopelijk heb je geen grijze haren van mij gekregen, maar bedankt voor al je hulp en het inplannen van alle studies.

Voor de humane studies wil ik de MNW-ers bedanken voor het uitvoeren van de scans met de, toch niet altijd even makkelijke, proefpersonen. In het bijzonder Johan (W), Remko en Yvonne: bedankt voor jullie hulp. De artsen, Jan, Riemer, Adrienne en Klaas-Pieter, bedankt voor het prikken van de arterielijnen. Arja en Erna, ik wil jullie natuurlijk bedanken voor het inplannen van al mijn humane studies. Antoon, bedankt voor al je onmisbare hulp bij de data-analyse en bij het beantwoorden van al mijn vragen hierover.

En als laatste van de NGMB collega's: Philip, bedankt voor je adviezen en je uitstekende taak als sectiehoofd, Annie van Zanten, bedankt voor alle hulp bij administratieve zaken en financiën, Anne Paans, bedankt voor alle goede adviezen en voor het (tijdelijk) ter beschikking stellen van je kamer en Klaas-Willem, bedankt voor alle hulp bij ICT-problemen.

Dan zijn er natuurlijk ook buiten de afdeling NGMB veel personen die ik wil bedanken voor hun hulp bij alle studies. Als eerste de personen die belangrijk zijn geweest voor het uitvoeren van de humane studies. Rixt Elgersma, ik wil jou bedanken voor het begeleiden van de patiënten naar de PET en MRI scans en weer terug. Zonder jouw steun was het voor de patiënten waarschijnlijk nog moeilijker geweest om tijdens de scans stil te blijven liggen. Voor het beoordelen van de MRI scans is een goede radioloog onmisbaar. Jan Cees de Groot, bedankt voor de tijd die je in het beoordelen van de scans hebt gestopt. Het Neuroimaging Center wil ik bedanken voor de mogelijkheid de MRI scans te maken op de 3T. Anita, bedankt voor alle MRI scans die je voor mij hebt gemaakt.

Als tweede de personen die belangrijk zijn geweest voor de dierstudies. De mensen van de centrale dienst proefdieren wil ik bedanken voor hun hulp bij de dierstudies. Wiebe Hofstra, voor het beoordelen en bespreken van de werkprotocollen en Hester voor het bestellen van alle ratten. Silvia, Yvonne, Annemiek en Maurice, jullie wil ik bedanken voor jullie hulp bij het infecteren en het verzorgen van de ratten. Sietske Welling-Wester en Björge Meijdam, bedankt voor al jullie hulp bij vragen over HSV-1 en bij het kweken van nieuwe badges HSV-1 (en het opsporen van oude badges…). Voor de immunohistochemische kleuringen van de microglia in hersencoupes, PCR's en Western Blot: Nieske Brouwer, bedankt voor je hulp hierbij. Een aantal van mijn studies heb ik mogen uitvoeren op de afdeling Biologische Psychiatrie, Folkert,

Christel en Petra bedankt hiervoor. Fokko Bosker bedankt voor al je hulp met het startle apparaat en voor het mogen uitvoeren van de laatste studies.

Tijdens mijn promotieonderzoek heb ik de studentes Namkje en Camilla mogen begeleiden. Thank you for your help and enthusiasm in performing research.

Na het bedanken van al mijn fijne collega's, rest mij niets anders dan mijn familie te bedanken. Jullie hebben mij altijd bijgestaan (en aangehoord) en dat is zeker niet minder belangrijk.

Allereerst wil ik mijn ouders bedanken. Piet en Thea, Pap en Mam, jullie hebben altijd achter me gestaan, bij alle studiekeuzes die ik heb gemaakt en dat is erg belangrijk voor mij geweest. Het gevolg is dat er nu een proefschrift voor jullie ligt. Hopelijk heb ik jullie enthousiast weten te maken over mijn onderzoek. Ik heb jullie in ieder geval wel vaak lastig gevallen met al mijn verhalen, dus bedankt voor het luisteren. Jullie zijn de beste.

Daarna, maar niet minder belangrijk, mijn broer(tje). Jonne, hoewel je niet altijd in de buurt was, ben je toch altijd erg geïnteresseerd geweest in mijn onderzoek en hebben we er toch vaak over kunnen kletsen. Je hebt zelfs actief een bijdrage willen leveren (hoewel dat niet zo'n succes was…). Nu krijg je een tweede kans door mijn paranimf te zijn en ik ben erg blij dat je dat wilde doen. Hopelijk krijg je ook je ook nog eens de kans om te promoveren, want ik kan je vertellen: het is de moeite waard. Mijn schoonzusje, Janet, ook jij was altijd geïnteresseerd in mijn onderzoek en hoe de zaken er voor stonden en dat vond ik erg fijn.

Mijn schoonouders, Jules en Alma Doekhi, jullie wil ik bedanken voor jullie enthousiasme en omdat jullie altijd voor me klaar hebben gestaan. Ook mijn zwagers en schoonzussen, Johnny, Lilian en John, Roy en Willemien, Rudy en Sandra, en Richard en Mirella wil ik bedanken voor jullie interesse, steun en vooral gezelligheid. Mirella, ik kon altijd bij jou terecht met mijn verhalen en problemen. We hebben altijd gezellig gekletst en veel gelachen, en ik ben blij dat je mijn paranimf wilde zijn.

En als laatste, maar niet de minste, mijn vriend. Lieve Rémy, je was er altijd voor mij en je hebt me enorm gesteund tijdens mijn promotieonderzoek. Ook wanneer ik weer eens langer door moest werken of in het weekend experimenten moest doen. Ik vond bij jou ook altijd een luisterend oor wanneer ik weer eens enthousiast was over mijn onderzoek of wanneer er soms iets minder leuk was. Je weet hoe belangrijk je voor me bent geweest en ook altijd zal blijven.

Appendix

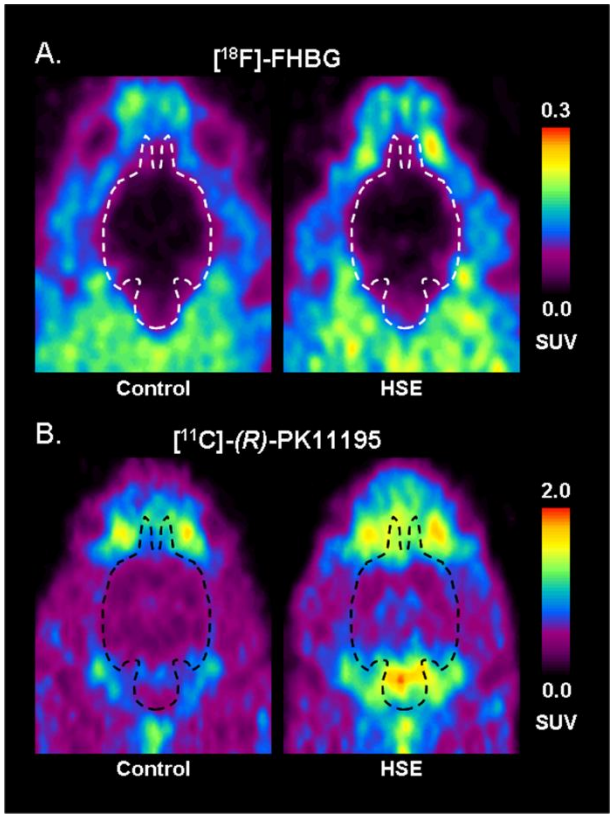

Chapter 3 Figure 2 [^{18}F]-FHBG (**A**) and [^{11}C]-*(R)*-PK11195 (**B**) PET images of a control rat (control) and a rat inoculated with 1x10^{7} PFU of HSV-1 (HSE), on 7 after inoculation. The PET images represent tracer uptake between 30 and 45 minutes after injection.

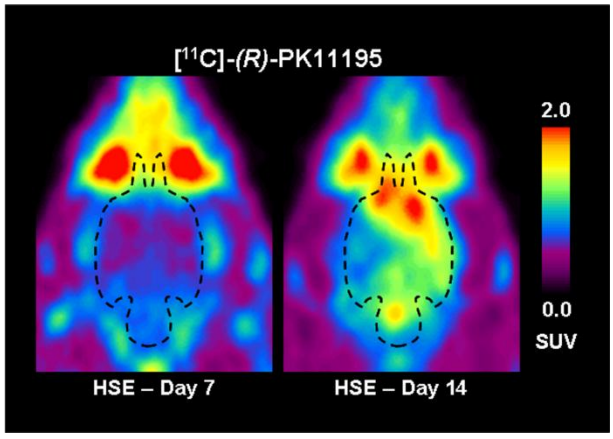

Chapter 3 Figure 3 [^{11}C]-*(R)*-PK11195 PET images of one rat that was inoculated with 1x10^{4} PFU of HSV-1 that showed the development of severe neuroinflammation in frontal brain areas from day 7 to day 14 after inoculation. The PET images represent tracer uptake between 30 and 45 minutes after injection.

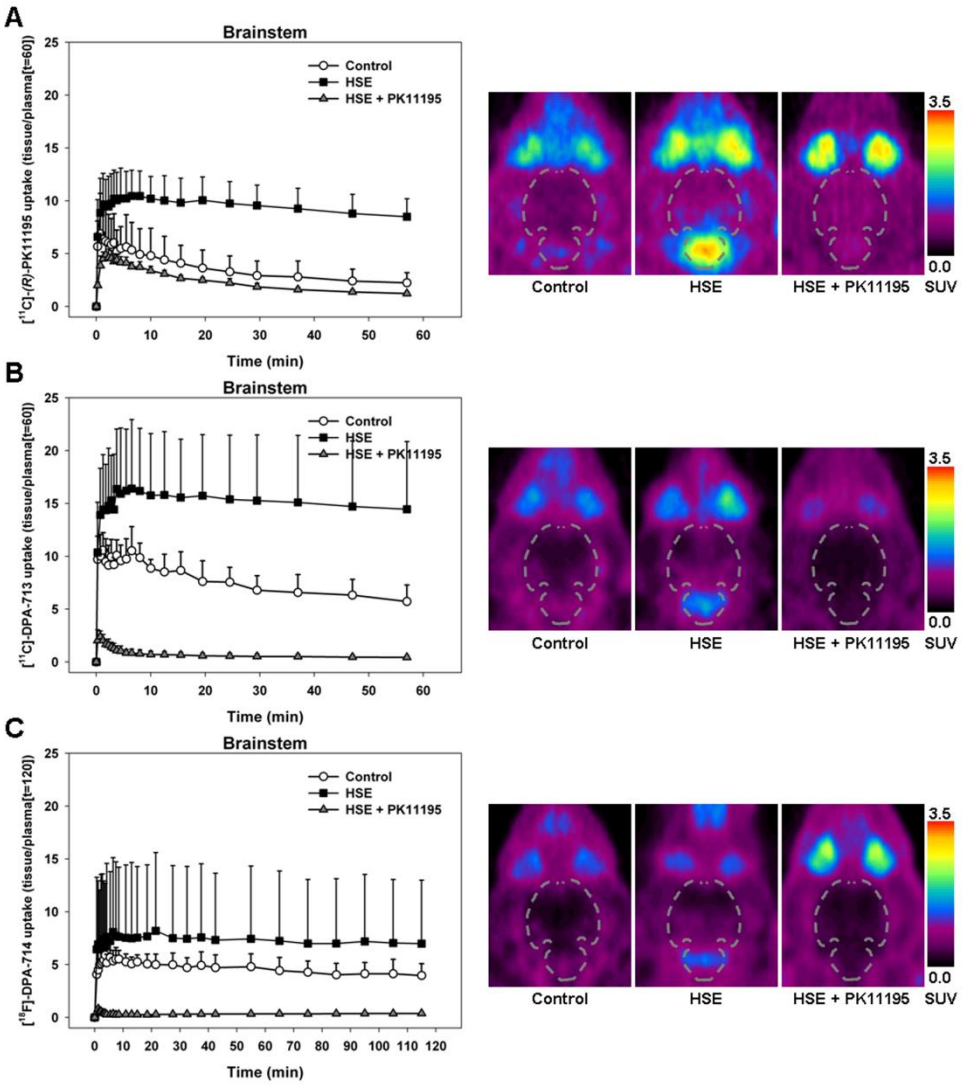

Chapter 4 Figure 3 Time-activity curves (left) of the brainstem for [^{11}C]-*(R)*-PK11195 (**A**), [^{11}C]-DPA-713 (**B**) and [^{18}F]-DPA-714 (**C**), and small animal PET images (right) of control rats (control), rats infected with HSV-1 (HSE) and rats infected with HSV-1 injected with 5 mg/kg PK11195 5 minutes before tracer injection (HSE + PK11195). The time-activity curves are expressed as tissue uptake divided by the *ex-vivo* plasma uptake at t=60 for [^{11}C]-*(R)*-PK11195 and [^{11}C]-DPA-713, and at t=120 for [^{18}F]-DPA-714. The small animal PET images display a coronal plane of the rat head at the level of the brainstem, in which the brain is delineated by a dashed line. The images are summed images between 16 and 60 minutes for [^{11}C]-*(R)*-PK11195 and [^{11}C]-DPA-713, and between 12 and 120 minutes for [^{18}F]-DPA-714.

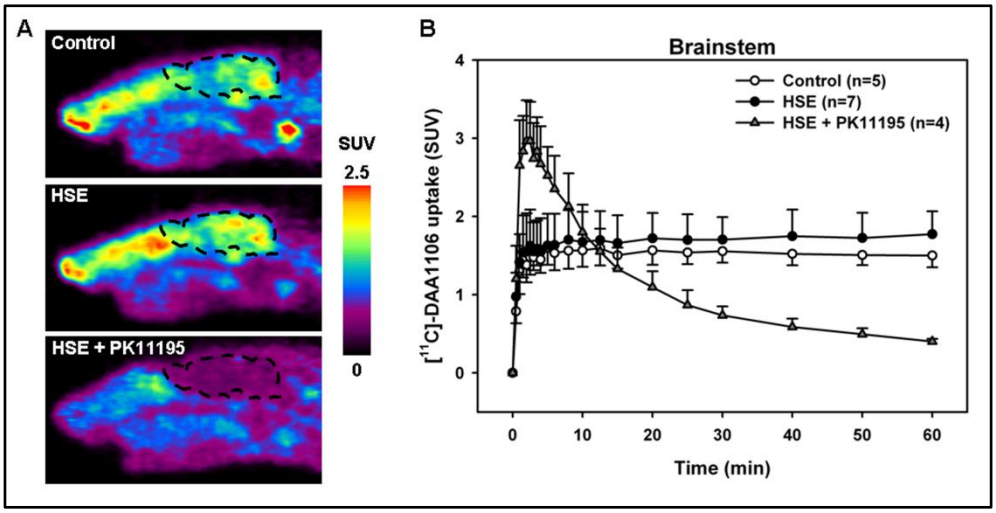

Chapter 5 Figure 1 Small animal PET images and time-activity curves of [^{11}C]-DAA1106. **A** Sagittal view of the head of a control rat (control), rat infected with HSV-1 (HSE) and rat infected with HSV-1 pretreated with 5 mg/kg PK11195 (HSE+PK11195), in which the brain is delineated by a dashed line. The images represent tracer uptake between 30 and 60 minutes after injection of [^{11}C]-DAA1106 (44±14 MBq). During the 60 minute small animal PET scan, the rats were aneasthesized with a combination of ketamine (25 mg/kg) and medetomidine (0.2 mg/kg) **B** [^{11}C]-DAA1106 time-activity curves of the brainstem, expressed as standardized uptake values (mean ± standard deviation), of control rats (n=5), HSE rats (n=7) and HSE+PK11195 rats (n=4).

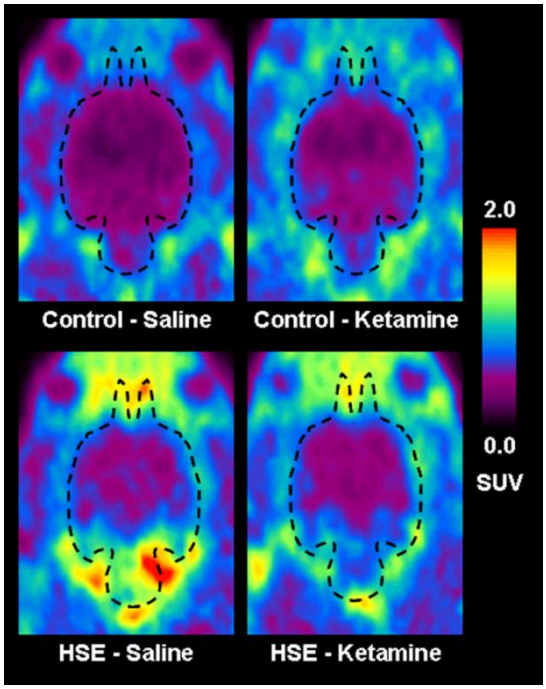

Chapter 6 Figure 5 [^{11}C]-PK11195 small animal PET images of control rats (control) and rats inoculated with HSV-1 (HSE), that received a daily administration of saline or ketamine, on day 5 after inoculation. The images display a coronal plane of the rat head at the level of the brainstem, in which the brain is delineated by a dashed line. The images represent brain uptake between 15 and 60 minutes after injection.

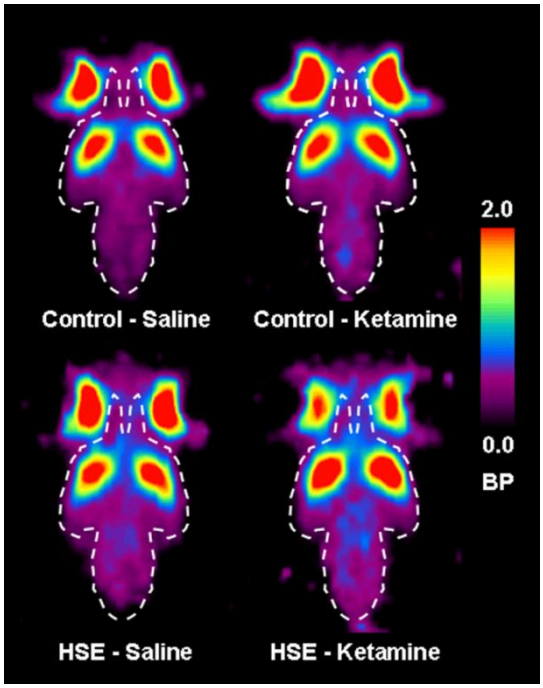

Chapter 6 Figure 6 Small animal binding potential (BP) images of the [^{11}C]-raclopride binding potential of control rats (control) and rats inoculated with HSV-1 (HSE), which received a daily administration of saline or ketamine, on day 5 after inoculation. The images display a coronal plane of the rat head at the level of the brainstem, in which the brain is delineated by a dashed line.

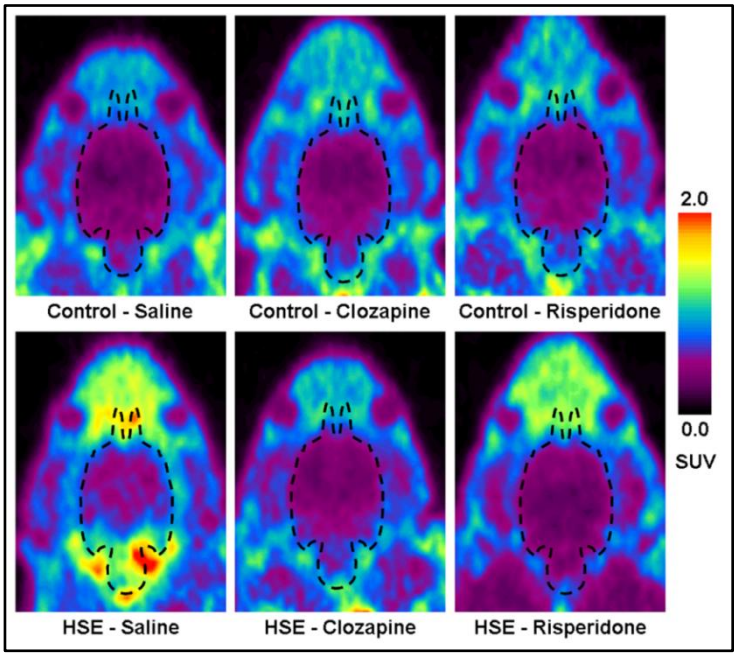

Chapter 7 Figure 4 [^{11}C]-PK11195 small animal PET images of control rats (control) and rats inoculated with HSV-1 (HSE), treated with saline, clozapine or risperidone, on day 5 after inoculation. The images display a coronal plane of the rat head at the level of the brainstem, in which the brain is delineated by a dashed line. The images represent brain uptake between 15 and 60 minutes after injection.

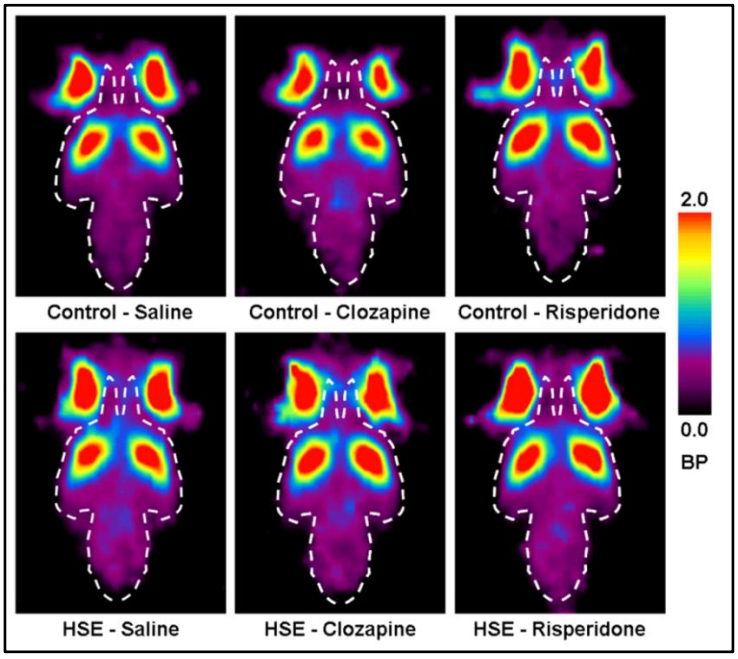

Chapter 7 Figure 5 Small animal PET images of the [^{11}C]-raclopride binding potential (BP) of control rats (control) and rats inoculated with HSV-1 (HSE), treated with saline, clozapine or risperidone, on day 5 after inoculation. The images display a coronal plane of the rat head at the level of the brainstem, in which the brain is delineated by a dashed line.

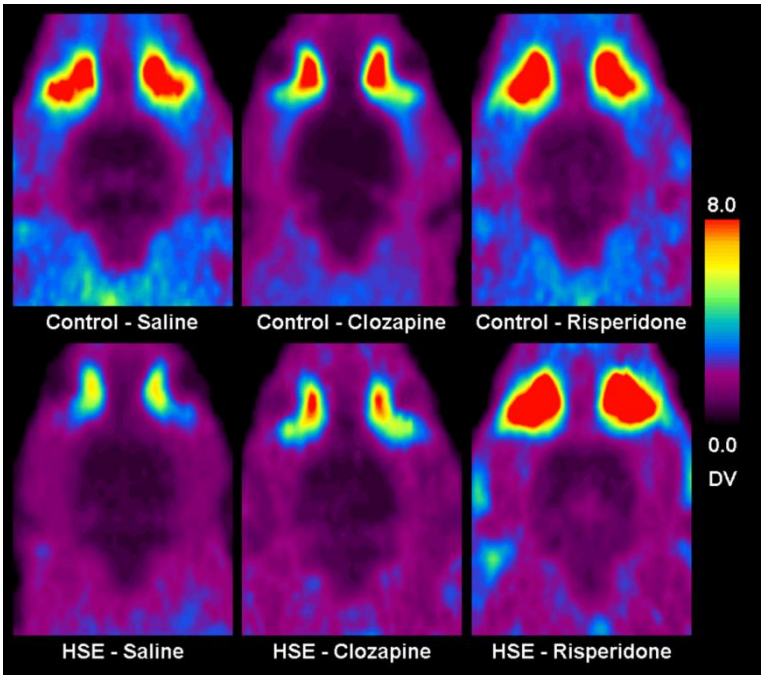

Chapter 8 Figure 2 Small animal PET images of the [^{11}C]-verapamil distribution volume (DV) on day 6 post-inoculation in control rats (control) and rats inoculated with HSV-1 (HSE) that were treated with saline, clozapine or risperidone from day 0 until day 4 post-inoculation. The images display a coronal plane of the rat head, at the level of the brainstem.